Whitbread, Katie (2012) *Postglacial evolution of bedrock rivers in post-orogenic terrains: the NW Scottish Highlands.*

PhD thesis

http://theses.gla.ac.uk/3499/

Postglacial evolution of bedrock rivers in post-orogenic terrains: the NW Scottish Highlands

Katie Whitbread

MA, MSci Natural Sciences, University of Cambridge

Submitted in fulfilment of the requirements for the degree of

Doctor of Philosophy

School of Geographical and Earth Sciences
College of Science and Engineering
University of Glasgow

June 2012

Abstract

Postglacial bedrock river erosion is likely to be a major control on the evolution of deglaciated landscapes. This study provides a quantitative assessment of bedrock channel change in a postglacial, post-orogenic terrain, encompassing the long-term evolution of bedrock channel distribution, geometry and the timing and rate of fluvial incision.

In the NW Scottish Highlands, fluvial incision is focused on steep valley headwalls and at knickpoints formed at inherited glacial valley-floor steps (riegels). Holocene average incision rates of 0.4 – 1.3 m/kyr were measured using cosmogenic surface exposure dating (^{10}Be) at five strath terrace sites. Incision rates of 0.1 m/kyr were quantified from active channel beds and are lower than the Holocene average. This finding is consistent with a paraglacial decline in sediment supply being responsible for a reduction in fluvial incision in detachment-limited channels. Further support for a paraglacial sediment influence on bedrock channels is found in the long-term increase in the proportion of bedrock-exposure, reflecting a decrease in the critical slope threshold for the alluvial to bedrock channel transition. In reaches that have undergone a switch from alluvial to bedrock channel conditions, the onset of fluvial incision into bedrock was found to lag deglaciation by 2 – 4 kyr, suggesting that a substantial reduction in sediment availability occurred within several thousand years of ice retreat.

Hydraulic conditions and substrate resistance are also major controls on the distribution and geometry of bedrock channels, and the rate of fluvial incision, in the NW Highlands. The geometry of both bedrock and alluvial channels was found to be strongly hydraulically scaled, with bedrock channels significantly narrower than coarse-grained alluvial channels. Lithology also governs the critical slope for alluvial to bedrock channel-transition; resistant metasedimentary bedrock produces relatively coarse-grained bed material with a high threshold for sediment entrainment, meaning that alluvial channels occur up to comparatively steep channel slopes. Lithological resistance also constrains the process and rate of fluvial incision. A new lithological resistance index, the ratio of joint spacing to intact rock strength, successfully discriminates between abrasion and plucking dominated channels and is non-linearly related to incision rate.

The pulse of postglacial incision in bedrock channels has resulted in 2 – 8 m of entrenchment into valley floors since deglaciation. Bedrock channels narrow during entrenchment, achieving a consistent hydraulic geometry when entrenched to between 1 and 2 times the bankfull flow depth. Width adjustment occurs within 8 – 17 kyr of ice retreat, but adjustment of channel slope takes considerably longer and the long profiles of NW Highland rivers remain strongly glacially conditioned. Entrenchment disconnects channels from floodplains and may have contributed to the decline in paraglacial sediment flux, suggesting that fluvial incision may be a self-limiting process in post-orogenic postglacial terrains.

Declaration

I declare that, except where explicit reference is made to the contribution of others, this dissertation is the result of my own work and has not been submitted for any other degree at the University of Glasgow or any other institution.

Acknowledgements

Table of Contents

List of Tables

List of symbols

Symbol	Description
A	Upstream drainage area
A_r	Reference drainage area
b and b'	Width-drainage area and width-discharge coefficients
C	Concentration of cosmogenic ^{10}Be
C_n	Initial concentration of cosmogenic ^{10}Be
c and c'	Width-drainage area and width-discharge exponents
d	Channel depth
d_n	Normalised reach-averaged channel depth
d_r	Reach-averaged channel depth
D	Sediment grain size (diameter)
D_0	Initial sediment grain size
E_c	Nominal erosional capacity of the stream
e and e'	Depth-drainage area and depth-discharge coefficients
f and f'	Depth-drainage area and depth-discharge exponents
h	Sediment supply-drainage area exponent
H_{GT}	Reach-average total entrenchment depth (i.e. average gorge depth)
H_{HF}	Bankfull flow depth
H_{LF}	Flow depth on day of measurement (low flow)
H_P	Height of strath terrace sample point above channel bed
H_T	Terrace height
H_G	Inner gorge height
h_{pg}	Predicted postglacial entrenchment depth
I_j	Joint index
I_R	Lithological resistance index
I_s	Rock strength index
I_j/I_s	Resistance ratio: ratio of joint index and rock strength index

K	Coefficient in detachment-limited stream power erosion model
k_p	Coefficient in transport capacity stream power model
k_r	Sediment supply-drainage area coeffecient
k_s	Channel steepness index (slope-drainage area coefficient)
k_{wf}	Coefficient for width- QS relation of Finnegan et al. (2005)
k_{ww}	Coefficient for width- QS relation of Whittaker et al. (2007)
L	Downstream distance
L_{KP}	Distance downstream of a knickpoint
L_R	Reach length
m	Exponent on A in stream power erosion model
n	Exponent on S in stream power erosion model
P_D	Nominal 'force' required to loosen blocks from bedrock
P_T	Nominal 'force' required to entrain grains
P_z	Cosmogenic ^{10}Be production rate at depth z
P_0	Cosmogenic ^{10}Be production rate at the surface
Q	Discharge
q_c	Stream transport capacity
Q_f	Discharge at frequency (f)
Q_{MA}	Median annual flood discharge
q_s	Sediment supply
R	Schmidt hammer 'R' value
R_s	Nominal substrate resistance factor
r	Discharge-area coefficient
s	Discharge-area exponent
S	Reach scale channel bed slope
S_c	Critical slope for alluvial to bedrock channel transition
$S_c^{\ r}$	Reference critical slope
S_{CB}	Channel bed slope from linear regression of dGPS data
S_{ST}	Strath terrace slope from linear regression of dGPS data
S_n	Normalised reach scale channel slope
S_r	Reference reach scale channel slope
T_P	Model ^{10}Be age of strath terrace sample
T_{SA}	Average strath terrace age
t	Time
$u(x)$	Uncertainty on x
W_{LF}	Channel width on day of measurement (low flow)
W_G	Gorge width
W_{HF}	Bankfull equivalent channel width

w	Channel width
w_{IC}	Reach-average inner channel width
w_{ST}	Pre-strath channel width
w_n	Normalised reach-averaged channel width
w_r	Reach-averaged channel width
X_{IC}	Inner channel cross-sectional area
V_{IC}	Inner channel volume
z	Depth below the rock surface
α	Rate of downstream fining of sediment
E_F	Volumetric erosion rate per unit channel length at strath sites
E_F^{PG}	Volumetric erosion rate per unit channel length from inner gorge geometry
ε	Vertical incision rate
ε_A	Abrasion rate
ε_B	Plucking rate
ε_{CB}	Modern vertical incision rate: cosmogenic ^{10}Be in channel bed
ε_P	Holocene vertical incision rate at strath sampling point
ε_{PA}	Average of ε_P values at each strath site
ε_{PG}	Holocene average vertical incision rate from inner gorge geometry
ε_n	Normalised vertical incision rate
ε_R	Holocene average vertical incision rate at a strath site
ρ_r	Density of bedrock
ρ_s	Density of sediment
ρ_w	Density of water
θ	Concavity index (slope-area exponent)
γ	Specific weight of water
Λ	Absorption mean free path
λ	Rate of radioactive decay of ^{10}Be
σ	Standard deviation
Ω	Total stream power (per unit channel length)
ω	Unit stream power (per unit channel width)

Chapter 1

Introduction

1.1   Context: fluvial incision in postglacial landscapes

The landscapes of many mountain ranges and high-latitude regions have been formed by a combination of glacial and fluvial processes (e.g. Roberts and Rood, 1984; Augustinus, 1995; Whipple at al. 1999). Oscillations between glacial and interglacial climate states during the Quaternary have resulted in spatial and temporal variations in the distribution and rate of fluvial and glacial erosion (Braun et al., 1999; Tomkin, 2009). The distinct landforms produced by these processes condition transient geomorphic regimes in which rivers and glaciers rework sediment deposits and reconfigure the topography (e.g. Sugden and John, 1976; Braun et al., 1999; Ballantyne, 2002b; Tomkin, 2009; Hobley et al., 2010; Norton et al., 2010).

During the latest glacial stage (the Late Devensian c. 35 – 11.7 ka, e.g. Bradwell et al., 2008c), northern Europe and North America were covered by extensive ice sheets, and ice masses developed over many mountain belts in mid to low latitudes (Figure 1-1). Many of these areas are now ice free due to climatic warming after ~14.5 ka (Ballantyne, 2010), and rivers have inherited a glacially-conditioned landscape (e.g. Cotton, 1941; Brardinoni and Hassan, 2006; Norton et al., 2010). Using numerical models that combine parameters describing glacial and fluvial erosion, Braun et al. (1999) and Tomkin (2009) predict that a pulse of fluvial erosion will follow deglaciation as postglacial rivers readjust topography and rework sediment deposits. They also suggest that feedback links between bedrock

channels, hillslope form and rates of mass-wasting drive long-term adjustment of hillslopes throughout catchments, thus tending to 're-fluvialise' the landscape (cf. also Dadson and Church, 2005).

A wealth of field evidence indicates that a phase of rapid mass-wasting of hillslopes and enhanced sediment flux in rivers, termed the 'paraglacial' period, is characteristic of postglacial terrains (Church and Ryder, 1972; Ballantyne, 2002b; Slaymaker, 2009). Yet, despite its potential control on hillslope processes and long-term landscape adjustment, the fluvial response to deglaciation, particularly the fluvial *erosional* response, is poorly understood (cf. Hobley et al., 2010). The few quantitative field studies of postglacial fluvial erosion rates are restricted to reach-scale assessments of incised inner gorges and report fluvial incision rates that equal or exceed long term Cenozoic denudation rates in both post-orogenic and orogenic terrains (McEwen et al., 2002; Valla et al., 2010a; Jansen et al., 2011). At catchment- to regional-scales, Norton et al. (2010) show that glacial inheritance is a strong control on the distribution of postglacial fluvial erosion in the European Alps, with local incision rates up to ten times greater than regional uplift and denudation rates. Similarly, Brardinoni and Hassan (2006) find that the inherited glacial landscape form determines the distribution of bedrock channels in British Columbia, but they also show that postglacial fluvial incision has led to little overall adjustment of rivers. Furthermore, Montgomery and Korup (2011) suggest that, in some areas of the European Alps, postglacial fluvial incision has been minimal and deep inner gorges are actually pre-existing features that were preserved under sediment during glaciation and re-excavated by postglacial streams.

These contrasting field observations highlight the need for further research to clarify the role of fluvial incision in postglacial landscape evolution. Three elements of particular importance are: (1) the potential control exerted by the inherited landscape form and paraglacial sediment flux regime on the distribution and rate of postglacial fluvial incision; (2) the influence of glacio-isostatic rebound on postglacial fluvial systems; and, (3) the nature of the relationships between channels and hillslopes that control how fluvial incision affects the wider landscape. The research presented in this thesis primarily addresses the first two elements by providing a quantitative assessment of bedrock channel distribution and morphology together with measurements of the rate of fluvial erosion in a postglacial terrain. The results are then discussed in terms of their implications for channel-hillslope coupling and postglacial landscape evolution.
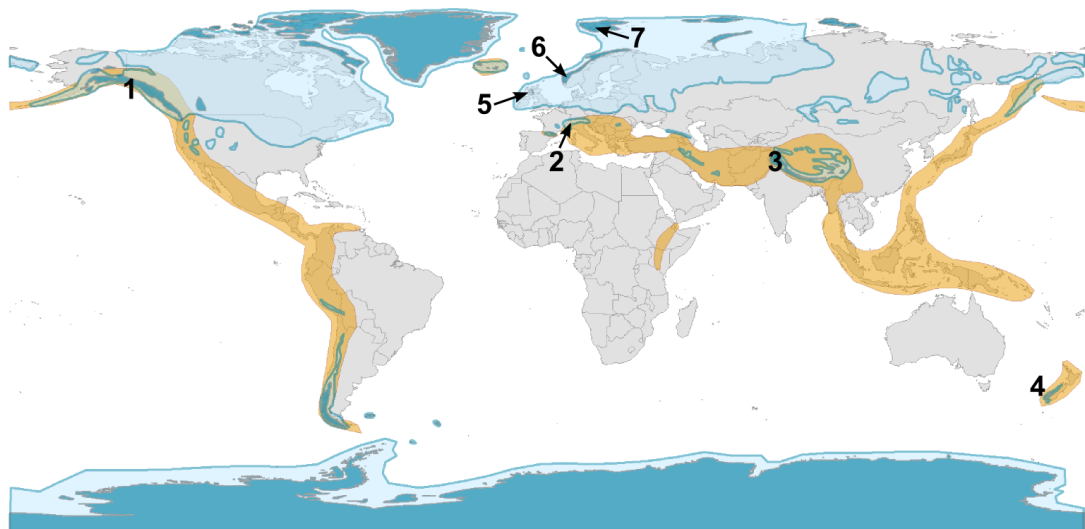
Figure 1-1. The extent of Late Devensian ice sheets and ice caps (light blue) and modern glaciers (dark blue) after Ehlers and Gibbard (2007). Approximate extent of land area affected by tectonic and volcanic activity associated with major plate boundaries also shown (orange shading). Numbers mark locations of published studies of postglacial or glacially-influenced rivers with estimated or measured incision rates discussed in the text. 1) Meigs et al., 2006. 2) Brocard et al., 2003, Valla et al., 2010a. 3) Burbank et al. 1996, Leland et al., 1998. 4) Litchfield and Berryman, 2006. 5) Bishop et al., 2005, Jansen et al., 2011. 6) McEwen et al., 2002. 7) Büdel, 1982.

1.2   Postglacial landscapes and rivers

The distribution of Late Devensian ice sheets and ice caps is compared with the modern distribution of glaciers in Figure 1-1 (Ehlers and Gibbard, 2007). The areas covered by ice during the Last Glacial Maximum (c. 26 – 21 ka, e.g. Ballantyne, 2010) have been repeatedly glaciated through the Quaternary, with the initial fluvial landscape form extensively modified by periods of erosion by both glaciers and rivers during glacial-interglacial cycles, resulting in the overprinting of glacial and fluvial landforms (e.g. Holtedahl, 1967; Roberts and Rood, 1984). At regional scales, the distribution of drainage basins and major valleys is largely preserved from pre-Quaternary times, though glacial erosion locally modifies drainage patterns through breaching of watersheds (e.g. Linton, 1949; Tricart, 1970; Haynes, 1977; Hall, 1991). The extent of glacial modification at sub-catchment scales has been shown to be influenced by both the duration of glaciation (Kirkbride and Matthews, 1997; Harbor et al., 1988) and the erosive capacity of the glacier, which depends on climate, ice thickness and topography (e.g. Brocklehurst and Whipple, 2004). Glacial modification of mountain landscapes appears to begin with cirque formation at higher altitudes followed by erosion of lower valleys as the equilibrium line altitude (ELA; elevation at which ice ablation balances accumulation) lowers and glaciers

extend into the lower parts of catchments (Kirkbride and Matthews, 1997; Brocklehurst and Whipple, 2004). Glacial erosion tends to deepen and widen existing 'V' shaped fluvial valleys, forming characteristic 'U' shaped troughs (Figure 1-2, Harbor et al., 1988; Hirano and Aniya, 1988). Glacial erosion may also 'overdeepen' valley long profiles forming flat-floored trough valleys and fjords in areas below sea level (Holtedahl, 1967; Oerlemans, 1984; Roberts and Rood, 1984; Anderson, 2006).
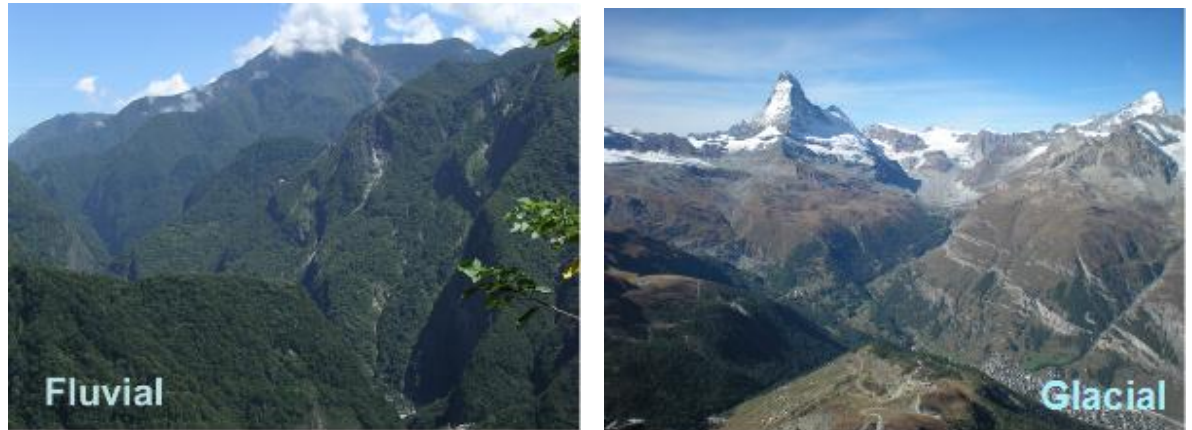
Figure 1-2.   Typical mountain landscapes formed by fluvial erosion (Taiwan) and glacial erosion (Swiss Alps).

1.2.1   Postglacial landscape change: Paraglacial systems

Inheritance of the glacially-conditioned landscape and glacigenic sediments results in disequilibrium in postglacial geomorphic systems (e.g. Ballantyne, 2002b). Church and Ryder (1972) note that high rates of sediment flux are observed in postglacial rivers as streams rework glacial sediments and rates of sediment supply from unstable hillslopes are elevated. They coin the term 'paraglacial' to describe "nonglacial processes that are directly conditioned by glaciation". This term has been widely applied to a range of hillslope processes in postglacial landscapes, including gullying and rock slope failures, and used to denote a period of landscape adjustment following deglaciation (Ballantyne, 2002b). At the heart of the paraglacial concept is a long-term decline in the rate of hillslope processes and sediment flux in rivers as glacial sediment deposits are exhausted and hillslopes stabilise (Church and Ryder, 1972; Schumm and Rea, 1995; Ballantyne, 2002a; Slaymaker, 2009). Although poorly quantified empirically, the temporal decline in sediment flux may be generally approximated by an exponential 'exhaustion' curve (e.g. Ballantyne, 2002a, 2008) and spatio-temporal variations in sediment flux may be modelled as a sediment 'wave' passing through a catchment (Harbor and Warburton, 1993; Ballantyne, 2002b).

To date, bedrock rivers have not been explicitly considered in a paraglacial context, although glacial-conditioning of the landscape is recognised as a major control on the distribution and rate of fluvial erosion (Brardinoni and Hassan, 2006; Hobley et al., 2010; Valla et al., 2010b; Norton et al., 2010). Moreover, only in the work of Hobley et al. (2010) are the responses of fluvial systems to deglaciation considered directly. In other studies, the process of fluvial incision has been considered mainly in the context of the impact of paraglacial landslides on fluvial systems in orogenic terrains (Korup, 2006; Korup et al., 2006; Hewitt et al., 2008; Ouimet et al., 2008). The omission of bedrock channels and fluvial erosion processes from consideration as paraglacial landforms and processes appears to be due to a combination of: a restricted focus on sediment flux; a longer timescale for fluvial adjustment compared to hillslopes (Dadson and Church, 2005); and confusion over the meaning and application of the term 'paraglacial'. In a major review of paraglacial research, Ballantyne (2002b) explicitly linked the paraglacial concept with one of 'glacially conditioned sediment availability', a focus which neglects the fundamental significance of these landscapes, namely that postglacial terrains are transient settings in which unstable, inherited landscape forms are being readjusted by geomorphic processes. In effect, the focus has been on the *effect* of landscape change rather than its *cause*. In different terms, this issue has been highlighted by Slaymaker (2009) who suggests that the term 'paraglacial' is better used as "a descriptor of landforms and landscapes that are in transition from glacial to non-glacial conditions" (pg 79). He also proposes that new approaches to assessing paraglacial landscapes should focus on quantifying the rate and 'trajectory' of landscape change. Put in terms of a question, we should ask: what are postglacial landscapes evolving towards, and how and how quickly do they get there?

The discussion above suggests that fluvial incision is the fundamental control on long-term landscape change in postglacial terrains. By considering bedrock channels and fluvial incision as paraglacial landforms and processes, major advances in the study of these landscapes can be made because: (1) numerical and conceptual frameworks of steady-state fluvial channel and landscape morphology can be used to assess the degree to which glacial topography has been adjusted by paraglacial rivers (i.e. the 'trajectory' of change can be assessed); and, (2) Fluvial incision rates are likely to be a fundamental constraint on the rate of paraglacial landscape adjustment, and techniques developed to measure incision rates can be applied to postglacial settings.

In quantifying the distribution of bedrock channels and measuring fluvial incision rates in a postglacial terrain, this research assesses the rate and trajectory of postglacial landscape change (Slaymaker, 2009), utilising existing knowledge of fluvial systems to assess the degree of adjustment of postglacial rivers to the climatic and tectonic conditions that prevail on deglaciation. Furthermore, the transient conditions of postglacial landscapes, particularly the declining sediment flux regime, provide the opportunity to assess key controls on fluvial incision processes and rates.

1.3   Fluvial bedrock incision: postglacial controls

Postglacial fluvial incision rates have been found to equal or exceed long-term denudation rates and/or uplift rates in both post-orogenic and orogenic terrains. In Scotland Cenozoic denudation rates of 0.02 – 0.03 m/kyr are an order of magnitude lower than measured postglacial fluvial incision rates of 0.4 – 2.4 m/kyr (Persano et al., 2007; Jansen et al., 2011). In the European Alps, local fluvial incision rates of 7 – 13 m/kyr and denudation rates in postglacial catchments of ~1 m/kyr compare with regional uplift rates of ~1 m/kyr (Norton, et al., 2010; Valla et al., 2010a), and in New Zealand, Litchfield and Berryman (2006) measure fluvial incision rates up to 11.5 m/kyr, 1.5 – 5 times regional uplift rates. In addition, two recent studies suggest that there may be temporal variations in postglacial fluvial incision rates; Jansen et al. (2011) have shown that postglacial fluvial incision rates in Scottish Highland rivers are up to ten times greater than current incision rates derived from cosmogenic nuclide analysis of bedrock channel beds; they also find that knickpoint retreat rates have slowed over the Holocene. Valla et al. (2010a) show comparable results from an Alpine gorge where Holocene incision rates are 7 – 13 m/kyr compared to modern incision rates of 0.5 – 3 m/kyr.

Differences between postglacial incision rates and regional and/or long-term uplift rates may reflect the different measurement timescales and spatial scales of the studies. However, a period of elevated fluvial incision in postglacial landscapes mirrors the paraglacial response of hillslopes and the results detailed above suggest that locally, and/or briefly, postglacial fluvial incision may outpace uplift. The main factors controlling fluvial incision, and how they may be influenced by glacial conditioning, are discussed below. Potential feedbacks between evolving postglacial channel morphology and fluvial incision are also discussed.

1.3.1   Incision processes

Fluvial erosion of bedrock occurs by a range of mechanisms which are described in detail by Hancock et al. (1998) and Whipple et al. (2000). The main processes are plucking, abrasion, cavitation and solution. Plucking, the loosening and removal of blocks of bedrock, and abrasion, the incremental wear of bedrock surfaces due to sediment impacts, are the main incision processes found in natural settings in non-carbonate rocks. The relative rates of abrasion and plucking are controlled by lithological factors such as rock strength and the spacing of joints (e.g. Whipple et al., 2000), and the rates of both processes are also dependent on stream power and sediment flux, as discussed below.

Solution is significant only in carbonate rocks and therefore is unlikely to result in substantial rock removal in most settings. Cavitation involves the formation and implosion of air bubbles due to pressure fluctuations resulting from local variations in flow velocity. Shock waves generated by the implosion may have sufficient force to erode bedrock (e.g. Barnes, 1956; Wohl, 1992). In relatively deep, fast moving flows with irregular channel bed morphologies, cavitation and abrasion may work together in the formation of flutes and potholes. As there is currently no known way of distinguishing the contribution of cavitation to bedrock erosion (Whipple et al., 2000), it is assumed here that flutes and potholes form largely due to abrasion but it should be noted that some component of apparent abrasion wear may actually be due to cavitation (Wohl, 1992).

1.3.2   Postglacial controls on fluvial incision

1.3.2.1   Hydrological controls: shear stress and stream power

Fluvial erosion involves bedrock being detached from the channel bed and then transported away by the flow (e.g. Whipple and Tucker, 2002). Fluvial erosion can thus be considered in terms of two end-member scenarios where the overall incision rate is limited by the rate of rock detachment (detachment-limited) or the rate of transport (transport-limited). These scenarios provide a useful conceptual framework for considering fluvial incision (discussed below), but purely detachment-limited erosion is unlikely in most settings due to the need for sediment flux to drive incision (discussed in the next section) (e.g. Whipple and Tucker, 2002).

Detachment-limited fluvial erosion is commonly related to stream power (or shear stress) (e.g. Howard and Kirby, 1983; Howard et al., 1994; Snyder et al., 2000, Whipple, 2004). 'Total stream power' (Ω, per unit length of channel) has been defined as:

$$\Omega = \gamma Q S \qquad\qquad\qquad \text{Eq 1.1}$$

where γ is the specific weight of water, Q is discharge and S is the channel slope (e.g. Bagnold, 1966; Bull, 1979; Jain et al., 2006), with "unit stream power" (ω, per unit channel width) expressed as:

$$\omega = \frac{\gamma Q S}{w} \qquad\qquad\qquad \text{Eq 1.2}$$

where w is the channel width. For detachment-limited channels, formulation of erosion rates in terms of stream power is based on assumed hydraulic scaling between discharge and drainage area (A) and channel width and discharge, and the assumption that most erosion occurs during high discharge events when the boundary shear stress greatly exceeds a critical shear stress for particle entrainment (e.g. Howard and Kirby, 1983; Snyder et al., 2003; Attal et al., 2008). The 'standard' stream power erosion model is formulated thus:

$$\varepsilon = K A^m S^n \qquad\qquad\qquad \text{Eq 1.3}$$

where K is a constant that depends on sediment flux, lithological resistance, and discharge variability amongst other factors, and exponents m and n vary with the erosion process (e.g. Howard and Kirby, 1983; Whipple and Tucker, 1999; Whipple et al., 2000). The stream power model forms the basis for fluvial components of landscape evolution models, and although generic it is relatively successful at reproducing realistic topographies and has been empirically verified with field and topographic data (e.g. Howard and Kirby, 1983; Whipple and Tucker, 1999; Snyder et al., 2003; Whipple et al., 2004).

In postglacial settings, rivers inherit glacially-conditioned valley floors, with steep valley headwalls, overdeepened basins, and valley-spanning steps or ridges termed 'riegels' (e.g. Cotton, 1941; MacGregor et al., 2000). Steep channel slopes, and therefore high stream power, may contribute to the high incision rates seen in bedrock reaches located at hanging valleys (Valla et al., 2010a), 'riegels' (e.g. McEwen et al., 2002) and knickpoints formed through base level fall related to glacio-isostatic uplift (Jansen et al., 2011). Temporal variations in discharge due to deglaciation and climatic change may also influence fluvial incision rates (e.g. Whipple, 2001).

1.3.2.2   Sediment and incision

Sediment plays a fundamental role in fluvial erosion; at low sediment concentrations erosion rates are limited due to a lack of tools for doing erosive work ('tools effect') and, at high concentrations erosion rates are low due to sediment cover on the channel bed ('cover effect') (e.g. Sklar and Dietrich, 1998, 2001; Whipple and Tucker, 2002). The degree of sediment cover is determined by the capacity of the flow to transport sediment (q_c) which, as for bedrock detachment, is commonly related to stream power. Where/when the flux of sediment in the channel (q_s) exceeds the transport capacity, sediment is deposited and alluvial channels form. Bedrock channels are thus characteristic of settings where $q_s<q_c$ (e.g. Massong and Montgomery, 2000).

The non-linear relationship between sediment flux and abrasion rates has been relatively well defined through physical experiments (e.g. Sklar and Dietrich, 2001), but the sediment flux control on plucking is poorly understood. Whipple et al. (2000) suggest that rates of crack propagation may depend on the frequency of bedload sediment impacts, but as crack propagation may also occur through weathering and seasonal freezing, sediment flux may play only a minor role in plucking in some settings.

The dual role of bedrock channels as conduits for sediment and agents of erosion (Whipple and Tucker, 2002), together with the potential for local sediment cover to influence the distribution of erosion within channels, means that changes in sediment flux may also influence channel geometry (e.g. Finnegan et al., 2007; Yanites and Tucker, 2010). Both physical and numerical modelling have shown that a reduction in sediment flux may result in channel narrowing, with important feedback implications for channel transport capacity and fluvial incision rates (Finnegan et al., 2007, Johnson and Whipple, 2007, 2010).

As noted above, the highly variable slope of postglacial channels, and consequent variation in transport capacity, is a strong control on the distribution of bedrock channels (Brardinoni and Hassan, 2006). Furthermore, the paraglacial decline in sediment flux has fundamental implications for postglacial fluvial systems:

- It may be responsible for a decline in postglacial incision rates in detachment-limited bedrock channels (via the tools effect);
- In transport-limited bedrock channels, a decline in sediment flux may increase erosion rates (via a decrease in sediment cover);
- It would be expected to drive long-term changes in the distribution of channel types

- It may result in channel narrowing.

To date, only a possible sediment-flux controlled decline in erosion rate has been documented in detachment-limited postglacial channels (Jansen et al., 2011). Postglacial settings thus have the potential to provide a much needed 'natural' test of the developing models of sediment flux controls on fluvial incision.

1.3.2.3   Lithological resistance

The key parameters controlling lithological resistance are the intact rock strength and the spacing of joints and bedding surfaces, with the balance between the two controlling the relative rates of abrasion and plucking (Hancock et al., 1998; Whipple et al, 2000). Where the joint spacing yield blocks sufficiently small to be moved by the flow (generally blocks of sub-metre size), rates of plucking have been found to be considerably greater than abrasion rates (Whipple et al., 2000; Hartshorn et al., 2002). Laboratory measured rock tensile strength has been shown to be a reasonable proxy for abrasion resistance (Sklar and Dietrich, 2001).

In most numerical and physical modelling studies, bedrock or equivalent substrates are homogenous, and field study areas are frequently selected to minimise lithological variations (e.g. Snyder et al., 2000; Johnson et al., 2010; Attal et al., 2011). However, in most natural settings, lithological resistance is highly variable and will drive spatial variations in the process and rate of fluvial incision (e.g. Whipple et al., 2000). Thus, variations in lithological resistance are likely to be important controls on postglacial channel evolution and must be accounted for in field assessments of fluvial incision.

1.3.2.4   Ice and fluvial incision in cold landscapes

Seasonal freezing of rivers and ground ice in the channel bed and banks may also affect erosion in postglacial and periglacial rivers (e.g. Büdel, 1982; McEwen and Matthews, 1998; McEwen et al., 2002, Whipple, 2004). Crack propagation due to ice formation in joints may loosen blocks in the channel banks and bed, which are then available for transport by the stream. Despite field observations suggesting that cryogenic processes may be an important component of fluvial incision in 'cold' landscapes (McEwen et al., 2002), very little is known about the influence of seasonal freezing on the rate of plucking, or on the distribution of incision within channels. In addition, the effect of ice-dams,

formed during the break-up of seasonally frozen high-latitude rivers, on the channel banks and bed is unknown.

1.3.3   Channel evolution and incision feedbacks

1.3.3.1   Base level change

During deglaciation, glaciers in trunk valleys may act as a local base level for unglaciated tributary streams (Meigs et al., 2006; Korup and Montgomery, 2008). Deglaciation of the trunk valley results in a considerable base level fall in the tributary stream driving river incision into sediments and bedrock (e.g. Benn and Evans, 1998, p.620). Brocard et al. (2003) and Meigs et al. (2006) describe this scenario in valleys in the European Alps and Alaska, respectively, where substantial postglacial channel incision was caused by base level fall of up to 800m following glacier retreat.

Regional base level change can also be triggered by glacio-isostatic rebound of the land surface due to the unloading of ice during deglaciation. Where postglacial streams are directly connected to sea level, variations in base level are driven by the competing influences of this glacio-isostatic uplift, and eustatic sea level rise caused by the melting of the continental ice sheets. The combination of sea level rise and land uplift may result in a rapid relative base level rise, followed by an extended period of base level fall when uplift outpaces the sea level rise (e.g. Lambeck, 1993; Shennan et al., 2005). Bishop et al. (2005) and Jansen et al. (2011) show that a regional postglacial base level fall has driven the formation of retreating bedrock knickpoints in postglacial streams in Scotland.

1.3.3.2   Channel evolution and internal feedbacks

Fluvial incision rates may be stabilised over long timescales by feedbacks between channel geometry, channel-hillslope coupling and the discharge and sediment flux conditions that drive erosion. Under stable climate and constant rates of tectonic uplift, negative feedbacks in fluvial systems result in stable, or 'steady-state' topography and channel geometry, and/or a state of 'dynamic equilibrium' in which mass fluxes between different geomorphic components of the landscape are in balance (e.g. Howard et al., 1994; Ahnert, 1994; Whipple, 2004).

In response to climatic or tectonic perturbations, fluvial systems tend to re-adjust their morphology in order to: (1) balance erosion with uplift (detachment-limited systems); and/or to (2) transport the sediment supplied from upstream (transport-limited systems)

(Whipple and Tucker, 2002). Numerical modelling studies suggest that postglacial rivers will tend to adjust the inherited glacial landscape to the prevailing postglacial climate and tectonic regime by 'smoothing' knickpoints in the channel long profile (Tomkin, 2009) and driving adjustment of glacial valley walls through channel bed lowering (Dadson and Church, 2005). Changes in channel slope and width through incision, as well as changes in the nature of channel-hillslope coupling as channels are entrenched, may result in spatial and temporal variations in fluvial incision rates. Thus in postglacial channels, the extent to which long-term variations in fluvial erosion rates may reflect changes in 'external' controls (climate, paraglacial sediment flux) or 'internal' controls (channel slope and width and coupling with hillslopes) is an important, but unresolved issue.

1.3.4   Fluvial erosion landforms and the duration of incision

Long-term changes in channel geometry during incision may result in the formation of a range of fluvial-erosion landforms, including knickpoints, inner gorges and strath terraces. These landforms have formed the basis for the measurement of fluvial incision rates using geometric assessment (e.g. McEwen et al., 2002; Bishop et al., 2005; Valla et al., 2010a), and/or surface-exposure dating (e.g. Burbank et al., 1996; Valla et al., 2010b; Jansen et al., 2011). However, some inner gorges in postglacial settings may have pre- or sub-glacial origins (Holtedahl, 1967; Tricart, 1970; Montgomery and Korup, 2011), and conversely, some surface exposure ages indicate that the onset of incision may lag deglaciation by several thousand years (Valla et al., 2010a; Jansen et al., 2011). Thus it is important to consider the timing of onset of fluvial incision when quantifying erosion rates from fluvial erosion landforms.

1.4   Research objectives and thesis structure

Comprehensive assessments of fluvial bedrock incision in postglacial landscapes that address the distribution, timing and rate of fluvial incision and the nature of channel evolution are needed to understand their contribution to postglacial landscape evolution. As noted in section 1.1, the influence of glacial conditioning on fluvial incision and the nature of feedback relationships between channels and hillslopes are of particular interest. The main focus of this study is on the former aspect. The primary objective of this research is: *to quantify the erosional fluvial response to inheritance of landscapes conditioned by glacial erosion.*

To achieve the primary objective, four specific research aims are identified:

1. To assess the distribution of postglacial bedrock channels (chapter 3)

2. To quantitatively assess the geometry (slope, width and depth) of postglacial bedrock channels (chapters 3 and 4)

3. To date the onset of fluvial erosion following deglaciation and to measure postglacial fluvial incision rates (chapter 5)

4. To quantify the distribution of postglacial fluvial incision at catchment scales (chapter 6)

These aims were addressed using a combination of field survey, topographic analysis and cosmogenic nuclide surface exposure dating. Potential controls on bedrock channel distribution, geometry and fluvial incision rates were also quantitatively assessed using field measurements and topographic data. The post-orogenic, postglacial terrain of the northwest (NW) Scottish Highlands was selected as the study area. The rationale for this selection and the geological and geomorphological characteristics of the NW Highlands are discussed in chapter 2 along with an outline of core aspects of the field survey and topographic analysis methodology.

The research methods and data analysis procedures specific to each research component are outlined in the relevant chapters, prior to the presentation and discussion of the results. In chapter 7, the findings from all components are synthesised, and conclusions in chapter 8 review the wider implications of the findings and suggest future research directions.

Chapter 2

Study area and research methods

2.1   Study area and data requirements

The objective of this research is to *quantify the erosional fluvial response to inheritance of landscapes conditioned by glacial erosion*. For this objective to be achieved, the study area must fulfil the following criteria:

1. It must be formerly glaciated, and it should retain enough evidence of the landscape form at deglaciation to allow assessment of the extent of postglacial fluvial adjustment.

2. It must have low rates of tectonic uplift so that tectonic influences on fluvial processes can be minimised.

3. It must be suitable for the use of cosmogenic nuclide analysis to quantify the timing and rate of fluvial bedrock incision.

The postglacial, post-orogenic terrain of the northwest (NW) Scottish Highlands fulfils these criteria and has the additional advantages of readily available, high resolution digital topographic data, a reasonably well constrained deglaciation history, a relative abundance of bedrock channels (e.g. Jansen et al., 2010), and abundant lithologies suitable for cosmogenic nuclide analysis (e.g. Jansen et al., 2011). The main geographical, geological and geomorphic characteristics of the NW Scottish Highlands are outlined in section 2.2.

Achievement of the research objective requires a holistic consideration of the range of potential morphological and process changes in postglacial bedrock channels. Four main components of fluvial systems that may change as bedrock channels evolve after deglaciation were identified in section 1.4, namely, the distribution, geometry and entrenchment of channels, and the rate of fluvial bedrock incision. The approaches taken to quantify these aspects of postglacial channels in the NW Highlands are outlined in section 2.3.

2.2   Study Area: NW Scottish Highlands

The NW Scottish Highlands are located in the north of the mainland British Isles. The main section of the range stretches over 160 kilometres from the Great Glen in the south to Assynt in the north, reaching a maximum elevation of ~1200m above sea level (Figure 2-1). The topography of the range is markedly asymmetrical, with the main watershed located close to the west coast. As a result, west-draining catchments are generally small and steep (c. 100 km^2) whereas east-draining catchments are considerably larger (c. 1000 km^2).

2.2.1   Geological context of the NW Scottish Highlands

The Scottish Highlands form part of a post-orogenic terrain, characterised by resistant metamorphic bedrock and low rates of tectonic uplift. The geological context of the study area is shown in Figure 2-2. The Great Glen, forming the southern limit of the NW Highlands, follows a major NE-SW trending fault bisecting the country from Loch Linnhe to the Moray Firth. The NW Highlands are predominately formed from the metasediments of the Moine Supergroup, which largely consist of metmorphosed sandstone, siltstone and mudstone (termed psammite, semipelite and pelite respectively). Near the western coast, the Moine thrust separates these metsediments from the underlying, highly metamorphosed Lewisian Gneiss and weakly metamorphosed Torridonian sandstone (Figure 2-2). In the east, around the inner Moray Firth, the Moine rocks are unconformably overlain by unmetamorphosed sandstones and conglomerates of Devonian age (~400 Ma) that were deposited in alluvial fans and river floodplains at the margin of an ancient mountain belt under an arid climate (Trewin and Thirlwall, 2002). Rocks younger than Devonian age do not crop out in the NW Highlands, and it is thought that much of the Highlands were eroded to a comparatively low relief landscape, and probably submerged below sea level by the latter part of the Cretaceous (~100 – 65 Ma) (Hall and Bishop, 2002).
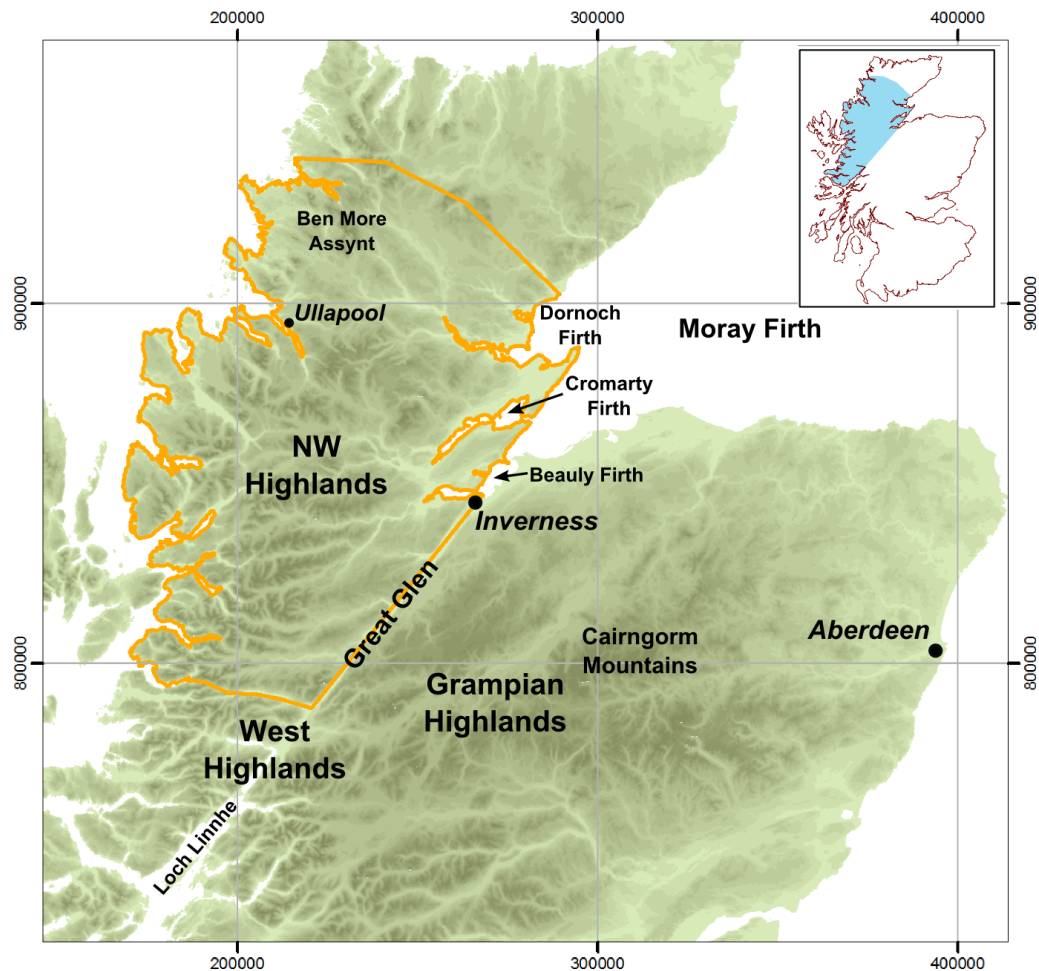
Figure 2-1. Topographic elevation map of northern Scotland derived from STRM data (USGS (2004), Shuttle Radar Topography Mission) (dark green = high elevation, light green = low elevation), geographical terms and places mentioned in the text. The inset map highlights the location of NW Highlands field area.

The general elevation of the NW Highlands, and the asymmetric form of the topography, were established during a phase of uplift and tilting of the land surface associated with the passage of the Iceland plume in the early Cenozoic (c. 65 – 50 Ma) (Hall and Bishop, 2002; Persano et al., 2007). Surface uplift of over 350 m drove a period of rapid denudation during which the pre-Cretaceous erosion surface was exhumed and the pre-glacial drainage network was established (e.g. Sissons, 1967; Hall, 1991; Hall and Bishop, 2002; Persano et al., 2007). The short duration of this pulse of uplift (1 – 10 Ma) and substantially lower denudation rates over the remainder of the Cenozoic have yielded a relatively low Cenozoic-average denudation rate of 0.02 – 0.03 m/kyr (Persano et al., 2007). Glacio-isostatic rebound following Quaternary deglaciations produced very rapid but short-lived pulses of surface uplift. Uplift rates following the most recent major glaciation of Scotland were 10 – 30 m/kyr during deglaciation with the highest rates in the western Highlands (Firth and Stewart, 2000). Within several thousand years of deglaciation uplift rates had fallen to 4 – 5 m/kyr and currently range from 0.5 m/kyr in

peripheral areas up to 2 m/kyr in the western Highlands (Shennan et al., 2000; Firth and
Stewart, 2000). Because of their short duration, these pulses of uplift have had little
influence on topographic relief (Jansen et al., 2010), meaning that uplift rates can be
considered as essentially low and uniform across the study area. The effects of glacio-
isostatic uplift on NW Highland rivers are considered in section 2.2.3.2.
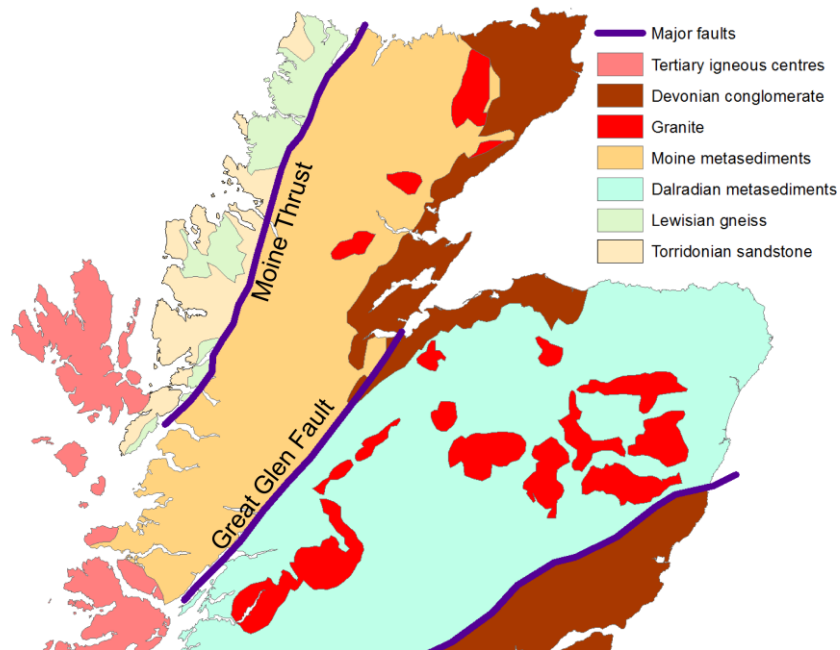
**Figure 2-2. Geology of the NW Scottish Highlands. Simplified representation of key geological units
and structures constructed from digital 1:50,000 scale British Geological Survey bedrock geology maps.**

2.2.2   Glacial erosion and the NW Highlands landscape

Global cooling at the onset of the Quaternary (~2.6 Ma) led to the development of ice caps
over the mountains of the NW Highlands (Lee et al., 2011). As the Quaternary glacial-
interglacial cycles became established, later glaciations resulted in the development of
major ice sheets over the whole of northern Britain (Sejrup et al., 2004; Lee et al., 2011).
The latest of these major glaciations occurred during the Late Devensian (LD) (31 – 11.7
ka) with the British-Irish Ice Sheet (BIIS) reaching a maximum extent between ~21 and 26
ka (Bradwell et al., 2008c; Ballantyne, 2010; Lee et al., 2011) (Table 2-1). The BIIS,
centred over the Scottish Highlands, thinned and receded throughout the latter part of the
Late Devensian (21 – 11.7 ka), probably reaching the location of the current shoreline
between 17 – 15 ka (Bradwell et al., 2008c; Ballantyne, 2010). In the NW Highlands,
further retreat of glaciers into the upland valleys occurred during the Late Glacial
Interstadial (14.5 – 12.9 ka), with some short-lived re-advances (Bradwell et al., 2008a). A
return to cool climate conditions during the Younger Dryas (YD) (12.9 – 11.7 ka), drove
an expansion of the remnants of the Late Devensian ice caps in the Scottish Highlands.

This cold phase is commonly termed the 'Loch Lomond Stadial' in Scotland (e.g. Ballantyne, 2010), but here the term YD is preferred for consistency with palaeoclimate and northern Hemisphere glacier reconstructions (Golledge, 2010). The cool phase was short-lived, and climatic warming brought an abrupt end to the YD with complete deglaciation of the NW Highlands by ~11.7 ka (Bradwell et al., 2008c), and the establishment of temperate climatic conditions by ~11 ka (Brooks and Birks, 2000).

Marine Isotope Stage	Stage			Age (ka)
1	Holocene			
1			Younger Dryas *(Loch Lomond Stadial)*	11.7
1				12.9
2	Devensian (Weichselian)	Late	Late Glacial Interstadial	14.5
2	Devensian (Weichselian)		Dimlington Stadial	LGM 26-21
	Devensian (Weichselian)			31
3	Devensian (Weichselian)	Mid		
	Devensian (Weichselian)			58
4	Devensian (Weichselian)	Early		
	Devensian (Weichselian)			116
5	Ipswichian (Ermian)			

Table 2-1.   Terminology used for Late Quaternary time periods, after Bradwell et al. (2008), Lowe et al. (2008), Ballantyne (2010) and Golledge (2010). All terms are standard for British Isles, with equivalent terms used in NW Europe shown in brackets apart from the Younger Dryas Stadial for which the original British term is shown in italics. Blue bands indicate the timing of the Last Glacial Maximum (LGM) and the glacial episode of the Younger Dryas. Not to scale.

Glacial erosion over the Quaternary has substantially modified the Scottish Highland landscape. Clayton (1996) estimates an average glacial erosion depth of ~100 – 175 m over the NW Highlands and reports glacial erosion rates for the whole British Isles of 0.23 m/kyr averaged over the Quaternary and up to 1.2 – 2.3 m/kyr when only the duration of glacial episodes is considered. Spatial variations in the mechanisms and extent of glacial erosion across the NW Highlands have resulted in regional differences in the assemblages of glacial landforms (cf. Sugden and John, 1976; Haynes, 1977; Benn and Evans, 1998). Three main types of 'glacial erosion terrain' have been identified in the NW Highlands: regions dominated by landforms resulting from areal scouring under ice-sheet conditions; those dominated by landforms produced by alpine-type glaciation; and areas of relatively

limited glacial modification (Sugden and John, 1976; Haynes, 1977; Rea and Evans, 1996; Benn and Evans, 1998). The distribution of these landscape types is shown in Figure 2-3.

The northern part of the study area is characterised by an 'areal-scouring' terrain of relatively low relief but undulating bedrock topography with abundant striated bedrock knolls, roche moutonnées and lakes filling overdeepened rock basins (termed 'knock and lochain' topography by Linton (1963)) (Figure 2-3). This landscape was produced by erosion under relatively extensive wet-based glaciers which striped away the sediment cover and scoured the bedrock surface through abrasion (cf. Sugden and John, 1976; Gordon, 1981; Rea and Evans, 1996; Bradwell et al., 2008b). Another feature of this areal-scouring terrain is the high connectivity of valleys resulting from extensive breaching of drainage divides, probably through erosion of topographic highs due to offsets between the ice-shed and the main topographic divide (e.g. Linton, 1949; Haynes, 1977).

The southern part of the study area and the uplands of the Beinn Dearg Massif are dominated by an 'alpine-type' landscape of narrow, deep glacial troughs separated by ridges or narrow plateaus (Figure 2-3). These form due to excavation by valley glaciers that develop through the amalgamation of ice from tributary cirques or as outlet glaciers from an ice-cap (Benn and Evans, 1998). Many of the glacial troughs in this area form roughly dendritic networks with headwater and tributary cirques, although there is also localised breaching of drainage divides (Haynes, 1977). Excavation of these breached divides may be due, in part, to valley/cirque headwall retreat (e.g. Brocklehurst and Whipple, 2002) as well as 'trans-topographic' ice flow under ice-sheet conditions (Haynes, 1977).

The east of the study area is lower relief and less distinctly glacial in character with relatively broad, and largely 'V' shaped, valleys indicating a lesser degree of glacial modification (Haynes, 1977). Localised areas of 'streamlined' and striated bedrock, and minor glacial troughs suggest that limited glacial erosion occurred during both ice-sheet and valley glaciation.

The different valley morphologies of the areal-scouring, alpine and low-modification terrains provide different constraints on the initial long-profile form of postglacial streams. The variability in terrain means that the influence of inheritance of a range of glacial landforms resulting from both ice-sheet and alpine-type glaciations on channel form and

evolution can be assessed in the study area. The different glacial erosion terrains were taken into account in the selection of study catchments (section 2.3.1).
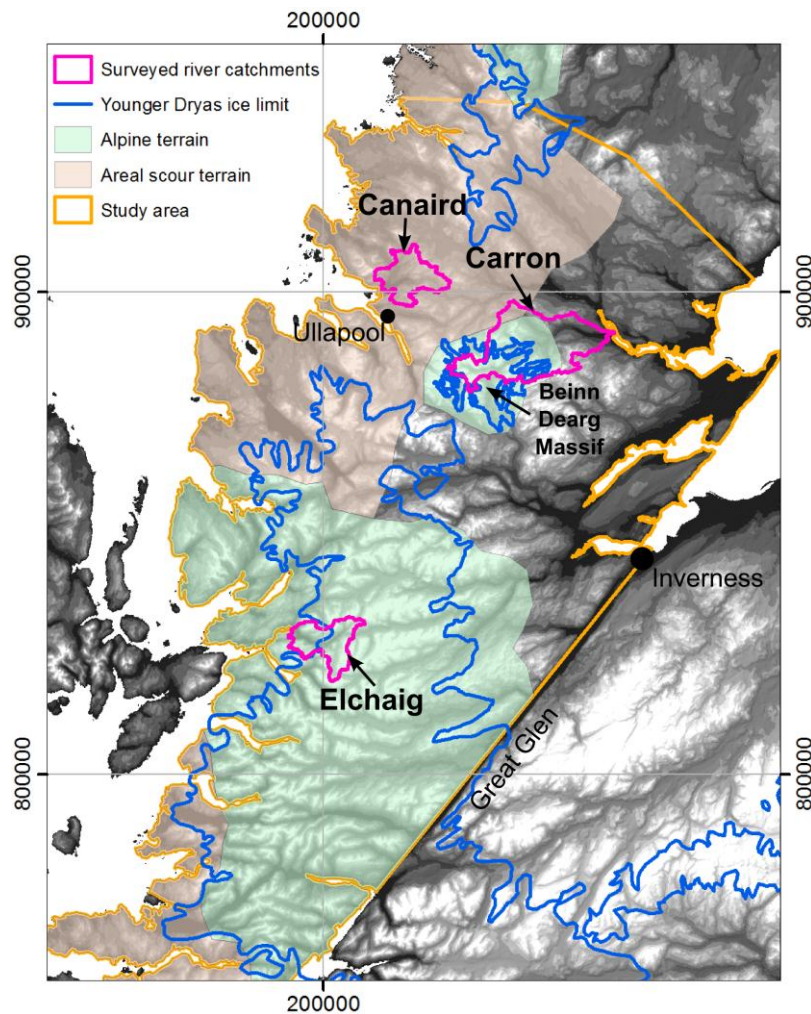
Figure 2-3. Glacial erosion terrains in the NW Highlands study area, simplified from Haynes (1977). Unshaded area in the east is the 'low-modification' terrain. Topography shown by STRM digital elevation model (white is high elevation, black is low elevation). Younger Dryas ice limit based on Bennett and Boulton (1993) and Golledge (2010) with reconstruction of Beinn Dearg ice cap by Finlayson et al. (2011). Study catchments highlighted and named are discussed in section 2.3.1. Scale is British National Grid (m) with grid at 100 km intervals.

2.2.3   Postglacial landscapes and rivers in the NW Highlands

2.2.3.1   Postglacial landscape change

Since deglaciation, the landscape of the Scottish Highlands has been modified by a range of geomorphic processes. Evidence for paraglacial hillslope adjustment through rock-slope failures, rock falls and debris flows, and for the reworking of glacial sediment deposits by rivers, was comprehensively reviewed by Ballantyne (2008). Stratigraphic evidence from gullies and dating of debris cone and landslip deposits indicate formation soon after deglaciation either during the Late Glacial following retreat of the BIIS, or during the early Holocene following the YD deglaciation. A period of rapid adjustment of unstable

hillslopes and sediment deposits following deglaciation suggests that sediment flux to NW Highland rivers may also have been elevated in early postglacial times.

Alluvial and glacio-fluvial terraces are almost ubiquitous features of NW Highland streams, indicating that periods of net aggradation during and after deglaciation were followed by erosion (Maizels and Aitken, 1991; Ballantyne, 2008). This general pattern is consistent with a paraglacial sediment flux regime characterised by high supply rates in early postglacial times followed by a long-term decline (e.g. Church and Ryder, 1972; Ballanytne, 2002b). However, dating of alluvial terraces in the Scottish Highlands suggests that the controls on aggradation and erosion may be more complicated (Lewin and Macklin, 2003). The few alluvial terraces that have been dated in the Scottish Highlands commonly yield mid to late Holocene ages (2 – 6 ka) suggesting relatively recent aggradation of valley floors. Lewin and Macklin (2003) note that the preservation potential of alluvial terraces in Highland catchments is likely to be low due to relatively narrow valley floors and the potential for reworking during floods. They suggest that the relatively recent aggradation in upland catchments is probably due to the superimposition of short, climatically-controlled periods of increased sediment supply on a long-term trend of channel incision. Thus, early Holocene terraces are not found because of the tendency for channels to incise and rework earlier deposits. Though complicated by shorter term variations in sediment flux, the tendency for Highland channels to deposit then incise over long-timescales is consistent with the hypothesis of a paraglacial sediment flux regime in NW Highland rivers.

Records of lacustrine sedimentation reviewed by Edwards and Whittington (2001) indicate that sedimentation rates in four lakes studied in the NW Highlands have generally stayed constant or decreased over the Holocene. They interpret this as reflecting both limited anthropogenic impacts and the development of stabilising peat cover during the mid to late-Holocene. But decreasing sedimentation rates are also consistent with a paraglacial decline in sediment supply due to slope stabilisation and exhaustion of glacial sediment deposits.

Jansen et al. (2011) show that a paraglacial decline in sediment flux is likely to have been responsible for the long term decrease in rates of knickpoint retreat in rivers in western Scotland. This use of evidence from bedrock channel processes to infer past sediment flux conditions suggests that careful consideration of postglacial bedrock channel distribution and form, as well as quantification of postglacial incision rates, may yield further

indications of the role of sediment in postglacial channel evolution despite an absence of measured sediment flux rates. This possibility is explored further in subsequent chapters in the context of the results obtained.

2.2.3.2   Glacio-isostatic uplift

Deglaciation of the BIIS caused relative base level fall in Scotland as glacio-isostatic surface uplift outpaced the postglacial eustatic sea level rise. As noted in section 2.2.1, the rate of base level fall was greatest during deglaciation (~14 – 13 ka), reaching rates of up to ~30 m/kyr in the western Highlands, and ~ 10 m/kyr in northern and eastern parts of the NW Highlands (Shennan et al., 2000, 2005). Rates of base level fall during the Late Holocene have been lower, typically ~0.5 – 2 m/kyr, and c. 8 ka, there was also a slight rise in sea level to ~2 – 4 m above present levels as eustatic sea-level rise briefly out-paced glacio-isostatic rebound (Shennan et al., 2000; Firth and Stewart, 2000). In the NW Highlands, raised glacio-marine sediments and beach deposits indicate sea levels were up to ~30 m above present when the retreating BIIS glaciers reached the modern coastline (e.g. Hansom, 1991; Haggart, 1986; Shennan et al., 2000; Firth and Stewart, 2000). Base level falls of up to 15 m during the Holocene are marked by raised beaches and erosional notches in many coastal areas (e.g. Sissons, 1983; Firth, 1989; Smith et al., 1992).

The effects of the Holocene base level fall on bedrock rivers in western and eastern Scotland have been assessed by Bishop et al. (2005), Jansen et al. (2011) and Castillo (2011). These studies indicate that knickpoints (KPs) have formed at the coastal outlet of many streams. Fluvial incision has driven upstream retreat of the KP, resulting in the regrading of the channel profile below the KP to the lower base level (cf. Castillo, 2011). These 'glacio-isostatic' KPs have retreated a relatively small distance upstream (up to ~10% of the total stream length), possibly due to a slowing of erosion due to declining paraglacial sediment flux (Jansen et al., 2011). Upstream from the glacio-isostatic KP, channels remain 'unaware' of the base level fall and are thus likely to respond directly to instabilities introduced by the inheritance of the glacially-eroded landscape form.

The observations of Bishop et al. (2005) and Jansen et al. (2011) suggest that postglacial base level fall might have caused KP incision in NW Highland streams. In contrast to western and eastern Scotland, however, many of the coastal outlets of NW Highland rivers are characterised by thick sediment fills and low-angle tidal plains, especially in the Firths of the east coast, but also in the inner fjords of the west coast (e.g. Firth, 1989; Smith et al.,

1992). It is likely that the presence of these sediments and the morphology of the near-shore environment may restrict the formation of glacio-isostatic bedrock KPs in many NW Highland channels (cf. Schumm, 1993; Snyder et al., 2002).

2.2.3.3   Postglacial climate and vegetation

Following the close of the YD, temperate conditions similar to the present day were rapidly established in the Scottish Highlands (Brooks and Birks, 2000; Ballantyne, 2010). The relatively wet and warm climate of the early Holocene encouraged the early development of peat and growth of birch and Scots Pine forests; Anderson (1998) records ^{14}C ages of ~8 – 10 ka (cal BP) from the bases of three peat cores from the NW Highlands. The temperate climate has persisted throughout the Holocene, with the exception of short-lived cold phases at ~8.2 ka and during the Little Ice Age c. 1500 – 1700 AD that may have seen increased snow cover over the study area (e.g., Whittington, 1985; Klitgaard-Kristensen et al., 1998). Precipitation proxy records for the Scottish Highlands cover only the mid to late Holocene and few peat core records exist for the early Holocene period (Anderson, 1998; Macklin, 2005). These records indicate that there have been multiple shifts between wetter and drier peat conditions since ~5 ka in peat bogs studied in the NW Highlands (Anderson, 1998), and phases of increased flood frequency since ~ 6 ka (Macklin et al., 2005). Pollen records from peat cores indicate that increasing wetness of peat between 5 and 4 ka was associated with a decline in Scots Pine forests and an increase in blanket peat in many areas. This advance of peat was followed by a reversal to drier conditions and a redevelopment of some of the pine forests, which terminated in another shift to wetter conditions between 4 and 3 ka. This latter decline in pine and the growth of peat may have also been influenced, in some areas, by human activity such as by the effects of burning for land clearance (Anderson, 1998).

2.2.3.4   Anthropogenic impacts on NW Highland rivers

The NW Highlands are sparsely populated, with fewer than 8 people per km^2 (2001 Population Report, Scotland), consequently the upland rivers are among the least affected by human activity in the UK (Gilvear et al., 2002). The main anthropogenic factors affecting NW Highland rivers are land use changes and the extraction of water for hydro-electric power generation (Gilvear et al., 2002).

Large hydro-electric power schemes have been developed on most of the larger east-draining rivers of the study area. Flow regulation has caused significant changes in the

hydrological regimes, with reduction in peak flow and elevation of base flow relative to un-regulated channels (e.g. Gilvear et al., 2002). Flow regulation and reduction in sediment flux downstream from dams will have dramatically influenced the morphology of affected channels, with potential changes in channel type and geometry throughout the lower parts of the catchments (Gilvear et al., 2002). In contrast to the east-draining streams, few of the smaller west-draining catchments of the NW Highlands are affected by hydro-electric power schemes. Due to the substantial influence of flow regulation on channel morphology, only channels with limited to no flow regulation were selected for field survey.

The most significant recent land use change to affect the NW Highlands has been the spread of pine plantations and the associated drainage and reduction in the extent of peat mire and grass/heather moorland. A lack of published studies means that the effects of afforestation on the form of Highland channels are poorly understood, but changes in bank vegetation, run-off and sediment supply have been observed to influence the morphology of alluvial channels (Gilvear et al., 2002). The short timescale of these changes means that the effects of afforestation are unlikely to influence the geometry of bedrock channels but the degree to which the distribution of bedrock channels may be affected is not known.

2.3   Research methods

The distribution and geometry of bedrock channels in the NW Highlands were assessed through a combination of field survey and topographic analysis. Fluvial incision rates were quantified using cosmogenic ^{10}Be surface exposure dating of strath terraces following the method of Jansen et al. (2011). The locations of the strath terrace sites and the method of cosmogenic nuclide analysis are outlined in chapter 5.

Digital topographic analysis was conducted data using the NEXTMap 5m horizontal resolution digital terrain model (DTM) (InterMap Technologies, 2004, 2007) and the Geographic Information System (GIS) software ArcGIS. This analysis was conducted to derive stream lines, channel longitudinal profiles ("long profiles"), drainage area and channel slope for the nine largest catchments spanning the N-S trending drainage divide in the NW Highlands (Figure 2-4). The data are used to assess controls on the long-profile form of NW Highland channels (section 3.3.1), and form the basis for calculations of discharge and stream power for three main stem channels assessed during field survey. The data sources and methods used in the topographic analysis are outlined in section 2.3.3.

The distribution of reach types and the measurements of channel geometry and entrenchment were obtained during field surveys of three NW Highland streams (Figure 2-4). The characteristics of these three streams are outlined in section 2.3.1. The approach to the field survey and key aspects of the survey methodology are discussed in section 2.3.2.

2.3.1   Study catchments: selection and characteristics

The three surveyed streams are the east-draining River Carron and the west-draining Elchaig and Canaird (Figure 2-4, Table 2-2). These streams were selected because they represent different glacial landscape terrains (Figure 2-3). The River Canaird is dominated by landforms of areal scouring, whereas the River Elchaig is characterised by alpine-type glacial landforms (Figure 2-3). The larger, east-draining River Carron catchment crosses two of the glacial terrains, with the upper half located in the alpine-type terrain of the Beinn Dearg massif, and the lower half characterised by limited glacial modification (Figure 2-3). The geographic and geological characteristics of these catchments are shown in Figure 2-5, Figure 2-6 and Figure 2-7. All the study rivers are sourced in small lakes in the catchment headwaters. The rivers Canaird and Elchaig have substantial lakes filling overdeepened basins along the main valleys. The River Carron has no lake in the main valley, but a wide, flat alluvial plain consisting of fine sand overlain by peat at Deanich (Figure 2-5) is interpreted to be an in-filled lake. The Scottish term 'loch' is used in the names of specific fjords and lakes referred to in the following chapters.
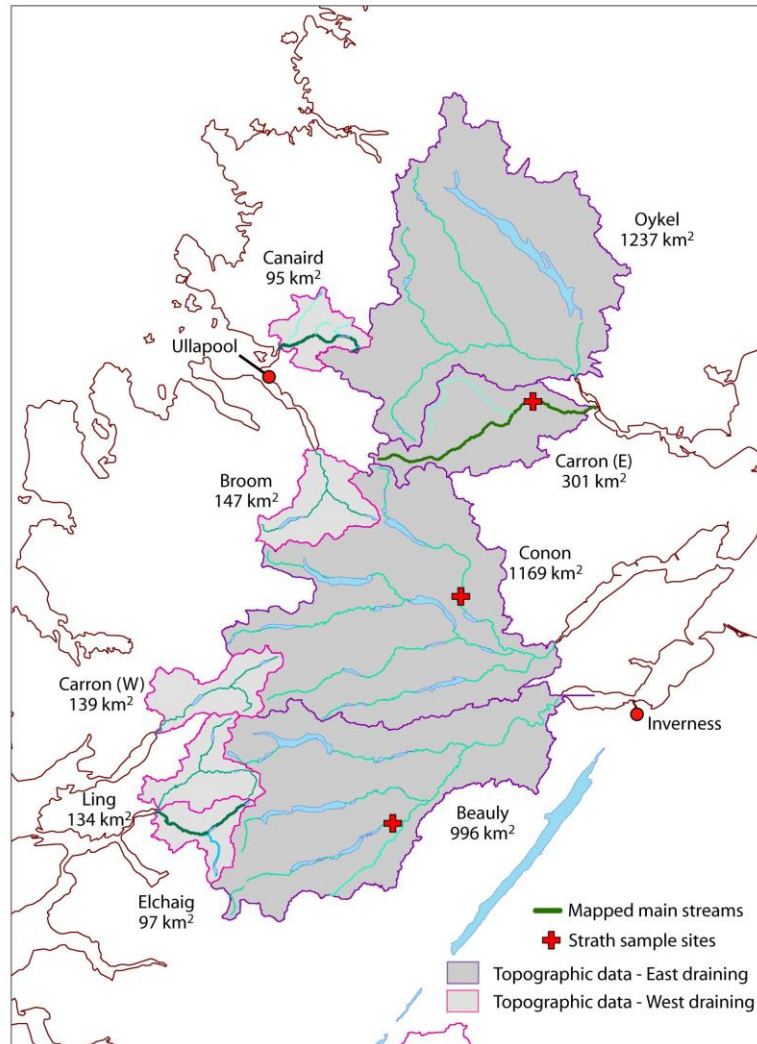
Figure 2-4. The main east-draining (dark grey) and west-draining (light grey) catchments of the NW Highlands, showing stream lines (derived from the NEXTMap 5m DTM using ArcGIS), major lakes and reservoirs. The rivers Carron, Elchaig and Canaird, assessed during field survey, are highlighted (thick green line). Three strath sample sites also shown, two further strath sites are outside the NW Highlands area (shown in figure 5-2).

Parameter	Carron	Elchaig	Canaird
Drainage area (km^2)	301	97	95
Stream Length (km)	44.5	19.5	17.1
Max. channel elevation (m)	740	423	196
Max. catchment relief (m)	928	1075	448 *(769)*
% Forest (plantation)	12.7	0.8	0 *(4.8)*

Table 2-2. Data for surveyed rivers. Drainage area, stream length and maximum channel elevation derived using digital topographic analysis (section 2.3.3). Maximum channel elevation is taken as the stream elevation close to the channel head where drainage area equals 1 km^2. Maximum catchment relief and percentage forest cover for the River Canaird are based on the trunk stream catchment area only. Values given in brackets include the sub-catchment of the River Runie (not mapped).
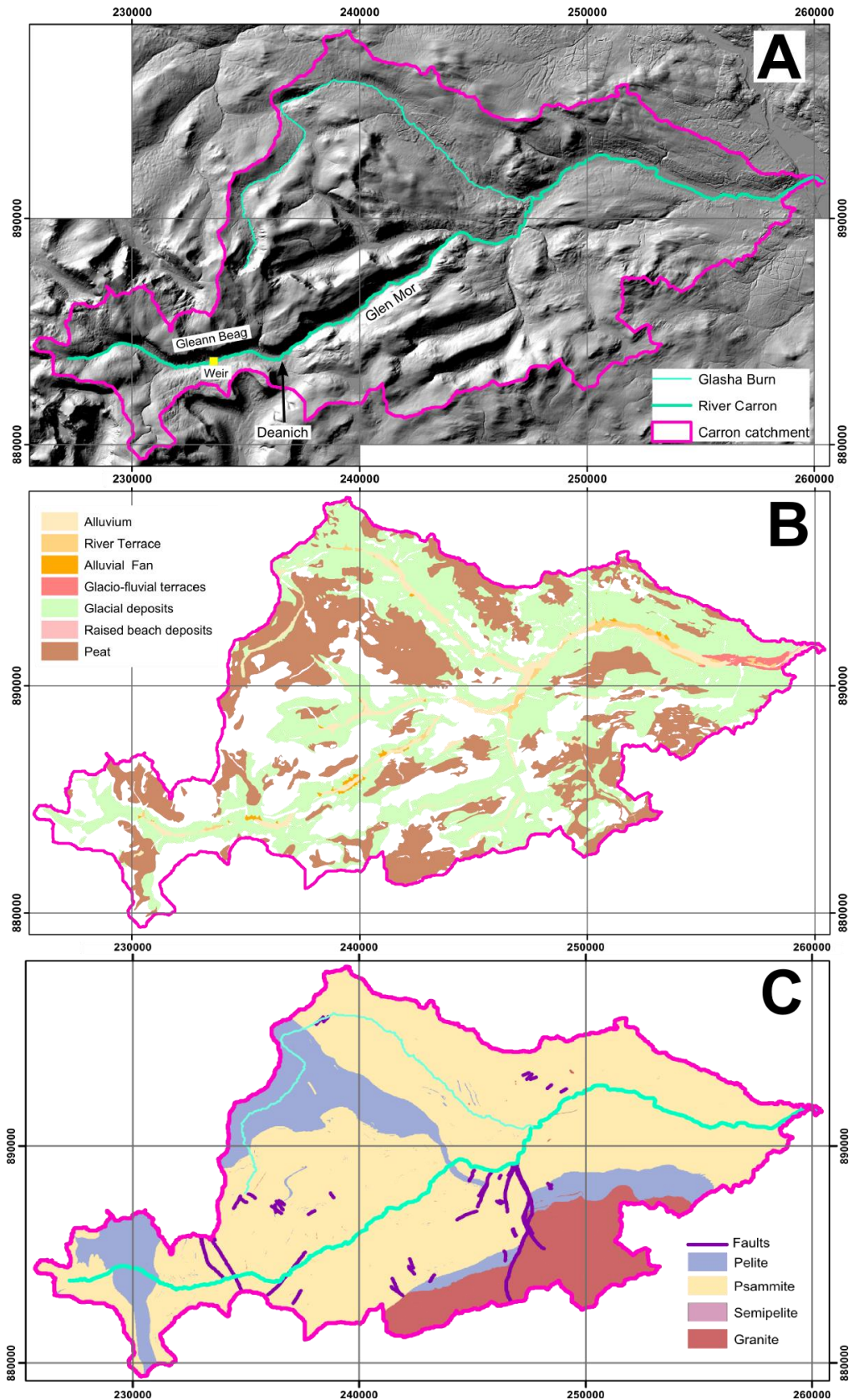
Figure 2-5. Carron catchment maps. Stream lines and catchment boundary derived from NEXTMap 5m horizontal resolution Digital Terrain Model (DTM) (Intermap Technologies, 2007) using ArcGIS Hydrology processing tools (section 2.3.1) A) Hillshade NEXTMap image showing topography. Note contrast between deep trough valleys of upper catchment and less incised lower catchment. B) Superficial deposits simplified from British Geological Survey (BGS) 1:50,000 scale digital superficial deposits maps. Peat is only represented on BGS maps where it is thicker than 1m. Peat <1m thick is extensive in the upper half of the catchment. C) Bedrock geology simplified from BGS 1:50,000 scale digital bedrock geology maps.
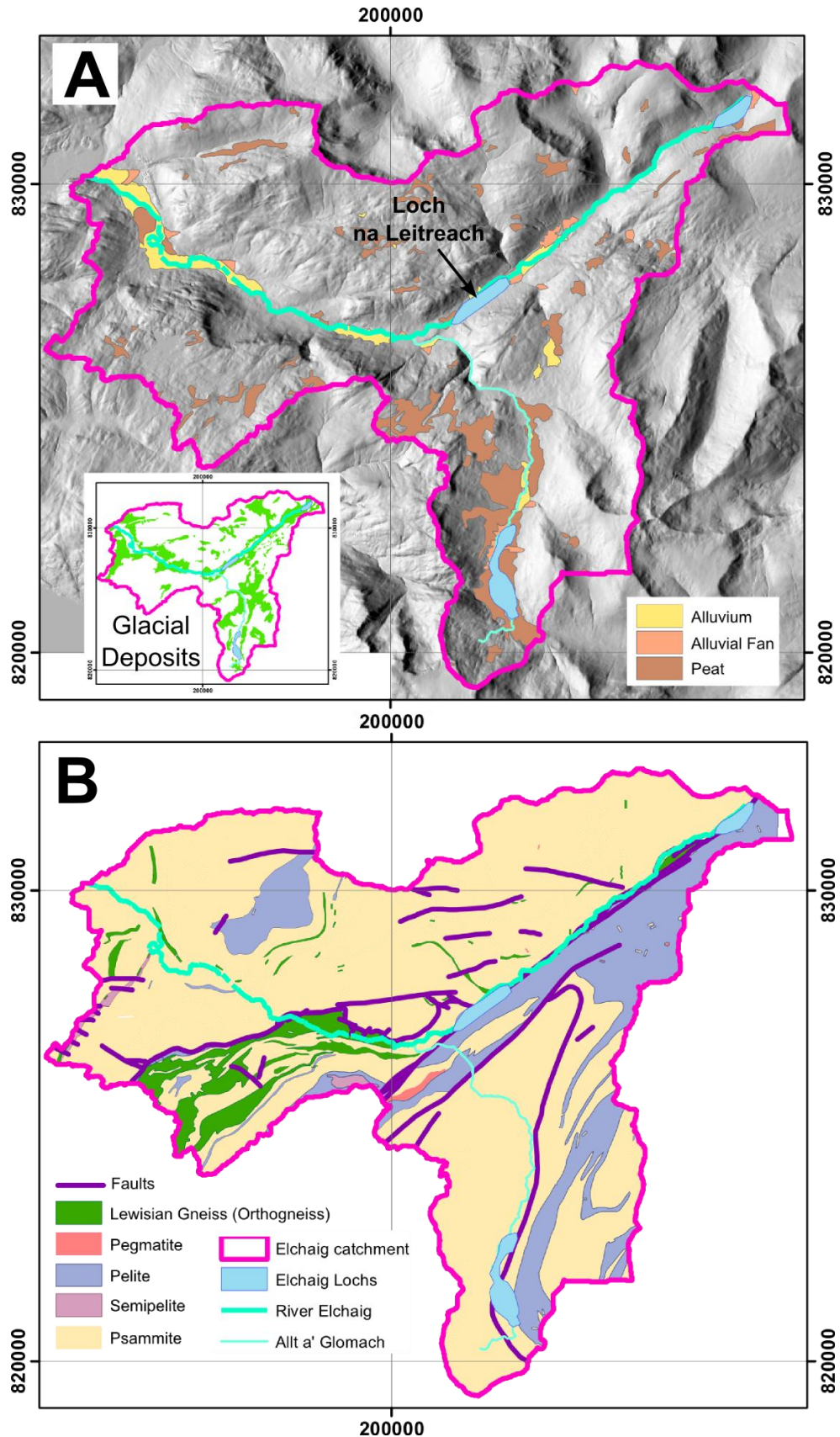
Figure 2-6. Elchaig catchment maps. A) Hillshade NEXTMap DTM image showing topography overlain by superficial deposits simplified from BGS 1:50,000 scale digital superficial deposits maps. Glacial sediment deposits not shown on main map for clarity (see inset map). As for the preceding figure, peat cover is under-represented. B) Bedrock geology simplified from BGS 1:50,000 scale digital bedrock geology maps.
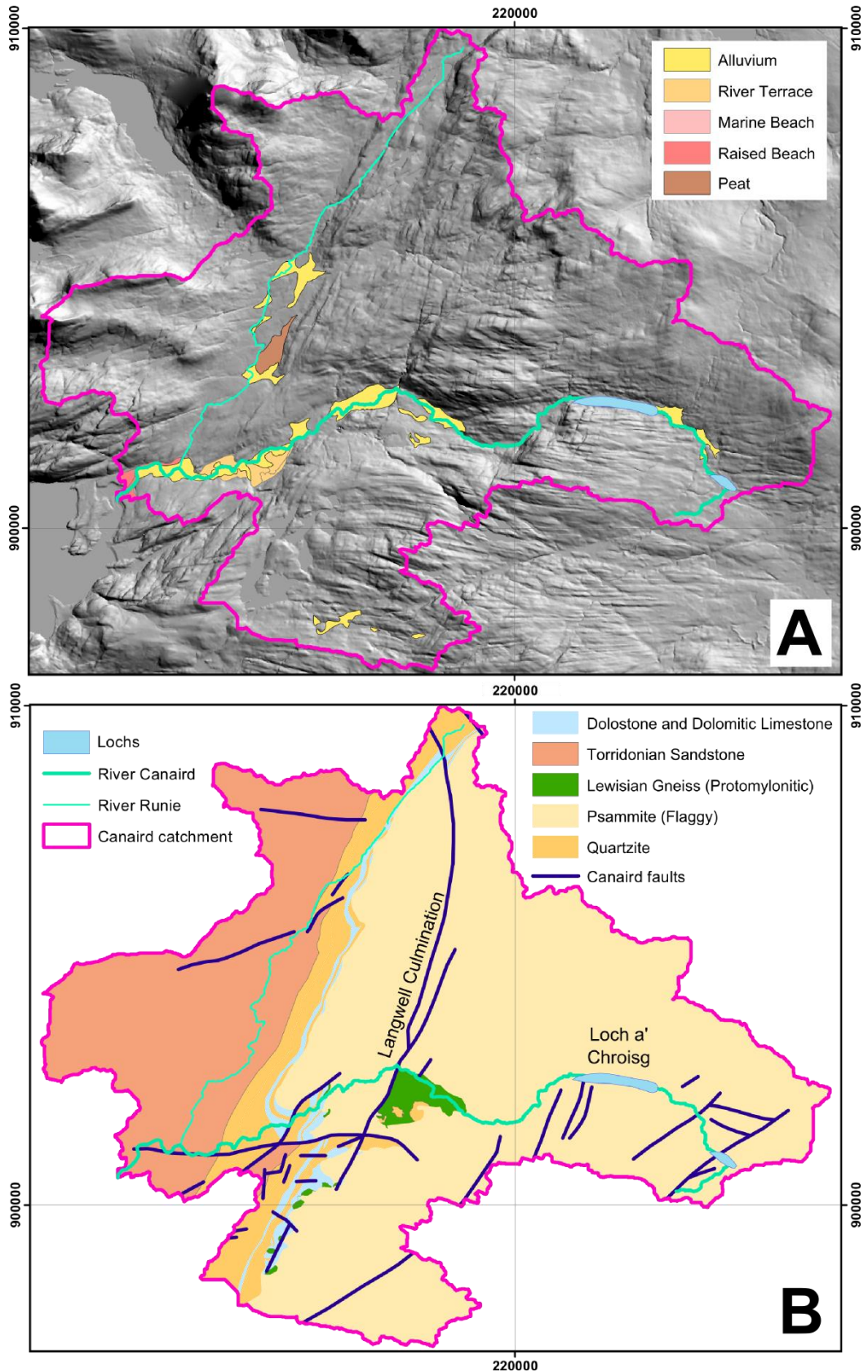
Figure 2-7. Canaird catchment maps. A) Hillshaded NEXTMap showing topography with trunk and major tributary streams and lakes. Note streamlined, 'areally-scoured' topography throughout catchment. Distribution of superficial deposits summarised from 1:50,000 scale digital British Geological Survey (BGS) map SC101-East (Strathkinaird). Glacial deposits are not included in BGS mapping. As for preceding figures, peat cover is under-represented. B) Bedrock geology summarised from BGS 1:50,000 scale digital maps.

2.3.1.1   Deglaciation history of the study catchments

The Canaird catchment was deglaciated during the retreat of the BIIS in the Late Glacial Interstadial (14.5 – 12.9 ka). Cosmogenic [10]Be ages from moraines located near the present coastline in the outer parts of Loch Broom indicate that a substantial valley glacier occupied the fjord between 13.5 and 14 ka (Bradwell et al., 2008a; Ballantyne et al., 2010) (Figure 2-8). The Loch Broom Glacier retreated during the latter part of the Late Glacial Interstadial, resulting in the deglaciation of the Canaird catchment between ~13.5 and 13 ka (cf. Bradwell et al., 2008a). The Canaird catchment, at the northern edge of the NW Highland mountain range, was outside the limits of the YD glacial readvance and would have experienced a periglacial climate between 12.9 and 11.7 ka before rapid warming at the onset of the Holocene (Bennet and Boulton, 1993, Brooks and Birks, 2000; Golledge, 2010).

Reconstruction of the deglaciation history for the Elchaig catchment is hampered by a lack of evidence for retreat of BIIS glaciers in outer Loch Broom, and contrasting interpretations of the extent of YD ice. It is assumed here that the pattern of retreat of BIIS glaciers in this area was similar to that described for Loch Broom, possibly occurring slightly later as the Elchaig area is closer to centre of the ice sheet (cf. Figure 2-3). Thus the Elchaig catchment was glaciated (by a tributary of the main Loch Alsh glacier) until at least 13.5 ka. Evidence for the extent of YD glaciation of the catchment is limited because, in contrast to other valleys in the area, there are no significant moraine ridges or other ice-margin indicators in the lower catchment. In a reconstruction of YD ice margins throughout Scotland, based on regional assessments of the patterns of moraine ridges, Bennet and Boulton (1993) suggest a maximum YD ice margin position in the middle of Glen Elchaig, approximately halfway down the catchment (Figure 2-8). May et al. (1993), on the other hand, suggest that the YD ice margin may have been located much further west, near the outlet of Loch Long, citing a conspicuous absence of Late Glacial raised marine terraces and other shoreline features within the fjord. Numerical models of the YD ice cap also suggest that the Elchaig catchment may have been completely glaciated during the YD, but the model predictions have not been validated by field assessments in this area (Golledge et al., 2008). For the purposes of this study, the partial glaciation of the catchment proposed by Bennett and Boulton (1993) is assumed, and the lower half of the catchment is thus interpreted to have been deglaciated between 13.5 and ~12.9 ka with the upper half of the catchment becoming ice free at the close of the YD (c. 11.7 ka). Where

relevant, the implications of the alternative 'full glaciation' scenario for this catchment are discussed in the following chapters.

In the Carron valley, the Late Devensian Carron glacier formed a tributary of the Dornoch glacier, occupying the Dornoch Firth. Deglaciation, probably during the latter part of the Dimlington Stadial (c. 17 – 15 ka), drove the retreat of the Dornoch glacier up the Kyle of Sutherland isolating the tributary glaciers. Near Ardgay, at the mouth of the Carron valley, substantial glacio-fluvial deposits that grade into a raised beach indicate a former position of the Carron glacier (Figure 2-8) (Hansom, 1991). This ice margin position is not dated, but a timing between ~14.5 and 15.5 ka is assumed on the basis of regional reconstructions (e.g. Phillips et al., 2008; Ballantyne, 2010). Deglaciation was thought to have proceeded throughout the Late Glacial Interstadial (14.5 – 12.9 ka), with the Carron glacier probably retreating into the corries of Beinn Dearg, in the catchment headwaters, by ~13 ka (cf. Finlayson and Bradwell, 2007) Recent reconstructions of the extent of a YD ice cap located over the mountain of the Beinn Dearg massif by Finlayson and Bradwell (2007) and Finlayson et al. (2011) indicate a readvance of the Carron glacier to a maximum position approximately halfway down the catchment. Cosmogenic ^{10}Be ages from a moraine associated with the equivalent ice margin position in the adjacent valley of Glen Alladale yield an age of ~12.6 ka. Thus, the lower half of the Carron catchment is interpreted to have been deglaciated between ~15 and 13 ka, with the upper half deglaciated at the close of the YD (c. 11.7 ka).

2.3.1.2   Anthropogenic influences

The three catchments selected for field survey show limited evidence for recent land use change, especially in the upland areas. Plantation forests cover less than 13% of the catchment area (Table 2-2) and are not located in the vicinity of the main stream. The catchments are sparsely populated with isolated farmsteads restricted to the lower reaches. In these areas the floodplains and lower valley slopes are grazed by sheep. Stabilisation of the channel banks, and straightening of the channel line were observed in the lower alluvial reaches of the rivers Canaird and Elchaig and these sections were not surveyed in detail. Parts of the lower the River Carron were also found to be affected by bank stabilisation measures.

Figure 2-8. (Following page) Late Devensian glacier extents in the regions of the Canaird (A), Elchaig (B) and Carron (C) catchments. Topographic elevation indiated by shaded STRM data (30m horizontal resolution) dark green shading is high elevation, light green shading is low elevation. Grid is British National Grid in metres. Named features are mentioned in the text.
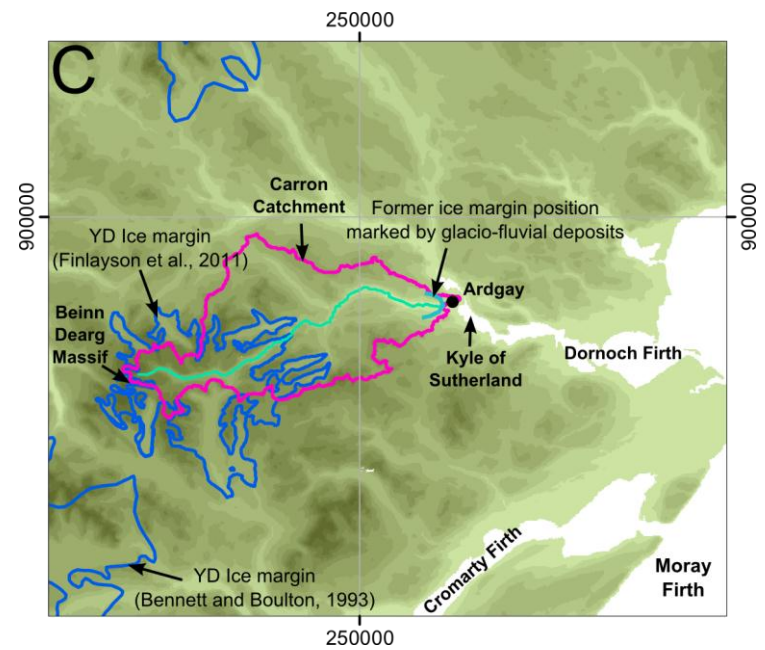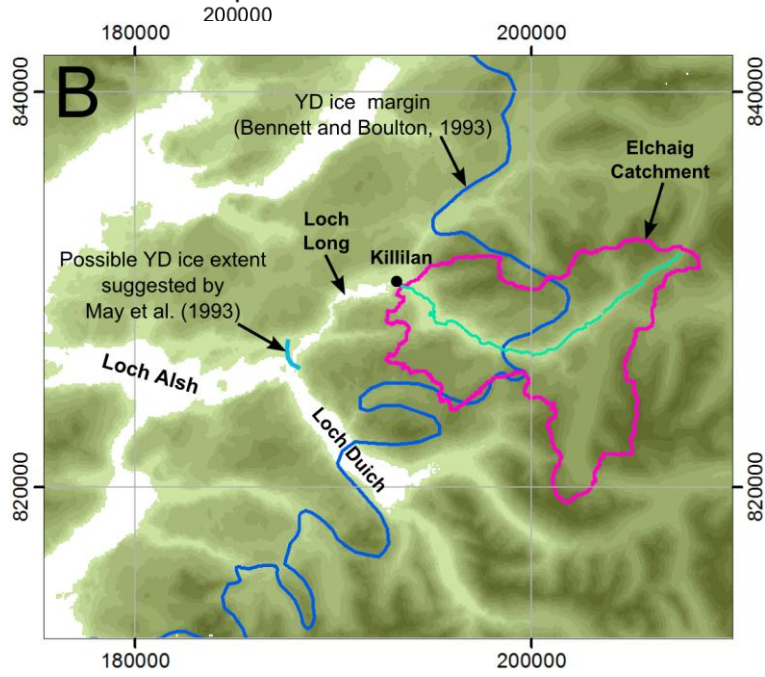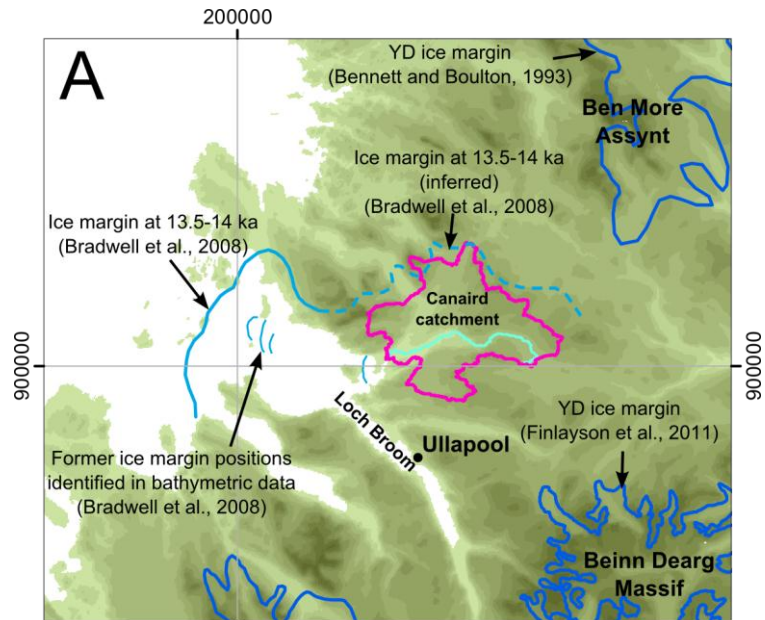
The east-draining River Carron is the only one of the study catchments to be affected by flow regulation for hydro-electric power generation. Part of the flow from the upper catchment is diverted at medium to high flows by a weir located in Gleann Beag (Figure 2-5 A). This may slightly reduce the peak discharges downstream, but as the partial flow diversion affects only the upper 10% of the catchment area the impact on the channel morphology is likely to be minimal. Limited aggradation upstream of the weir suggests also that sediment supply from the upper catchment is low and the presence of the weir is thus likely to cause only a minor reduction in sediment flux downstream.

2.3.2   Field data and methods

The rivers Carron, Elchaig and Canaird were surveyed during low-water conditions in June and October 2010 and April 2011. The distribution of reach types was mapped along the full length of the main stem channels (a total of 71 km). Measurements of channel cross-section geometry and depths of entrenchment into sediment and/or bedrock were made for all mapped reaches and channel bed forms, sediment cover conditions, sediment sources and lithological features were recorded. Reaches were mapped directly onto digital Ordnance Survey topographic maps at 1:10,000 scale (supplied through EDiNA) using ArcGIS software on an iExplore tablet PC. The methods for measurement of channel cross-section geometry and channel entrenchment are discussed in detail in chapters 4 and 6 respectively. The classification of reach types and lithological units are outlined below.

2.3.2.1   Reach designation

Channel reaches are defined as lengths of channel ranging from c. 50 – 2000m in length (>5 channel widths) that are characterised by a consistent substrate type and morphology (cf. Montgomery and Buffington, 1997; Wohl and Merritt, 2001). Reach 'types' were distinguished in the field according to the main substrate making up the bed and banks of the channel (cf. Montgomery and Buffington, 1997). Three main categories were identified: alluvial (AL); mixed bedrock-alluvial (BR-AL); and bedrock (BR) (Table 2-3, Figure 2-9). Bedrock channels are defined as channels in which over 70% of the channel boundary is exposed rock. This threshold is higher than the 50% bedrock exposure threshold suggested by Tinkler and Wohl (1998). The higher threshold was chosen because NW Highland channels are strongly detachment-limited with abundant bedrock in the channel boundary. A higher exposure threshold thus allows a more sensitive discrimination of the distribution of reach types and may improve assessments of the influence of substrate on channel form and processes. Sub-types of the alluvial and bedrock-alluvial

channel types were also identified to distinguish reaches influenced by peat in the channel banks and small channels dominated by locally-sourced coarse-grained bed material (Table 2-3). The reach type designation forms the basis for the assessment of controls on bedrock channel distribution (chapter 3) and cross-section geometry (chapter 4). Reaches were also characterised according to the main channel bed forms, e.g. pool-riffle/step-pool/plane bed, using the classification schemes of Montgomery and Buffington (1997) for mountain alluvial channels and Wohl (1998) for bedrock channels. This classification does not form a major component of the analyses here, but does influence the characterisation of reach-scale channel geometry (section 4.2.1.2), and facilitates qualitative assessments of the influence of channel roughness on channel morphology and fluvial erosion processes.

Substrate Type	Code	Description	Subtype	Description
Alluvial	AL	Bed and banks 100% in unconsolidated sediment. Sediment generally coarse sand to boulder, occasionally medium to fine sand.	AL-BR	Dominantly alluvial reach with 1-15% the channel boundary (classed as alluvial unless stated)
			AL-P (Peat)	Channel with alluvial bed and >25% peat in the banks ("Peat" used when AL-P and BR-AL-P reaches are grouped)
			AL-B (Boulder)	Small channel dominated by medium to large boulders that are roughly half the channel width or greater ("Boulder" used when AL-B and BR-AL-B reaches are grouped)
Bedrock-Alluvial	BR-AL	15-70% bedrock in the bed and banks. Varying morphology including reaches with bedrock bed and those with short bedrock-constrained sections alternating with alluvial sections	BR-AL-P (Peat)	Mixed bedrock-alluvial channel with >25% peat in the banks ("Peat" used when AL-P and BR-AL-P reaches are grouped)
			BR-AL-B (Boulder)	Small bedrock alluvial channel dominated by medium to large boulders that are roughly half the channel width or greater ("Boulder" used when AL-B and BR-AL-B reaches are grouped)
Bedrock	BR	Bed and banks 70-100% bedrock	Subtypes classified according to lithology	

Table 2-3.   Reach classification according to substrate type. Codes for the main substrate types and subtypes are used in the following chapters. Bedrock channel subtypes are discussed in section 2.3.2.3.

This classification of bedrock channels implicitly assumes that the distribution of bedrock channels observed during the field surveys reflects the long-term distribution (over $10^3 - 10^4$ years) and does not reflect the passage of 'pulses' in sediment supply resulting from recent flood events (cf. Benda and Dunne, 1997). This assumption is judged to be valid for the study catchments as vegetation and peat cover, established within ~1000 years of deglaciation (e.g. Anderson, 1998), has stabilised hillslopes and limited the effect of precipitation variations on sediment supply rates (e.g. Edwards and Wittington, 2001).

Long-term changes in channel type, potentially due to declining paraglacial sediment flux, are discussed in more detail in chapter 3.
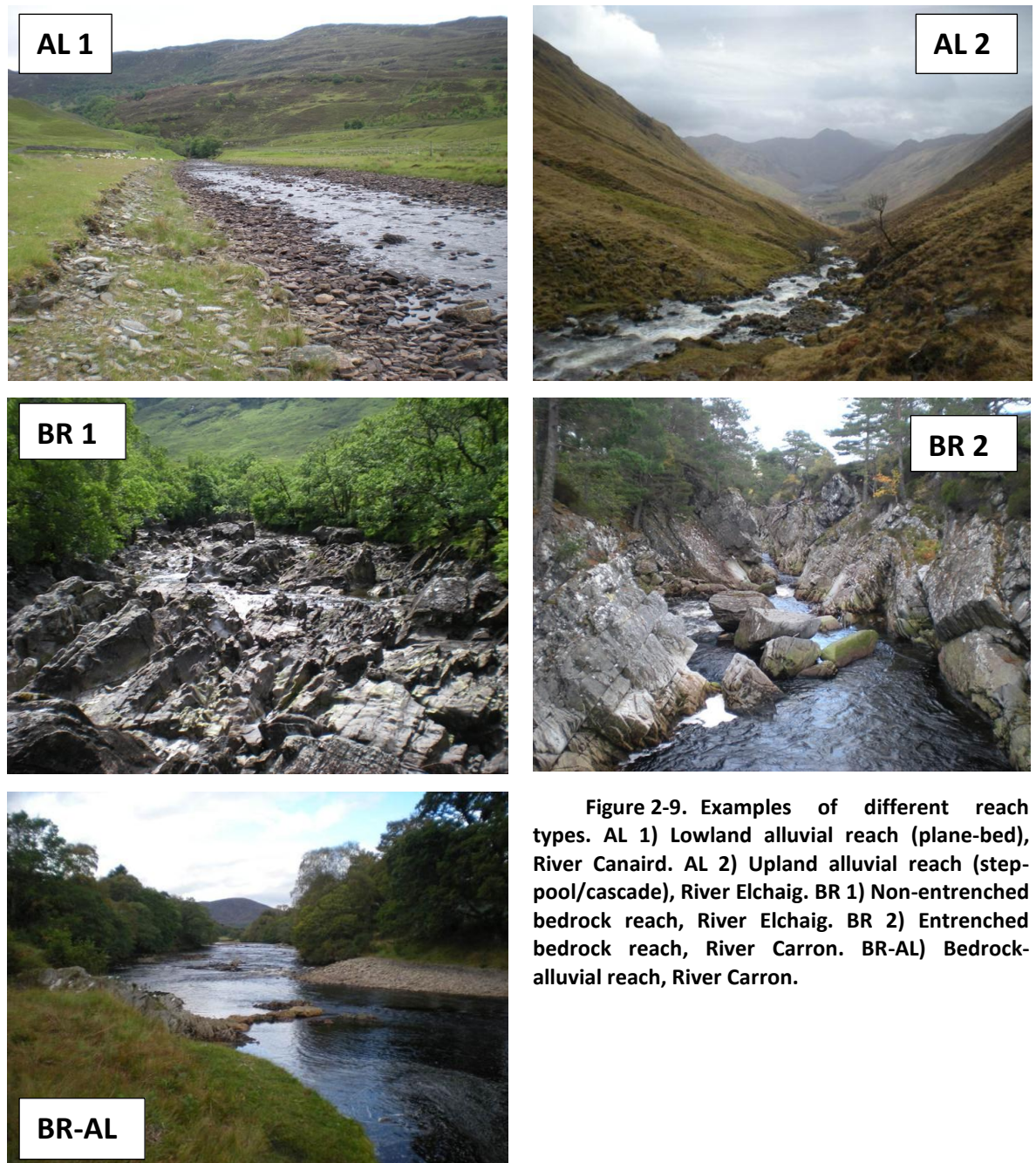
Figure 2-9. Examples of different reach types. AL 1) Lowland alluvial reach (plane-bed), River Canaird. AL 2) Upland alluvial reach (step-pool/cascade), River Elchaig. BR 1) Non-entrenched bedrock reach, River Elchaig. BR 2) Entrenched bedrock reach, River Carron. BR-AL) Bedrock-alluvial reach, River Carron.

2.3.2.2   Sediment cover and sources

A visual estimate of the degree of sediment cover of the bed (%) was used to classify BR and BR-AL reaches. The main characteristics of the sediment, including the general range of grain-sizes and angularity were also described for each AL, BR-AL and BR reach. In the lower parts of the catchments, channel sediment was found to be fine gravel to cobble-grade, with upland channels dominated by coarser sediments (up to boulder-grade). Systematic grain-size analysis was not conducted during the field survey due to the

extended time required to sample the coarse to very coarse sediment characteristic of the study channels.

The location, type, and characteristics of the sediment inputs to the channel, both active and inactive, were recorded. These sources include relict alluvial fans, debris cones and gullies, tributary streams, areas of active alluvial bank erosion, steep gorge or valley walls prone to rockfalls and landslip deposits that reach the active channel.

2.3.2.3   Bedrock   geology: classification   and   lithological resistance

The distributions of the main lithologies and geological structures of the study catchments are shown in Figure 2-5, Figure 2-6 and Figure 2-7. Each BR reach was sub-classified according to the main lithology of the channel bed. Rather than use the classic stratigraphic designations for the rocks of the study area (e.g. Johnstone, 1989; Strachan et al., 2002), the main lithologies found in the study channels were categorised on the basis of their general composition and structure (Table 2-4). This approach was taken in order to account for the key lithological properties thought to influence fluvial incision processes, namely, the intact rock strength and the density of joints and bedding planes (e.g. Selby, 1982; Sklar and Dietrich, 2001; Whipple et al., 2000; Hartshorn et al., 2002). Rock strength and joint density were quantified at type localities for each of the main rock types (discussed below). The type of bedforms and the degree of smoothing and fluting of bedrock surfaces, as indicators of the relative prevalence of plucking and abrasion (Whipple et al, 2000), were noted for each bedrock reach, along with the location and type of geological features such as lithological contacts, faults and igneous intrusions and their effects on the channel morphology.

Lithological classification

The main rock types in the study rivers are metasediments, detailed descriptions of which are given in Table 2-4. Psammite is the most common lithology and is found in all three catchments. Two types of psammite were distinguished on the basis of major differences in the degree of jointing: standard 'psammite' is found in the rivers Carron and Elchaig, whereas strongly bedded and jointed 'flaggy psammite' is found in the River Canaird. Pelite is also found along the rivers Carron and Elchaig, but is not present in the River Canaird. More intensely metamorphosed Lewisian gneiss is found in the Rivers Canaird and Elchaig. Two types of gneiss, 'protomylonitic gneiss' and 'orthogneiss', distinguished

by their internal structure (or lack thereof), occur in the River Canaird and River Elchaig respectively. In addition to these main lithological types, reaches strongly affected by faulting were identified. These reaches are characterised by local variations in lithology (on 10 cm – 10 m scales), and strong variations in structure, with brecciated zones, lenses of fault gouge and very sparsely jointed igneous intrusions. Fault-affected reaches are mainly located in the River Elchaig above Loch na Leitreach (Figure 2-6 B), with some also located in the upper River Carron.

Measuring lithological resistance

Although it is widely recognised that both the 'intact' rock strength and the density and orientation of joints influence fluvial erosion processes and rates, there is no current consensus on the best method of quantifying lithological resistance to fluvial erosion (e.g. Whipple et al., 2000; Snyder et al., 2003; Whipple, 2004; Whittaker et al., 2008). Wohl and David (2008) and Whittaker et al. (2008) quantify rock strength on the basis of the Selby rock mass strength index (Selby, 1982), which was developed for use in determining hillslope stability and includes criteria for assessing joint spacing, orientation and continuity. Despite its recognised limitations (Wohl and David, 2008), the Selby scheme was used here to derive a semi-quantitative measure of lithological resistance to fluvial erosion at characteristic 'type' locations for the main lithologies in the mapped channels. The intact rock strength was measured using an 'N' type Schmidt hammer, following the method outlined by Day (1980) and Selby (1982). The Schmidt hammer 'R' value was taken as the average of 30 measurements taken randomly in a $1m^2$ area of bedrock at least 6 cm from any joints. All surfaces measured were sub-horizontal (max. surface slope ~15 degrees). Corrections for the orientation of the Schmidt hammer were made using the theoretical normalisation curves of Basu and Aydin (2004). The average spacing of joints was derived from a survey of 30 – 50 joints conducted along 15 to 25 m transects roughly parallel to and perpendicular to the flow direction between the high flow and low flow levels. The resulting scores are shown in Table 2-5. The high variability in both rock type and structure in fault-affected reaches means that 'type' locations could not be identified. Selby scores for fault-affected reaches were estimated by assuming a mid-range Schmidt hammer reading (46) and an estimated fracture spacing of 2 – 15 cm with a vertical joint orientation and good continuity, giving a Selby rock mass index score of 59.
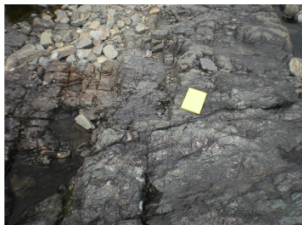
	Sub type/Picture	Lithological description	Structural description
Psammite	Psammite 	Resistant metamorphosed sandstone, commonly interbedded with quartzite and/ or semipelite on cm-m scales. Medium grained, dominantly quartz with feldspar and variable but generally minor amounts of mica.	Beds 5cm - 2m thick. Moderately to sparsely jointed yielding sub-rectangular blocks 20cm - 2m in diameter. Psammites in the River Elchaig are thinly bedded and complexly folded in places. In the River Carron, well bedded psammites
	Flaggy psammite 		Only found in the River Canaird; thin (2 - 15cm), horizontally bedded with strong vertical joints yielding platy blocks 5 - 50cm in diameter and 2 - 15cm thick
Pelite		Metamorphosed mudstone, fine grained with a high proportion of clay minerals, mica and fledspar and limited amounts of fine grained quartz. Commonly interbedded with semipelite.	Beds 1 - 20cm thick, may be laminated. Commonly folded especially in the River Elchaig and weakly and sparsely jointed
Gneiss	Orthogneiss 	Only found in the River Elchaig; strongly metamorphosed, originally igneous rock. Strongly banded with alternating quartz and mica/feldspar rich bands.	Commonly complexly folded and poorly jointed.
	Protomylonitic gneiss 	Only found in the River Canaird; very strongly metamorphosed, originally sedimentary rock. Consisting of green 'patches' dominated by chlorite and irregular pink areas dominated by quartz and feldspar.	Despite a 'rubbly' texture due to an abundance of minor, very weak discontinuities, there are few significant joints and the rock is massive with no regular internal structures
Fault	Designates channel reaches alligned along major faults. Variable lithologies and fault-related structures visible in channel bed and banks.	Depends on adjacent rock types, but can also contain intrusive igneous dykes (including lamprophyre, basalt, pegmatite), fault gouge and calcite veins.	Variable structure: where formed in resistant rocks, subvertical fault planes, fault-related joints or dykes may form channel margins. Some areas strongly brecciated.

Table 2-4.   Lithological units of the study streams.

Parameter	Protomylonitic gneiss		Orthogneiss		Flaggy psammite		Psammite		Pelite	
	'Score'	Rating	'Score'	Rating	'Score'	Rating	'Score'	Rating	'Score'	Rating
Intact rock strength (corrected R value)	53	18	53	18	50	17	52	18	40	12
Weathering	slight	10	none	10	slight	10	none	10	none	10
Spacing of joints	0.7m*	25	0.2-0.3m	20	0.02-0.40m	12	0.7m	25	0.98m	27
Joint orientations	random	18	upstream	18	vertical	9	cross stream	12	horizontal	16
Widths of joints	0.5-1mm	6	1-5mm	5	1-8mm	4	1-5mm	5	1-5mm	5
Continuity of joints	none continuous	7	few continuous	6	continuous thin infill	4	few continuous	6	few continuous	6
Outflow of ground water	none	6	none	6	none	6	None	6	None	6
Total rating	Strong	**90**	Strong	**83**	Moderate	**62**	Strong	**82**	Strong	**82**

Table 2-5. Selby rock strength index data for main lithological types in the surveyed streams. Fault affected reaches were not assessed due to high variability in lithology and structure (see text).
* The protomylonitic gneiss is criss-crossed by fine discontinuities in random orientations spaced at 2 – 5 cm (Table 2-4), but these features do not form coherent fracture planes and are therefore not considered as joints.

2.3.3   Topographic and calculated data

Channel long profiles, slope and drainage area were derived from digital topographic data for eighteen streams from the nine largest NW Highland catchments, including the three surveyed rivers (Figure 2-4). The main data source was the 5 m grid NEXTMap digital terrain model (DTM) (Intermap Technologies, 2004, 2007) from which the stream parameters were calculated using ArcGIS Hydrology processing tools (cf. Wobus, 2006; Addy, 2010).

The primary data derived were stream line (planform), elevation profile (i.e. the long profile), stream length and drainage area. Channel slope was then calculated from the long-profile data (section 2.3.3.2) and drainage area and channel slope were used in the calculation of discharge and stream power (sections 2.3.3.3 and 0). This method for the calculation of channel slope was used in preference to measurement during field survey due to the logistical difficulty of surveying channel profiles either through traditional survey methods or a static-base station differential GPS. The time needed to measure channel slope accurately in the field would have considerably reduced the scope of the fieldwork.

2.3.3.1   Topographic data and GIS analysis

The NEXTMap surface elevation and terrain models (Intermap Technologies, 2007) are the most detailed digital dataset available for the study area, with a 5 m grid size and 1 m vertical resolution. The 'raw' product is the digital surface model (DSM) which provides a topographic model of the Earth's surface that includes objects such as trees and buildings (Intermap Technologies, 2004). The DTM is a derivative of the DSM produced by Intermap using the proprietary software 'TerrainFit' which estimates the elevations of the ground surface underneath objects based on 'bare ground' regions in the original DSM (Wang et al. 2001). The DTM was used in this study because test analyses of the DSM highlighted problems with flow routing around surface objects.

Smoothing and warping of the surface by the TerrainFit algorithm may influence the apparent stream elevation in forested areas and where channel and valley-side slopes are steep. In addition, a number of factors associated with InSAR acquisition may influence the accuracy of surface elevation data, including shadow and layover effects (Intermap Technologies, 2004). Modelled stream lines and long profiles, derived using GIS Hydrology processing tools (Appendix 1.1), were checked against digital Ordnance Survey 1:10,000 and 1:25,000 scale topographic maps to identify errors which were then manually corrected. Errors in the modelled channel reflect the local topography of the valley floor (cf. Reinfelds et al., 2004; Addy, 2010). Where valley-floors are dominated by extremely low slope floodplains, the model channel is subject to planform errors such as missed meander loops and offsetting of tributary junctions. Where valley floors are extremely confined and/or densely forested, the channel line is accurately delineated, but step-artefacts are found to affect the channel elevation. These errors affect less than 10% of reaches in the three study streams, and were mitigated by manual corrections based on 10m contour data and blue stream lines from 1:10,000 scale Ordnance Survey topographic maps.

2.3.3.2   Channel slope

Channel slope (m/m) was derived from the corrected modelled channel elevations. Massong and Montgomery (2000) compared reach-scale channel slopes derived from digital elevation models (DEMs), with field measured slopes, finding differences of up to 100%, but uncertainties associated with the derived slopes vary depending on the resolution of the original data and the calculation methods used (Wobus et al., 2006). Massong and Montgomery (2000) used a 10m grid DEM derived from 12m contours,

significantly coarser resolution than the NEXTMap DTM used in this study. Wobus et al. (2006) noted that slope errors can be reduced by resampling the DTM elevation and/or using a moving-window to calculate spatially averaged slope values for individual profile pixels. The NEXTMap DTM was resampled to 1m vertical intervals and 200m and 50m moving-windows were used to calculate channel slopes for 5m spaced 'pixels' along the stream line. This procedure has the effect of smoothing 'step' artefacts in the channel profile. The mean of all 5m 'pixel' slopes in each reach was then calculated to give reach-averaged 200m and 50m slopes. These channel slopes were then compared with a third measure of reach slope, calculated from the difference in elevation between the top and base of the reach (derived from the corrected long profile) and the reach length measured in the GIS. The reach slopes derived using different methods are compared in Figure 2-10.
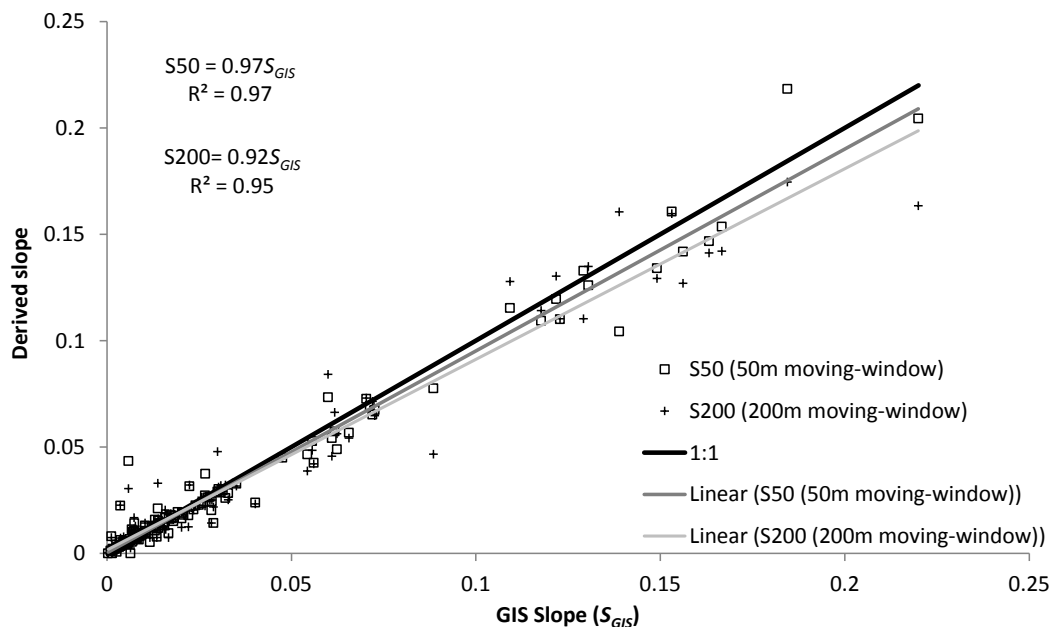
Figure 2-10. Comparison of reach slopes (m/m) derived by three methods from NEXTMap DTM data for all study rivers. S50 and S200 are the reach slopes derived using 50m and 200m moving-windows respectively. These are plotted against the 'GIS slope' (S_{GIS}) derived from the GIS measured stream length and the elevation of the top and base of the reach. Linear regressions are significant at p<0.001 and forced through the origin (intercepts are not significantly different from zero p>0.1).

Reach slopes derived using the 50m (S50) and 200m (S200) moving-windows are in good agreement with the GIS slope, and variability in S50 with respect to the GIS Slope is lower than that for S200, as expected due to the narrower smoothing window (Figure 2-10). The use of a moving-average window results in slightly lower slope values for most reaches than the GIS slope, with a larger offset for the 200m smoothing window. This may be due to the effects of reach length, with many steeper reaches being relatively short, 50 – 200m in length, and flanked by shallower reaches which causes the slope to be underestimated

when calculated using a moving-window. As these short, steep reaches are generally the bedrock reaches, the GIS slope was used in this study.

2.3.3.3   Discharge derivation from drainage area

In natural channels, discharge at a given point varies as a result of climatic variations in precipitation. Two different approaches to deal with the complexity of climatically driven changes in discharge have been employed in studies of gravel-bed and bedrock channels. The first assumes that channel form and sediment transport or erosion depend on a 'formative discharge' defined by the frequency-magnitude distribution of flows (e.g. Wolman and Miller, 1960; Pickup, 1976; Knighton, 1998). The second assumes that all flows may influence the channel form and employ stochastically varying discharge in numerical simulations of channel processes (e.g. Pickup and Rieger, 1979; Lague, 2010). Whilst the latter approach may better represent processes in many natural channels, the assumption of a formative discharge remains widely used in studies of bedrock channels due to the need for a reference discharge when undertaking assessments of channel geometry (c.f. Montgomery and Gran, 2001; Wohl and David, 2008) and a strong relation between a given reference discharge and catchment area which facilitates studies in areas with limited or no gauged flow records (e.g. Knighton, 1998). A reference discharge, the formative discharge, is thus used to derive stream power estimates and as a basis for channel geometry assessment in this study.

The use of a formative discharge assumes that the frequency distribution of discharge events has remained roughly constant over timescales of up to 10^4 years. This assumption has been made in this study on the basis that the temperate climatic regime established following the Younger Dryas deglaciation has remained largely stable (e.g. Brooks and Birks, 2000). Furthermore, the lack of long-term records precludes a more detailed approach to the assessment of discharge variability over Holocene timescales.

The downstream increase in discharge (Q) with drainage basin area (A) can be estimated from empirically determined power law relationships of the form;

$$Q_f = rA^s \hspace{6cm} \text{Eq. 2.1}$$

Where Q_f is a discharge of a given frequency (f) and the values of r and s are empirically determined constants (e.g. Knighton, 1998). The constants can be derived using gauging data, and vary depending on the discharge frequency 'level', e.g. mean flow versus peak

flow, catchment relief and vegetation, and the presence and distribution of lakes (Knighton, 1998; Galster, 2009). The effects of catchment characteristics on the scaling exponent (*s*) are greater for higher discharges such as peak flows and median annual floods (Galster, 2009). These flows are strongly affected by precipitation gradients, relief, water extraction and the location of lakes.

The Scottish Environmental Protection Agency (SEPA) operates a network of gauging stations in the NW Highlands. But there is only one gauging station located on the River Carron and no gauging data for the rivers Canaird and Elchaig. Discharge for the study catchments was therefore estimated using regional power law *Q-A* relationships derived from subsets of gauging data from the SEPA network (e.g. Jansen et al., 2010). The subsets of gauging stations were selected to account for the effects of a west to east precipitation gradient and the attenuating effect of lakes on higher discharges in the rivers Canaird and Elchaig. Thus two different *Q-A* relationships were derived: one for the River Carron and one for the rivers Canaird and Elchaig (see below). These relationships were derived using flow records from ~1960 to 2009 (Marsh and Hannaford, 2008). Following recent practice, the median annual flood (~ two year return time) is taken as the 'formative discharge' (Q_{MA}) and is assumed to be approximately equivalent to the bankfull stage in alluvial channels (e.g. Wharton, 1995; Barker, 2009; Addy, 2010; Jansen et al. 2010). The concepts of the formative discharge and bankfull stage are discussed in detail with reference to the channel geometry in section 4.2.1.

Flow regulation and water extraction for hydro-electric power generation have a major influence on the flow regime of most of the larger east-draining catchments of the NW Highlands. In the smaller west-draining catchments, natural lakes are the main influence on the flow regime. These two factors prevent good correlations between Q_{MA} and *A* in both east-draining and west-draining rivers in the study area (Figure 2-11). Gauging data from rivers in the eastern Grampian Highlands, with limited flow regulation and a more extensive network of gauging stations were used to estimate *r* and *s* for the east-draining River Carron. For the rivers Elchaig and Canaird, gauging data from a number of west-draining catchments were used to derive a Q_{MA}-*A* scaling applicable to streams with lakes.

River Carron discharge

Empirical *Q-A* regressions for the rivers Dee and Spey in the eastern Grampian Highlands are compared with those from east- and west-draining NW Highland rivers in Table 2-6. In

contrast to the NW Highland data, the Dee and Spey regressions are highly significant (p<0.01) and increasing drainage area accounts for over 95% of the variability in Q_{MA} in these rivers.

Although the River Dee has a substantially larger catchment than the River Carron, it has a similar topographic form, with the upper reaches located in a steep mountain range, and a low relief lower catchment (cf. Addy, 2010). For this reason, the Q_{MA}-A regression for the River Dee was used to approximate median annual flood discharges for the River Carron:

$$Q_{MA} = 1.65A^{0.79} \hspace{4cm} \text{Eq. 2.2}$$

The calculated discharge was compared to the median annual flood for a single gauging station located on the River Carron at a drainage area of 241.1 km^2 (Sgodachail). The median annual flood at the station, derived from gauged daily flows between 1974 and 2009, is 108 m^3/s. This compares with a value of 126 m^3/s calculated for an equivalent drainage area using Eq. 2.2. The slightly lower measured value for the River Carron is likely to be due to the diversion of water at high flows from the upper catchment (section 2.3.1.1). Eq. 2.2 is thus thought to provide a good estimate for the median annual flood discharge prior to the construction of the hydro power scheme.
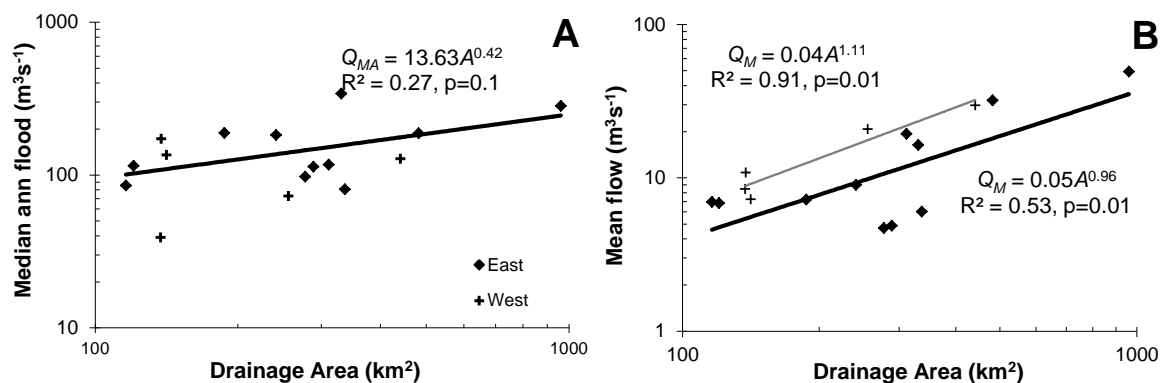
Figure 2-11. Log-log plots of drainage area versus discharge for data from gauging stations in the NW Highlands based on flow records from 1950 to 2005 in the UK Hydrometric Register. A) Median annual flood discharges (Q_{MA}) B) Mean flow (Q_M).

Rivers Elchaig and Canaird discharge

The west-draining Elchaig and Canaird have both headwater and main-stem lakes. In order to derive an empirical Q_{MA}-A relation for these streams, all gauging data for rivers in western Scotland, from the Loch Linnhe area to Assynt, were compiled and gauging stations were classified according to whether they were downstream of moderate to large lakes or located in catchments with no lakes. Figure 2-12 A indicates that two different

Q_{MA}-A relationships can be distinguished for rivers with lakes and those without, but mean flow is unaffected by the presence of lakes (Figure 2-12 B). Median annual flood discharges for the rivers Elchaig and Canaird were calculated using the equation for rivers with lakes ($Q_{MA} = 0.27A$, Figure 2-12 A).

River / Region	Number of gauges	Mean flow			Median annual flood (Q_{MA})			Peak flow		
		Coeff. (*r*)	Exponent (*s*)	R^2	**Coeff. (*r*)**	**Exponent (*s*)**	**R^2**	Coeff. (*r*)	Exponent (*s*)	R^2
Dee	9	0.02	1.05	0.97	**1.65**	**0.79**	**0.97**	4.45	0.72	0.88
Spey	12	0.02	1.00	0.97	**1.47**	**0.69**	**0.94**	3.24	0.71	0.89
NW Highlands - East	11	0.05	0.96	0.53	**13.63**	**0.42**	**0.27**	4.08	0.76	0.48
NW Highlands - West	5	0.04	1.11	0.91	**44.88**	**0.15**	**0.02**	76.21	0.14	0.01

Table 2-6.   Data from power law *Q-A* regressions between drainage area and gauged flow data for two rivers in the eastern Grampian Highlands compared with east-draining and west-draining NW Highland channels.
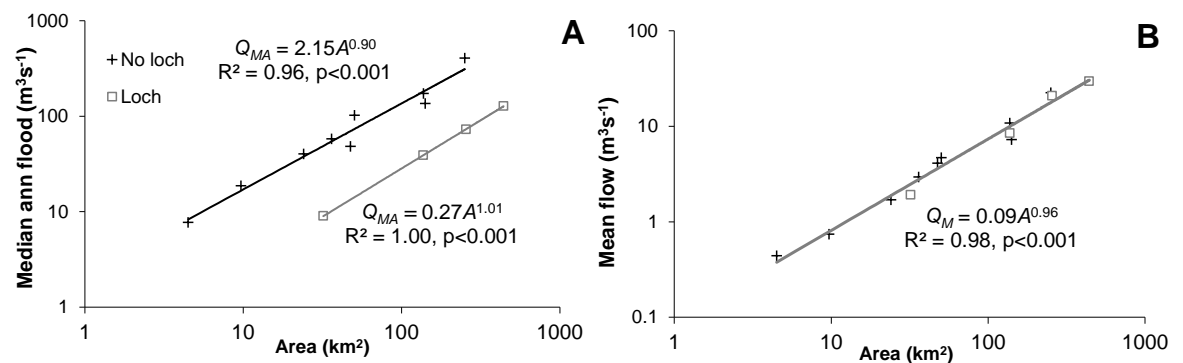
Figure 2-12. Log-log plots of drainage area versus discharge for gauging stations in west-draining catchments in the west and NW Highlands. A) Median annual flood; power law regressions for gauging stations downstream from lakes (black line) and unaffected by lakes (grey line) B) mean flow; with power law regression for all data (dark grey line).

2.3.3.4   Stream power

Total stream power (Ω) and unit stream power (ω) were derived for the three survey rivers from equations 1.1 and 1.2 (section 1.3.2.1) using the GIS derived channel slope and calculated median annual flood discharge estimates. Thus total stream power was calculated for the River Carron using equation 2.3 and for the rivers Elchaig and Canaird using equation 2.4.

$$\Omega = \gamma(1.65A^{0.79})S \qquad\qquad\qquad\qquad\qquad\qquad\qquad\text{Eq 2.3}$$

$$\Omega = \gamma(0.27A)S \qquad\qquad\qquad\qquad\qquad\qquad\qquad\qquad\text{Eq 2.4}$$

Unit stream power was derived for each reach in the study streams using the reach-averaged channel widths presented in chapter 4.

The discharge data and channel slopes used in the calculation of stream power reflect the conditions in modern channels. However, slow rates of fluvial incision mean that bedrock channel morphology generally reflects hydraulic conditions averaged over considerably longer timescales (e.g. Whipple, 2004). As discharge is strongly correlated to drainage area in non-glaciated areas, substantial changes in discharge over the Holocene are not thought to have been significant in the study rivers. However, discharges in partially glaciated and deglaciating catchments are likely to have been substantially higher. Based on analysis of glacio-fluvial terrace sequences, Maizels and Aitkin (1991) calculated palaeodischarges during deglaciation in rivers in the eastern Grampian Highlands up to 17 times greater than modern levels. Maizels and Aitkin (1991) also noted that discharges associated with glacial outburst floods will have been considerably higher than the estimated proglacial discharges. The extent to which bedrock channel morphology and distribution are adjusted to the postglacial (i.e. Holocene) hydraulic regime is assessed in the following analysis, and the influence of proglacial discharge regimes on channel morphology is considered. The potential influence of spatio-temporal changes in stream power arising from progressive adjustments in channel slope and geometry due to postglacial fluvial incision are also assessed.

Chapter 3

Distribution of postglacial bedrock channels

3.1   Introduction

3.1.1   Context

Bedrock channels form where the transport capacity of the stream exceeds the sediment supply (e.g. Gilbert, 1877; Montgomery et al., 1996). The transport capacity is commonly formulated in terms of stream power (cf. section 1.3.2.1). Hence, the key factors controlling the distribution of bedrock channels include channel slope, discharge, sediment flux, and sediment grain-size (Massong and Montgomery, 2000). In postglacial regions, these factors are influenced by inherited glacially-conditioned landscape forms and sediment deposits, and by postglacial climatic change. Variations in sediment flux and discharge, and long-term adjustments in channel slope during postglacial channel evolution may result in spatially and temporally variable bedrock channel distributions (e.g. Brardinoni and Hassan, 2006).

Bedrock rivers effectively have 'excess' stream power and thus also the capacity to erode the channel bed through the force exerted by the flow and impacts of mobile sediment (e.g.

Howard and Kerby, 1983). The exposure of bedrock in channels is coupled to fluvial incision and has strong implications for postglacial fluvial adjustment.

The distributions of bedrock channels in three trunk streams in the NW Highlands were assessed during field surveys. The main controls on the distribution of bedrock channels in these postglacial streams are assessed in this chapter using these field data and GIS analysis of digital topographic data.

3.1.2   Controls on bedrock channel distribution

3.1.2.1   Transport capacity versus sediment supply

The conceptual basis for understanding the controls on the distribution of channel types has changed little since first postulated by Gilbert (1877). He proposed that bedrock channels, i.e. channels that lack a consistent alluvial cover, form where the transport capacity of the stream (q_c) exceeds the sediment supply (q_s). Conversely, alluvial channels form where q_s equals or exceeds q_c. Assessing controls on the distribution of channel types in rivers in the northwest USA, Montgomery et al. (1996) and Massong and Montgomery (2000) proposed a stream power approximation for q_c and estimated q_s using a power law relation between q_s and A,

$$q_c = k_p A^m S^n \hspace{6cm} \text{Eq 3.1}$$

$$q_s = k_r A^h \hspace{6.5cm} \text{Eq 3.2}$$

where the coefficients k_p and k_r depend on climate, geology and other regional characteristics, and the exponent h is likely to be less than 1 due to the potential for long-term sediment storage in floodplains. They showed that the distribution of bedrock and alluvial channels is largely determined by a drainage-area dependent critical slope (S_c) for the transition between alluvial and bedrock channel types:

$$S_c = \left(k_r/k_p\right)^{\frac{1}{n}} A^{\left(\frac{h-m}{n}\right)} \hspace{4.5cm} \text{Eq 3.3}$$

This critical slope was found to discriminate well between most alluvial and bedrock channels, supporting the use of equation 3.2 to model q_s. However, local variations in channel type were found where q_s is locally high, such as at large tributary inputs, or reduced by deposition upstream, as may occur at log-jams. Affected reaches have a 'forced' morphology not controlled by the critical slope. This simple model (eq 3.3) is used

as a basis for the analysis of regional controls on bedrock channel distribution in rivers in the NW Highlands.

3.1.2.2   <u>Controls on stream transport capacity</u>

Channel slope and drainage area are considered as the main controls on the spatial variation in stream power within the study catchments. Equation 3.1 is formulated in terms of *total* stream power (section 1.3.2.1), and implicitly assumes that channel width varies systematically with drainage area. This assumption is valid for the study rivers, as shown in the analysis of channel width presented in chapter 4. In fluvial systems at steady-state, channel slope and drainage area are commonly found to be related by inverse power law functions of the form,

$$S = k_s A^{-\theta}$$ Eq 3.4

where k_s is the channel steepness index and θ the concavity index (Flint, 1974). However, a number of complicating factors may cause spatial and/or temporal variations in erosion rates forming breaks-in-slope, or convexities, in the channel long-profile and affecting k_s and θ. For the purpose of this study, channel profile convexities are termed knickzones at length scales of 2 − 10 km and knickpoints at < 2 km. Knickzones and knickpoints may be produced by spatial variations in erosion rates associated with thresholds in erosion processes (e.g. Crosby and Whipple, 2006; Wobus, 2006), sediment flux and grain size changes at tributary junctions (Sklar and Dietrich, 1998), resistant lithologies (Miller, 1991; Jansen et al., 2010) and spatial or temporal variations in uplift rates or climate (e.g. Snyder et al. 2000).

As discussed in section 1.2.3.1, glacially-conditioned valley floors are characterised by deep concavities, riegels and overdeepened basins (Cotton, 1941; Evans, 1997; MacGregor et al., 2000; Anderson et al., 2006; Hobley et al., 2010). The steep valley-wide convexities that form riegels may result from; spatial variations in glacial erosion rates arising from abrupt changes in ice discharge at tributaries (e.g. MacGregor et al., 2000; Anderson et al., 2006), longitudinal variations in ice discharge along the glacier related to the position of the equilibrium line altitude (e.g. Oerlemans, 1984; Anderson et al., 2006), and basal water pressure fluctuations driven by crevassing at steps in the glacier bed (e.g. Hooke, 1991). In the latter case, the locations of riegels may be affected by bedrock lithology and structure, particularly the degree of jointing and fault related fracturing (e.g. Augustinus, 1995; Benn and Evans, 1997; Dühnforth et al., 2010). These riegels form knickpoints in rivers

following deglaciation, and thus are likely to be a key control on reach-scale channel slope (e.g. Cotton, 1941; Brardinoni and Hassan, 2006; Jansen et al., 2010).

At catchment scales, the long profile form of postglacial channels may be strongly influenced by the degree to which drainage divides have been breached by glacial erosion under ice sheets, or glacial headwall retreat (section 2.2.2), and by the overdeepening of glacial valley floor profiles (Oerlemans, 1984; Anderson et al., 2006). Flat channel headwaters in breached drainage divides and abrupt changes in channel slope associated with valley overdeepening are predicted to have a major impact on the distribution of bedrock reaches in postglacial channels.

3.1.2.3   Sediment supply and grain-size

The grain-size and rate of sediment supply to channels is a third important control on bedrock channel distribution. These factors have the potential for considerable spatial and temporal variability in postglacial landscapes (e.g. Church and Ryder, 1972; Ballantyne, 2002b). The spatial distribution of sediment sources may be strongly influenced by the inheritance of wide, flat-floored glacial troughs in which channels are effectively decoupled from hillslopes because mass-wasting material is deposited at the foot of the valley walls, at the margin of the floodplain. In these areas only major tributary streams and debris flow gullies, and large rock-slope failures contribute sediment directly to the channel. Sediment supply in larger basins may be dominated by the reworking of glacio-fluvial and alluvial floodplain sediments (e.g. Brardinoni and Hassan, 2006). Lakes formed by glacial overdeepening of the valley floor, or dammed by moraines, are common in glaciated valleys and act as sediment traps, restricting the through-flow of sediment along the channel (e.g. Korup and Montgomery, 2008). Moraines, talus, debris fans, rockfalls and steep tributaries may all supply coarse sediment to channels. Strong local variations in the grain-size of sediment sources may lead to longitudinal variation in the distribution of bedrock channels as the threshold stream power for particle entrainment is greater for larger grain-sizes.

In addition to these spatial variations, temporal variations in sediment flux reflecting a paraglacial decline in sediment supply to channels may be expected (sections 1.2.1 and 2.2.3.1). A long term decline in sediment flux will alter the critical slope threshold for the alluvial to bedrock channel transition, thereby exerting a first order control on the distribution of bedrock channels within postglacial landscapes.

3.1.3   Research questions and outline

Analysis of the distribution of bedrock channels in the NW Highlands is guided by three main research questions identified from the preceding discussion:

1. What controls channel slope and the form of the postglacial channel long-profile?
   a. Does channel slope show a strong inverse power law scaling relationship with drainage area (as observed in non-glaciated channels)?
   b. What are the main controls on channel slope at catchment, sub-catchment and reach scales?

2. What controls the distribution of bedrock channels?
   a. Is there a critical slope threshold for the alluvial - bedrock transition?
   b. Or, is the transition complicated by strong longitudinal variations in q_s and/or grain-size?

3. Has the distribution/extent of bedrock channels changed over time?
   a. How has it changed and what are the causes of this change?

These research questions are addressed in the remainder of this chapter using field and topographic data from the rivers Carron, Elchaig and Canaird in the NW Highlands (section 2.3.1).

3.2   Data and Methods

Channel reach types were mapped in the study streams during field surveys (section 2.3.2), and the controls on channel morphology were assessed on the basis of channel slope and drainage area measurements derived from digital topographic data (section 2.3.3). The distribution and characteristics of sediment sources and sinks, recorded during field survey, were used to assess the influence of spatial variations in q_s and grain-size on the distribution of channel types. The early Holocene (i.e. early postglacial) distribution of channel types was reconstructed on the basis of field observations of valley floor deposits and topographic and geological data (section 3.2.3).

3.2.1   Reach classification

The classification system used to designate reach type is discussed in detail in section 2.3.2.1. Channel reaches are defined as channel segments over 5 channel widths in length

characterised by a consistent substrate type and morphology. Three main reach 'types' were distinguished in the field according to the main substrate making up the bed and banks of the river; alluvial (Al), bedrock (BR) and mixed bedrock-alluvial (BR-AL) (Table 3-1, cf. Montgomery and Buffington, 1997).

The distribution of reach types may be influenced by the recent flow and sediment flux conditions in the channel system. Depending on sediment availability, flood events may deposit sediment or scour the channel bed resulting in local changes in channel morphology. The potential influence of recent events on the channel type distribution in the study catchments cannot be evaluated here, but the relatively high bedrock exposure criteria (70%) for bedrock channel classification will reduce the potential for short term sediment flux variations to affect the distribution or bedrock and alluvial channels. In effect, it is expected that recent flood events are likely to have influenced the proportion and/or distribution of sediment cover within bedrock-alluvial reaches rather than driven substantial changes in the channel type distribution at the reach scale.

Reach type	Code	Description
Alluvial	AL	Bed and banks 100% alluvial sediment
Bedrock	BR	Bed and banks 70 – 100% bedrock
Bedrock-Alluvial	BR-AL	15 – 70% bedrock in bed and banks: varying morphology including reaches with bedrock bed and alluvial banks, and those with short bedrock constrained sections alternating with alluvial sections.
Alluvial-Bedrock	AL-BR	Minor type with 1 – 15% bedrock in the channel boundary

Table 3-1.   Channel reach classification.

3.2.2   Topographic data and valley-floor profiles

Channel long-profiles, slope and drainage area were derived for the three survey catchments from the 5m horizontal resolution NEXTMap DTM using ArcGIS Hydrology processing tools (section 2.3.3). Similar data were derived for fifteen trunk streams and major tributary channels from six other catchments in the NW Highlands (Fig 2-4). These data are compared with results for the study catchments and provide a broader basis for assessment of the controls on channel slope. Discharge and stream power were calculated from drainage area and channel slope using the equations and methods described in sections 2.3.3.3 and 2.3.3.4.

In addition to these data, valley-floor profiles, following the top of depositional terraces flanking the channel or the outer edge of inner gorges cut into bedrock, were constructed from the NEXTMap DTM along valley parallel profile lines. These profiles were used to assess the distribution and elevation of depositional terraces in the study catchments. The terrace profiles were also used to derive slope estimates for the reconstructed 'Early Holocene' reaches (discussed below).

3.2.3   Early Holocene channel reconstruction

Field observations indicate that bedrock channels are commonly flanked by alluvial terraces on the valley floor. These alluvial terraces have not been dated in the study catchments, but deposition must have occurred after ice retreat, i.e. in the Late Glacial (14.7 – 11.7 ka) or Holocene (since 11.7 ka; Table 2-1). As discussed in section 2.2.3.1, there is a dearth of information on alluvial landforms in the Scottish Highlands, particularly a lack of dates for alluvial terrace deposition (Ballantyne, 2008). The few quantitative studies yield mid to late Holocene ages suggesting that early Holocene alluvial deposits have been reworked during later floods (Lewin and Macklin, 2003; Lewin et al., 2005). However, this scenario is unlikely in channels that have incised through valley floor sediments and into bedrock, as floodplain reworking is restricted in these channels. Alluvial terraces on valley floors adjacent to entrenched bedrock channels in the study catchments thus most probably date to soon after deglaciation (e.g. Werritty and McEwen, 1997; Jansen et al., 2010). It is hypothesised that a change from depositional to erosional fluvial systems occurred during the mid to Late Holocene (cf. Ballantyne, 2002b), and that the distribution of alluvial terrace deposits indicates a former distribution of alluvial channels and floodplains. It is acknowledged that catchments are unlikely to have experienced a smooth decline in q_s over postglacial timescales (e.g. Werritty and McEwen, 1997), and that floodplain deposition followed by entrenchment to form terraces is likely to be diachronous within and between catchments. However, the distribution of alluvial terrace deposits is hypothesised to represent, to a first-order, the distribution of alluvial channels in early postglacial times and thus provides a broad comparison with the present-day distribution of channel types.

On this basis, an 'Early Holocene' distribution of bedrock and alluvial channels was reconstructed by reclassifying the modern channel reaches mapped during the field survey according to their probable 'early Holocene' type. The reclassification was based on; alluvial terrace deposits as shown in 1:50,000 scale British Geological Survey (BGS)

digital superficial geology maps, the valley floor topography assessed using 1:25,000 scale OS topographic maps and valley floor profiles, and field observations. Channel slope for these early Holocene reaches was estimated from the elevation of depositional terraces adjacent to the top (upstream) and base (downstream) of each reach, and the reach length, which is assumed to have remained constant. As reach length was measured along the channel centre-line, this assumption implies that the channel planform has not changed significantly since the early Holocene. Yet, many of the early Holocene alluvial channels were likely to have been braided, and therefore straight, whereas many modern alluvial channels meander (e.g. Werritty and McEwen, 1997); hence, Early Holocene channel slope estimates for some alluvial reaches (~10% of all channels) may be underestimated. Where channels have switched from alluvial to bedrock, the straight bedrock channel length is likely to provide a reasonable estimate of the early Holocene braided alluvial channel length. Drainage area is assumed to have remained constant over time as none of the study catchments shows evidence of significant postglacial drainage rearrangement.

3.2.4   Canonical discriminant analysis

Critical channel slopes (Eq 3.3) were derived from log-transformed slope and drainage area data using canonical discriminant analyses (Montgomery et al., 1996; Massong and Montgomery, 2000), performed in the statistical software package R. In canonical discriminant analysis, differences between two or more separate data groups can be assessed with respect to a range of discriminating variables simultaneously. Here, the procedure was used to assess the variation between the alluvial and bedrock reach datasets (the data groups) on the basis of drainage area ($log\ A$) and slope ($log\ S$) (the discriminating variables). A linear function, the canonical discriminant function, was derived which maximises the differences between the two data groups in terms of both $log\ A$ and $log\ S$. The coefficients of this linear function, the 'canonical coefficients', were used to compute a power law critical slope function defining the transition from alluvial to bedrock channels in terms of channel slope and drainage area (Eq 3.3). The mathematical basis for this analysis is outlined by Klecka (1980) and the R code is given in Appendix 1.2.

3.3   Results

The controls on channel slope are assessed in section 3.3.1 through analysis of channel long profiles and slope-area relationships, followed by an assessment of the controls on the distribution of bedrock channels in section 3.3.2.

3.3.1   Postglacial channel long profiles and slope

The long-profiles of the rivers Carron, Elchaig and Canaird are shown in Figure 3-1, with slope-area plots in Figure 3-2. The form of the channel long profiles and slope-area relationships, and the controls on channel slope are discussed for catchment (whole profile), sub-catchment (2 – 10 km) and reach (<2 km) scales in the following sections.

3.3.1.1   Catchment scale

The rivers Elchaig and Carron have concave-up profiles with steep headwater channels, whereas the River Canaird has a sigmoidal profile with a convex-up upper half and low-slope headwater channels (Figure 3-1). These differences are also highlighted in the nature of the slope-area relationships (Figure 3-2, Table 3-2): the rivers Elchaig and Carron show significant negative power law relationships between channel slope and drainage area despite considerable variability in the data (R^2= 0.34 - 0.71, p<0.01), but for the River Canaird, only the 200m slope regression is significant at p<0.01, and even this has a very low R^2 (0.13) suggesting that slope is very poorly related to drainage area in this channel (Table 3-2).

Slope-area relationships were used to derive channel steepness (k_s) and concavity (θ) indices (Eq 3.4, Table 3-2). Due to the strong covariance between k_s and θ, a normalised channel steepness index (S_r) was derived following the method of Sklar and Dietrich (1998) and Jansen et al. (2010), using a reference drainage area (A_r) at the midpoint of the dataset:

$$S_r = k_s\left(A_r^{-\theta}\right)$$ Eq 3.5

A_r was set to 10 km^2 in order to enable direct comparison of normalised channel steepness indices with those derived by Jansen et al. (2010) for postglacial rivers in western Scotland. An extensive regional dataset was generated by supplementing the steepness and concavity indices from the three surveyed channels with those from 15 other NW Highland rivers (locations shown in Figure 2-4, data in Appendix 2).
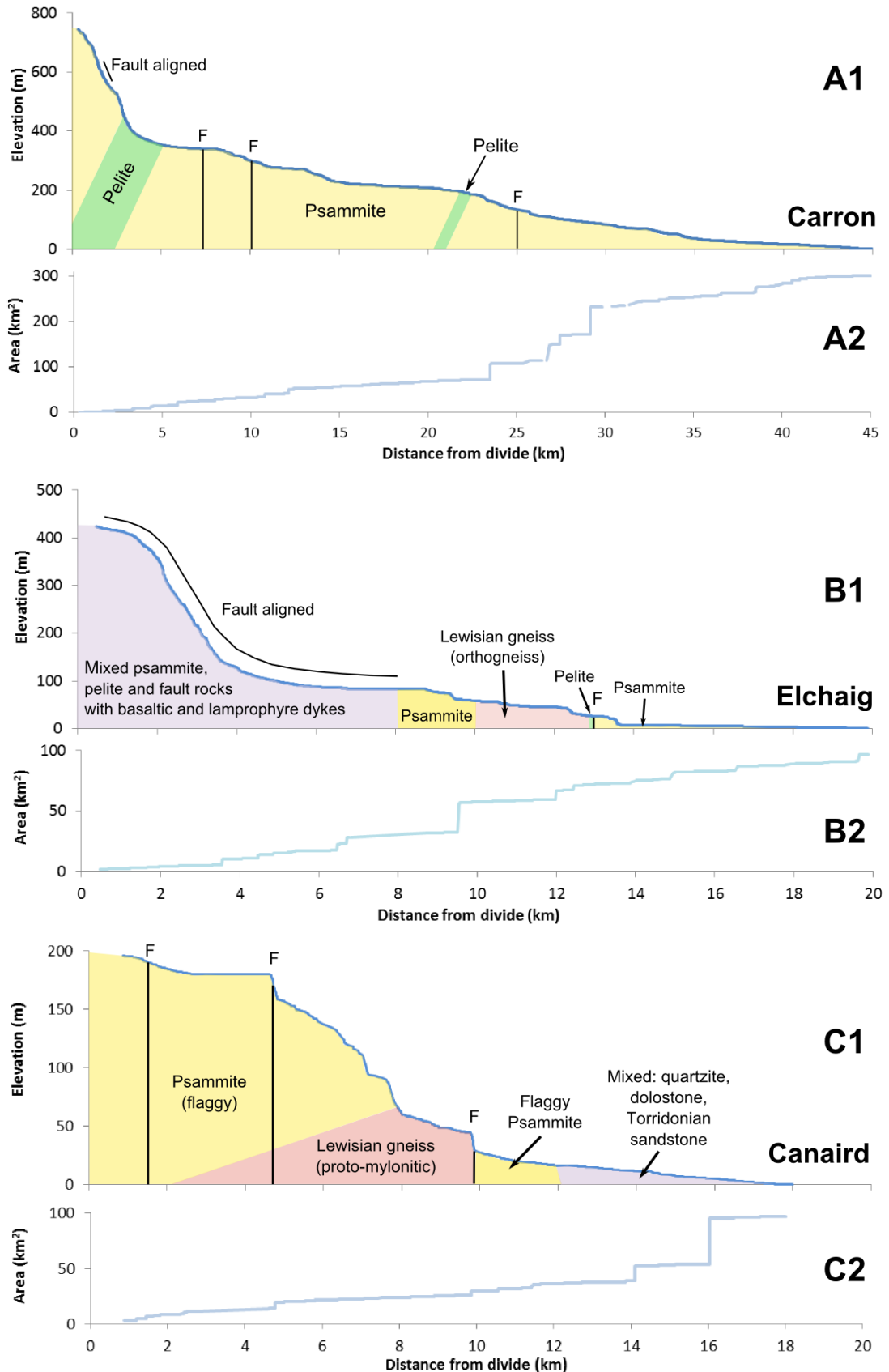
Figure 3-1. Long profiles and plots of drainage area versus distance from divide for the rivers Carron (A1 and A2 respectively), Elchaig (B1 and B2) and Canaird (C1 and C2). Note the different horizontal and vertical scales. The distribution of main lithologies was mapped in the field; F signifies fault, other terminology outlined in chapter 2. Note that this is a general outline intended to highlight the distribution of different lithological types along the channel line; structural relationships such as fault and contact dips are represented schematically.
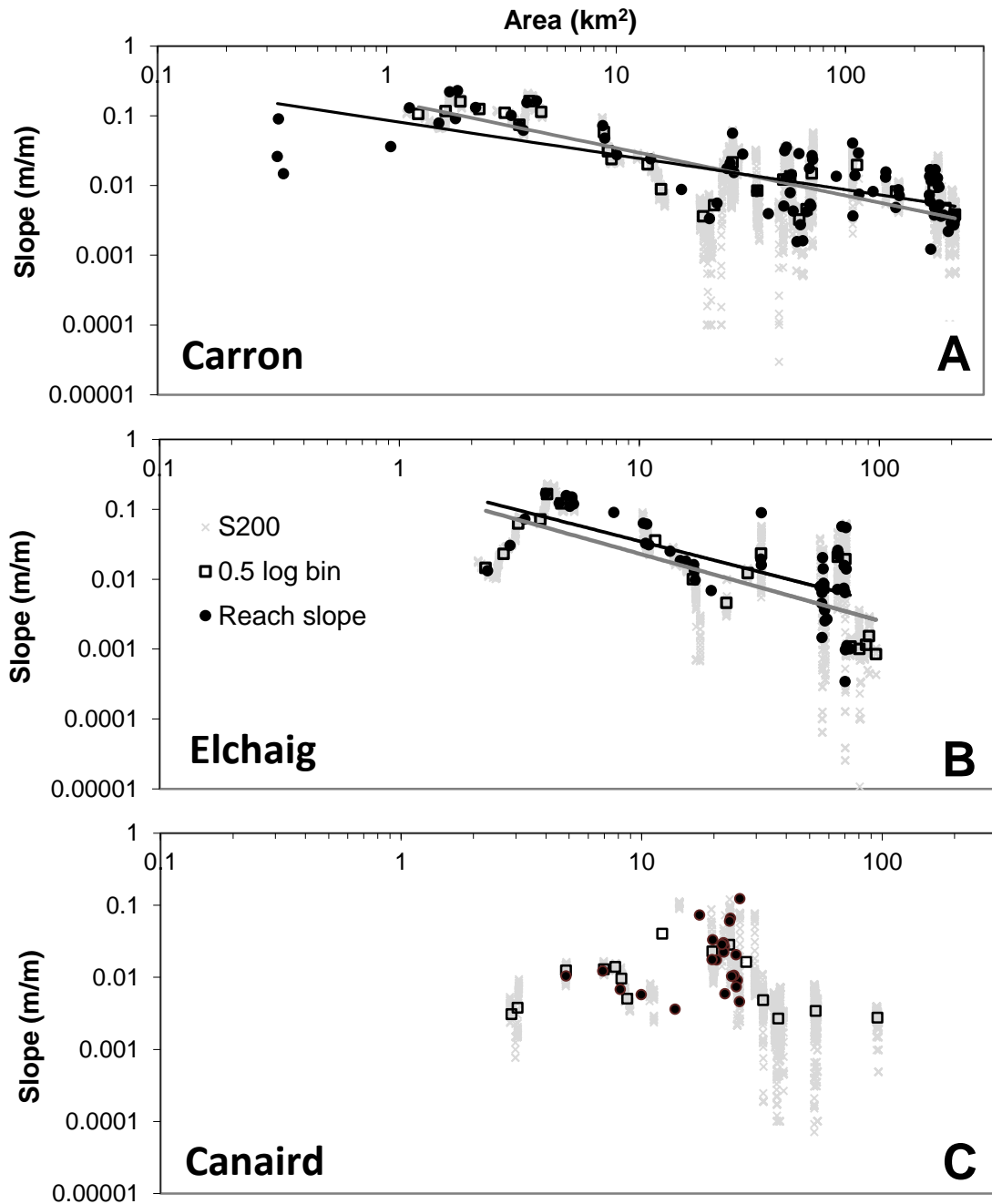
Figure 3-2. **Slope versus drainage area (logarithmic axes) for the rivers Carron (A), Elchaig (B) and Canaird (C). Three methods of deriving channel slope are compared here: i) S200 is calculated using a 200m moving window (grey crosses). ii) *0.5 log-bin* represents the 200m-Slope smoothed using 0.5 log bins (open squares, grey regression line). iii) *Reach-slope* is calculated using the reach length and elevation of top and base (filled circles, black regression line). Regressions shown where significant at p<0.05, regressions for S200 data not shown. Regression statistics are given in Table 3-2. All slope-area data for the rivers Canaird and Elchaig were restricted to the trunk stream below the outlet of minor lakes, which are found in the catchment headwaters at drainage areas of 2.5km² on the Canaird and 2 km² on the Elchaig. For the river Carron, reach data were taken from below a small headwater lake at ~0.3 km² drainage area, but a drainage area limit of 1km² was used for all other data.**

	Data type	Coefficient (k_s)	Standard error of k_s	Exponent (θ or m/n)	Standard error of θ	R^2	p
River Carron	S200	-1.11 (0.08)	0.02	0.56	0.01	0.34	<0.001
	Half log bins	-0.78 (0.17)	0.13	0.68	0.08	0.71	<0.001
	Reach average	-1.06 (0.09)	0.10	0.50	0.05	0.52	<0.001
River Elchaig	S200	-0.46 (0.35)	0.03	1.17	0.02	0.53	<0.001
	Half log bins	-0.65 (0.22)	0.17	0.97	0.13	0.60	<0.001
	Reach average	-0.61 (0.25)	0.22	0.86	0.15	0.43	<0.001
River Canaird	S200	-1.47 (0.03)	0.05	0.57	0.03	0.13	<0.001
	Half log bins	-1.95 (0.01)	0.29	0.12	0.24	0.00	0.633
	Reach average*	-2.60 (0.003)	0.54	-0.66	0.42	0.10	0.137

Table 3-2. Regression statistics for slope-area data for the three study catchments, employing three different channel slope derivations (see caption to Figure 3-2). Linear regressions were calculated in Minitab for logged area and slope data and are shown as power law trends in Figure 3-2. Bracketed values are power law coefficients calculated from the linear *log A – log S* intercepts.
*No data for lower alluvial section, hence this regression yields a positive drainage area exponent.

Following the rationale and methods of Jansen et al. (2010), potential lithological controls on k_s and θ were assessed using lithological indices quantifying the proportion of the catchment underlain by resistant quartzite rocks ("quartzite fraction" in Figure 3-3), and the proportion of the channel line that is aligned along fault zones ("fault fraction" in Figure 3-3). The effect of glacial inheritance on the long profile form was assessed by comparing k_s and θ with two metrics that quantify the extent of glacial breaching of the drainage divide:

- the "breach depth ratio", which is the ratio of the breach depth to the estimated un-breached ridge height derived from the elevations of the 'intact' adjacent ridgeline; and

- the "breach cross-section area" calculated from the breach width and depth at the divide, on the basis of a triangular valley form. The breach width and depth were measured from the break in slope between the breach walls and the adjacent ridge using OS digital 1:50,000 scale topographic maps and 10 m contours in ArcGIS.

These two metrics were derived for the NW Highland channels, and the western Highland channels studied by Jansen et al. (2010), and are presented alongside the other indices in Figure 3-3. Fault-aligned channel segments constitute 14% of the combined length of all 18 NW Highland rivers. However, the degree of fault alignment of the stream has no relation to S_r or θ (Figure 3-3, G and H), supporting the findings of Jansen et al. (2010). The extent of resistant quartzite in the catchment also appears to have no effect on the channel profile form (Figure 3-3, E and F), though it should be noted that resistant

quartzite is relatively sparse in the NW Highland catchments. This finding is contrary to that of Jansen et al. (2010) who describe a weak positive scaling between S_r and the extent of quartzite outcrop in western Highland catchments. The lack of correlation with lithology metrics contrasts with highly significant negative correlations between channel profile indices and the glacial breach indices; S_r and θ are inversely correlated with the breach depth ratio and breach cross-section area for both NW Highland ($p<0.01$, $R^2 = 0.43 - 0.57$) and western Highlands datasets ($p<0.05$, $R^2=0.35 - 0.44$). Thus, the extent of glacial breaching of the drainage divide appears to be a major control on the channel profile form, whereas lithology has limited to no influence on the channel at the catchment scale. Glacial erosion across the drainage divide lowers the maximum elevation of streams that inherit the catchment after deglaciation. Divide breaching effectively decapitates the long-profile and introduces convexities in the mid to upper catchment. This process has a limited effect on the drainage area of the postglacial stream in most cases, although extensive breaching may result in drainage rearrangement in some catchments, and hence a change in both A and S (cf. Haynes, 1977).

3.3.1.2   Sub-catchment scale

In non-glaciated settings, variations in S-A relationships within a catchment are commonly associated with different geomorphic process domains and inflexions between different S-A 'segments' are interpreted as transition points between, for example, colluvial (commonly debris flow dominated) and fluvial channel domains (Montgomery and Foufoula-Georgiou, 1993). In postglacial rivers in British Columbia, Brardinoni and Hassan (2006) noted that variations in S-A relationships result from inheritance of glacially conditioned valley-floor slopes, and suggested that this inheritance controls the distribution of hillslope, colluvial and fluvial process domains within catchments of drainage area 10^{-2} to 10^1 km^2. In this study, channels were surveyed over a range of drainage areas of 10^{-1} to 10^2 km^2; despite relatively steep channel slopes, all streams at drainage areas > 1 km^2 are dominated by fluvial processes with no evidence for debris flow activity along the main channel. The lack of debris flow activity in modern channels is probably the result of limited sediment availability and is discussed further in section 3.4.3.
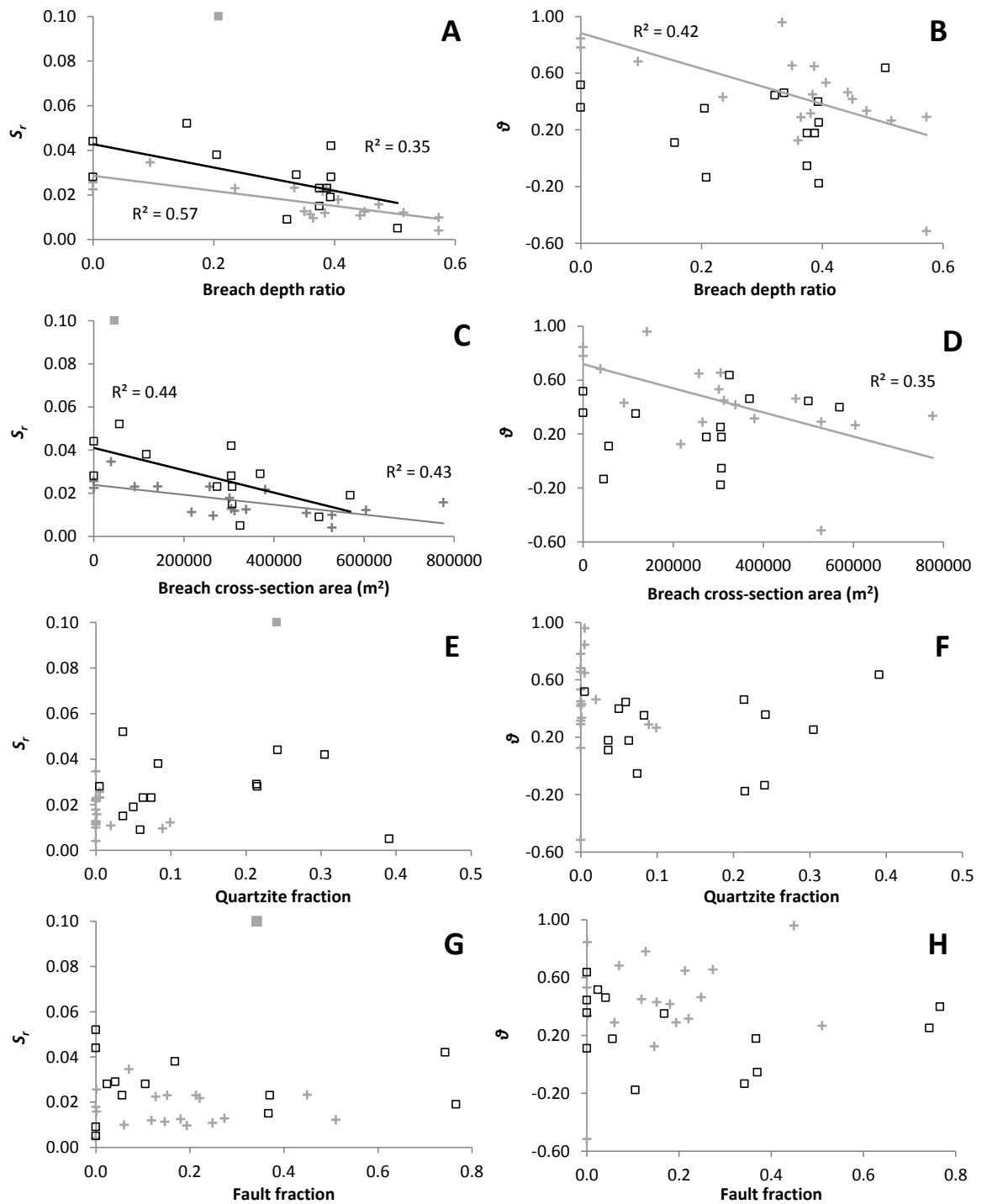
Figure 3-3. Channel steepness and concavity indices for NW Highland channels (crosses, this study), and western Scotland (open squares, Jansen et al. 2010). The outlier (filled square in plots A, C, E and G) is Esragan, western Scotland data (Appendix 2). A) normalised channel steepness versus breach depth ratio; B) channel concavity versus breach depth ratio; C) normalised channel steepness versus breach cross-section area; D) channel concavity versus breach cross-section area; E) normalised channel steepness versus fraction of the catchment area underlain by resistant quartzite; F) channel concavity versus fraction of catchment area underlain by resistant quartzite; G) normalised channel steepness versus fraction of channel line aligned along fault zone; H) channel concavity versus fraction of channel line aligned along fault zone. Linear regressions with R^2 values are shown where correlations are significant ($p<0.05$); grey regression lines for NW Highlands data, black lines for western Highlands data.

Comparison of Figure 3-1 and Figure 3-2 indicates that positive trends in the *S-A* relationship at low drainage areas are related to the flattening of headwater reaches where drainage divides have been breached by glacial erosion. Negative *S-A* trends between 5 and 12 km^2 correspond to hyper-concave segments in narrow upland glacial troughs. In catchments with major breached divides, this segment may be absent (e.g. River Canaird, Figure 3-1 C1 and Figure 3-2 C). At drainage areas greater than ~12 km^2, channel slope generally declines with increasing drainage area, but is highly variable at reach-scales. These observations suggest that rather than being indicative of differences in geomorphic process, variations in the *S-A* relationships within catchments reflect the inheritance of a glacially conditioned landscape form (e.g. Jansen et al., 2010).
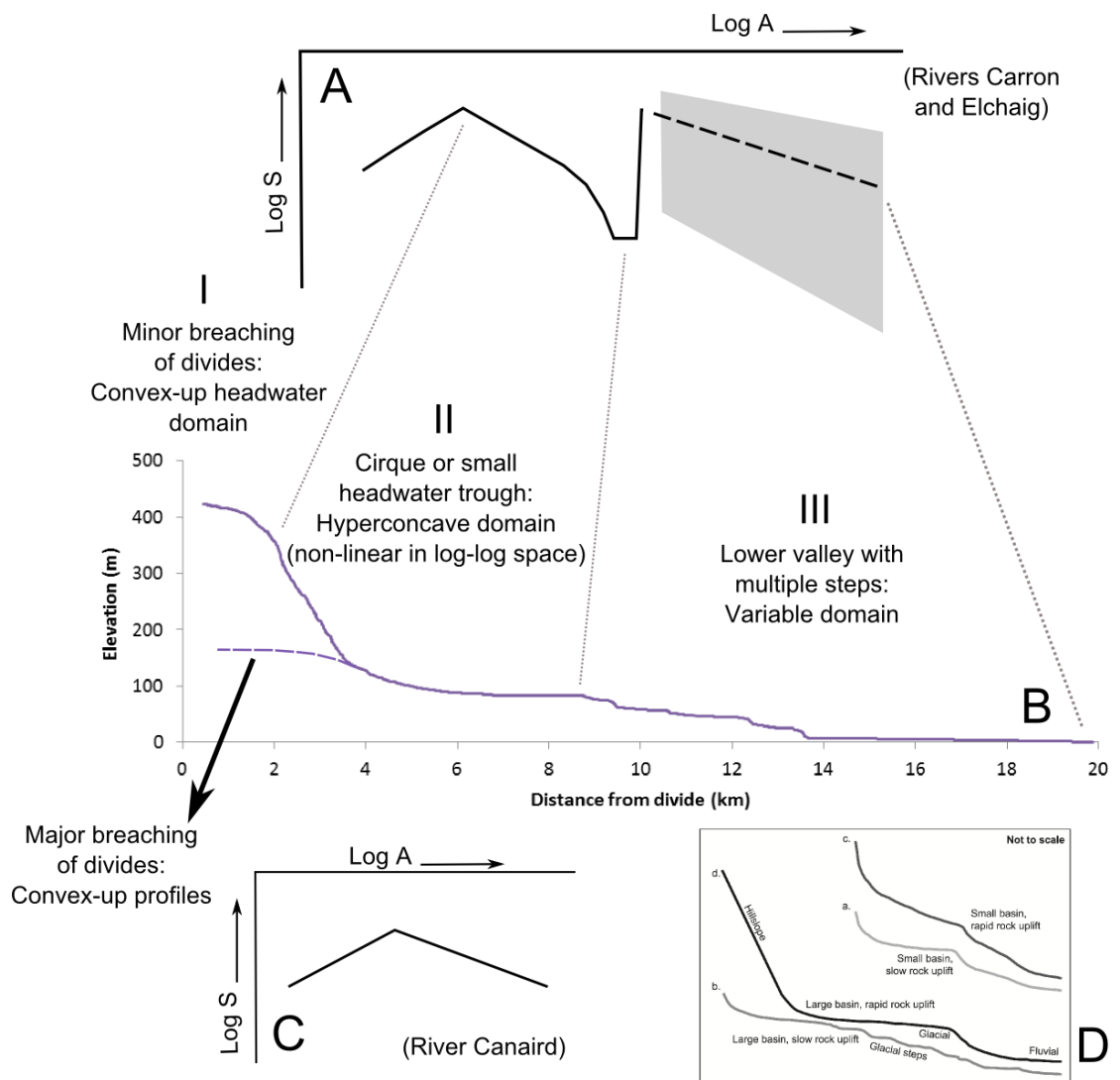
Figure 3-4.   **Glacio-morphological domains in postglacial landscapes. A) diagrammatic slope-area plot for a typical (non-breached) glaciated catchment. B. Long-profile for the River Elchaig with glacio-morphological domains linked to segments of the slope-area plot. The dashed line illustrates alternative profile of catchment affected by major breaching of the drainage divide. C) diagrammatic slope-area plot for catchment affected by major divide breaching (e.g. the River Canaird). D) sketch plot from Brocklehurst and Whipple (2007) depicting typical glaciated valley floor profiles in large (b and d) and small (a and c) catchments with low (a and b) and (c and d) high rates of tectonic uplift.**

The form of the *S-A* relationship can be used to delineate major glacio-morphological domains within the postglacial catchment (Figure 3-4). Similarities between the form of the NW Highland channels those in other settings (cf. D in Figure 3-4) suggests that these domains may be applicable to postglacial fluvial systems worldwide.

3.3.1.3   Reach scale

Reach-scale channel slopes range from 0.001 to 0.25 m/m and are highly variable, especially in the mid to lower parts of the study catchments (domain III, Figure 3-4). This local variability is due to the presence of multiple knickpoints (KPs) that give the profile a 'stepped' form. Controls on reach-scale channel slope are assessed in this section by comparing reach-average channel slopes with semi-quantitative lithological resistance data and reviewing the position of KPs with respect to tributary inputs and other valley-floor features.

When all reach-scale data from the three rivers are combined, there is a significant inverse power law scaling of channel slope with drainage area ($S_{GIS} = 0.1507A^{-0.563}$, $R^2 = 0.44$, $p<0.001$) (Appendix 2, Figure A2-1). In order to assess the influence of lithological resistance on reach-scale channel slope, reach slope values (S_{GIS}) were normalised using the power law *S-A* relationship derived using all the data,

$$S_n = \frac{S_{GIS}}{0.1507A^{-0.563}}$$ Eq 3.6

Normalised reach slope (S_n), together with reach-averaged total stream power (Ω) values were classified according to bedrock lithology and associated Selby rock mass strength (RMS) index (section 2.3.2.3). S_n and Ω are not scaled with lithological resistance in the study channels (Figure 3-5). This may be because the Selby RMS index poorly represents bedrock resistance to fluvial erosion (cf. section 7.2.2), but the result confirms field observations indicating that bedrock lithology and structure have only local, or sub-reach scale control on channel morphology. Strong geological control on reach slope was seen only at the lower KP on the River Canaird (9.8 km from the divide, Figure 3-1 C1), where a faulted contact occurs between the flaggy psammite and protomylonitic gneiss (Figure 3-6). These rocks have the lowest and highest Selby RMS scores (62 and 90 respectively) in the dataset and hence the largest observed difference in rock strength. By contrast, the geological contact between psammite (R=82) and orthogneiss (R=83) in the River Elchaig has no influence on channel slope, nor does the alignment of channel reaches along fault lines (Figure 3-1 B1).

KPs are not widely associated with tributary inputs, which are indicated by step increases in drainage area in graphs A2, B2 and C2 in Figure 3-1. Although the characteristics of tributary streams have not been assessed in detail, this observation suggests that local variations in discharge and sediment supply or grain-size at tributary junctions may be accommodated by changes in channel width or roughness with limited effect on channel slope in these catchments.
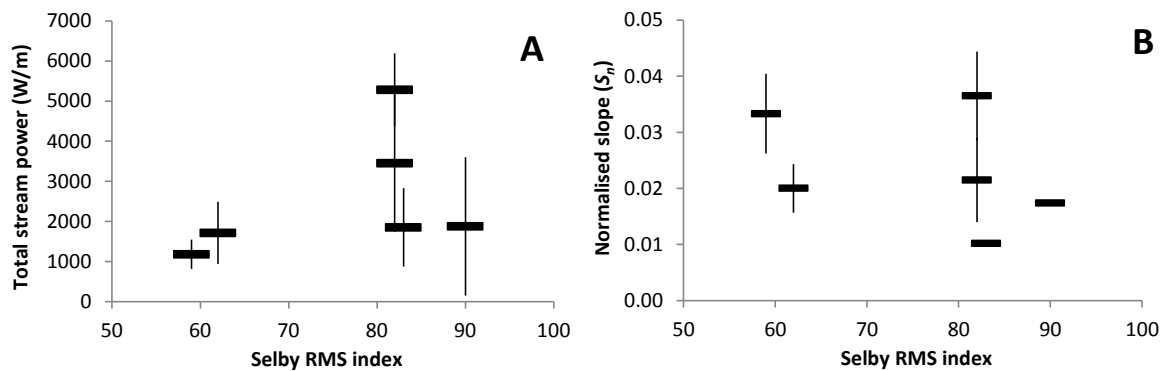
Figure 3-5.   **A) Mean reach-average total stream power and B) Mean normalised reach slope (S_n) for channel reaches underlain by different lithologies; flaggy psammite (R=62), fault (R=59), orthogneiss (R=83), pelite (R=82), psammite (R=82) and protomylonetic gneiss (R=90). Error bars show standard error at 2σ; where no error bars are visible, error bars are smaller than the symbol.**
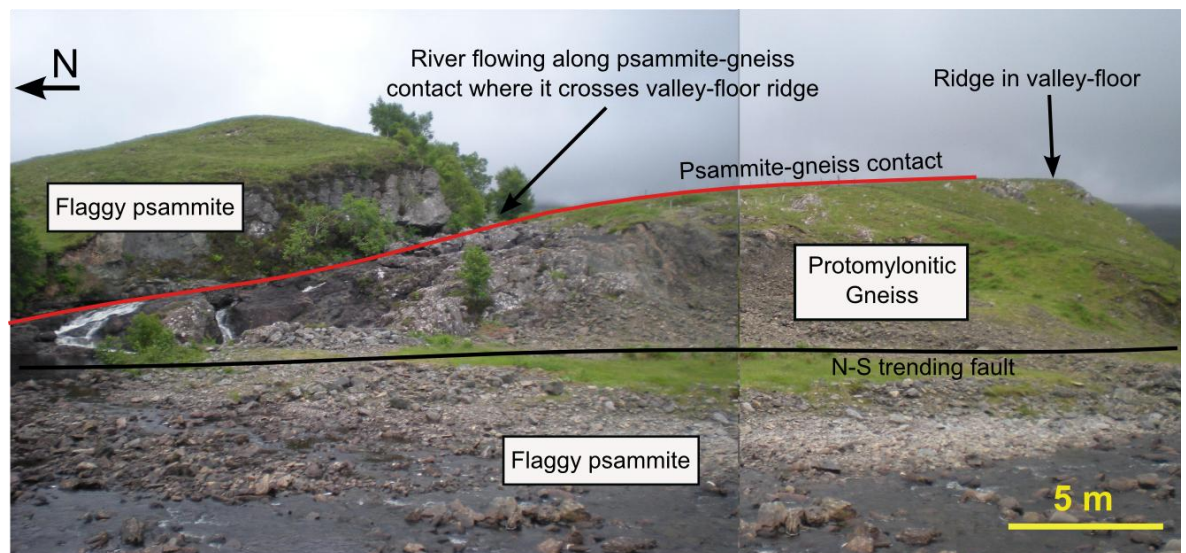
Figure 3-6.   **Annotated photograph of lower KP on the River Canaird (9.8 km from divide in Figure 3-1 C1) showing relationship of channel to lithological contacts and faults.**

Comparison of channel and valley-floor profiles indicates that the channel slopes remain largely similar to valley-floor slopes, as indicated for the River Canaird in Figure 3-7. This river has the deepest entrenchment and thus the largest difference between valley floor and channel long-profiles of the study rivers (chapter 6). KPs are generally formed at the site of

steep 'steps' (i.e. riegels) in the valley floor, and KP retreat or lowering through fluvial incision at these steep reaches has not yet 'smoothed' the channel profile (discussed in detail in chapter 6). The lithological KP in the lower Canaird (Figure 3-6) is also associated with a valley-spanning ridge following the line of the faulted contact between the protomylonitic gneiss and flaggy psammite. Thus it is likely that the apparent lithological control on channel slope in that reach is due to inheritance of a lithologically controlled riegel. The presence of multiple riegels thus exerts a strong control on reach-scale channel slope in postglacial rivers.
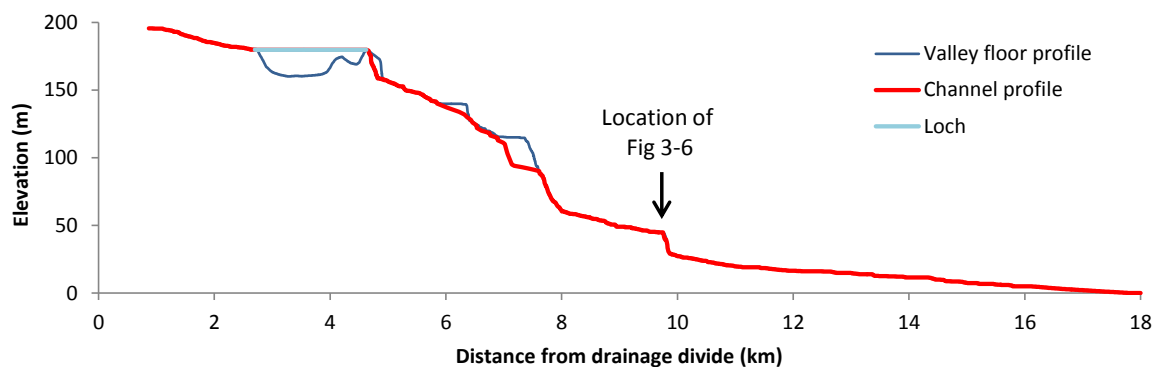
Figure 3-7.   River Canaird long profile compared with the valley floor profile

3.3.1.4   Glacio-isostatic rebound and the channel profile

Base-level fall driven by glacio-isostatic uplift of the land surface following deglaciation is responsible for the formation of retreating bedrock KPs in the lower reaches of many rivers in the Scottish Highlands (Bishop et al., 2005; Jansen et al., 2011). In the study rivers the presence of raised beaches and shoreline platforms near the outlets indicate that the rivers Canaird and Elchaig have experienced 15 – 20 m and the River Carron ~13 m of glacio-isostatic uplift since deglaciation. However, the presence of sediment mantles over the bedrock valley floor at the outlets to all three rivers has affected the fluvial response to this postglacial uplift.

In the lower 6 – 8 km of the rivers Elchaig and Canaird, alluvial channels with active floodplains are graded to contemporary sea level. In both streams, these lower alluvial reaches terminate abruptly at their upstream end in riegels that mark a major change in the valley floor elevation and morphology and form KPs in the channel long-profiles. Remnants of raised alluvial terraces along the lower Canaird suggest that the lower valley was previously graded to higher relative sea level and has subsequently incised in response to a relative fall base-level (Figure 3-8 A). Thus glacio-isostatic uplift appears to have been largely accommodated by regrading of the alluvial reach in the lower channel, with the

lower KP (a lithologically-controlled riegel) retarding upstream transmission of any residual base-level fall (Figure 3-8 A). A similar scenario is assumed for the Elchaig although no raised terraces are found in the lower catchment and it is possible that the postglacial uplift has exhumed a low-slope sediment plain deposited in the tidal inlet at the channel mouth and hence has not caused the stream to incise.

In the lower River Carron, raised alluvial terraces suggest that there may have been incision resulting from a base-level fall. Here the alluvial cover is relatively thin and incision has exposed the undulating bedrock valley floor surface, with bedrock reaches and minor KPs forming at bedrock convexities. It is probable that a larger KP located ~12 km upstream from the river mouth (33 km from the divide in Figure 3-8 B) is the upper limit for sediment excavation due to base-level fall at the river mouth, acting as a local base-level for upstream reaches. Sediment excavation in this channel may also reflect changing discharge or declining sediment flux, meaning that entrenchment of the lower Carron could be a response to both base-level lowering driven by glacio-isostatic uplift, and long-term changes in discharge and/or sediment flux.

The influence of glacio-isostatic rebound is limited to the lower $6 - 8$ km of the rivers Elchaig and Canaird, coinciding with the unmapped alluvial segments at the base of the channel profile, and the lower 12 km of the River Carron. All reaches upstream of these limits are unaffected by the glacio-isostatic base-level fall.

3.3.1.5   Summary of channel slope results

- At the catchment scale, long profile steepness (k_s) and concavity (θ) depend upon the degree of glacial breaching of the drainage divide.
- At sub-catchment scales, glacio-morphological domains can be identified in channel long profiles that relate to different components of the glacial landscape and control variations in channel slope-area relationships.
- At the reach-scale, channel slope is locally influenced by bedrock geology where strong contrasts in lithological resistance exist across geological contacts, but mainly depends upon the location of riegels that form knickpoints in the postglacial channel.
- The effects of glacio-isostatic uplift on the channel long profile are restricted to the lower reaches of the studied rivers, affecting less than one-quarter of the total channel length.
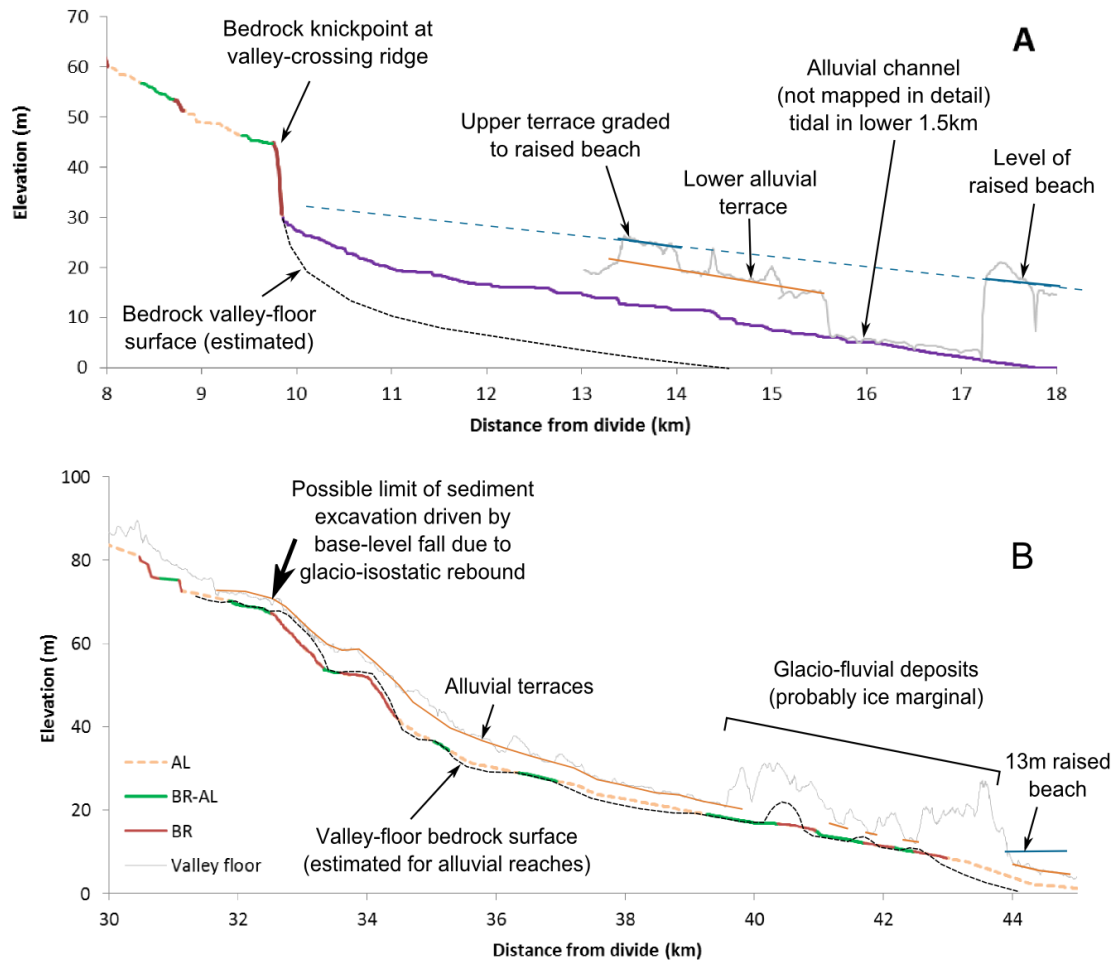
Figure 3-8. Glacio-isostatic uplift effects indicated by the relationship between the lower sections of the channel long-profile and adjacent terraces. A: River Canaird (similar to the situation in the River Elchaig). B: River Carron: incised bedrock reach at 33km from divide, with thin sediment cover on surrounding valley floor, is likely to have acted as a local base-level control, restricting upstream incision into sediments until after the KP was incised.

3.3.2   Distribution of bedrock channels

The controls on the distributions of channel types are assessed in this section by testing whether the alluvial to bedrock channel transition can be explained by a critical slope threshold (cf. Massong and Montgomery, 2000).

3.3.2.1   Modern distribution of channel types

Bedrock channels occupy 16 – 29% of the total length of the study streams and mixed bedrock-alluvial channels account for 12 – 20% of the stream length (Table 3-3). The downstream distributions of channel types are shown in Figure 3-9. Bedrock reaches are located predominantly in the steeper sections of the channels where stream power is higher. Two-sample t-tests show that the mean reach slope and stream power of bedrock channels are significantly greater than those of alluvial channels (p<0.001, Table 3-4).

Mean slopes and stream power values for bedrock-alluvial channels are significantly lower than for bedrock channels ($p < 0.001$), but not significantly different to those for alluvial channels ($p > 0.05$).
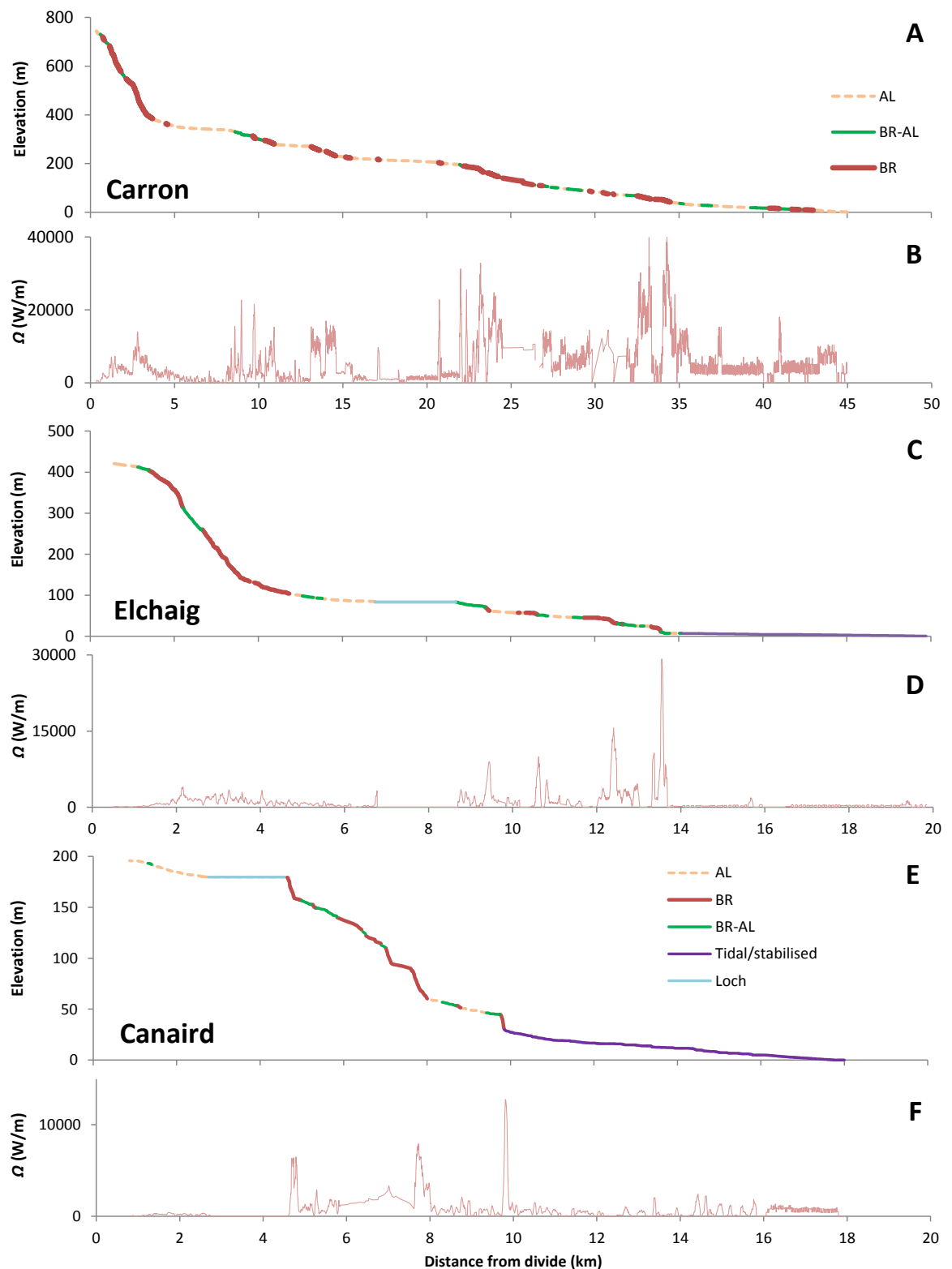
Figure 3-9.   Long-profiles with channel type distributions for the rivers Carron (A), Elchaig (C) and Canaird (E). Key to reach types in plot A. Total stream power (Ω) versus distance from the drainage divide for the respective rivers (B, D and F). Note the different horizontal and vertical scales for study rivers.

Total stream length	Carron	Elchaig	Canaird	Combined
% AL	51.3	60.1	71.9	57.5
% BR-AL	19.9	16.2	12.0	17.5
% BR	28.8	23.7	16.1	25.1
Total length (km)	44.7	19.5	17.1	81.3
Number of reaches	82	48*	24*	154

Table 3-3.   Proportion of the main channel types in the study streams as fractions of the total stream length (i.e. including lower alluvial reaches of the rivers Elchaig and Canaird that were not mapped in detail). AL=Alluvial, BR-AL= mixed bedrock-alluvial, BR=bedrock. *Lower alluvial section (not mapped) is represented as one reach.

Channel type	n	Slope			Stream power (W/m)		
		Mean	SE	t-test p	Mean	SE	t-test p
Modern AL	46	0.010	0.002	<0.001	235	34	<0.001
Modern BR	55	0.058	0.007		706	84	
Modern BR-AL	35	0.018	0.004	0.056 (vs AL) <0.001 (vs BR)	313	37	0.129 (vs AL) <0.001 (vs BR)

Table 3-4.   Mean slope and total stream power data for modern channel types.
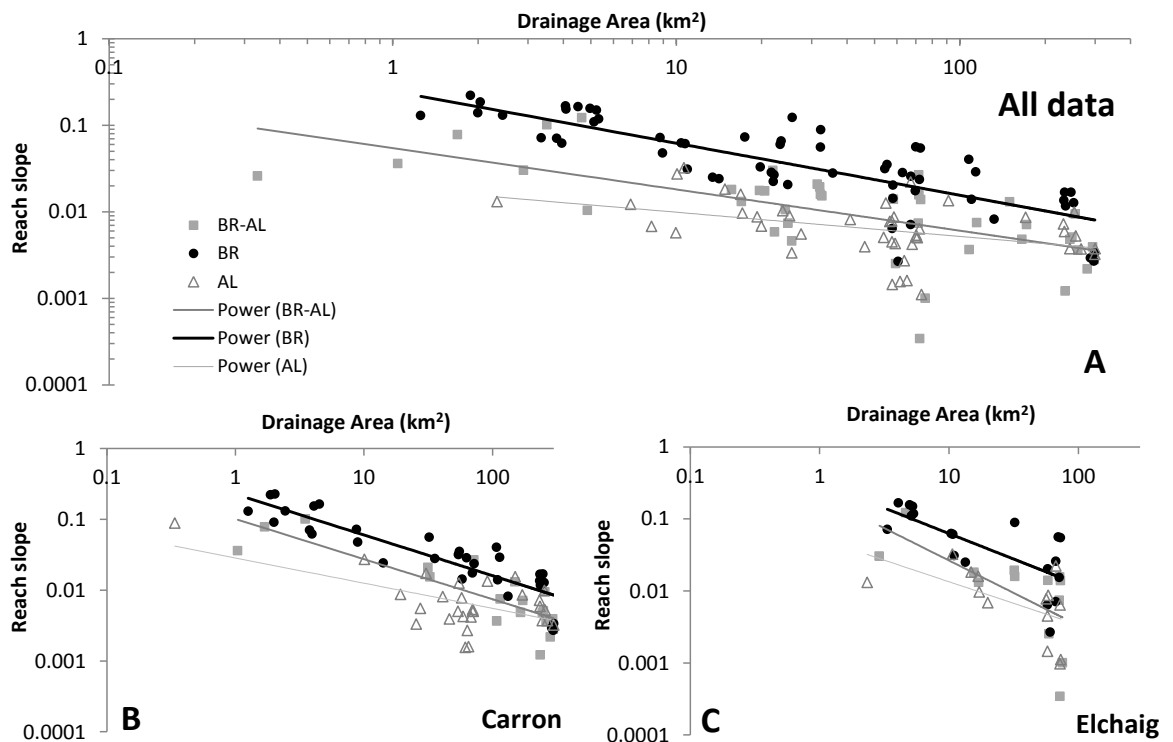
Figure 3-10.   Reach slope versus drainage area (logarithmic axes) for A) all reaches from the three surveyed channels, B) all reaches from the River Carron, C) all reaches from the River Elchaig. Data are classified according to reach type (legend in plot A), with power law regressions (significant at p<0.05). Alluvial and bedrock-alluvial channels include 'peat' and 'boulder' channel subgroups (Table 2-3). River Canaird regressions are not shown due to insufficient data.

Bedrock and alluvial channels are strongly segregated in slope-area space (Figure 3-10). ANCOVA indicates that the exponents on the S-A regressions for bedrock (-0.60) and alluvial (-0.30) channels are significantly different ($p<0.05$) for combined data and for data from the River Carron. Only the coefficients of the relationships are significantly different for data from the River Elchaig (Appendix A3-2). The exponent on the S-A regression for bedrock-alluvial channels (-0.48) is not statistically different from those for bedrock or alluvial channels ($p>0.05$), but the coefficient is significantly different ($p<0.05$). As for the 2-sample t-test results, the slope-area values for mixed bedrock-alluvial channels fall in between those of alluvial and bedrock channels.

Canonical discriminant analysis was used to derive a function describing the critical slope threshold (S_c) for the transition between alluvial and bedrock channel types (Figure 3-11). The critical slope function correctly identifies 93% of the modern alluvial and bedrock reaches. BR-AL channels form at total stream power values that are intermediate between bedrock and alluvial channel end-members. The slope-area distribution of mixed BR-AL channels suggests that they are forming close to the critical slope threshold, although the BR-AL regression has a slightly higher exponent (0.48 ± 0.09) than the critical slope function (Figure 3-11). The implications of the critical slope function, comparison with data from other regions, and potential controls on the critical slope are discussed in section 3.4.1.

Assessment of alluvial and bedrock reaches that are misclassified by the discriminant function indicates that local variations in q_s and q_c probably have a minor influence on channel distribution. Misclassified alluvial reaches (4) are either short reaches (<100m in length) between steeper bedrock channels, or they have minor bedrock outcrops (i.e. they are AL-BR reaches). The latter type are likely to be close to the threshold slope, hence misclassification may be due to natural variability or errors in slope. Misclassification of short alluvial reaches proximal to gorges could reflect local increases in the sediment grain-size; large, angular boulders and rock slabs are commonly deposited at the gorge outlet as the channel widens and q_c falls. Short alluvial reaches are also prone to errors in slope due to errors in the DTM elevation in confined valley-floor settings (cf. Massong and Montgomery, 2000). The four misclassified bedrock reaches are short bedrock gorges formed at minor riegels. These reaches may also be affected by errors in slope where the DTM 'misses' the gorge, but the narrow gorges may also be responsible for local increases in stream power (therefore q_c) resulting in the formation of bedrock channels despite moderate channel slopes.

The S_c derived in this study shows a good fit to Addy's (2010) dataset of 42 mountain-alluvial and 4 bedrock channels from the Cairngorm Mountains in northeast Scotland (Figure 2-1). Despite the Cairngorms being characterised by abundant granite and comparatively lower rainfall than the NW Highlands, 87% of channels were correctly discriminated by the S_c function (Figure 3-12), suggesting that such an approach is regionally applicable and that variations in sediment flux, grain-size or discharge across the Scottish Highlands have only minor influence on the S_c.
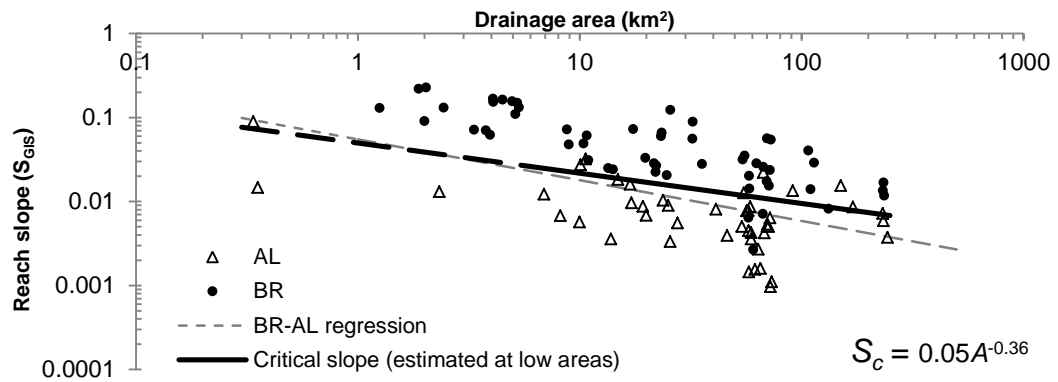
Figure 3-11.   Log-log plot of reach slope (m/m) versus drainage area for modern bedrock (filled circles) and alluvial (open triangles) channels in the NW Highlands; data from the lower 12km of River Carron was excluded due to possible influence of glacio-isostatic uplift. Critcal slope function (S_c) for alluvial to bedrock channel transition (solid black line, dashed where estimated). Bedrock-alluvial regression for NW Highland data shown for reference (dashed grey line, S=0.055A$^{-0.48}$).
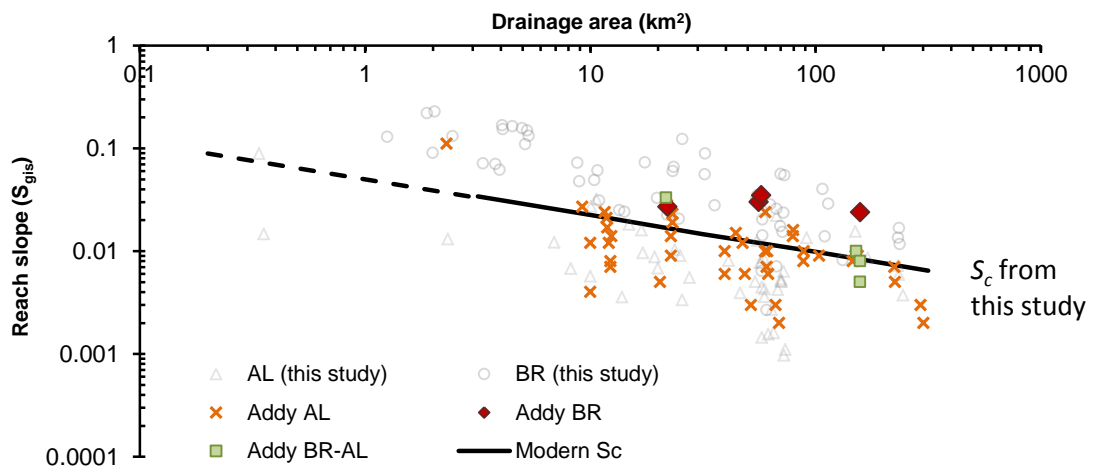
Figure 3-12.   Log-log plot of slope versus area for data from Addy (2010) for mountain alluvial (orange crosses), bedrock (dark red diamonds) and mixed bedrock-alluvial (light green squares) channels in the Cairngorm Mountains, northeast Scotland (Figure 2-1). Critical slope function (black line) is that derived from the data in this study (modern), with bedrock (pale pink circles) and alluvial channels (pale orange triangles) shown for reference.

The results indicate that bedrock reaches form where channels are steep and therefore have high stream power (high q_c). Variations in channel slope, relative to the S_c, thus strongly control the location of bedrock reaches in the study rivers. Bedrock channels are found

predominantly on the headwalls of upland glacial troughs and corries and at steep knickzones and knickpoints formed where channels inherit glacial or glacio-lithological riegels in the mid to lower reaches of the trunk valleys (the 'variable domain' in Figure 3-4). Where drainage divides have been substantially lowered by glacial breaching, bedrock channels are absent in the catchment headwaters. The implications of the glacially conditioned landscape form for fluvial processes in postglacial channels are discussed in section 3.4.2.

3.3.2.2   Early Holocene distribution of channel types

The distribution of channel types in the early Holocene (i.e. the early postglacial) was reconstructed on the basis of the distribution of alluvial terraces (section 3.2.3). The proportion of bedrock channels in the surveyed streams has increased over the Holocene, with bedrock and bedrock-alluvial channels accounting for 25% and 18% of the modern stream length, but only ~15% and 8% of the length of 'Early Holocene' streams respectively (Table 3-5). The increase in bedrock and bedrock-alluvial channels has been predominantly in the mid to lower sections of the mapped streams (Figure 3-13). Changes of channel type in the lower Carron, 33 – 45 km from the divide (Figure 3-13), may be related to entrenchment in response to base-level fall (section 3.3.1.4) and these reaches are excluded from further analysis. Potential controls on the distribution of channel types, and reasons for the temporal changes in channel distribution are explored below through comparison of channel *S-A* distributions and critical slope functions for 'Early Holocene' and modern channels.

'Early Holocene'	Carron	Elchaig	Canaird	Combined
% AL	78.6	67.2	85.6	77.4
% BR-AL	6.4	14.9	2.0	8.0
% BR	15.0	17.9	12.4	14.6
Total length (km)	44.7	19.5	17.1	81.3
Number of reaches	82	48	24	154

Table 3-5.   Proportion of the main channel types in the reconstructed 'Early Holocene' streams as fractions of the total stream length.
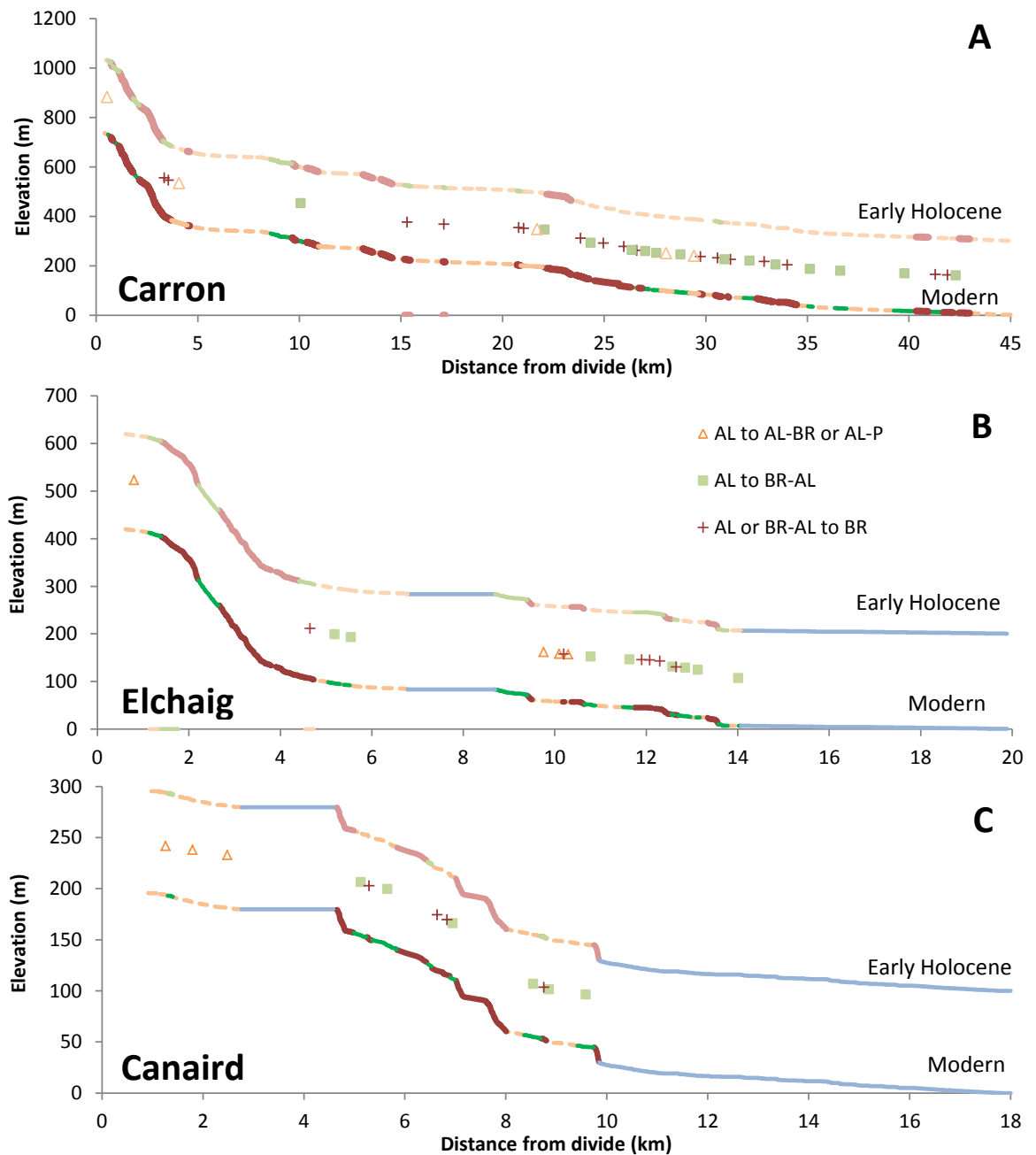
Figure 3-13. **Comparison of the distribution of channel types in the modern channel (lower profile) and for reconstructed the 'Early Holocene' channel (upper profile). Reach types are coloured as for figure 3-9. For display purposes, the elevations are offset (by 300m for the River Carron (A), 200m for the River Elchaig (B) and 100m for the River Canaird (C)). Symbols mark locations of changes in channel type, key to symbols in plot B. Note different vertical and horizontal scales for each stream.**

AL or BR-AL to BR channel transitions could result from local increases in channel slope driven by incisional lowering or KP retreat. The importance of channel slope changes since the early Holocene was assessed by comparing 'before' and 'after' slopes for the sixty 'switch' reaches using a paired sample t-test. The mean of the difference between 'before' and 'after' channel slopes (-0.0036 ± 0.0053 at 95% confidence) is not significantly different from zero and mean channel slopes for 'before' and 'after' groups were also not significantly different (p=0.18). These findings indicate that the transition from AL or BR-

AL to BR channels was not generally due to an increase in channel gradient. In other words, local steepening of channels due to knickpoint incision has had only a minor influence, if any, on the distribution of channel types. However, possible errors in the DTM-derived channel slopes for both modern and past channels may mean that subtle differences in channel slope cannot be distinguished.

Slope-area data for 'Early Holocene' and modern channels are compared in Figure 3-14. The power law slope-area regressions for Early Holocene BR, AL and BR-AL channels tend to have lower exponents than their modern counterparts (Figure 3-14 C). However, these relationships are not significantly different due to relatively high variability in the data, especially for AL and BR-AL channels (ANCOVA p>0.05).

Similar to the pattern seen in the power law regressions, the critical slope (for the AL to BR transition) calculated for 'Early Holocene' channels, is higher for a given drainage area than the equivalent function for modern channels and has a lower exponent (0.27 for early Holocene versus 0.36 for modern channels) (Figure 3-14 A). The Early Holocene critical slope function correctly discriminates 95% of the reconstructed 'Early Holocene' BR and AL channels. These results indicate that the maximum slope of 'Early Holocene' alluvial channels was higher than that in modern channels.

3.3.2.3   Summary of bedrock channel distribution results

- Bedrock channels are steeper than are alluvial channels and have higher stream power.
- The proportion of bedrock channels in the surveyed streams has increased from ~15 % to 25% over the Holocene, with most of the increase in the mid to lower parts of the catchments.
- Critical slope thresholds for the alluvial to bedrock channel transition, where $q_c=q_s$, have been estimated from the slope-area distributions of the two channel types for modern and 'Early Holocene' channels. These critical slope thresholds correctly predict the channel type of 89 – 93% of all reaches.
- Local increases in sediment grain-size or narrow channels may be responsible for isolated reaches that deviate from the predicted channel type.
- In early postglacial times alluvial channels were maintained at higher maximum slopes than that observed in modern channels.
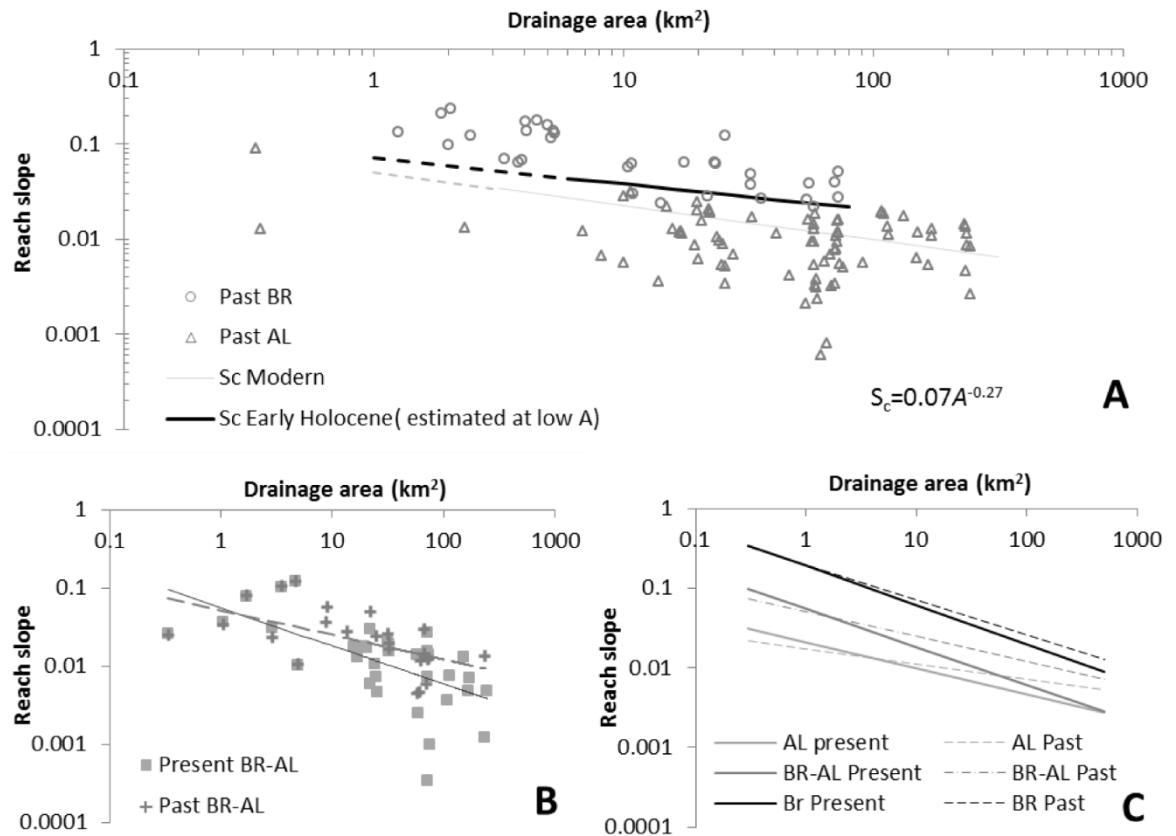
Figure 3-14. **Slope versus area plots for data from present channels and reconstructed 'Early Holocene' channels ("Past"). A) 'Early Holocene' bedrock (BR) and alluvial (AL) channel data with canonical discriminant function (S_c) for all data excluding the lower Carron (black line). The modern canonical discriminant function is shown for comparison (grey line). B) bedrock-alluvial (BR-AL) channel data for 'Early Holocene' and modern alluvial channels (key in plot) with power law regressions for modern data (solid line) and early Holocene data (dashed line), C) comparison of regressions for each channel type, past and present, all regressions are significant ($p < 0.05$).**

3.4   Discussion

These results show that the long profiles of NW Highland rivers remain strongly constrained by inherited glacial valley floor slopes. The irregular forms of the long profiles are reflected in strong spatial variations in stream power and alternations between bedrock and alluvial reaches. The distribution of these two channel types is determined by the regional critical slope threshold for the alluvial to bedrock transition and the local channel slope and sediment characteristics that determine the transport capacity of a particular reach. These regional and local controls on channel type are discussed below.

The finding that fluvial processes are dominant in the study streams despite steep channel slopes contrasts with observations from other non-glaciated and postglacial settings (e.g. Montgomery and Buffington, 1997; Brardinoni and Hassan, 2006). The relative roles of fluvial and debris flow processes in the NW Highlands are discussed in section 3.4.3.

3.4.1 The critical slope threshold: regional controls on channel distribution

The critical slope threshold (S_c) for the alluvial-bedrock channel transition is effectively the channel slope at which the transport capacity (q_c) equals the sediment supply (q_s), thus factors such as the discharge regime (i.e. discharge relative to drainage area), sediment supply rate and the sediment grain-size, may all be expected to influence the value of S_c.

In Figure 3-15 and Table 3-6, critical slope functions from this study are compared with published data for streams Washington State (NW USA) (Montgomery et al., 1996; Massong and Montgomery, 2000). The differences between S_c values for modern and early Holocene channels in the NW Highlands, and between the NW Highlands and catchments in the NW USA, are discussed with respect to potential controls on the critical slope.
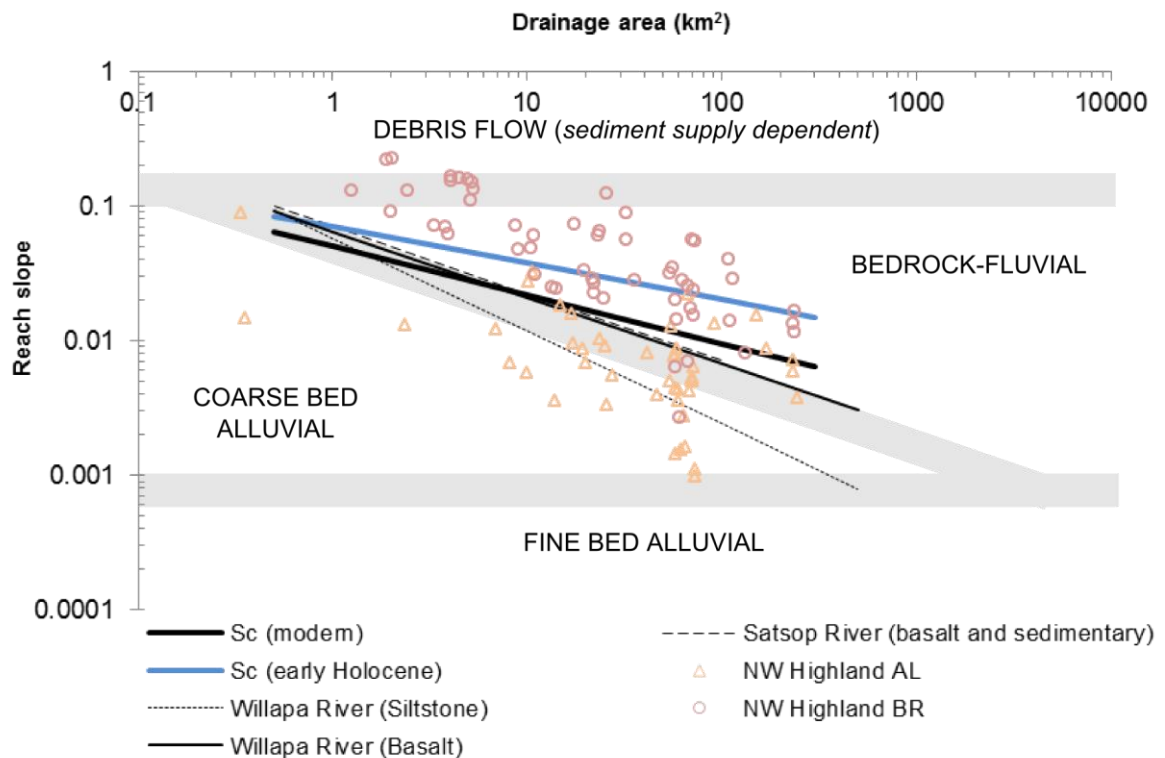
Figure 3-15. **Slope-area process domains after Sklar and Dietrich (1998), transitions between domains are marked by grey bands. Critical slope functions (S_c) for modern channels and 'Early Holocene' channels from this study, and for the Satsop River (Montgomery et al., 1996), and two regions of the Willapa River with different lithological types (Massong and Montgomery, 2000). Regression equations shown in Table 3-6. Modern bedrock and alluvial channel data from this study shown for reference.**

Statistical procedures for comparing the exponents and coefficients of critical slope functions are complex and have not been attempted here and it should be noted that differences between the relationships have not been statistically verified. The following

discussion is intended to highlight potential controls on S_c as a basis for generating hypotheses that can inform on-going research. Development of statistical tests for comparing discriminant functions is a priority for further research.

Region/catchment	Data sub-group	Critical slope function
NW Highlands	Modern	$0.05A^{-0.36}$
	Early Holocene	$0.07A^{-0.27}$
Willapa River, NW USA	Basalt	$0.07A^{-0.49}$
	Siltstone	$0.06A^{-0.69}$
Satsop River, NW USA	Mixed basalt and siltstone	$0.08A^{-0.52}$

Table 3-6. Critical slope functions for modern and 'Early Holocene' channels in the NW Scottish Highlands (this study), note drainage area (A) measured in km^2. Critical slope functions for the Willapa and Satsop rivers are modified from Montgomery et al. (1996) and Massong and Montgomery (2000) from original functions derived for A in m^2.

3.4.1.1   Modern vs 'Early Holocene' critical slope thresholds

The distribution of alluvial terrace deposits flanking bedrock channels indicates that there have been long-term changes in the distribution of channel types in NW Highland rivers since deglaciation. A compelling explanation for this change involves a decrease in the critical slope threshold for the alluvial to bedrock channel transition over time. A higher S_c in the early Holocene may be due to either; i) lower discharge, ii) higher sediment flux, or iii) coarser-grained sediment.

In the NW Highlands, temperate conditions similar to today were rapidly established at the close of the Younger Dryas glaciation, and it is unlikely that discharge was considerably different in the early Holocene than it is at present (Maizels and Aitken, 1991; Brooks and Birks, 2000; Ballantyne, 2008). Modern bed material in the NW Highland channels is relatively coarse-grained throughout the catchments; field observations indicate predominantly gravel to boulder-grade sediment (20 – 1000 mm) with estimated average grain sizes of 50 – 150 mm. Much of this material is sourced from reworking of paraglacial debris fans and talus accumulations, rock falls in confined gorges and reworking of glacio-fluvial and alluvial terraces. As the resistant metasedimentary rocks in the study area weather slowly, the size of bed material in modern channels is unlikely to be considerably different from that in early Holocene channels, it may even be coarser if fine sediment was mobilised preferentially during the Holocene.

As discussed in section 2.2.3, the early Holocene in the NW Highlands was probably characterised by an elevated paraglacial sediment flux regime in rivers (cf. Ballantyne, 2008). A long-term decline in sediment flux is thus the most likely cause of the difference in S_c between modern and 'Early Holocene' channels in the study catchments. This postglacial decline in S_c reflects a long-term change in the balance between sediment flux and transport capacity which has resulted in the entrenchment of many alluvial channels and an increase in the proportion of bedrock reaches over time.

3.4.1.2   Regional variations in the critical slope

Comparison of the S_c functions of Montgomery et al. (1996) and Massong and Montgomery (2000) with the NW Highlands data indicates that the S_c coefficients are all relatively similar (0.05 – 0.08), but there is considerable variation in the exponents ($(h - m/n)$ in Eq 3.3), with a value of 0.36 in modern NW Highland channels compared to 0.49 – 0.69 for those in Washington (Figure 3-15 and Table 3-6). As for the temporal variation in S_c, regional differences in discharge regime, sediment flux and sediment grain size may be responsible for the regional differences in S_c (Massong and Montgomery, 2000).

Comparing the critical slope functions for the Satsop and Willapa Rivers, Massong and Montgomery (2000) concluded that different grain-size distributions of channel sediment are the most likely cause of differences in the S_c exponents. They suggest that lower S_c exponents (0.49 and 0.52) (i.e. higher S_c values) for the Satsop River and basalt-dominated section of the Willapa River are due to coarse-grained sediment (median grain-size of 33 – 68 mm), whereas the higher S_c exponent (0.69) for sections of the Willapa River underlain by siltstone is due to finer sediment (median grain-size 14 – 34 mm). Furthermore, they link differences in sediment grain-size to lithology, with more resistant igneous rocks forming the bulk of the coarser sediment in the Satsop and basalt-dominated Willapa rivers and softer sedimentary rocks forming the smaller clasts of the siltstone-dominated portions of the Willapa River.

The S_c exponent of 0.36 for modern NW Highland channels is lower than values for the Washington channels (i.e. the critical slope is higher) (Figure 3-15, Table 3-6). Both Scotland and the NW USA have temperate maritime climate regimes and receive up to 3 m of annual rainfall. As the studies were conducted in catchments with similar drainage area ranges (0.1 – 400 km^2), it is unlikely that differences in discharge regime are responsible

for the lower S_c exponent in the NW Highlands. Similarly, higher sediment flux is unlikely to be the cause of the higher S_c as sediment flux rates in modern NW Highland channels are relatively low. But, as noted above, sediment throughout the study channels is relatively coarse, with estimated average grain sizes of $50 - 150$ mm. A lower S_c exponent (higher S_c value) for NW Highland channels due to coarse-grained bed material is consistent with the conclusion of Massong and Montgomery (2000) that the S_c exponent is inversely related to grain-size (Figure 3-16). Massong and Montgomery (2000) also suggest that differences in grain-size between their study catchments are primarily due to differences in bedrock lithology, with smaller grained sediment in catchments underlain by mudstone relative to streams in a basaltic terrain. The resistant metamorphic bedrock of the NW Highlands may be responsible for the coarse-grained sediment in the study channels, potentially supporting the conclusions of Massong and Montgomery (2000). However, it should be noted that grain-size may also depend on the location within the catchment, the sediment supply rate and channel slope (e.g. Sternberg, 1875; Hoey and Bluck, 1999; Chatanantavet et al., 2010).
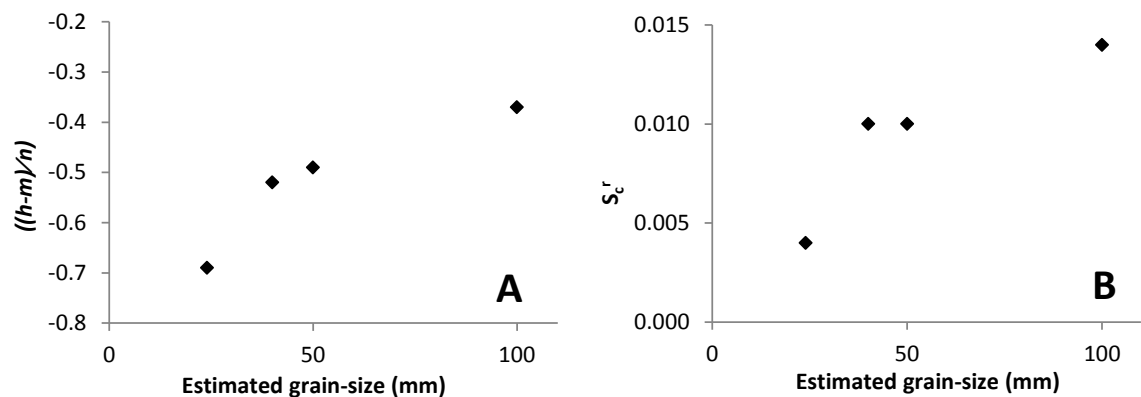
Figure 3-16.   Plots of estimated median grain-size for Willapa River (siltstone) (24mm), Willapa River (basalt) (50mm), Satsop River (40mm) and NW Highland rivers (100mm) versus (A) the critical slope exponent, $(h - m/n)$ from eq. 3.3 and (B) a reference critical slope (S_c^r) calculated at drainage area of 50 km^2. Grain-size estimates based on ranges of median grain sizes given in Massong and Montgomery (2000) – Willapa River, Collins and Dunne (1989) – Satsop River, and Jansen et al. (2010) and Addy et al. (2011) for the Scottish Highlands.

3.4.2   Local controls on channel type

The strong segregation of bedrock and alluvial channels with respect to channel slope and drainage area suggests that catchment-scale approximations of sediment flux rates (where q_s~A) and transport capacity (where q_c~Ω) are relatively robust. However, small-scale variations in transport capacity, sediment supply and grain-size may locally influence the channel morphology (Montgomery et al., 1996; Massong and Montgomery, 2000). In the

NW Highlands, variations in channel width, and the distribution of 'point' sediment sources may result in local variations in channel type.

In chapter 4, the width of both alluvial and bedrock channels is found to be strongly dependent on discharge (drainage area) which is consistent with a strong stream power control on q_c. However, ~20% of the variation in bedrock channel widths is not related to drainage area and lithological control and inheritance of pre-existing gorges may be responsible for relatively narrow channels in some areas. Of the four bedrock reaches that fall below the critical slope threshold, (i.e. are expected to be alluvial for their slope and area conditions), two are slightly narrow for their drainage area (*w-A* regression residuals of -2.1 and -1.2, cf. Figure 4-10) suggesting that narrow channels, and therefore higher q_c, may be responsible for local variations in the critical slope. The widths of the remaining two 'low slope' bedrock channels are consistent with those expected for their drainage area and it is possible that these reaches may be affected by errors in the DTM-derived channel slope. Four alluvial channels fall above the critical slope threshold, i.e. they are expected to be bedrock given their slope and drainage area. These are all short reaches and may also be affected by slope errors. However, two of these 'high-slope' alluvial reaches are located at the downstream end of gorges and are dominated by coarse boulder-grade bed material consisting of angular blocks sourced from the gorge upstream. It appears that this coarse sediment has been deposited due to a reduction in q_c where the channel widens at the gorge outlet.

3.4.3   Channel form and process domains

3.4.3.1   Debris flows and channel form

Debris flow processes are commonly found to dominate in channels with slopes steeper than ~0.1 – 0.2 m/m, especially in catchment headwaters (colluvial channels) (e.g. Montgomery and Foufoula-Georgiou, 1993; Sklar and Dietrich, 1998). In postglacial streams, debris flows have also been found to be significant sediment sources to channels formed at hanging valleys in British Columbia (Brardinoni and Hassan, 2006). By contrast debris flows appear to have a limited impact on NW Highland streams; field observations indicate that fluvial processes are dominant throughout the main-stem study channels, including in steep reaches on valley headwalls and riegels (Figure 3-15).

Headwater channels with drainage areas < 1 km^2 were not assessed in this study as main stream channels were mapped to small 'source' lakes located in corries or breached divides in all three study catchments. The presence of these lakes in the catchment headwaters suggests that source colluvial channels are likely to have a negligible impact on the channel system downstream. The lack of debris flow activity along the main stem channels, even in the steep headwall sections of the upper Elchaig and Carron and middle Canaird, is likely to be due to generally low sediment availability. These steep channels are formed in resistant bedrock and surrounding hillslopes have little drift cover or regolith and are stabilised by peat and vegetation (e.g. Ballantyne, 1986). Thus even during intense rainfall events, little sediment is mobilised from hillslopes and sediment-starved conditions prevail in modern channels. However, relict gully systems on till-mantled hillslopes in the upper Elchaig and Carron (cf. Figure 7-7), and relict debris fans from steep tributaries in all of the study catchments, suggest that debris flows may have sourced sediment directly to the channels in the past.

Curry (1999) found that gully systems on till-mantled slopes in Norway begin to form immediately after deglaciation, and frequent debris flows drive rapid incision of gullies into the glacial drift (c. 80 – 150 mm/yr). Till-slope gullies stabilise once the drift has been incised to bedrock, with vegetation growth further stabilising the gully form. In regions with thin till deposits, such as the NW Highlands, gully activity on till slopes is thus likely to be short lived with gullies stabilising within 10 – 100 years of deglaciation (cf. Curry, 1999, 2000). Relict till-slope gullies are confined to the 'alpine' valleys of the upper Elchaig and Carron catchments. Glacial deposits in 'areally-scoured' terrains are sparse and extremely thin (Rea and Evans, 1996), which has prevented the development of gully systems in the Canaird catchment (e.g. Ballantyne, 1986).

Debris fans associated with steep tributary streams and large bedrock gullies in the study catchments have not been dated, but evidence from other areas of the Scottish Highlands indicates that debris fan formation occurred largely in the early Holocene, although many have remained periodically active (Brazier et al., 1988; Curry, 2000; Ballantyne, 2008). Most debris fans in the study catchments have been deposited at the foot of the valley walls, indicating that, even when active, they were not directly coupled to the main channel. However, a debris fan deposit (now relict) appears to have locally diverted the River Canaird at the outlet of Loch a' Chroisg (Figure 2-7), and large debris fans in the narrow valleys of the upper Carron and Elchaig are also likely to have sourced sediment directly to the main stream when active.

Relict gullies and debris fans suggest that debris flow activity may have contributed to stronger channel-hillslope coupling and higher early postglacial sediment flux conditions in the study rivers. However, the long term impact of debris flows on the main stem channel appears to be extremely limited, with no lasting influence on the channel morphology. Channel geometry too appears to be unaffected by debris flow activity; the strong hydraulic scaling identified in chapter 4 suggests that the fluvial system is well adjusted to the Holocene discharge regime and channel widening due to debris flow scour is not seen (cf. Montgomery and Gran, 2001).

3.4.3.2   Glacial conditioning and bedrock channel distribution

Channel slope remains strongly controlled by glacial inheritance at catchment to reach scales. Postglacial channel incision has not been sufficient to smooth inherited knickpoints and thus channel slope adjustments are incomplete and are generally restricted to sub-reach scales (cf. chapter 6). The extent and distribution of bedrock channels in the NW Highlands thus remains strongly controlled by the inheritance of glacially-conditioned valley-floor slopes.

In catchments affected by divide breaching, dramatic reductions in the maximum elevation of trunk streams, and the removal of steep headwaters, lowers the channel steepness and concavity. Bedrock channels are less extensive in these streams and they lack bedrock channels in their headwaters (domain I, Figure 3-4). This distribution has major implications for sediment supply regimes, and may influence the timescale of landscape response to deglaciation, as well as the sensitivity of the channel system to short-term climatic perturbations (Harvey 2007). In the hyper-concave upper segments of Alpine-type catchments (domain II, Figure 3-4), bedrock channels dominate the steep headwater section, with alluvial channels and over-deepened lake basins in the lower half of the domain. Low discharge in the bedrock reaches of the cirque headwall mean that stream power is low despite high channel slopes (Figure 3-9), potentially restricting fluvial incision in these reaches. The variable slopes of domain III, in the mid to lower parts of the study catchments, mean that domain III channels are the most responsive to declining paraglacial sediment flux, and may also have the highest potential for postglacial channel adjustment through fluvial bedrock incision. The entrenchment of bedrock reaches in the study channels is assessed in chapter 6. The influence of glacial-conditioning and the

distribution of channel types on the degree of channel-hillslope and reach-reach coupling in the study rivers is discussed in section 7.3.

3.5   Conclusions and implications

The distribution of bedrock channels in the NW Highlands is strongly controlled by the inheritance of glacially-conditioned valley floor slopes and sediment supply. Breaching of drainage divides and the formation of riegels by glacial erosion are major determinants of the extent and distribution of bedrock channels in postglacial rivers. The supply of coarse-grained paraglacial sediment resulted in a high critical slope threshold for the alluvial to bedrock channel transition following deglaciation. This critical slope threshold has declined over the Holocene, due to declining paraglacial sediment flux, resulting in a long-term increase in the proportion of bedrock channels. The switching from depositional alluvial to erosional bedrock regimes has important consequences for the development of channel geometry (chapter 4), the formation of strath terraces and the timing of onset of fluvial incision in NW Highland rivers (chapter 5), and the degree of postglacial channel entrenchment (chapter 6).

Chapter 4

Form of postglacial bedrock channels

4.1 Introduction

4.1.1 Context

In addition to the channel slope, the width and depth of streams are strong controls on the amount and distribution of shear stress (or stream power) exerted by the flow against the channel banks and bed. The channel slope, width and depth, collectively determining the channel 'geometry', may thus influence the distribution of bedrock channels by controlling sediment transport capacity (chapter 3), and fluvial incision rates by controlling the rate of bedrock detachment (chapter 5). In landscapes with spatially and temporally uniform rates of tectonic uplift, bedrock channel geometry is thought to adjust to balance the fluvial incision rate with the long-term uplift rate and the stable configuration of channel slope, width and depth is thought to depend on discharge, sediment flux and substrate resistance (e.g. Whipple, 2004; Turowski et al., 2007; Yanites and Tucker, 2010). In landscapes responding transiently to changes in climate or tectonic regime, inheritance of channel widths and slopes configured under different conditions adds more complexity to the potential controls on channel geometry. In these areas, the timescale over which channels adjust to new conditions may control the degree to which the channel geometry reflects the current discharge regime, sediment flux and uplift rate.

In the post-orogenic, postglacial terrain of the NW Highlands, the inheritance of glacially-conditioned valley floor slopes and spatially and temporally variable sediment flux, as well as resistant metasedimentary bedrock, may give rise to spatially and temporally variable bedrock channel geometry. Analysis of the geometry of the three study rivers, presented in this chapter, is used to assess the degree to which channel geometry is adjusted to the postglacial discharge regime. The results highlight key controls on channel form, and can be used to infer relative rates of adjustment of channel slope, width and depth following deglaciation.

4.1.2   Controls on channel geometry: numerical frameworks

Bedrock channel geometry is accounted for in stream power fluvial incision models by assuming empirically-based power law relationships between the main channel geometry components and discharge or drainage area (e.g. Howard et al., 1994),

$$S = k_s A^{-\theta}$$ Eq 3.4

$$w = bA^c \text{ or } w = b'Q^{c'}$$ Eq 4.1a and 4.1b

$$d = eA^f \text{ or } d = e'Q^{f'}$$ Eq 4.2a and 4.2b

where w is channel width, d is channel depth, A is drainage area and Q is discharge. Coefficients b, b', e and e', and exponents c, c', f and f' are empirically determined (equation 3.4 is discussed in section 3.1.2.2). Values for the width scaling exponent, c or c' are commonly assumed to be 0.5 for bedrock channels, a value derived from empirical assessment of gravel-bed rivers (e.g. Leopold and Maddock, 1953; Bray, 1982; Miller, 2005), and supported by a study of bedrock channel width by Montgomery and Gran (2001). In simple stream power models, channel depth is neglected on the basis of the implicit assumption that the width to depth (w/d) ratio is constant for bedrock channels (e.g. Howard et al., 1994; Brocard and van der Beek, 2006; Attal et al., 2008). But, a number of recent developments in numerical modelling, supported by empirical data, suggest that these assumptions are likely to be too simplistic for bedrock channels.

Modelling of detachment-limited bedrock channel erosion indicates that channel width may depend on slope (e.g. Finnegan et al., 2005; Wobus, 2006; Attal et al., 2008), and is supported by field evidence from rivers experiencing spatial or temporal variations in uplift rate (e.g. Whittaker et al., 2007). Empirical equations relating channel width to discharge and slope have been derived,

$$w = k_{wf}Q^{0.38}S^{-0.19} \qquad\qquad \text{Eq 4.3 (after Finnegan et al., 2005)}$$

$$w = k_{ww}Q^{0.38}S^{-0.44} \qquad\qquad \text{Eq 4.4 (after Whittaker et al. 2007)}$$

where k_{wf} and k_{ww} are constants. These relationships are reviewed and discussed extensively by Attal et al. (2008). But field observations of channel slope control on width in areas affected by spatially and temporally variable uplift rates are not all in agreement (e.g. Whipple, 2004). Furthermore, published data suggest that the w/d ratio may not be constant, but depends on discharge and channel slope, contrary to the predictions, or assumptions, of detachment-limited bedrock channel geometry models (e.g. Finnegan et al., 2005; Wobus, 2006). These discrepancies have led to the suggestion that sediment flux may play a key role in constraining channel geometry (Whipple, 2004; Turowski et al., 2007; Yanites and Tucker, 2010). Physical modelling supports this suggestion, indicating that declining sediment flux drives channel narrowing by focusing incision on a smaller area of the channel bed, whilst higher sediment flux drives channel widening as sediment cover limits incision of the bed and increases lateral erosion of the channel banks (Finnegan et al., 2007; Johnson and Whipple, 2010).

Field observations also indicate that substrate resistance may influence channel geometry. Montgomery and Gran (2001) observed that channels may narrow rather than steepen in resistant bedrock relative to softer sedimentary bedrock or alluvium, but an assessment of worldwide channel geometry data by Wohl and David (2008) found no dependence of channel width on substrate resistance. Both studies also indicate that hydraulic scaling relationships of channel widths (Eq 4.1 a and b) for bedrock and gravel-bed alluvial channels are similar, a finding that has led to the suggestion that channel width may be set by bedload flux (Montgomery and Gran, 2001; Whipple, 2004). However, the numerical channel-geometry model of Turowski et al. (2007) suggests the possibility that substrate resistance has an important but non-linear control on channel geometry. Their model predicts a morphological threshold conditioned by the balance between the erosive capacity of the stream and the substrate resistance. At relatively low substrate resistance, channel geometry was found to depend primarily on hydraulic conditions, but for hard substrates channel width decreased with increasing substrate resistance. A comparable morphological threshold was found by Wohl (2004) for transport-limited mountain alluvial streams. In these channels, the development of consistent downstream hydraulic geometry scaling was found to depend on a threshold conditioned by the ratio of stream power to the sediment grain-size.

4.1.3   Postglacial channels: controls on channel geometry development

Glacially conditioned valley-floor slopes (chapter 3) and spatially and temporally variable sediment flux, as well as variations in lithological resistance and postglacial climatic change, are expected to influence the development of scaled channel geometries in postglacial settings. The strong spatial and temporal variability in these factors could prevent the development of strong hydraulic scaling in bedrock channels or prolong the timescale of adjustment following deglaciation. If channel width and depth are poorly scaled with A, or A and S, then the assumptions of hydraulic or A-S scaling underpinning stream power based fluvial incision models will cause them to poorly estimate the transport and erosive capacity of postglacial rivers.

The long-term decline in paraglacial sediment flux characteristic of postglacial landscapes may also offer an opportunity to test the predictions of experimental models in a field setting. The experimental models of Finnegan et al. (2007) and Johnson and Whipple (2010) indicate that bedrock channel narrowing in response to a decline in sediment flux may produce a suite of landforms including inner channels and strath terraces at the channel margins. Strath terraces have been used to quantify vertical erosion rates in bedrock channel systems (Burbank et al., 1996; Leland et al., 1998; Reusser et al., 2006; Jansen et al., 2011). Strath surface exposure ages may also be used to quantify the timing of changes in channel geometry (chapter 5), thus providing a record of temporal changes in the controls on channel form (cf. Hancock and Anderson, 2002). Quantitative assessment of postglacial strath terraces in the Scottish Highlands forms the basis of chapter 5.

4.1.4   NW Highland Rivers: opportunities and research questions

Recent theoretical advances and the on-going development of numerical modelling frameworks are beginning to provide insights into the complex controls on channel geometry and explanations for contrasting field observations of controls on channel width and slope. However, the relative roles of discharge, sediment flux and substrate resistance in determining channel geometry, and the physical processes by which the channel geometry is adjusted to prevailing conditions remain poorly understood (e.g. Tucker and Hancock, 2010). In postglacial landscapes these controls are particularly diverse and may constrain both the stable channel geometry and the potential timescale for adjustment. The

role of channel geometry in determining stream power, and thus the transport and erosive capacity of the stream means that the controls on channel width have fundamental implications for fluvial incision in postglacial channels, and thus the wider landscape response to deglaciation.

In postglacial NW Scotland it has already been shown that bedrock channel slope remains strongly controlled by glacial inheritance (chapter 3; Jansen et al., 2010), but the controls on bedrock channel width and depth remain poorly known. Resistant bedrock lithologies and generally low sediment flux, together with the inheritance of glacially-conditioned valley floor slopes, gives rise to strongly detachment-limited bedrock channels at a wide range of drainage areas (chapter 3). If sufficient erosion has occurred to adjust channel geometry to postglacial conditions these streams provide a key opportunity to test the predictions of numerical models for natural systems characterised by low erosion rates and low sediment flux conditions, especially the potential for substrate control on channel geometry and the importance of substrate-erosion thresholds.

Recent studies indicate that Scottish Highland streams have developed hydraulic scaling regimes over postglacial timescales. Measured channel widths and depths from coarse-grained alluvial mountain streams in the River Dee catchment in the Grampian mountains of northeast Scotland are hydraulically scaled with exponents $c = 0.53$ for *w-A*, and $f = 0.16$ for *d-A* (Addy, 2010; Addy et al., 2011). Jansen et al. (2010) quantified bedrock channel widths in several rivers in the western Scottish Highlands from digital topographic maps, finding that widths conform to hydraulic scaling patterns with exponents (*c*) of 0.14 − 0.65, and that channels developed in resistant quartzite may be narrower than those in other lithologies. However, for a given *A*, they found that channel widths may vary by an order of magnitude. This may be due to the use of digitally-derived channel widths spaced at approximately 10m intervals rather than reach-averaged width values that remove sub-reach scale width variability. A systematic reach-scale assessment of channel geometry in the NW Highlands will provide a more detailed assessment of the controls on channel geometry by addressing three main research questions:

1. Do bedrock channel width and depth in NW Scotland show similar empirical hydraulic scaling regimes to those found in many non-glaciated channels (e.g. $w{\sim}A^{0.5}$). Or, is channel width better described by an *A-S* relationship, as found in transiently adjusting channels and predicted by detachment-limited channel evolution models (e.g. equations 4.3 and 4.4)?

a. Do channel width and slope adjust at similar rates?

2. Is bedrock channel geometry similar to that of coarse-grained alluvial channels?

    a. Do bedrock and alluvial channels have different w-A and/or d-A scaling exponents?

    b. Does bedrock lithology affect bedrock channel w-A or d-A scaling?

3. Do bedrock channels in the NW Highlands show constant *w/d* ratios, or do *w/d* ratios scale with substrate resistance, drainage area and/or slope?

These questions form a hierarchy, with the identification of consistent geometry scaling in bedrock channels of the NW Highlands (question 1) fundamental to the assessment of questions 2 and 3. Channel slope has been considered in detail in chapter 3; this chapter focuses on the cross-sectional channel geometry, i.e. width and depth.

4.2   Data and methods

Channel width and depth measurements were made during the survey of 71 km of main stream along the rivers Canaird, Elchaig and Carron (section 4.2.1). Channel slope and drainage area were quantified for mapped reaches, and individual width and depth measurement points, through topographic analysis of NEXTMap DTM data, as described in section 2.3.3. The hydrological parameters of discharge, stream power, shear stress, and a regional estimate of sediment flux were also calculated from topographic data. The main quantified parameters of the channel geometry, and the terms used to denote them are shown in Figure 4-1.

4.2.1   Field data

A total of 486 width and depth measurements were recorded in the three study streams over a range in drainage area of $0.5 - 300$ km^2. Several width and depth readings were taken, where possible, for each of the 155 reaches surveyed and were used to derive reach-averaged width and depths. The designation of channel reach types and lithological descriptions used in the results section are as outlined in section 2.3.2.

4.2.1.1   Channel width and depth measurements

Channel width and depth measurements were made in the field using an Impulse 200LR laser range finder (Laser Technology Inc.) and measuring pole during June and October 2010 and April 2011. Width and depths were measured at the same locations, at frequent intervals along the channels. The location of individual measurement points, and their spacing were determined by the reach length and the distribution of bed form components associated with the reach morphology.

Reference discharge

All the channel surveys were conducted during low flow conditions in the study channels. As channel width and depth at any point on the river depend on discharge, variations in width and depth can only be assessed by specifying a reference discharge (e.g. Montgomery and Gran, 2001; Wohl and Merritt, 2008). Width and depth measurements were made for both the low flow (LF) (on the day of measurement) and high flow (HF) levels (Figure 4-1). LF widths are not used in subsequent analysis. The HF level is the main reference discharge, and is synonymous with the 'bankfull' stage in alluvial channels. The alluvial 'bankfull' stage is commonly used as a reference discharge in a wide range of fluvial studies because it is associated with a 'formative discharge' and is generally morphologically marked by the strong break-in-slope between an active alluvial channel and its floodplain (e.g. Knighton, 1998). The 'dominant' or 'formative' discharge is considered, in this context, as the flow stage that is largely responsible for determining channel form, roughly equivalent to the $1 - 2$ year return flood (comparable to 'median annual flood, section 2.3.3.3) (e.g. Wolman and Miller, 1960; Knighton, 1998). Bankfull equivalent stages in bedrock channels are more difficult to assess due to the irregular nature of bedrock banks. However, a number of features were used to determine the effective bankfull level in channels with bedrock banks, including the bank geometry, the distribution of lichens and vegetation and the presence of 'wash lines' consisting of debris deposited at the margin of the channel at high flow (Montgomery and Gran, 2001; Wohl and David, 2008; Wohl and Merritt, 2008). The channel widths and depths measured in this work are comparable with data from other published field studies of channel geometry (Montgomery and Gran, 2001; Wohl and David, 2008; Wohl and Merritt, 2008).
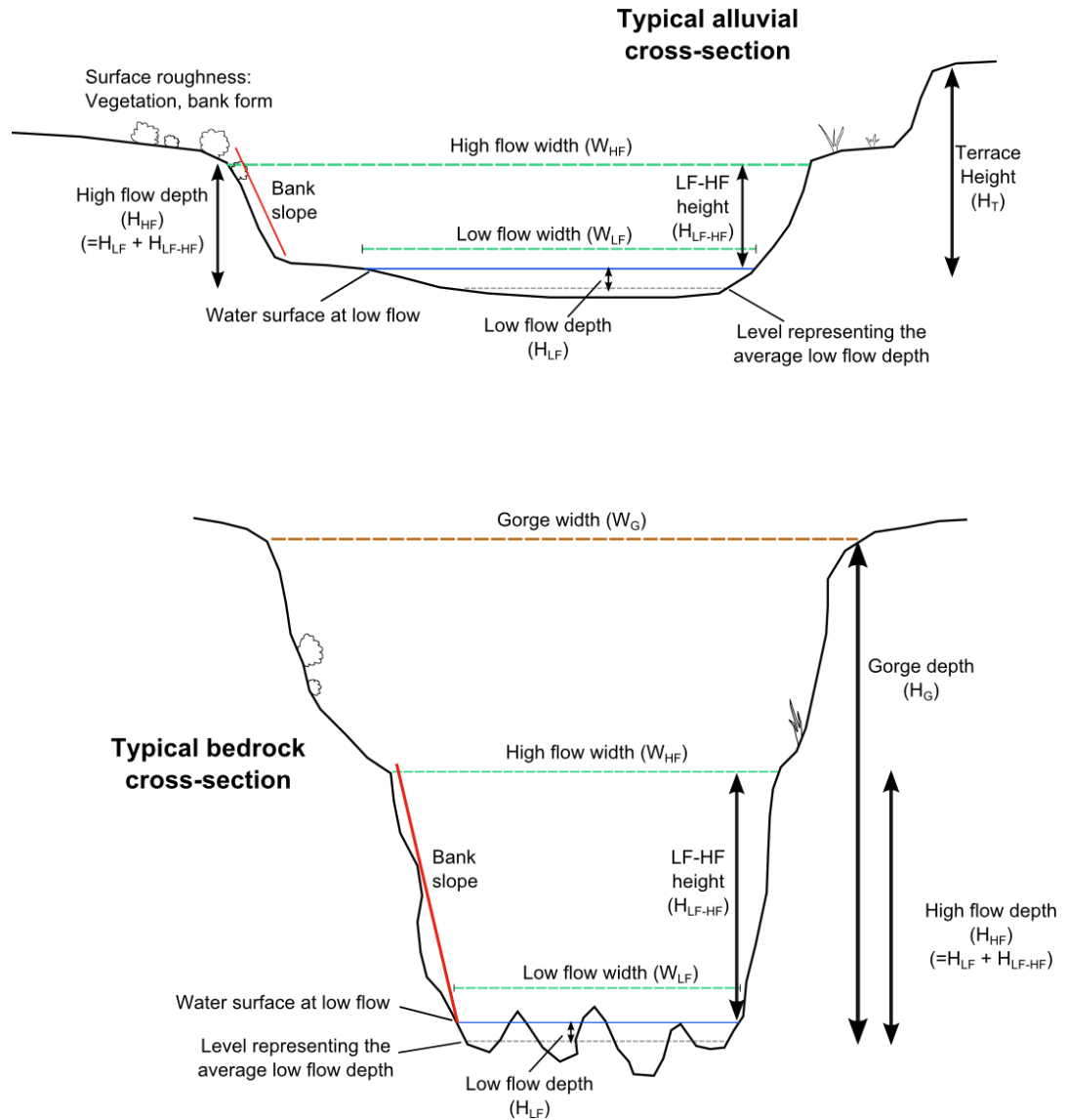
Figure 4-1. Field measurements of channel geometry at typical cross-sections for alluvial and bedrock channels.

Width

Channel width was recorded by sighting with the laser range finder from the LF or HF line on one bank to the estimated position of the LF or HF line on the opposite bank, with the line of sight perpendicular to the direction of channel flow at the measurement point. The published accuracy of the Impulse 200LR laser range finder is ±0.05m over the range of measured distances in this study ($2 - 50$ m) (Laser Technology Inc., 2011).

Depth

The average LF channel depth was estimated for the channel at each measurement location using a measuring pole graded at 1 cm intervals up to 1.9 m in height and a visual assessment of the channel shape. Due to the distorting effect of the measuring pole on the water surface when inserted into the flow, depths were measured to the nearest 5cm. Where channels were deeper than 1.9 m, a weighted tape measure was used, where

possible, to gauge the channel depth. When this method was used, the tape was lowered into the channel several times, at slightly different locations, to gain a representative depth value. However, the real variability of the channel depth in such locations could not be assessed. The average HF depth was derived by adding the vertical height, measured with the measuring pole, between the LF line and the HF line to the average LF depth (Figure 4-1). Where the vertical distance between the LF and HF levels exceeded 1.9 m, the laser range finder was used to derive the vertical height between these two levels. Where steep terrain restricted access to the channel, the laser range finder was used to estimate HF widths and depths when a good vantage point from which to view of the base of the gorge was available.

Data from individual measurement points are not considered in detail in the following analysis as reach-averaged width and depth values are preferred (section 4.2.1.2). Therefore the derivation of the uncertainty on individual channel width and depth measurements is not given in detail here. The main sources of uncertainty in channel width and depth, for both individual measurements and reach-average data are shown in Table 4-1. Uncertainty associated with individual measurements is relatively small compared to the uncertainty in reach-averaged data that arises from longitudinal variations in channel geometry along a reach (cf. Figure 4-4).

4.2.1.2   Reach-averaged width and depth

HF channel widths and depths show considerable variation along the river course. Much of this variation is likely be due to key controlling factors such as discharge and substrate, and the degree to which these factors control width is the subject of this research. However, variations in along-channel width and depth are also strongly influenced by sub-reach scale controls such as vegetation, geological features, and by hydraulic processes that produce rhythmic channel forms such as pool-riffle or step-pool sequences, or knickpoints/plunge pools and bedrock step-pools in bedrock reaches (e.g. Montgomery and Buffington, 1997). Reach-averaging effectively filters sub-reach scale channel width or depth variations to provide a 'smoothed' geometry with which to determine the key controls on channel width and depth over larger spatial scales. Comparison of data from individual measurement points with reach-averaged data should indicate the same trends in scaling, but reach-averaging the data is expected to considerably lower the variability.

Reach-averaged widths (w_r) and depths (d_r) are derived as the arithmetic mean of the measured HF widths and depths from each reach (Montgomery and Gran, 2001; Wohl and Merritt, 2008). To provide accurate reach-averaged values, the width and depth measurements were distributed so that they proportionally represent the distribution of the major morphological components of the reach, such that if pools are twice as long as riffles, two pool widths and depths were taken for every riffle width and depth. In practice, this control was achieved by measuring at the extremes of the respective features in the reach, for example, the widest part of the pool and narrowest of the riffle, as these locations are the most easily identified in the field (Figure 4-2). A minimum of three width-depth readings per reach were taken, where possible.

Point data	Width	Depth
Precision	Precision of laser range finder	Precision of measuring pole and tape
Accuracy	High flow line/ bankfull level	High flow line/ bankfull level
	Irregular or vegetated banks	Access to channel bed
	Slope of bank	Bed roughness
	Orientation of laser	Slope of bank
Reach scale	Proportion of various channel features or bedforms sampled along the reach e.g. pools vs. riffles in alluvial reaches, steps/rapids and pools or knickpoints/plunge pools in bedrock reaches	

Table 4-1. Sources of uncertainty on individual measurements and reach-average width and depths.

In some incised bedrock reaches, irregularity in the distribution of bedforms meant that precise representation of the true width and depth data was more difficult. In such reaches, geometry measurements were taken more frequently and the variability is accounted for in the calculation of uncertainties for the reach-averaged data (Figure 4-2). Proportional sampling was restricted by a lack of access in some gorge reaches, but efforts were made to gain a representative set of readings for the reach even where sampling was limited. Reaches with only one measured width were excluded from further analysis (<2% of all reaches).

Due to the highly variable channel geometry at the sub-reach scale (sometimes up to ~70% of the maximum channel width) uncertainty associated with reach-averaged HF width or depth is dominated by the intra-reach variability. The proportional sampling method described above attempts to account for intra-reach variability and to provide a reliable measure of the average reach geometry. However, the method also maximises the

variability of the reach sample data, in some cases producing a bimodal distribution of reach widths and depths (Figure 4-2). Standard errors ($s/\sqrt{n}$, at 1σ) calculated for each reach are thus conservative estimates of the uncertainty on the w_r and d_r, i.e. they are likely to over-estimate the 'true' uncertainty in the data. For this reason standard errors are not converted to expanded errors (i.e. at 2σ). The reach-average standard errors are roughly an order of magnitude greater than uncertainties associated with individual measurements of channel width, ranging from 1 – 25% (average 8%) of reach-averaged width, but are only slightly greater than uncertainties on individual channel depths, ranging from 1 – 40% (average 12%) of reach-averaged channel depth.
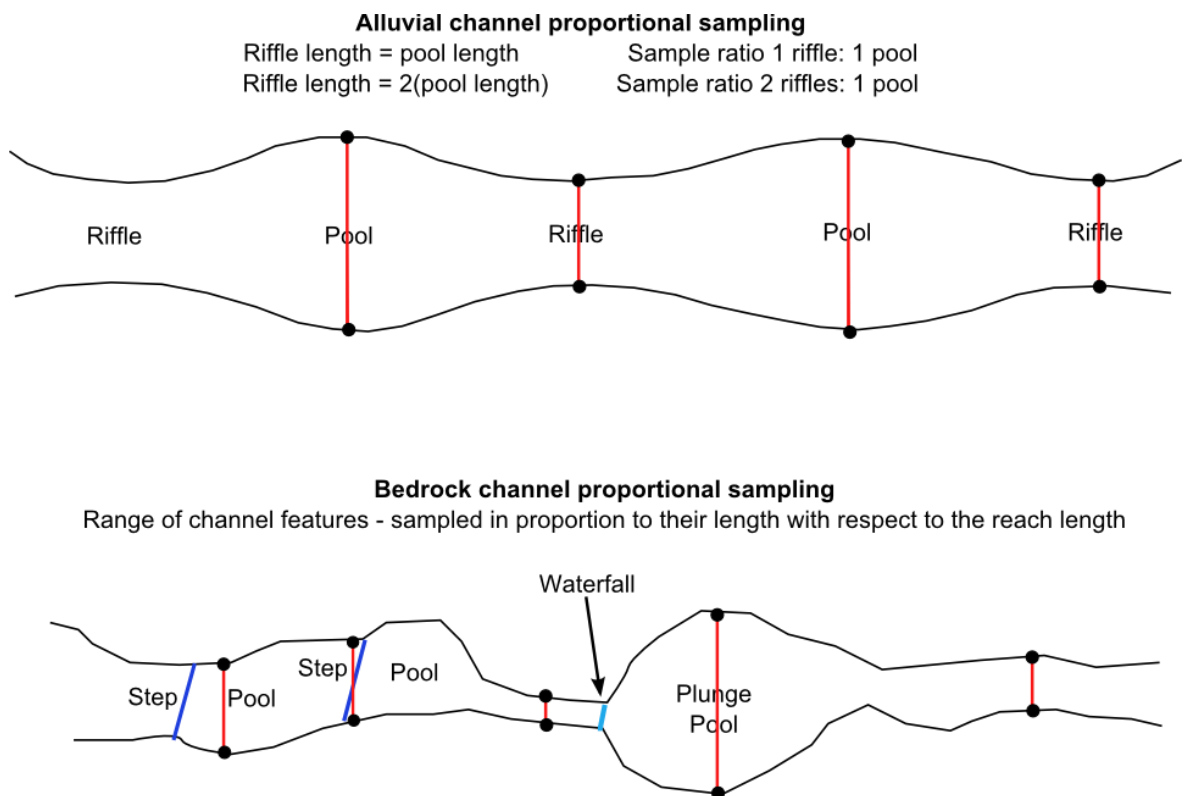
Figure 4-2. Sketch of typical proportional sampling measurement strategy for channel width and depth in alluvial channels (upper) and bedrock channels (lower), with respect to the distribution of major bed forms.

4.3   Results

4.3.1   Spatial distribution of widths and depths

The spatial distribution of HF channel width and depth data, with respect to the long profile of the mapped streams is shown in Figure 4-3. HF width and depths from individual measurement points and reach-averaged values (w_r and d_r) follow similar trends, with widths and depths increasing downstream. The increase in width downstream appears to be

greater for each channel than the increase in depth. Superimposed on the general downstream increase in width and depth are smaller scale variations that may be related to the distribution of channel types.
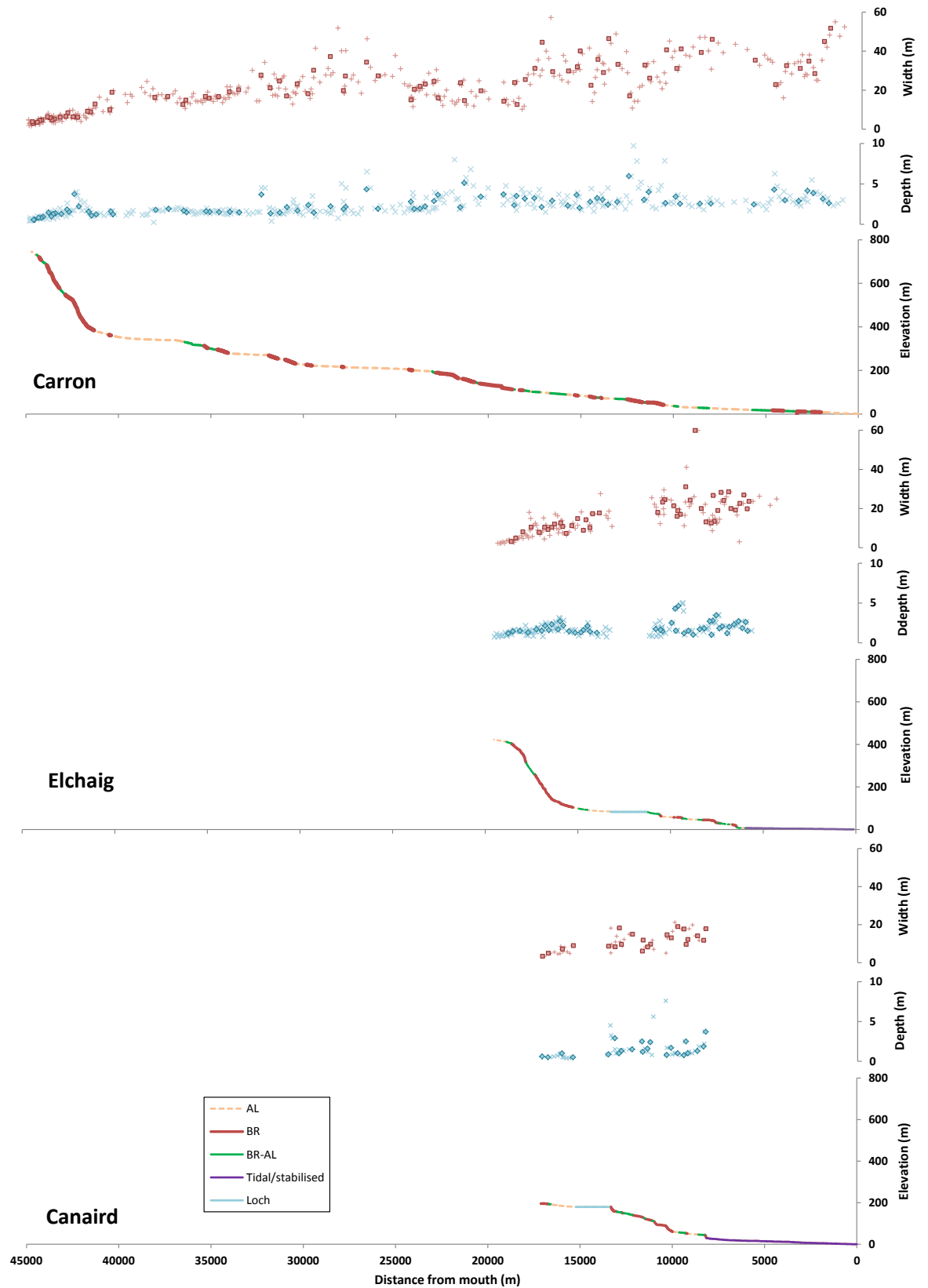
Figure 4-3. Long-profiles for the three mapped streams showing the distribution of reach types, together with the distribution of HF width (red/pink) and depth data (blue/sky blue) from individual measurement points (crosses) and reach averaged data (squares/diamonds).

4.3.2   Drainage area and slope control on channel geometry

4.3.2.1   Hydraulic geometry: initial results

Reach-averaged width and depths are strongly correlated with drainage area in the study channels (p<0.01) (Table 4-2, Figure 4-4). R^2 values indicate that variation in drainage area (*A*) accounts for 82% of the variation in w_r, but for d_r, variation in *A* accounts for less than 50% of the data variation (Table 4-2). R^2 values for w_r-*Q* and d_r-*Q* correlations are slightly lower than those for *A* (Table 4-2); possibly due to differences between actual discharge in the study channels and that predicted by the regional empirical *A*-*Q* relationship (section 2.3.3.3), or due to a disparity between median annual discharges calculated from c. 50 year gauging records and the long-term discharge regimes over timescales of 10^2-10^4 years during which the channels develop. Drainage area is likely to have remained constant at most points along the channels since deglaciation and is used as the main hydraulic scaling factor in the remainder of this analysis, although discharge correlations may be presented in a few cases in order to compare with published studies.

Reach-averaged width and depth are more strongly correlated with drainage area (and discharge) than data from individual measurement points (Figure 4-4 A and B, Table 4-2 A). Comparison of the regression relationships for individual measurements and reach-averaged data using ANCOVA shows no statistical difference between the *w*-A and *d*-A regressions derived using the two datasets (p>0.05) (Appendix A3-4). This indicates that the process of reach-averaging accurately preserves the pattern of the data whilst removing the sub-reach scale variability, thus supporting the use of the reach-averaged data in further analysis.

The w_r-*A* and d_r-*A* regressions for each river are all highly significant (p<0.01) except for the d_r-*A* relationship for the River Elchaig which is significant at p<0.05 (Table 4-2 B). Combining the reach-averaged data from all rivers would provide a larger dataset with statistical advantages for the analysis of the controls on channel geometry. However, datasets from the different rivers have different w_r-*A* and d_r-*A* scaling trends (Figure 4-4 C and D; Appendix A3-3 and A3-5). The rivers Carron and Elchaig have similar w_r-*A* relationships (p>0.05) but significantly different d_r-*A* relationships (p<0.05) and both the w_r-*A* and d_r-*A* relationships from the River Canaird are significantly different from those of the two other rivers (p<0.05) (Appendix A3-4).

A		n	Width				Depth			
			Intercept	Exponent	R^2	p	Intercept	Exponent	R^2	p
A	Individual data	486	0.59 (3.92)	0.39	0.75	<0.001	-0.07 (0.86)	0.22	0.38	<0.001
	Reach-averaged	152	0.59 (3.93)	0.39	0.82	<0.001	-0.06 (0.88)	0.22	0.45	<0.001
Q	Individual data	486	0.73 (5.36)	0.37	0.69	<0.001	0.01 (1.02)	0.21	0.36	<0.001
	Reach-averaged	152	0.74 (5.52)	0.38	0.75	<0.001	0.02 (1.04)	0.22	0.44	<0.001

B		n	w_r-Area				d_r-Area			
			Intercept	Exponent	R^2	p	Intercept	Exponent	R^2	p
River	Carron	82	0.64 (4.39)	0.37	0.87	<0.001	-0.03 (0.94)	0.21	0.62	<0.001
	Elchaig	47	0.57 (3.68)	0.44	0.70	<0.001	0.09 (1.23)	0.11	0.12	0.018
	Canaird	23	0.05 (1.13)	0.74	0.65	<0.001	-0.75 (0.18)	0.69	0.32	0.005

Table 4-2. Regression data for channel width and depth calculated using least-squares linear regression of log width or depth and log *A* or *Q* in Minitab. A) Drainage area (*A* in km^2) and discharge (*Q* in m^3/s) regressions for individual measurements and reach-averaged data (whole dataset). B) Drainage area regressions for all reach-averaged data from each river. Bracketed values for intercepts are converted to power law coefficients, slope values from the linear regression of log data are equivalent to the power-law exponents.

The w_r-A and d_r-A regressions for data from the River Canaird are strongly affected by a few low width and depth values at small drainage areas (Figure 4-4 C and D). All of these low values are from channels in peat in the catchment headwaters. As discussed in the next section, peat has a strong effect on channel geometry and thus the significantly different relationships for the River Canaird are likely to be due to the distribution of substrate types within the channel. The influence of substrate can also account for the difference in the d_r-A scaling relationship between the rivers Carron and Elchaig. Subdividing the data for each river into alluvial and bedrock channel types shows that the difference in the overall scaling relationships between the two streams is largely driven by a difference in the alluvial channel depth scaling, whereas bedrock channels from the two rivers show similar scaling relationships (ANCOVA p>0.05) (Figure 4-5). The apparently inverse alluvial channel scaling for the River Elchaig is not significant (p>0.05) and is strongly influenced by two shallow channels at higher drainage areas. The differences in scaling relationships between the rivers arise largely due to differences in the distribution of channel types (i.e. channel substrate) along the stream profiles. As the role of substrate in controlling channel geometry is a key component of this research, and data are classified according to channel type in subsequent analyses, the effects of differences in scaling between the rivers will be

removed. Hence a combined dataset of reach-averaged data from all the rivers is used in the remainder of the analysis.
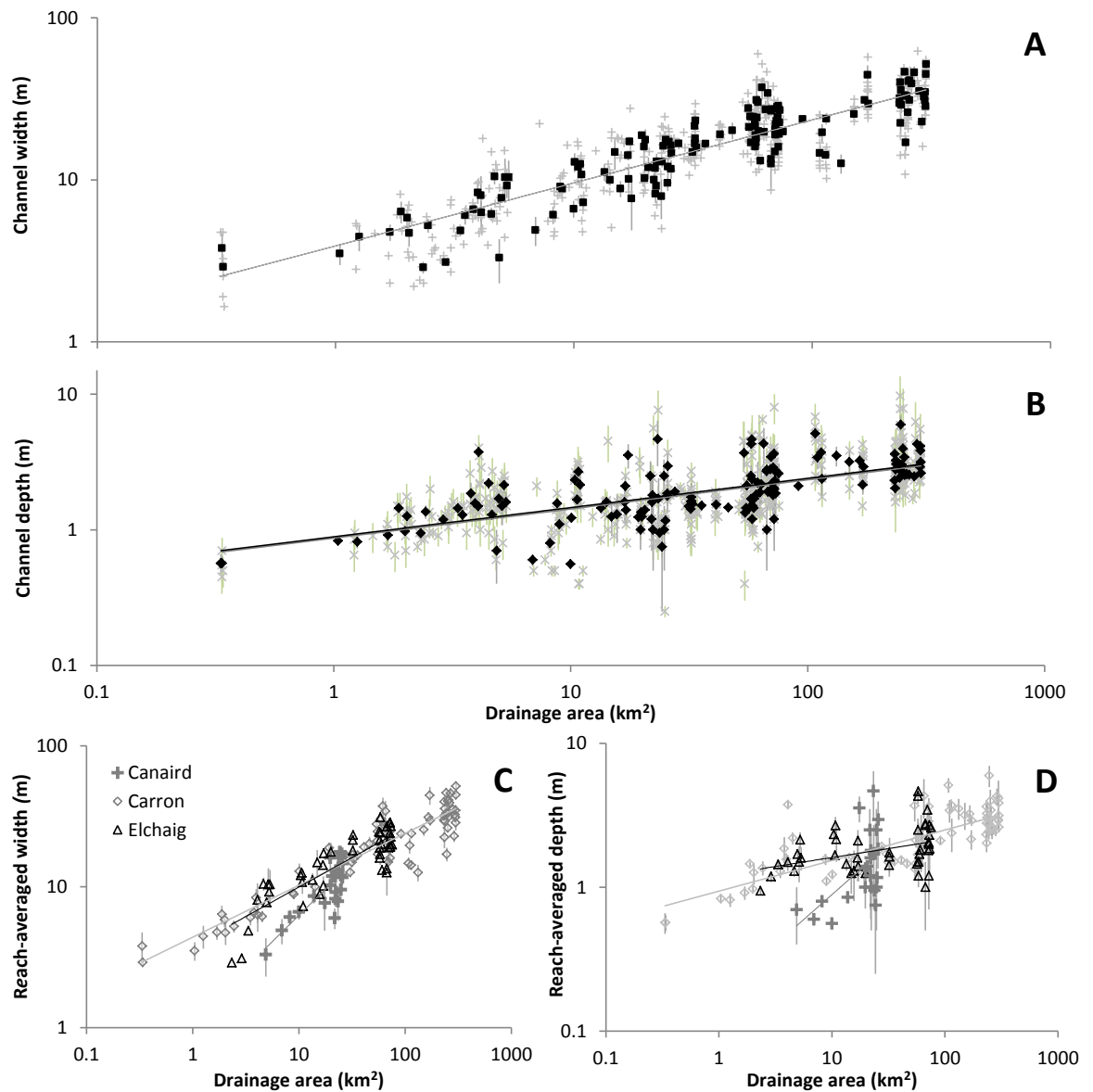
Figure 4-4. Reach-averaged channel width (w_r) and depth (d_r) versus drainage area (logarithmic axes). A) All channel width values for individual measurements (grey crosses) and reach-averaged data (black squares). B) All channel depth data for individual measurements (grey diagonal crosses) and reach-averaged data (black diamonds). Least-squares power law regressions in A and B for individual measurements (grey line) and reach-averaged data (black line) overlay one another. C) w_r versus A for each river (symbols in legend). D) d_r versus A for each river (symbols as for C). Power law regressions in C and D for River Carron (light grey line), River Elchaig (black line) and River Canaird (medium grey line). Error bars on reach-average data in all plots show standard error. Error bars on individual measurements in plots A and B show uncertainty at 1σ.
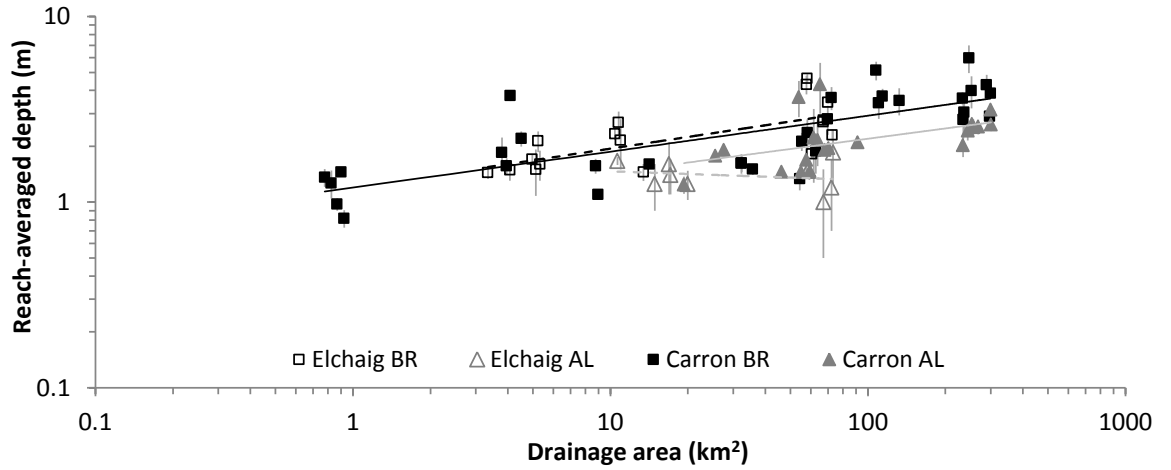
Figure 4-5. Log-log plot of reach-averaged channel depth (d_r) versus drainage area for data from the rivers Carron and Elchaig subdivided by substrate type. Regressions for individual channel data according to reach type; solid black line is Carron bedrock (BR), dashed black is for Elchaig bedrock, solid grey is Carron alluvial (AL) and dashed grey is Elchaig alluvial reaches. Error bars showing standard error on reach-average depth.

4.3.2.2   Slope control on channel geometry

As discussed in section 4.1.2, channel slope as well as drainage area may influence channel width (and depth) in detachment-limited bedrock channels. Channel slope and drainage area are inversely correlated for the rivers Carron and Elchaig (section 3.3.1), hence channel widths and depths were normalised to avoid autocorrelation. Normalised reach-averaged channel widths and depths (for bedrock channels only) were calculated by dividing the reach-averaged width or depth by the respective hydraulic scaling relationship, following the method of Yanites and Tucker (2010),

$$w_n = \frac{w_r}{bA_r^c}$$ Eq 4.5

$$d_n = \frac{d_r}{eA_r^f}$$ Eq 4.6

where w_n and d_n are the normalised width and depth, A_r the drainage area for the reach and b and c, e and f are derived from the relevant scaling relationship. w_n and d_n are not correlated with channel slope in the surveyed rivers (Figure 4-6, p>0.1). Hence negative correlations between channel width and slope, predicted by detachment-limited models and seen in some channels responding to changes in uplift rate (e.g. Whittaker et al., 2007), are not supported by the data.

4.3.2.3   Summary of initial results

- Reach-averaged width and depth are strongly scaled with drainage area as $w \sim 3.9A^{0.39}$ and $d \sim 0.88A^{0.22}$

- Combining all the data from the different rivers is justified when the data are classified according to substrate type.

- Channel width (normalised for drainage area) is not correlated with channel slope.
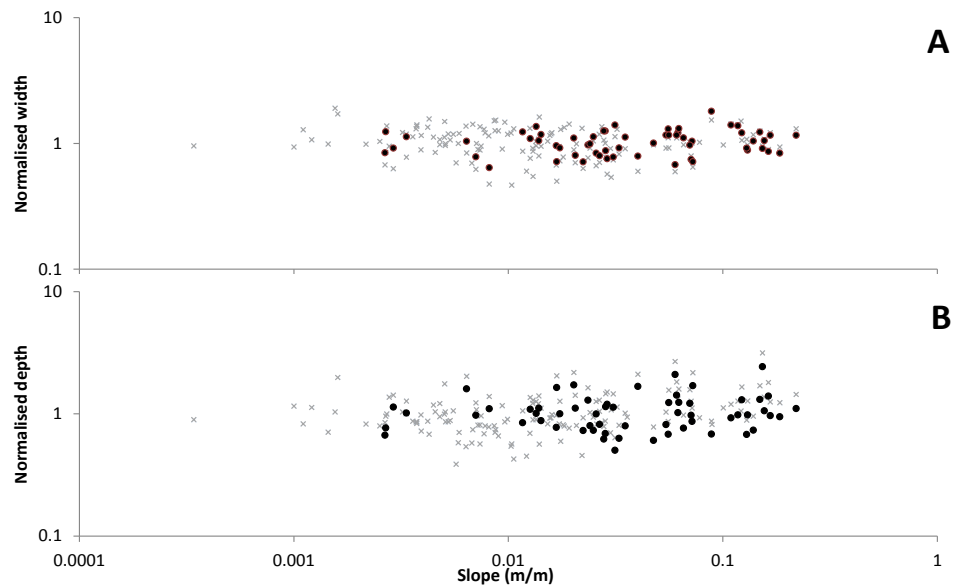
Figure 4-6. A) Log-log plot of normalised channel width (w_n) versus slope for all channel data (grey crosses, normalised using $w_n = w_r/3.93A_r^{0.39}$) and for bedrock channel data only (black circles, normalised using $w_n = w_r/4.54A_r^{0.30}$). B) Log-log plot of normalised channel depth (d_n) versus GIS-slope for all channel data (grey crosses, $d_n = d_r/0.88A_r^{0.218}$), and for bedrock channel data only (black circles, $d_n = d_r/1.51A_r^{0.21}$).

4.3.3   Hydraulic geometry and substrate control

Reach-averaged width and depths from all rivers were subdivided on the basis of the reach type, defined by the substrate comprising the channel bed and banks within the reach. Figure 4-7 indicates that w_r and d_r vary systematically with substrate type for a given drainage area. Differences in w_r-A and d_r-A scaling between reach types, shown in Table 4-3, are explored in the following sections.

4.3.3.1   <u>Bedrock vs alluvial channel geometry</u>

Both alluvial and bedrock channels show highly significant positive correlations with drainage area (p<0.001) (Figure 4-7, Table 4-3), with R^2 values of 0.89, 0.81 and 0.85 for alluvial, bedrock and bedrock-alluvial w_r-A regressions respectively. Thus, both bedrock and alluvial channel widths are strongly hydraulically scaled in the study rivers. The results of ANCOVA indicate that the exponent on the w_r-A regressions of alluvial (0.38) and bedrock (0.30) channels are significantly different (p<0.05) (Appendix A3-4). This result precludes a statistical comparison of the intercepts, but confirms that bedrock channels are systematically narrower for a given drainage area than alluvial channels (Figure 4-8). This

is illustrated by the reference channel widths, calculated from the w_r-A scaling relationships at a reference drainage area of 50 km^2, for bedrock (14.9 m) and alluvial channels (23.9 m). The significantly lower w_r-A scaling exponent for bedrock channels also indicates that rate of increase of bedrock channel width with drainage area is lower than that for alluvial channels. Furthermore, whilst the slope of the bedrock-alluvial w_r-A regression is not significantly different to either the alluvial or bedrock w_r-A regressions (p>0.05), the intercept is significantly different (p<<0.05) (Appendix A3-4). The reference width at 50 km^2 for bedrock-alluvial channels is 19.0 m, in-between those calculated for bedrock and alluvial channels.

		n	w_r-Area				d_r-Area			
			Intercept	Exponent	R^2	P	Intercept	Exponent	R^2	p
Substrate	Alluvial	29	0.73 (5.40)	0.38	0.89	<0.001	-0.12 (0.76)	0.22	0.34	<0.001
	Bedrock	57	0.66 (4.59)	0.30	0.81	<0.001	0.06 (1.15)	0.21	0.50	<0.001
	Bedrock - Alluvial	42	0.66 (4.54)	0.37	0.85	<0.001	-0.30 (0.50)	0.33	0.67	<0.001

Table 4-3. Regression data for w_r-A and d_r-A regressions for all data classified according to substrate type (only the three main types are shown), calculated using least-squares linear regression of log w_r or d_r and log A in Minitab. Bracketed values for intercepts are converted to power law coefficients, slope values from the linear regression of logged data are equivalent to the power law exponents.
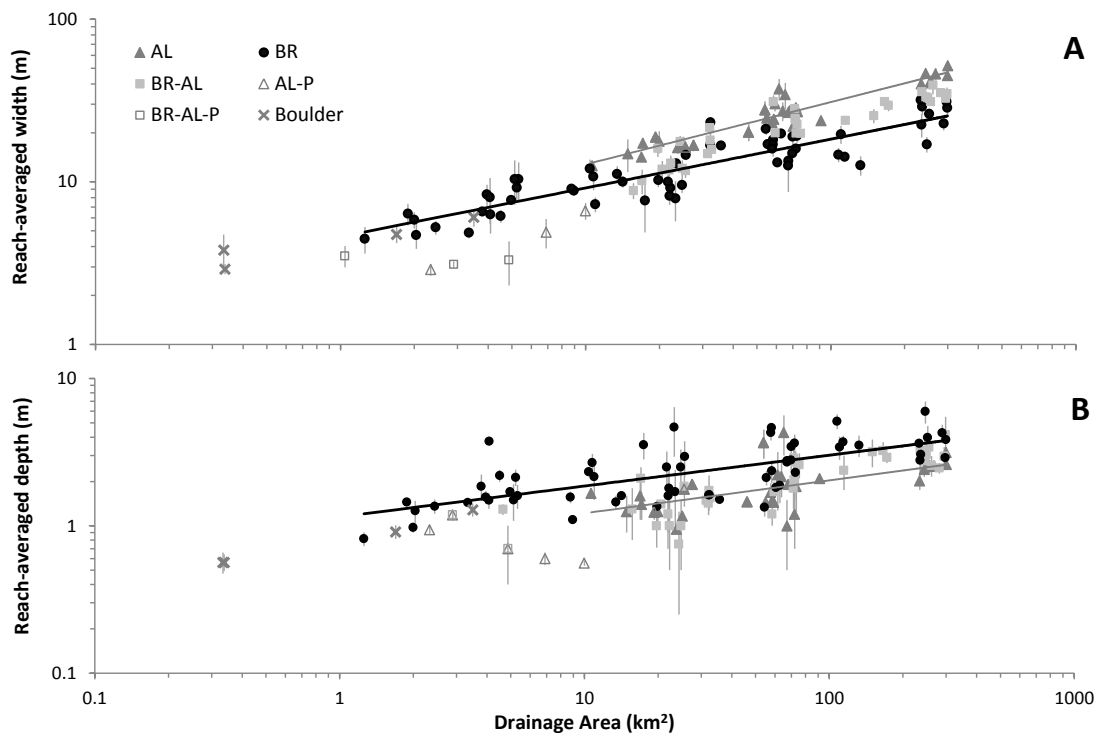
Figure 4-7. Log-log plots of (A) reach-averaged width (w_r) and (B) reach-averaged depth (d_r) as functions of drainage area for different substrate types. Power law regressions for bedrock channels (black line) and alluvial channel types (grey line) only, regressions for BR-AL, peat and boulder channels not shown for clarity. BR-AL regression data give in Table 4-3, peat and boulder channels discussed in sections 4.3.3.2 and 4.3.3.3 respectively. Error bars on all data are one standard error.

The lower scaling exponent in the d_r-A relationship (Figure 4-7, Table 4-4), together with the lower R^2 values (<0.70), indicate that channel depth is less strongly correlated with drainage area than channel width. However, the d_r-A relationships for the three main substrate types are all highly significant (p<0.01) (Table 4-4), and lower R^2 values may be partly due to the lower scaling exponent. The 95% confidence intervals on the regressions of alluvial and bedrock channels overlap (Figure 4-8 B), but the results of ANCOVA indicate that whilst the slope of the d_r-A relationship for bedrock channels is not significantly different to alluvial channels (p>0.05), the intercepts are significantly different (p<0.01), with bedrock reaches systematically deeper than alluvial reaches. Reference channel depths at 50 km^2 drainage area are 3.42 m for bedrock channels and 1.76 m for alluvial channels. The d_r-A scaling relationship for mixed bedrock-alluvial channels is not significantly different from the d_r-A relationship for alluvial channels (p>0.05), but is significantly different to the d_r-A relationship for bedrock channels (p<0.05). This indicates that bedrock-alluvial channel depths are similar to alluvial channels; the reference channel depth at 50 km^2 is 1.78 m, but are shallower for a given drainage area than bedrock channels (Appendix A3-4).
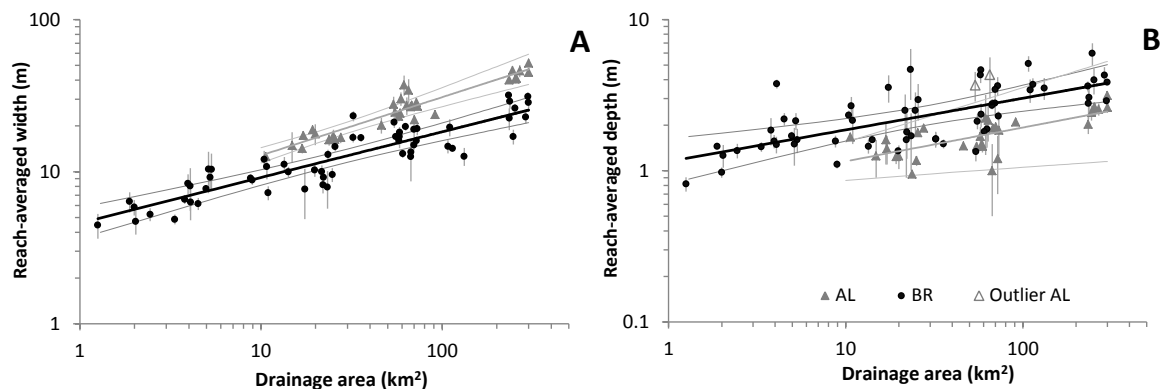
Figure 4-8. A) Reach-averaged width (w_r) and B) reach-averaged depth (d_r) versus drainage area for bedrock and alluvial channels only. Key in plot B. Power law regressions with 99% confidence intervals. Note that the two anomalously deep alluvial outlier reaches (open triangles) (standardised residuals are 3.1 and 2.7) are located at the sites of in-filled glacial lakes in the upper River Carron.

4.3.3.2   Peat and channel geometry

Vegetation cover has no discernible effect on the observed alluvial channel width (Appendix 4), but cohesive peat in the channel banks influences w_r and d_r for alluvial and bedrock-alluvial channels (Figure 4-9). Peat channel width is similar to alluvial channel width at higher drainage areas, but is considerably lower at low drainage areas. This observation may indicate that peat channels have a steeper w_r-A scaling than alluvial or bedrock channels, with a scaling exponent of 0.5 (Figure 4-9 A). However, an alternative

interpretation of the data, with a break in the scaling at a drainage area of ~15 – 25 km^2 (Figure 4-9 B) is possible. In this scenario, channels with peat banks at drainage areas >15 – 25 km^2 appear to scale with area in the same way as alluvial channels, but below this value, channels with peat banks are substantially narrower than would be expected for alluvial channels (assuming the power-law relationship can be projected to lower drainage areas), and are narrower even than bedrock channels at similar drainage areas (Figure 4-9 B). Statistically distinguishing which scenario best-fits the data is a complex procedure and is beyond the scope of this study.

4.3.3.3   Grain size and alluvial channel geometry

The widths and depths of small alluvial channels dominated by large boulders are shown in Figure 4-7. The widths of the boulder-affected channels are similar to bedrock channel widths for the same drainage area, whereas the depths of these channels fall ambiguously between bedrock and alluvial channel depths. As there are only a few channels affected by boulders in this way statistical assessment is not possible; however, these data suggest that where channels are unable to transport coarse bed material, they may 'switch' to a bedrock channel width scaling regime.

		n	w_r-Area				d_r-Area			
			Intercept	Exponent	R^2	p	Intercept	Exponent	R^2	p
Substrate	**Alluvial**	29	0.73 (5.40)	0.38	0.89	<0.001	-0.12 (0.76)	0.22	0.34	<0.001
	Bedrock	57	0.66 (4.59)	0.30	0.81	<0.001	0.06 (1.15)	0.21	0.49	<0.001
	Bedrock - Alluvial	42	0.66 (4.54)	0.37	0.85	<0.001	-0.30 (0.50)	0.33	0.67	<0.001
River and substrate	**Carron AL**	23	0.69 (4.92)	0.40	0.80	<0.001	-0.03 (0.93)	0.19	0.28	0.011
	Elchaig AL	11	0.61 (4.06)	0.48	0.67	0.004	0.25 (1.79)	-0.08	0.09	0.391
	Canaird AL	3	-	-	-	-	-	-	-	-
	Carron BR	32	0.65 (4.49)	0.31	0.90	<0.001	0.04 (1.08)	0.22	0.60	<0.001
	Elchaig BR	19	0.73 (5.42)	0.27	0.65	<0.001	0.08 (1.20)	0.21	0.46	0.002
	Canaird BR	9	-0.58 (0.26)	1.15	0.24	0.176	0.12 (1.31)	0.19	0.003	0.891

Table 4-4. Alluvial and bedrock channel hydraulic scaling relationships for combined data and individual streams. Shaded cells highlight R^2 values below 0.5 or p values >0.05, i.e. relatively weakly scaled parameters, or non-significant relationships.
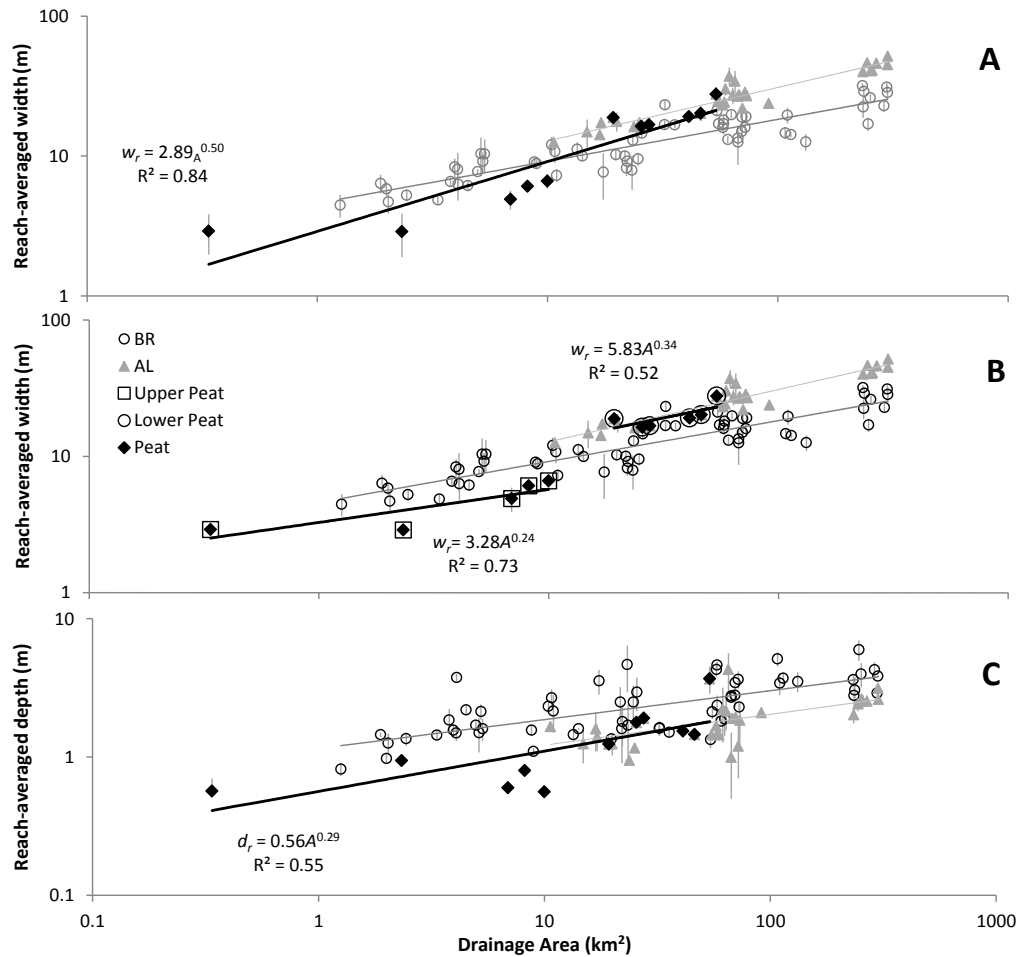
Figure 4-9. Log-log plots of w_r-A (A and B) and d_r-A (C) for alluvial and peat channels, bedrock channels shown for reference. Key to symbols in plot B. Power law regressions for bedrock (medium grey line), alluvial (light grey line) and peat channels (black line), plot B shows alternative scaling interpretation for peat channels. Error bars show standard error (1σ).

4.3.3.4   Lithology and bedrock channel geometry

Data for bedrock channels were subdivided according to the dominant lithology within the reach (Table 2-4). Figure 4-10 indicates that lithology has no systematic influence on the w_r-A or d_r-A scaling, over the range of lithologies found in the field area.

4.3.3.5   Summary of substrate results

- Alluvial channels are significantly wider and shallower than bedrock channels for a given drainage area or discharge.

- Alluvial channel width scales as $5.40A^{0.38}$ and $9.21Q^{0.31}$ and depth as $0.76A^{0.22}$ and $0.34Q^{0.21}$.

- Bedrock channel width scales as $4.59A^{0.30}$ and $5.96Q^{0.29}$ and depth as $1.15A^{0.2}$ and $1.42Q^{0.19}$.

- Channels with peat banks are narrower than bedrock channels at low drainage areas but have similar widths to alluvial channels at higher drainage areas.

- Alluvial channels at low drainage areas very coarse-grained (bouldery) boundaries have widths similar to bedrock channels.

- Lithology has no discernible effect on bedrock channel width.
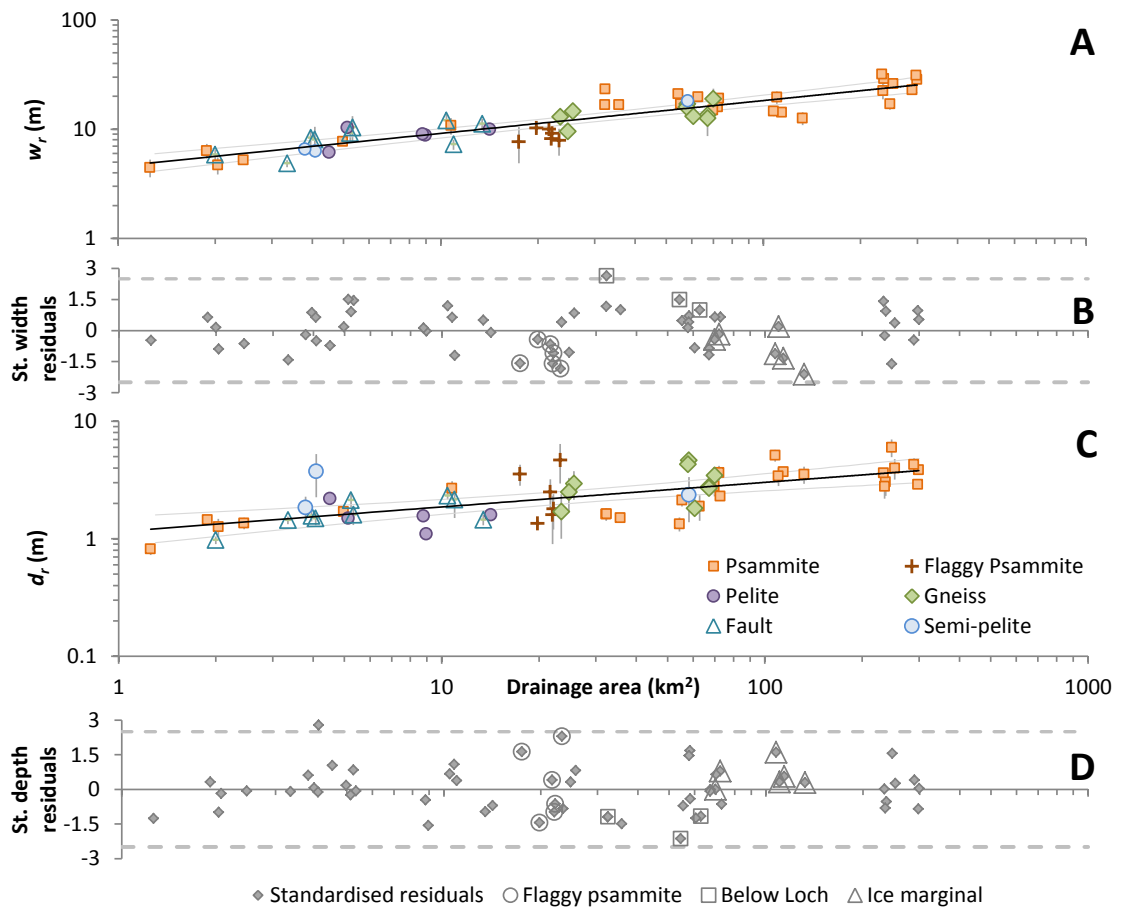
Figure 4-10. Log-log w_r-A (A) and d_r-A (C) plots for bedrock channels grouped by lithology, key on plot C. Power law regressions (solid line) for all bedrock channel data with 99% confidence interval (dashed lines). Standardised residuals from bedrock channel w_r-A (B) and d_r-A (D) regressions, key on plot D. Highlighted 'below lake' and 'ice marginal' channels are discussed in section 4.3.5.2.

4.3.4   Width versus depth: Controls on the channel cross-section

The *w/d* ratio of bedrock channels is commonly assumed to be, or is predicted to be, constant for a given substrate in numerical modelling studies (e.g. Finnegan et al., 2007; Wobus et al., 2006), though the numerical model of Turowski et al. (2007) predicts that the *w/d* ratio should scale weakly with drainage area. A weak *w/d* scaling with *A* is supported empirically by data from gravel-bed channels (e.g. Leopold and Maddock, 1953; Turowski et al., 2006) but not supported by published data from bedrock channels (Wohl and David, 2008).

The *w/d* ratio of NW Highland rivers varies with channel substrate (Figure 4-11). Bedrock channels have significantly lower *w/d* ratios for a given discharge than alluvial channels (p<0.01). The average *w/d* ratio of bedrock channels in this study (5.95, n=59, SE=0.37) is similar to that cited by Finnegan et al. (2005), and the average *w/d* ratio of the coarse-grained alluvial channels (14.70, n=32, SE=0.81) falls in between Finnegan's derived values for cobble-bed (21) and boulder-bed channels (9). The average *w/d* ratio of bedrock channels discussed by Wohl and David (2008) is 8 (n=44, SE=0.98), slightly higher the value from this study. The difference in the average *w/d* ratios of bedrock channels may reflect differences in the interpretation of the level of bankfull discharge, or may be due to the different definition of bedrock channels employed by Wohl and David (2008) (50% of channel in bedrock compared to 70% in this study).

The influence of lithology on the *w/d* ratio of bedrock channels was assessed by comparing residuals from the *w/d-A* regression in order to remove any potential influence of the spatial distribution of lithological units within catchments. Mean values of the residuals grouped according to lithological type or Selby rock mass strength index were not significantly different (p>0.05). Wohl and David (2008) also found no influence of lithological resistance on the *w/d* ratio of bedrock channels from a worldwide dataset.

The *w/d* ratio is weakly positively scaled with drainage area and weakly negatively scaled with channel slope (Figure 4-11 B and C, regressions significant at p<0.05). The scaling exponent of 0.09 for *w/d* versus A is within the range predicted by the numerical model of Turowski et al. (2007) (0.08 – 0.25) and similar to that observed in empirical data for gravel-bed rivers (~ 0.1) (cf. Turowski et al., 2006, 2007), but contrasts with the findings of Wohl and David (2008). The lack of relation between *w/d* and *A* in the worldwide bedrock channel dataset of Wohl and David (2008) may be due to the considerable scatter in the data obscuring the weak scaling. The finding of a weak scaling between the *w/d* ratio and drainage area supports the assertion of Turowski et al. (2007) that constant *w/d* ratios predicted by numerical models may be artefacts resulting from the omission of a critical shear stress for bedrock erosion.

4.3.4.1   Summary of *w/d* ratio results

- The mean *w/d* ratio of bedrock channels (5.95) is significantly lower than that of alluvial channels (14.69) and bedrock alluvial channels (11.29).

- Bedrock channel w/d is weakly positively scaled with drainage area (exponent = 0.09) and weakly negatively scaled with channel slope, but does not vary with lithology.
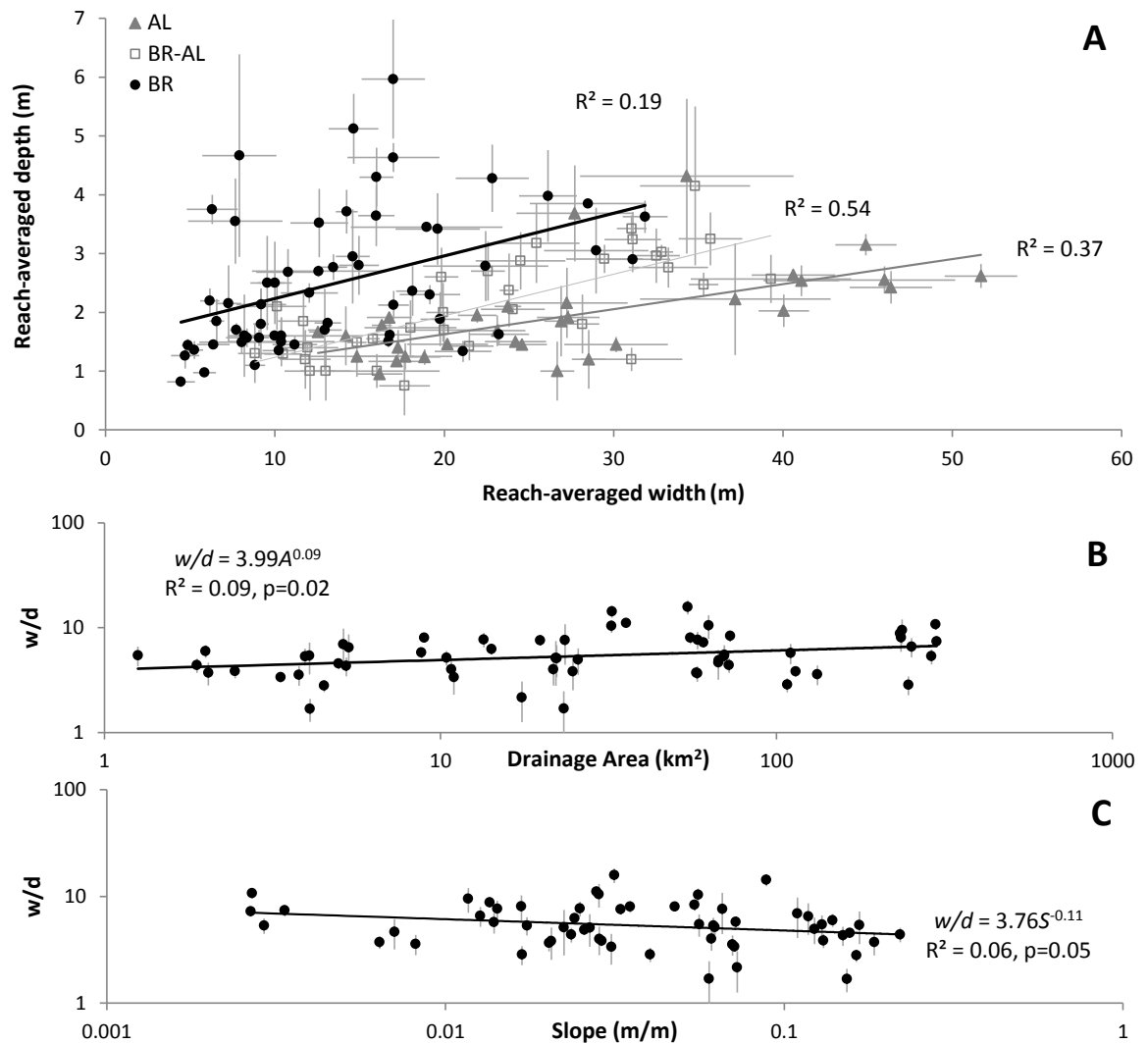
Figure 4-11. A) d_r **versus** w_r **for different substrate types. Linear regressions for alluvial (medium grey line), bedrock-alluvial (light grey line) and bedrock (black line) channels shown; all regressions are significant (p<0.01). The R^2 value of 0.37 for alluvial channels rises to 0.6 when two outlier reaches with standardised residuals of 2.9 and 3.5 are removed, these are located at the sites of two in-filled glacial lakes on the river Carron. Error bars show standard error (1 sigma). B) Log-log plot of bedrock channel** w/d **ratio versus drainage area. C) Log-log plot of bedrock channel** w/d **ratio versus channel slope. Power law regressions in B and C are significant (p<0.05). Error bars on** w/d **calculated from standard errors on** w_r **and** d_r**.**

4.3.5 'Postglacial' controls on channel geometry

Despite the complex glacial history of the study area, channel width and depth are strongly scaled with drainage area and there are significant differences in scaling between alluvial and bedrock channels. Channel slope, which remains largely glacially conditioned, does not directly control the channel cross-section, but indirectly influences channel geometry via its control on channel type (chapter 3).

4.3.5.1   Lakes and partial glaciation

The presence of large, sediment-trapping lakes along the trunk streams of the Rivers Elchaig and Canaird, and an in-filled lake on the River Carron (figures 2-5, 2-6 and 2-7), has no major influence on the observed bedrock channel geometry; standardised residuals from the bedrock channel w_r-A and d_r-A regressions for reaches downstream of lakes are within the range of other residuals (Figure 4-10). Similarly, the partial glaciations of the Elchaig and Carron catchments during the Younger Dryas stadial (12.9 – 11.5 ka) has not substantially disrupted the scaling of channel width and depth with drainage area (Figure 4-10).

4.3.5.2   Gorge inheritance and bedrock channel geometry

Inheritance of pre-existing gorges that were either preserved under ice or cut by sub-glacial meltwater channels may have locally influenced the channel geometry of the study rivers. In chapter 6, the distribution of inherited pre- or sub-glacial gorges along the surveyed streams has been estimated by comparing the expected depth of postglacial fluvial entrenchment, derived from extrapolation of the quantified fluvial erosion rates and the estimated deglaciation age (chapter 5), with the observed entrenchment depth of bedrock channels throughout the mapped streams. Bedrock channels have been classified according to the difference between the observed and predicted entrenchment depths (Figure 4-12):

- "Over-entrenched" channels have observed entrenchment depths greater than 125% of the predicted postglacial entrenchment; these channels are interpreted to be affected by the inheritance of pre- or sub-glacial gorges.
- "Under-entrenched" channels have observed entrenchment depths of less than 75% of the predicted postglacial entrenchment depth; these channels are interpreted to have had postglacial bedrock incision delayed by a thick overlying sediment cover.
- "Postglacial-entrenched" channels have observed entrenchment depths of ± 25% of the predicted postglacial entrenchment depth; in these channels bedrock incision is interpreted to have been initiated shortly after deglaciation.

The w_r-A regression for postglacial-entrenched bedrock channels is not significantly different to those of over- or under-entrenched channels (ANCOVA p>0.1, Figure 4-12). But, the slope of the w_r-A regression for under-entrenched channels is significantly different to that of over-entrenched channels (p<0.1). Inspection of Figure 4-12 indicates that under-entrenched channels are wider than over-entrenched channels at drainage areas >10km^2; with a reference width at A=50 km^2 of 16.4 m compared to 14.1 m for over-

entrenched and 14.7 m for postglacial-entrenched channels (Table 4-5). The slopes of the d_r-A regressions for all levels of entrenchment are not significantly different, but the intercept for the over-entrenched channel d_r-A regression is significantly different to those of the under-entrenched and postglacial-entrenched channels ($p<0.05$). This suggests that over-entrenched channels are significantly deeper for a given area than the less entrenched channels (Figure 4-12); reference depths at $A=50$ km^2 are 3.1 m for over-entrenched channels compared to 2.7 m for postglacial-entrenched and 2.2 m for under-entrenched channels (Table 4-5). A highly significant ($p<0.01$) negative correlation of the channel w/d ratio with the observed entrenchment depth of the reach also indicated that more deeply entrenched channels are both narrower and deeper than less entrenched channels (Figure 4-13).

4.3.5.3   Summary of 'postglacial' controls on channel geometry

- Bedrock channels in gorges interpreted to have formed during phases of pre or sub-glacial erosion have similar widths to those that have formed since deglaciation.

- The w/d ratio is negatively correlated with the depth of entrenchment.
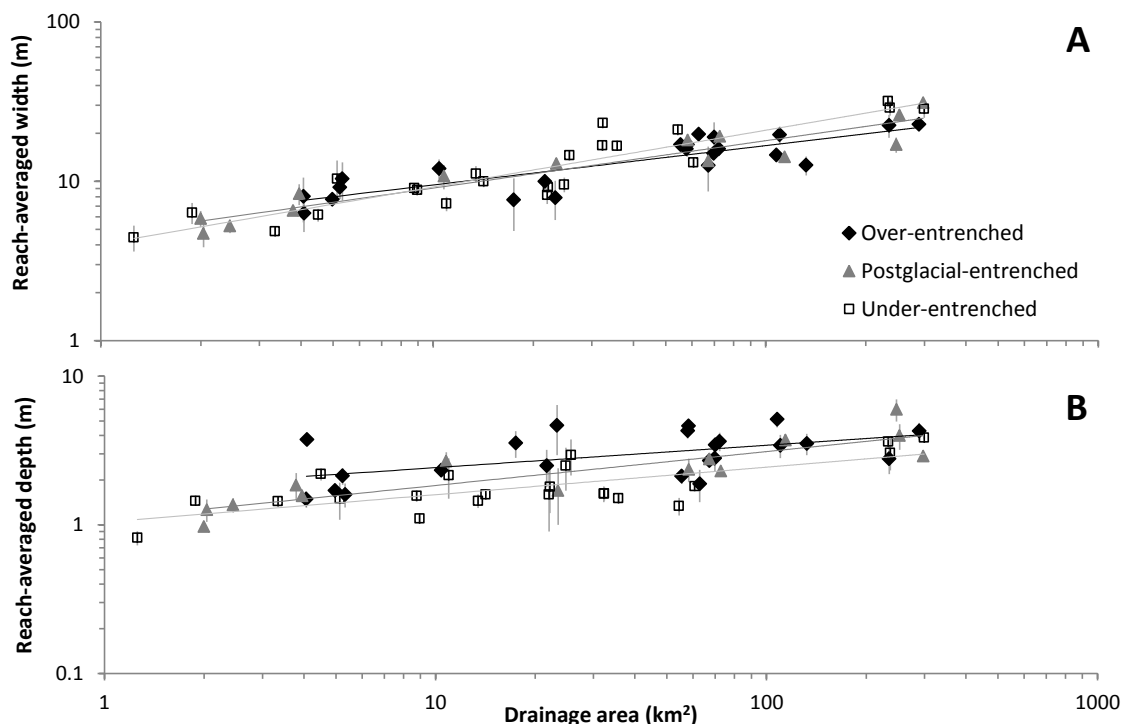
Figure 4-12. Log-log w_r-A (A) and d_r-A (B) plots for bedrock channels grouped according to the estimated timescale for the onset of fluvial incision within the reach (groups and derivation discussed in the text); Over-entrenched (black diamonds, black line), Postglacial-entrenched (grey triangles, medium grey line), and Under-entrenched (open squares, light grey line).

$$w/d = 8.47H_{GT}^{-0.3}$$
$$R^2 = 0.27, p<0.001$$
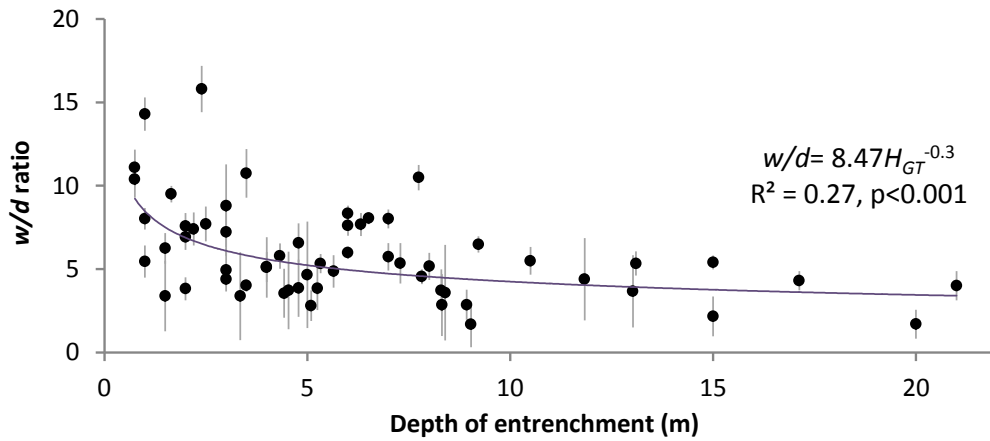
Figure 4-13. *w/d* ratio for bedrock channels versus observed depth of entrenchment (H_{GT}; see section 6.2.1 for details of the measurement of entrenchment depth).

Dataset	w_{ref}	d_{ref}
All bedrock	14.85	3.42
Postglacial-entrenched	14.69	2.66
Over-entrenched	14.14	3.09
Under-entrenched	16.37	2.15

Table 4-5. Reference bedrock channel widths (w_{ref}) and depths (d_{ref}) calculated from w_r-A and d_r-A regressions using a reference drainage area of 50 km^2. Regression equations used; All bedrock w_r=4.59$A^{0.30}$, d_r=1.15$A^{0.21}$, Over-entrenched w_r=5.38$A^{0.25}$ d_r=1.71$A^{0.15}$, Postglacial-entrenched w_r=4.58$A^{0.30}$ d_r=1.09$A^{0.23}$, Under-entrenched w_r=4.05$A^{0.36}$ d_r=1.04$A^{0.19}$.

4.4   Discussion

4.4.1   Controls on channel geometry

4.4.1.1   Hydraulic scaling of bedrock channel geometry

The overall w_r-A and d_r-A scaling relationships for NW Highland rivers of w~3.9$A^{0.39}$ and d~0.87$A^{0.22}$ are within the range of hydraulic scaling relationships derived for mountain streams and bedrock channels in Scotland (Addy et al., 2010; Jansen et al., 2010), and worldwide (e.g. Montgomery and Gran, 2001; Whipple, 2004; Wohl and David, 2008) (Figure 4-14, Table 4-6). The w_r-Q and d_r-Q scaling relationships are more variable between studies, and the data are generally more scattered leading to lower R^2 values. The higher variability in the w_r-Q and d_r-Q relationships may be due to the use of different methods to calculate the formative discharge for catchments, and/or the imperfect representation of long-term discharge regimes by regional empirical *Q-A* scaling relationships derived from short-term gauging records (e.g. Wohl and David, 2008).
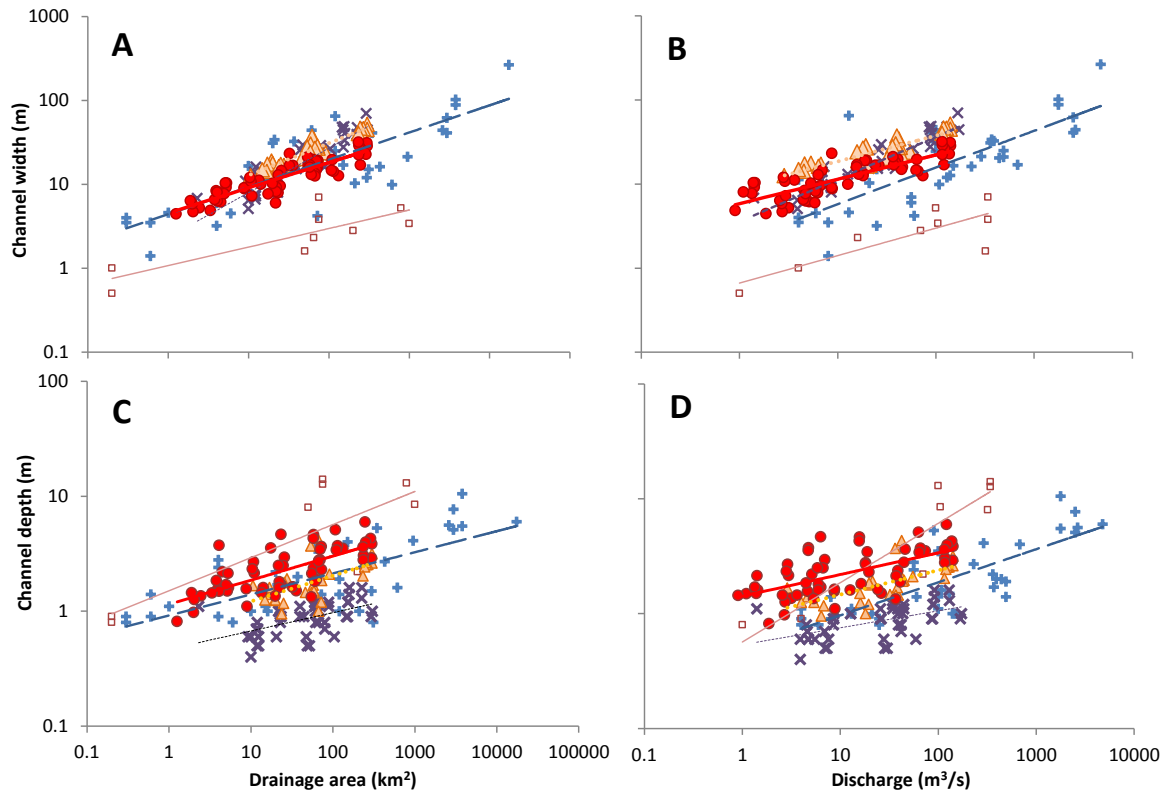
Figure 4-14. Comparison of NW Scotland channel *w-A* (A), *w-Q* (B), *d-A* (C) and *d-Q* (D) relationships with data from published studies. Worldwide bedrock channel dataset compiled by Wohl and David (2008) (small crosses, long dashed trendline), with slot-canyon subset (open squares, thin solid trendline). Data from mountain streams (coarse-grained alluvial) in the River Dee catchment, Cairngorm Mountains, northeast Scotland (Addy, 2010) (diagonal crosses, short dashed trendline). Bedrock channels (filled circles, thick solid trendline) and alluvial channels (filled triangles, dotted trendline) from this study.

The reach-averaged widths and depths of both bedrock and alluvial channels in NW Scotland fall within the range of data from the worldwide bedrock channels dataset of Wohl and David (2008), indicating that postglacial bedrock channel geometry is comparable with that of rivers in non-glaciated settings. The data from this study are less scattered than the worldwide data (Figure 4-14, Table 4-6), probably due to the smaller geographic scope which limits the potential variation in sediment flux, grain-size, discharge variability, and vegetation between sampled reaches. The fact that both alluvial and bedrock channel widths and depths fall within the range of the worldwide bedrock channel data suggests that differences between scaling relationships for transport-limited (i.e. alluvial) and detachment-limited (i.e. bedrock) channels may be relatively subtle.

The widths of alluvial and bedrock channels from the NW Highlands are comparable with those of mountain-alluvial channels in the Cairngorm Mountains, northeast Scotland (Addy, 2010) (Location in Figure 2-1), but the NW Highland channels are apparently systematically deeper (Figure 4-14 C and D). It is not known whether this difference in depths is real or an artefact of measurement techniques, measurement distribution, or

differences in the estimated reference discharge level. A standardised method of measuring channel depth is needed in order to facilitate comparisons between studies.

	Research study	Width		Depth	
		Drainage Area	Discharge	Drainage Area	Discharge
Bedrock	Wohl and David (2008)[a]	$3.06A^{0.32}$	$1.12Q^{0.50}$	$1.02A^{0.20}$	$0.58Q^{0.30}$*
	Wohl and David (2008) – No slot gorges	$4.41A^{0.32}$	$2.11Q^{0.43}$	$0.92A^{0.18}$	$0.50Q^{0.29}$
	Montgomery and Gran (2001)[b]	$0.002\text{-}0.54A^{0.30\text{-}0.53}$	-	-	-
	Tomkin et al. (2003)	$4.2A^{0.42}$	-	-	-
	NW Highlands	$4.54A^{0.30}$	$5.86Q^{0.29}$	$1.15A^{0.21}$	$1.42Q^{0.18}$
	Jansen et al. (2010)[c]	$0.0002\text{-}1.15A^{0.14\text{-}0.65}$	-	-	-
Alluvial (Mountain)	Montgomery and Gran (2001)	$0.001\text{-}0.05A^{0.32\text{-}0.55}$	-	-	-
	Wohl and Merritt (2008)	-	$4.9\text{-}9.2Q^{0.27\text{-}0.29}$	-	$0.24\text{-}0.31Q^{0.29\text{-}0.38}$
	Addy (2010)[d]	$2.33A^{0.53}$	$3.58Q^{0.50}$	$0.47A^{0.16}$	$0.54Q^{0.15}$
	NW Highlands	$5.30A^{0.38}$	$9.19Q^{0.31}$	$0.73A^{0.22}$	$0.90Q^{0.21}$
Alluvial	Park (1977)[e]	-	$\sim Q^{0.4\text{-}0.5}$	-	$\sim Q^{0.3\text{-}0..4}$
	Bray (1982)	-	$\sim Q^{0.53}$	-	$\sim Q^{0.33}$
	Hey and Thorne (1986)	-	$\sim Q^{0.52}$	-	$\sim Q^{0.39}$

Table 4-6. Selected published downstream hydraulic scaling relationships. Only bedrock channel data from studies where channels are defined according to the actual material of the channel boundary are shown.
[a] Compilation of worldwide field data. Values of regressions are as published and are derived from the whole dataset including the slot-gorge reaches. Relationships have been recalculated for the data with slot gorges excluded – these revised relationships are shown in the plots in Figure 4-14.
[b] Field data from catchments in the western USA
[c] Channel width data derived using GIS for the rivers Coe, Etive, Leven and Nevis in Western Scotland.
[d] Field data from the River Dee catchment, Grampian Highlands, northeast Scotland
[e] Compilation of published gravel-bed channel data, only modal range cited here, total range is 0.03-0.86 for *w-Q* and 0.09-0.70 for *d-Q* exponents
*not recorded in the published paper but derived from the data presented in table 2 of Wohl and David (2008)

4.4.1.2   Substrate control on channel geometry

Substrate type exerts a strong control on the channel geometry in the NW Highlands, with channels formed in cohesive substrates (peat and bedrock) narrower and deeper than those formed in non-cohesive sediment. The influence of peat and coarse sediment on alluvial

channel widths and depths at low drainage areas, supports previous observations from studies of gravel-bed streams (e.g. Hey and Thorne, 1986; Miller, 2005; Wohl, 2004). However, the value of the alluvial channel w_r-A scaling exponent derived from these data (0.38) is lower than those found in most studies of gravel-bed alluvial or mountain streams, which are generally between 0.45 and 0.55 (cf. Hey and Thorne, 1986; Miller, 2005; Wohl and Merritt, 2008; Parker et al. 2007). The high sensitivity of alluvial channel width to boundary resistance at low drainage areas has the potential to dramatically change the observed scaling relationship if vegetation, peat or grain-size effects are not accounted for. Inclusion of boulder dominated reaches or those affected by peat increases the observed w_r-A exponent to 0.41 and 0.48 respectively, closer to published values. Thus, the nature of topographic, vegetation and soil changes and the type of upland sediment sources and patterns of downstream sediment fining are likely to exert strong controls on the hydraulic scaling relationships of alluvial channels (cf. Hey and Thorne, 1986; Pizzuto, 1992).

The statistically significant difference between the w_r-A scaling exponents for bedrock and alluvial channels (0.30 compared to 0.38) in the study rivers contrasts with the findings of previous comparative studies (Montgomery and Gran, 2001; Wohl and David, 2008), and is inconsistent with the general assumption of similar w-A scaling for bedrock and gravel-bed alluvial channels (e.g. Whipple, 2004). Yet, lithological resistance was found to have limited impact on the observed hydraulic scaling, a similar result to that of Wohl and David (2008). These results contrast with the observation of local channel narrowing across a contact between limestone and resistant granite made by Montgomery and Gran (2001), suggesting that abrupt changes in lithological resistance may influence channel geometry, but at larger scales other factors, such as discharge, may be more important controls over channel width.

4.4.1.3   Erosion versus resistance thresholds

The numerical modelling of Turowski et al. (2007) suggests that bedrock resistance plays an important but complex role in controlling channel geometry. The balance between substrate resistance and the erosive capacity of the stream constrains a morphological threshold separating two different domains in which the channel geometry displays different sensitivity to 'hydraulic' and 'substrate' control factors (Figure 4-15 A). At rock strengths below the threshold, substrate resistance exerts very little influence on channel form, which is instead dictated by discharge and bedload flux, whereas at high rock strengths, substrate resistance acts as a strong control on channel geometry (Figure 4-15).

This threshold is discharge dependent, thus, in larger streams only extremely strong rocks are likely to exert any control on the channel geometry (Figure 4-15). A comparable complex control of lithological resistance and discharge on channel slope has been described by Brocard and van der Beek (2006) for channels in the French Alps. They found that lithological knickpoints, formed where streams cross resistant bedrock (limestone), occur only at drainage areas <30 – 45 km^2, with lower drainage area thresholds for less resistant lithologies. The contrasting observations of substrate versus hydraulic control on channel width in published field studies may be due to the effects of this erosion versus resistance threshold.

If erosion in both alluvial and bedrock channels is considered to depend on the capacity of the flow to detach and transport material at the channel boundary, all 'granular' substrates, from non-jointed resistant bedrock to non-cohesive sediment, can be considered conceptually on a single resistance scale across the spectrum of channel types. Substrate resistance (R_s) can be thus represented by a nominal 'detachment' term related to the force required to 'loosen' grains (P_D; a function of rock tensile strength and joint density, continuity and orientation), and a 'transport' term related to the force required to entrain grains (P_T; a function of grain-size and shape):

$$R_S = P_D + P_T \qquad\qquad\qquad\qquad\qquad\qquad \text{Eq 4.7.}$$

Assuming that channel geometry adjusts in order to balance the rate of erosion around the channel boundary (cf. Yanites and Tucker, 2010), the stable channel geometry will depend on the relative importance of P_D. Where $P_T \geq P_D$, the erosion rate depends on the rate of sediment transport, channels are transport-limited, and channel geometry adjusts so that shear stress around the channel margin matches that needed to entrain grains. Empirical measurements suggest that this adjustment yields downstream hydraulic scaling relationships where $w{\sim}A^{0.5}$. Where $P_T < P_D$, channels are detachment limited and higher shear stresses are needed to erode rock from the channel boundary, the corresponding stable channel geometry is narrower and deeper than for transport-limited channels with w-A scaling exponents <0.5.

The erosional capacity of the stream (E_c) is a function of discharge, slope and sediment flux. The balance between E_c and R_s constrains the main controls on channel geometry; the morphological threshold depicted in Figure 4-15 represents the E_c:R_s ratio that marks the transition between transport-limited and detachment-limited domains. As well as high R_s, high values of E_c, i.e. in large streams with high stream power, also affect the

morphological threshold. Where E_c greatly exceeds that needed to detach rock, the P_D term becomes unimportant, so that even where substrates are highly resistant, channel form will depend only on hydraulic parameters. Observations of similar bedrock and alluvial channel scaling relationships (e.g. Montgomery and Gran, 2001; Wohl and David, 2008), and the consequent assertion that channel geometry is primarily set by bedload flux (Montgomery and Gran, 2001; Whipple, 2004), may be due to the measured channels falling within the transport-limited geometry domain. This would be expected where substrates have low P_D, as for poorly consolidated sedimentary rocks and unconsolidated alluvium (Montgomery and Gran, 2001), or where E_c is large due to high discharge, steep slope or narrow channel. By contrast, observations of substrate control on channel width, with hydraulic scaling exponents c. 0.3, are only associated with highly resistant bedrock (high P_D) i.e. channels in the detachment-limited geometry domain (Montgomery and Gran, 2001; Jansen, 2006; Jansen et al., 2010).
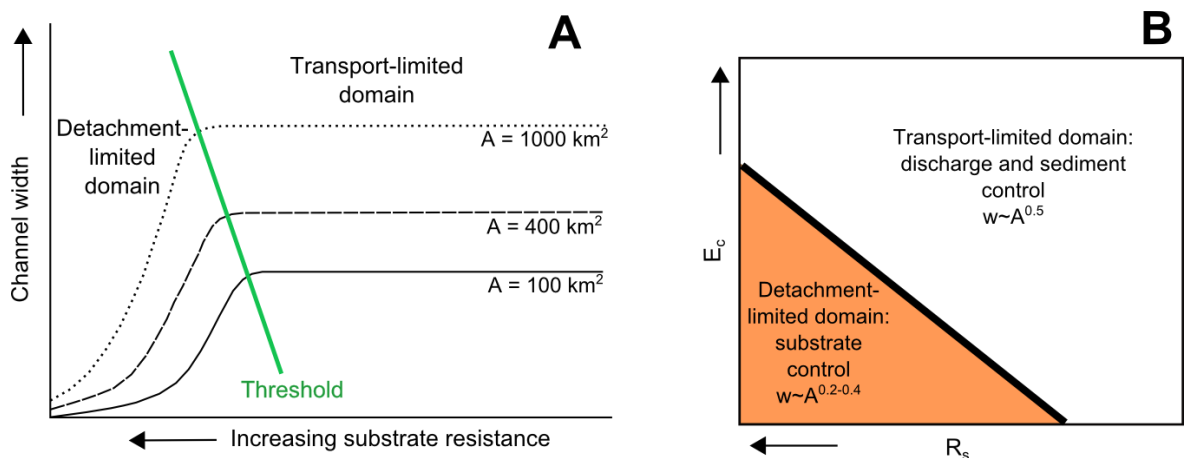
Figure 4-15. A) Sketch graph of model channel width versus substrate resistance (modelled as the ratio of Young's modulus to square of the rock tensile strength) after Turowski et al. (2007), indicating detachment-limited and transport-limited morphological domains (my addition). B) Schematic conceptual diagram indicating distribution of morphological domains in relation to the erosive capacity of the stream (E_c) and substrate resistance (R_s). Thick black line represents the threshold E_c/R_s ratio at the transition between detachment-limited and transport-limited conditions.

The difference between bedrock and alluvial channel hydraulic scaling relationships found in this study indicates that they fall into different morphological domains. This is driven by a major difference in P_D between the highly resistant bedrock and non-cohesive alluvial sediment. By contrast, the lack of lithological control on channel geometry suggests that relatively small differences in P_D between metamorphic lithologies may have, at best, only subtle effects on channel geometry that are obscured by variability in the data. The observation of a possible discharge threshold control on peat channel geometry in this study is also consistent with these suggestions, but the different processes of substrate

detachment in fibrous materials may lead to different constraints on the detachment versus transport threshold in these channels.

The complexity of the controls on both E_c and R_s, and the limited availability of quantitative field data, means it is not currently possible to estimate the threshold $E_c{:}R_s$ ratio. However, the threshold is synonymous with that quantified by Wohl (2004) for the coarse-grained mountain alluvial channels. The system studied by Wohl (2004) represents a simplified scenario in which $P_T > P_D$ and R_s is thus strongly related to the sediment grain-size, and E_c is equivalent to the sediment transport capacity, which can be reasonably estimated by stream power (cf. chapter 3). She finds that channels with a Ω/D_{84} ratio exceeding 10000 kg/s^3 develop strong hydraulic geometry scaling with an average w-A exponent of 0.43. Channels with a Ω/D_{84} ratio <10000 kg/s^3 were only weakly hydraulic scaled with an average w-A exponent of 0.2. Wohl (2004) suggested that this threshold spatially limits the development of hydraulic scaling in alluvial channels, but the results from this study indicate that small alluvial channels with large grain-sizes scale similarly to bedrock channels. Rather than a break-down in scaling as she proposed, the threshold marks a transition from transport-limited to detachment-limited geometry scaling.

4.4.1.4   Channel slope and the channel cross-section

The discussion above implies that channel slope, as a major control on stream power, is also a potential control on channel width and depth. Physical modelling and field studies have all shown an influence of channel slope on the cross-section geometry, with narrower channels formed where slopes are steeper (e.g. Finnegan et al., 2005; Whittaker et al., 2007; Attal et al., 2008). In the study channels, slope was found to have no observable effect on channel width or depth, but a very weak negative scaling with the w/d ratio. The lack of slope control on channel width in the study rivers may be due, in part, to the strong control of slope on channel type (discussed in chapter 3), which suggests that channel slope may have only an indirect influence on the channel cross-section. However, the dominance of alluvial channels at low channel slopes, reducing the range of slopes over which bedrock channels occur, and the high uncertainties on GIS-derived channel slopes may mean that any subtle slope control on channel geometry is obscured by variability in the data. Improvements in the measurement of channel slope are needed to clarify whether channel slope has a direct control on channel width and depth in this setting, or is only an indirect control on the cross-section geometry.

4.4.2   Postglacial bedrock channel geometry

4.4.2.1   Postglacial channel adjustment

Comparison of channel geometry for streams with probable inheritance of pre- or sub-glacially cut gorges indicates that inheritance does not substantially affect the channel width. This finding suggests that the inherited erosional features were formed either under similar discharge conditions, or that the postglacial rivers have adjusted their channel cross-sections to the prevailing postglacial discharge regime. The presence of sediment-trapping rock-bound lakes and the partial glaciation of two of the study catchments during the Younger Dryas stadial (12.9 – 11.7 ka) also appear to have had no long-term impact on the channel geometry despite probable spatial variations in peak discharges and sediment flux.

More entrenched channels are generally deeper than channels with limited entrenchment which commonly have higher *w/d* ratios. Bedrock channels with low degrees of entrenchment are generally found in areas of the valley floor mantled by alluvial or glacio-fluvial sediments, suggesting that these channels have been through prior phases of alluvial aggradation followed by erosion (section 3.2.3). As alluvial channels are wider and shallower for a given drainage area than are bedrock channels due to their more erodible boundaries, the alluvial-to-bedrock channel transition is accompanied by narrowing and deepening of the channels. In some areas, this process has resulted in the formation of strath terraces (chapter 5). Declining paraglacial sediment flux, which is thought to drive the postglacial alluvial-to-bedrock channel transition (chapter 3), may therefore indirectly influence channel geometry.

4.4.2.2   Timescales of response

The strong w_r-A and d_r-A scaling of bedrock channels in the NW Highlands suggests that the streams have had sufficient time (c. 11.5 – 14 kyr) and erosive capacity to adjust their cross-sectional geometry to the postglacial discharge regime and inherited valley-floor slopes. However, minor, but statistically significant, variations in channel geometry caused by a delayed onset of incision in bedrock reaches that were temporarily shielded by sediment cover indicates that some channels may only be partially adjusted. The exponential decrease in *w/d* shown in Figure 4-13, suggests that the *w/d* ratio stabilises at ~4 – 5 between entrenchment depths of 5 – 10 m, slightly higher than the range of bankfull flow depths. Variations in erosion rates along channels may mean that the timescale for

achieving stable cross-section geometries are spatially variable. However, for an assumed average erosion rate of 0.6 m/kyr (cf. section 5.4.3) the predicted 'response time' for channel geometry adjustment would be ~8 – 17 ka.

This result contrasts with the relatively weak *S-A* scaling due to the strong glacial conditioning of the long profiles (chapter 3). Although perfect steady-state *S-A* scaling may not be expected for the lithologically diverse study channels, the lack of lithological control on channel slope, even at the reach scale (section 3.3.1), suggests that channel slope remains poorly adjusted over the postglacial timescale. Rapid adjustment of channel cross-sectional geometry relative to channel slope has been noted in alluvial channels adjusting to perturbation (Parker et al., 2003), and may be simply due to the need for substantially more sediment or rock to be removed to adjust channel slope than channel width and depth.

4.5   Conclusions and implications

Bedrock channels in the NW Highlands have developed stable cross-section geometries adjusted for discharge and substrate resistance over postglacial timescales of 11.5 – 14 ka. Response times depend on the balance between local incision rates, conditioned by stream power and lithological resistance, and channel size, with channel adjustment achieved at entrenchment depths ~1 – 2 times the bankfull flow depth. Delayed bedrock incision due to temporary shielding by alluvial or glacio-fluvial sediment deposits prolongs the response time, leading to a spatial variation in the degree of channel adjustment.

The results highlight the potential importance of a morphological threshold arising due to differing controls on channel geometry in detachment-limited and transport-limited channels. This finding suggests that modelling frameworks must account for the influence of substrate resistance on the channel geometry, and especially that associated with thresholds of bed material entrainment. A standardised methodology for the measurement of substrate resistance in fluvial field studies is needed (cf. section 7.2.2), and should, ideally, be integrated with parameters used in theoretical and experimental modelling. In the meantime, it is clear that accurate descriptive characterisation of channel substrate is required in studies of channel form. Loose definitions of bedrock channels, such as those applied to 'mountain streams' where channels with alluvial banks and bed are classed as bedrock on the basis of modes of long-term landscape adjustment must be used with caution.

Chapter 5

Rate and timing of postglacial fluvial bedrock incision

5.1   Introduction

5.1.1   Context

The distribution of bedrock channels in the NW Scottish Highlands remains strongly controlled by glacially-conditioned valley floor slopes suggesting limited postglacial fluvial adjustment (chapter 3). But the hydraulically-adjusted geometry of these bedrock channels indicates that postglacial fluvial incision has been sufficient to reset the channel widths and depths (chapter 4). The rate of fluvial incision constrains the timescale for channel adjustment following deglaciation and is known to be controlled by the same factors that influence channel distribution and geometry; stream power, lithological resistance and sediment flux (Sklar and Dietrich, 1998; Whipple et al., 2000; Whipple, 2004). The glacial-conditioning of valley floor slopes (which set stream power) and sediment flux in postglacial settings has the potential to locally enhance rates of fluvial incision relative to background levels set by regional tectonic uplift rates (e.g. Valla et al., 2010a; Jansen et al., 2011). The common occurrence of erosional fluvial bedrock landforms such as gorges, waterfalls and strath terraces in many postglacial settings lends tacit support to this hypothesis. However, the origin of bedrock gorges in postglacial landscapes is debated and many are thought to be wholly or partly inherited from periods

of erosion by pre-glacial streams or sub-glacial meltwater channels (e.g. Holtedahl, 1967; McEwen et al., 2002; Montgomery and Korup, 2011).

The quantification of postglacial fluvial incision rates is fundamental to the assessment of the timescale of channel, and wider landscape, adjustment following deglaciation. It is also the key to determining the controls on fluvial erosion and how glacial conditioning of the landscape influences incision in postglacial streams. Methods of quantifying fluvial incision rates over postglacial timescales (c. 10^4 years) invariably rely on quantitative assessments of erosional fluvial landforms such as gorges and strath terraces (e.g. McEwen et al., 2002; Valla et al., 2010a; Jansen et al., 2011). But in view of the debate regarding the origin of gorges in postglacial settings, methods for quantifying postglacial fluvial incision rates, must *also* account for the timing of formation of fluvial erosion landforms. Surface exposure dating of strath terraces using *in situ* cosmogenic nuclide analysis can quantify both the timing of strath terrace formation and long-term fluvial erosion rates. Strath terraces at five sites in the Scottish Highlands have been analysed using this technique, quantifying the timing of strath formation, the rate of fluvial incision and highlighting key control factors on the incision process.

5.1.2   Research questions and chapter outline

Despite the potential importance of fluvial bedrock erosion for controlling the long-term landscape response to deglaciation there are few published rates of fluvial incision from postglacial regions, and the controls on the process in these settings remain poorly characterised. Erosion rates of 0.2 – 0.4 m/kyr were quantified in gorges in Norway by McEwen et al. (2002) and rates of 0.4 – 2.4 m/kyr were measured in rivers responding to glacio-isostatic uplift in western Scotland by Jansen et al. (2011). These two studies are the only existing quantitative assessments of fluvial erosion rates in post-orogenic, postglacial terrains comparable to the study area. Jansen et al. (2011) quantify postglacial incision rates using cosmogenic nuclide surface exposure dating of strath terraces associated with knickpoints. They measure a long-term decrease in knickpoint retreat rates, thought to have been caused by declining postglacial sediment flux. This study highlights the potential importance of temporal changes in postglacial incision rate in terms of long-term landscape adjustment to deglaciation.

Here the timing and rate of fluvial incision in the Scottish Highlands are assessed by addressing the following research questions:

1. When did the strath terraces form? - What controls the timing?

2. How fast is fluvial incision and does the rate change with time? - What controls the rate of incision?

Following the strategy of Jansen et al. (2011), cosmogenic nuclide analysis is used to derive surface exposure ages for strath terraces at five sites on Scottish Highland rivers which are then used to quantify fluvial erosion rates. These strath terraces are located at knickpoints formed where rivers cross riegels, and are above the glacio-isostatic response limit for these channels. The procedure for dating strath terraces through cosmogenic nuclide analysis is reviewed below, with particular attention paid to the geomorphic interpretation of strath terraces that underpins the method.

5.2   Dates and rates from strath terraces

Strath terraces are preserved remnants of bedrock channel bed that are abandoned by the river during fluvial incision (cf. Burbank et al., 1996; Hancock and Anderson, 2002; Wohl, 2008). Strath terraces form due to changes in boundary conditions for fluvial erosion that result in: 1) a change in the rates of lateral versus vertical channel incision; 2) a long-term change in bedrock channel width; and/or 3) a change in channel type accompanied by channel narrowing (e.g., a switch from an alluvial to a bedrock channel). The interpretation of cosmogenic nuclide concentrations in strath terraces, the basis for calculations of long-term incision rates, rests on the geomorphic interpretation of the landform and its formation history (Hancock and Anderson, 2002; Ouimet et al., 2008). The principles of cosmogenic nuclide analysis and the interpretation of strath formation histories thus provide the conceptual basis for this mode of analysis.

5.2.1   Principles of cosmogenic nuclide analysis

Cosmogenic radionuclides (e.g., ^{10}Be, ^{14}C, ^{26}Al and ^{36}Cl) are produced in exposed rock surfaces as a result of the interaction of cosmic radiation with atoms in the rock minerals (e.g. Lal, 1988; Gosse and Phillips, 2001). Cosmogenic ^{10}Be is one of the most widely used *in situ* cosmogenic radionuclides due to its production in quartz-rich rocks and relatively long half-life which makes it suitable for determining surface exposure durations of 10^3-10^5 years (e.g. Gosse and Phillips, 2001). These factors make it ideal for studies in the Scottish Highlands due to the prevalence of quartz-rich metasedimentary rocks, and the timescale of deglaciation since the Late Devensian (LD) and YD glaciations (c.15 – 11.7 ka). Cosmogenic ^{10}Be is produced largely by spallation of oxygen and silicon in the

mineral structure, and builds up in quartz over the duration of exposure. Surface exposure ages are calculated from the concentration of ^{10}Be in samples from bedrock surfaces by comparing with an independent estimate of the ^{10}Be production rate. Comprehensive explanations of the processes of cosmogenic nuclide analysis are given by Lal (1988, 1991) and Gosse and Phillips (2001).

5.2.2   Cosmogenic dating of fluvial surfaces

A cosmogenic nuclide concentration from a bedrock surface depends on the duration of exposure and the rate of bedrock erosion (e.g., Lal, 1991). In order to interpret a bedrock strath terrace ^{10}Be concentration as an exposure age, the surface must not have inherited any pre-existing cosmogenic nuclide concentration; the surface must have formed rapidly, and; it must not have been buried or substantially eroded since it was formed (Leland et al., 1998; Reusser et al., 2006). Thus the conceptual 'geomorphic' models assumed for the formation of strath terraces are fundamental to the interpretation of cosmogenic nuclide concentrations (Montgomery, 2004; Ouimet et al., 2008). Conflicts over the interpretation of published strath surface exposure ages have arisen when differences in assumed formation models have not been clearly outlined (cf. Hancock and Anderson, 2002).

In order to resolve these conflicts, a new classification of strath terrace forms and formation models has been developed, based upon descriptions in published studies and field observations from the Scottish Highlands. This classification is presented in the following section to provide a conceptual basis for the use of cosmogenic nuclide analysis to date strath terraces in Scottish Highland rivers.

5.2.3   Strath terrace formation: geomorphic models

Three main forms of strath terrace are shown in Figure 5-1 (cf. Burbank et al., 1996; Hancock and Anderson, 2002; Montgomery, 2004). Differences in the morphologies and geomorphic contexts of these strath terraces indicate that they have different formation mechanisms, these are outlined in the following sections.
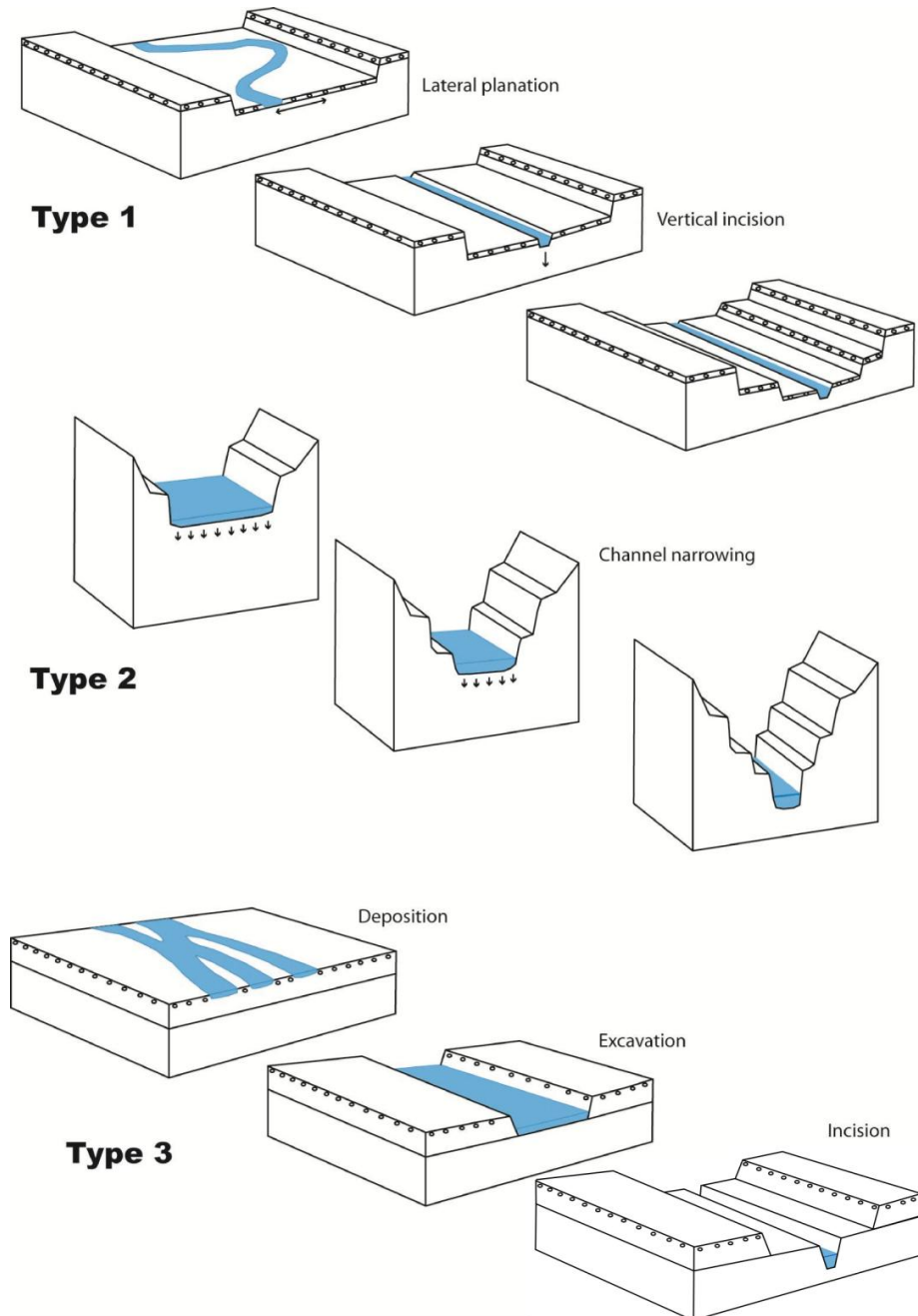
Figure 5-1.   Strath terrace types and proposed formation models (see discussion in the text).

5.2.3.1   Type 1 strath terrace formation

Type 1 strath terraces are wide, flat, longitudinally continuous surfaces with a thin cap of alluvial sediment (Figure 5-1). They are effectively raised, bedrock-cored floodplains, tens to hundreds of meters wide and up to several kilometres in length and commonly form flights of terraces in wide valley floors (Gilbert, 1877; Merritts et al., 1994; Hancock and Anderson, 2002; Montgomery, 2004; Fuller, 2009). The accepted formation model for these surfaces describes alternating phases of lateral planation by meandering streams and periods of vertical lowering (Gilbert, 1877; Hancock and Anderson, 2002). During the lateral planation phase the bedrock valley floor is widened by erosion of the valley wall at

the apex of meander bends, while the alluvial mantle is deposited by aggradation in the inner bend of the meander. The bevelled floodplain created during lateral planation is then abandoned when vertical erosion outpaces lateral erosion and the channel incises (Gilbert, 1877; Hancock and Anderson, 2002). Type 1 straths are found predominantly in terrains characterised by relatively weak bedrock (Montgomery, 2004), and their formation may be encouraged by rock fracturing due to weathering (Montgomery, 2004) or the effects of ground ice (Gibbard and Lewin, 2009; Murton and Belshaw, 2011).

Type 1 strath terraces are rare in the Scottish Highlands due to the resistant bedrock, which limits the rate of lateral planation, and the inherited glacial landscape form. Meandering channels are restricted to the alluvial reaches that occupy the flat floors of glaciated troughs already widened by glacial erosion; elsewhere channels are confined in gorges and narrow valley floors. Type 1 strath terraces are thus not used in the following analysis.

5.2.3.2   Type 2 strath terrace formation

Type 2 strath terraces are narrow, up to several channel widths wide, and discontinuous, and may have considerable surface relief and little-to-no sediment cover (Burbank et al., 1996; Leland et al., 1998; Wohl, 1992; Reusser et al., 2006; Jansen et al., 2011) (Figure 5-1). They occur in confined channel settings (gorges or narrow valleys) and are generally restricted to areas with resistant bedrock and/or high uplift rates (Montgomery, 2004; Wohl, 2008). Type 2 strath terraces appear to form as bedrock channels narrow during ongoing vertical incision or during the upstream passage of knickpoints (e.g. Gardner, 1983; Leland et al., 1998; Jansen et al., 2011). Channel narrowing may be guided by strong joint control on the channel geometry (Wohl, 2008), or as a result of changes in the distribution of fluvial incision due to declining sediment flux (cf. Finnegan et al., 2007; Johnson and Whipple, 2010). The tendency to narrow drives the formation of an inner channel leaving abandoned portions of the bed to become the Type 2 strath terraces. As sediment is concentrated in the developing inner channel, Type 2 straths are stripped of sediment during formation (Finnegan et al., 2007; Johnson and Whipple, 2010). This process results in a positive feedback mechanism which increases the rate of inner channel incision causing rapid abandonment of the strath. Cosmogenic nuclide concentrations from Type 2 strath terraces thus record the timing of abandonment of the strath surface by the river, i.e. the timing of changes in boundary conditions that control channel width.

5.2.3.3   Type 3 strath terrace formation

Type 3 strath terraces are narrow 'shoulders' of exposed bedrock valley floor adjacent to entrenched bedrock channels, flanked by alluvial or glacio-fluvial sediment terraces (Figure 5-1). In contrast to Type 1 and Type 2 strath terraces, Type 3 straths are not carved by active fluvial incision, but are formed when the river excavates a pre-existing bedrock surface, possibly a glacially eroded valley floor, from under sediment cover. As shown in chapter 4, alluvial channels formed in unconsolidated sediments are wider than bedrock channels formed in resistant lithologies. Thus, the transition from alluvial to bedrock channel systems that occurs where rivers incise across the sediment-bedrock boundary (chapter 3) may be accompanied by channel narrowing resulting in the incision of an inner gorge and the formation of Type 3 straths terraces. Assuming that there is no inheritance of cosmogenic nuclides, the cosmogenic surface exposure age of Type 3 straths thus quantifies the timing of surface excavation by the river and provides an upper limit for the timescale of entrenchment into bedrock by the active channel. The issue of inheritance of cosmogenic nuclides that may accumulate during any period of exposure before sediment burial, or during the cover period is addressed below.

5.2.4   Strath terraces in the Scottish Highlands

The formation models for Type 2 and Type 3 strath terraces provide a general justification for the use of cosmogenic nuclide analysis to date these strath surfaces and quantify incision rates. Application of this technique in the specific context of postglacial rivers in the Scottish Highlands also requires careful consideration to ensure that the key geomorphic 'assumptions' fundamental to the interpretation of strath surface cosmogenic nuclide concentrations are valid in this setting. First, the issue of potential inheritance of inner gorges and associated features from prior periods of erosion before or during glaciation is addressed (section 5.2.4.1). Following this, key assumptions of rapid pre-strath erosion and abandonment in the Scottish Highlands, characterised by low tectonic uplift rates and resistant bedrock, as well as the issue of inheritance in Type 3 straths, are considered (section 5.2.4.2). Both of these assessments include observations from the strath sites used in this study, which are described in section 5.3.1.

5.2.4.1   Strath terraces in postglacial landscapes

Some inner gorges in postglacial landscapes are interpreted to be pre-existing features formed by pre-glacial fluvial incision or erosion by sub-glacial meltwater streams

(Holtdahl, 1967; McEwen et al., 2002; Montgomery and Korup, 2011). This interpretation raises an important question as to the origin of the strath terraces and inner gorges in the study area, and thus whether the strath surface ^{10}Be ages and inner gorge geometry can be used to derive postglacial erosion rates. The key requirement for the derivation of postglacial erosion rates from these sites is a genetic relationship between the timing of strath exposure and the onset of incision of the inner gorge. If the inner gorges at the study sites were formed before or during glaciation, the ^{10}Be concentrations from the strath surfaces may be unrelated to postglacial bedrock incision. Because the postglacial ^{10}Be exposure ages from the strath terraces themselves cannot be used to suggest that the inner gorges formed during postglacial fluvial incision, observations from other sources are required to support the interpretation that the strath terraces and inner gorges here are indeed postglacial features.

The inner gorges at all sites used in this study are relatively small, no deeper than 16 m, and their geometry is consistent with that expected for the modern stream (cf. section 5.4.1). Assuming that inner gorges were incised following deglaciation (c. 14 – 11.7 ka), a basic assessment of predicted incision rates yields estimates of 0.3 – 1.1 m/kyr. These values are consistent with published postglacial fluvial incision rates for comparable regional settings, lithology, discharge and sediment flux conditions (section 5.1.2). At all sites there is evidence for ongoing fluvial erosion; the bed and lower gorge walls (within the active channel) are fluted and/or smoothed with 'clean' bedrock surfaces free from lichen cover. Towards the top of the inner gorge, and on strath terraces, bedrock surfaces retain fluvial erosion bed forms such as flutes, but are more weathered with increasing lichen cover and vegetation growth. The weathering gradient is also seen in a difference in Schmidt hammer 'R' values from tests conducted in the lower channel (near the low flow line) and towards the top of the inner gorge (near the high flow line). Values from the lower channel are consistently higher than those from the upper channel (Table 5-1) suggesting that erosion is outpacing weathering in the channel bed.

None of the sites is associated with glacial moraines or other features suggestive of ice marginal positions, nor do they have clear sub-glacial meltwater features such as incised dry tributary gullies or unusually large flutes or potholes. There are no remnants of glacial or glacio-fluvial sediment deposits found within the inner gorge at any site, nor are they found on the strath surfaces at the Type 2 sites (Glen Affric and the Monessie gorge, section 5.3.1).

Together, these observations provide strong evidence that the strath terraces and inner gorges at the study sites are genetically related and have formed since deglaciation. The issue of inheritance of pre-existing gorges is revisited, in light of the quantified cosmogenic surface exposure ages, in section 5.5.1.

5.2.4.2   Interpreting strath terraces in the Scottish Highlands

As noted in section 5.2.2, the key requirements for the interpretation of strath terrace cosmogenic nuclide concentrations as surface exposure ages are;

- that there is no inheritance of pre-existing cosmogenic nuclides,

- that the strath was rapidly abandoned by the river, and,

- that there was no significant burial or erosion of the surface after it was abandoned.

In previous studies of Type 2 strath terraces using cosmogenic nuclide analysis, assumptions of rapid pre-strath erosion and strath abandonment have been supported by measurements of high erosion rates in modern channels, i.e. very low [10]Be concentrations in modern channel beds (Leland et al., 1998; Reusser et al., 2006). But modern fluvial erosion rates in the Scottish Highlands are relatively low (Jansen et al., 2011) and consequently it is necessary to consider in more detail the implications of low pre-strath erosion rates and protracted abandonment on [10]Be concentrations in strath surfaces.

Numerical simulations were used to quantitatively assess the conditions that result in inheritance of [10]Be in Type 2 and Type 3 strath terraces. For Type 2 straths, simulations were used to assess the influence of 'pre-abandonment' incision rates and sediment cover on the [10]Be concentration of the strath surface at abandonment. For Type 3 strath terraces, the influence of incomplete shielding of the surface during the cover period prior to excavation was assessed. The implications of protracted strath abandonment for [10]Be concentrations in both strath types were also assessed through numerical simulations. The results of these simulations quantify criteria that were used to inform the selection of suitable sites in the Scottish Highlands, and are discussed with reference to observations made at the study sites in the following sections.

The numerical simulations were carried out using standard equations for calculating [10]Be production rate with depth (Eq 5.1) and exposure ages from sample [10]Be concentrations (Eq 5.2) (e.g. Lal, 1991):

$$P_z = P_0 e^{-\rho z / \Lambda}$$ Eq 5.1

Where P_z is the production rate in at/g/yr at depth z (cm), P_0 is the production rate at the surface, ρ is the density of substrate in g/cm^3 and Λ is the absorption mean free path (160 cm/g^2).

$$C = \left[\frac{P_i e^{-z\rho_r/\Lambda}}{\lambda + \varepsilon\rho_r/\Lambda}\right] \times \left(1 - e^{-(\lambda + \varepsilon\rho_r/\Lambda)t}\right) + \left(C_n e^{-\lambda t}\right) \qquad\qquad\text{Eq 5.2}$$

Where P_i is equivalent to P_0 or P_z depending on the simulation, C is the concentration of ^{10}Be in the sample (at/g), C_n is the initial concentration of ^{10}Be (assumed to be zero in the simulations), ρ_r is the density of the bedrock (assumed to be 2.5 g/cm^3 for psammitic bedrock), λ is the rate of radioactive decay for ^{10}Be (4.62 x 10^{-7} at/yr, e.g. Balco et al., 2008), ε is the erosion rate in cm/yr and t is time in years. Values for P_0 and a surface shielding factor that are representative of the study sites were used; P_0 = 4.96 atm/g (roughly equivalent to that expected at ~100m elevation, latitude 57°N), shielding factor = 0.9984. This surface shielding factor is an average of the shielding factors derived from sample points at the Dog Falls study site on the River Affric. A ^{10}Be concentration of 4000 at/g was used as the threshold concentration for inheritance. This value is equivalent to the approximate concentration of a good experimental blank, therefore defines a lower limit for a measurable concentration of ^{10}Be in a sample.

Inheritance of ^{10}Be in strath terraces

Inheritance of ^{10}Be would lead to an overestimation of the strath exposure age. As potential sources of inherited ^{10}Be differ for Type 2 and Type 3 strath terraces, they are considered separately.

For Type 2 strath terraces, the concentration of ^{10}Be in the channel bed at abandonment will depend on the rate of fluvial erosion and the average thickness of sediment cover during the period when the strath was part of the active channel bed. Under the simulation conditions, a model erosion rate of greater than 0.8 m/kyr would be necessary to yield active channel bed ^{10}Be concentrations of <4000 at/g. For higher production rates, i.e. at higher elevations and/or latitudes, this 'threshold' erosion rate would increase. This value of 0.8 m/kyr is at the high-end of erosion rates quantified for the Scottish Highlands (e.g. Jansen et al., 2011), suggesting that inheritance due to slow erosion of the strath surface prior to abandonment may contribute to observed ^{10}Be concentrations. However, mobile sediment cover passing through the bedrock reach and driving the incision also has a shielding effect on the channel bed. If the long-term average sediment cover (density 2 g/cm^3) on the active channel bed is assumed to be 50 cm thick, an erosion rate of c. 0.4

m/kyr would yield a sample concentration of approx. ~4000 at/g. For 1 m of sediment cover, the threshold erosion rate drops to ~0.2 m/kyr. These sediment thicknesses and erosion rates are both higher than those observed in modern Scottish Highland bedrock channels, but the model erosion rates are consistent with long-term Holocene vertical erosion rates measured in western Scotland (Jansen et al., 2010) and postglacial fluvial incision rates in Norway (McEwen et al., 2002) (similar bedrock lithologies and tectonic regime to those in northern Scotland). Early postglacial sediment flux is also likely to have been considerably higher than in the present day. Thus at abandonment, Type 2 strath terraces in the Scottish Highlands are likely to have had very low [10]Be concentrations and therefore no significant inheritance.

Inheritance in Type 3 strath surfaces may arise if the original surface concentration was not 'reset' through surface erosion prior to burial by sediment, if the bedrock valley floor was exposed prior to burial by sediment, and/or if the depth of sediment is insufficient to shield the bedrock valley floor during burial. As the study sites are located in the floors of trough valleys that were actively glaciated during the Late Devensian, it is likely that glacial erosion of >2 m depth occurred to reset the surface [10]Be concentration to zero and that burial under glacio-fluvial and/or alluvial sediment occurred during, or very soon after, ice retreat. There is no way of testing this directly for the study sites, but substantial inheritance would be expected to increase [10]Be concentrations such that apparent strath ages pre-date the expected deglaciation age. The potential for surface inheritance to affect the measured strath exposure ages is discussed in section 5.4.2.

Sediment depths over the bedrock valley floor adjacent to the Type 3 straths at the study sites range from 1.5 to >7 m (section 5.3.1). Taking the minimum depth of 1.5 m, and assuming a dry sediment density of 1.5 g/cm^3 (for sand and gravel, the wet density is ~2 meaning a slower rate of [10]Be accumulation), 3500 – 4000 years would be needed for the underlying bedrock to accumulate ~4000 at/g of [10]Be. The range in time is due to variations in production rate with altitude (c. 4.8 – 6.4 at/g/yr for 50 – 350 m elevation range in northern Scotland). For 2 m of sediment the time-span over which a site may accumulate [10]Be to measurable quantities rises to 6000 – 10,000 years. Thus, the time-scales required for measurable inheritance of [10]Be during the cover period at the study sites, even for fairly thin cover (c. 1.5 m), are relatively long and the inherited concentration gained during a prolonged cover phase does not compensate for the loss of accumulation due to the consequent shortening of the exposure period. Thus, [10]Be

inheritance due to partial shielding of Type 3 strath surfaces during the cover phase is not thought to be significant at the study sites.

Strath abandonment and ^{10}Be concentrations

The time taken for the river to abandon the strath surface may influence the accumulation of ^{10}Be. If the strath surface continues to be periodically eroded by the river after the inception of the inner channel, accumulation of ^{10}Be may be interrupted and the strath surface cosmogenic ^{10}Be concentration may underestimate the true surface age. Conceptually, the abandonment period may be considered as the time spent by the strath between the low flow and high flow water levels, although Reusser et al. (2006) point out that the lack of sediment in the upper parts of the flow means that erosion stops *before* the strath leaves the high flow channel.

The potential impact of a prolonged abandonment period is likely to be limited for Type 3 strath terraces, as these surfaces show limited evidence for fluvial sculpting, implying that the inner channel was relatively rapidly cut after excavation of the bedrock valley floor and fluvial modification of the strath was minimal. Therefore at these sites, the ^{10}Be concentration is thought to be a good representation of the timing of excavation of the surface from under sediment.

Type 2 straths are more likely to be affected by a prolonged abandonment period. The potential effects of abandonment periods of different durations on measured surface exposure ages were assessed using a simple numerical simulation in which periodic erosion of the strath is assumed to be most frequent soon after abandonment, and the effects of multiple incision events are approximated by a time-averaged erosion rate. The total duration of strath exposure used in the simulations was 12 kyr, with modelled abandonment periods of 2000, 4000 and 6000 yrs (i.e. up to half the total exposure period). An average strath lowering rate of 0.05 mm/yr was applied in the first half of each abandonment period, with a lowering rate of 0.01 mm/yr applied in the second half of the abandonment period. Under the model conditions, an abandonment period of 2000 years led to a 5% underestimation of the real strath age, with a 6000 year abandonment period causing an 8% underestimate. These values are within the range of uncertainty values on cosmogenic ^{10}Be surface exposure ages suggesting that prolonged abandonment may have a limited effect on the observed surface age. However, it is acknowledged that this is a very simplified model scenario and more detailed modelling of strath formation is needed

to shed light on the processes and timescales of strath abandonment. Cosmogenic ^{10}Be exposure ages for the Type 2 straths should therefore be considered as minimum ages for strath abandonment.

Strath terrace exposure and the accumulation of ^{10}Be

Degradation of strath terraces through weathering and surface erosion during the period of exposure may reduce the ^{10}Be concentration. Burial of the strath under alluvial sediment or debris from rockfalls or landslips would also result in lower ^{10}Be concentrations, causing underestimation of the strath surface exposure age.

All the Type 2 and Type 3 strath terraces assessed in this study are partially vegetated, and have associated surface weathering on less resistant pelite and semi-pelite where exposed; the quartz veins and psammitic bedrock sampled here are more weathering-resistant. These observations indicate that in most areas the strath surfaces are not being actively eroded by the river. Only short strath sections immediately downstream of the knickpoints, where bedrock surfaces are more exposed, may be active at high-flow levels, as indicated by 'clean' bedrock surfaces with little lichen growth and very limited vegetation. The implications of active erosion on the strath close to knickpoints are discussed further in section 5.4.2.

Geomorphic evidence from the study sites suggests that neither the Type 2 nor Type 3 strath surfaces were covered by sediment at or after abandonment. Apart from the main terrace tread at the outer edge of the Type 3 strath terraces, there are no sediment terraces or other substantial sediment deposits on any of the strath surfaces at the study sites.

The results of the numerical simulations described above indicate that strath terrace ^{10}Be concentrations in the Scottish Highlands should provide good estimates of the duration of surface exposure following abandonment by the active river. The method is thus considered to be a reliable means of quantifying the timing of strath terrace formation and fluvial incision rates in the study area.

5.3   Data and methods

The two main data components required to determine fluvial incision rates are the cosmogenic nuclide concentrations from strath surface samples and accurate measurements of the site geometry, particularly the vertical distance between the strath surface and the

channel bed, but also the width of the channel below the strath (for erosion flux calculations). Here the methodology for determining cosmogenic nuclide surface exposure ages is reviewed (section 0), and the procedure for measuring the site geometry is outlined (section 5.3.3).

5.3.1   Study site selection and site descriptions

To derive a representative range of incision rates for Scottish Highland rivers, five sites from a range of lithologies and drainage areas, and with differing deglaciation histories were selected. Channel reaches responding to glacio-isostatic uplift were avoided; all sites are located at knickpoints formed where postglacial rivers have inherited glacially eroded riegels or hanging valleys (Figure 5-3).

The distribution and main characteristics of the five selected strath sites are shown in Figure 5-2 and Table 5-1. Three of the strath sites are in the NW Highlands (rivers Carron, Blackwater and Affric), and two are in the western Highlands (River Spean) and Cairngorm Mountains (River Dee). The strath site at Croick Schoolhouse gorge on the River Carron, which was surveyed in detail, provides a direct link between the assessment of the timing and rate of fluvial incision and the evolution of postglacial channel type distribution and geometry discussed in chapters 3 and 4. Photographs of the strath sites are shown in Figure 5-4.

The lithological characteristics, drainage areas (surrogate for discharge) and deglaciation histories of the sites are given in Table 5-1. All sites apart from the Monessie gorge on the River Spean are located outside the Younger Dryas (YD) ice limit (Figure 5-2), although all experienced different degrees of glaciation of the upper parts of their catchments during that period. Deglaciation times for the sites (Table 5-1), are estimated on the basis of regional deglaciation histories for the YD ice cap (Monessie gorge only) or the Late Devensian (LD) British-Irish Ice Sheet (BIIS), described in chapter 2, together with quantitative evidence from lake sediments and cosmogenic nuclide-dated glacial moraines in the study catchments. The deglaciation histories of each catchment are outlined below.
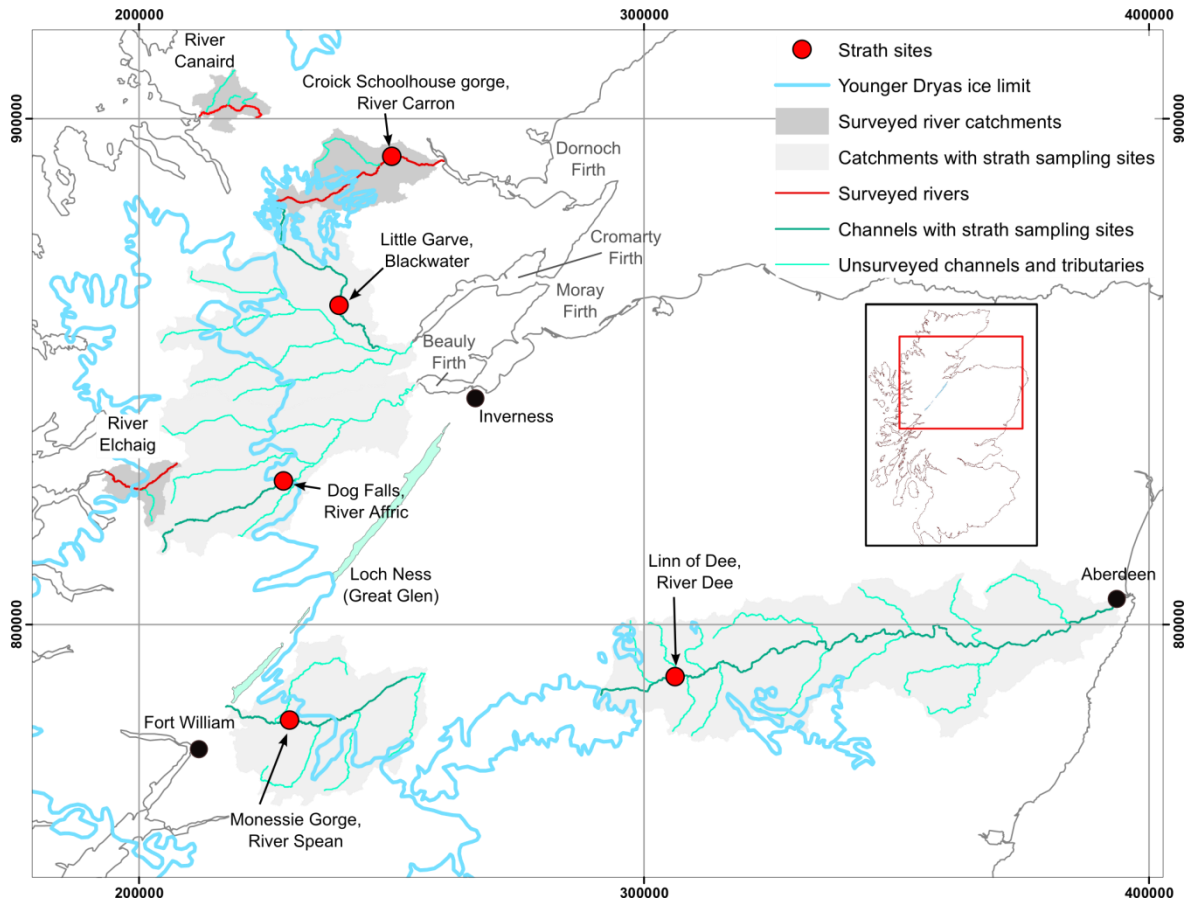
Figure 5-2. Location of strath terrace sampling sites in the Scottish Highlands. Surveyed rivers also shown. Inset map shows Scotland with location of main map marked by red box. Scale is indicated by 100km grid (British National Grid), named coastal inlets ('Firths') are referred to in the text, major cities (black dots) shown for reference. Younger Dryas ice limit based on Bennett and Boulton (1993), Golledge (2010) and Finlayson et al. (2011).

Site, River	Strath Type	Area (km²)	Lith.	Schmidt Hammer 'R' value		Joint spacing (m)	Selby index	Late-Devensian deglaciation[b] (ka)	YD glaciation context[b]
				High[a]	Low[a]				
Little Garve, Blackwater	3	266	Qzt / Psam	34.7	56.1	0.73	81	14.5-13.5	Headwater glaciers
Croick Schoolhouse, River Carron	3	246	Psam	47.6	50.1	0.17	77	14.5-13.5	Glacier 10km upstream
Linn of Dee, River Dee	3	158	Schist	30.6	31.7	0.86	79	15-14	Not glaciated
Dog Falls, River Affric	2	195	Qzt	57.1	58.6	0.47	82	14-13	Glacier 1km upstream
Monessie Gorge, River Spean	2	551	Pelite	32.3	38.1	0.98	80	-	11.5 ka glacier retreat and glacial lake drainage

Table 5-1. Data for strath terrace study sites.

[a] **Mean value derived from 30 readings taken at random in ~1m² areas of channel bed near the high-water level (high) and just above base-flow level (low).**
[b] **Estimated timing of BIIS/Late Devenisan deglaciation and context for site/catchment during the Younger Dryas (YD) stadial, discussed in the text.**

5.3.1.1   Linn of Dee, River Dee

The Dee catchment was fully glaciated during the LD glacial maximum (c. 20 ka), with ice retreating to the present coastline by approximately 17 − 15 ka (Brown, 1993; Bradwell et al., 2008c; Phillips et al. 2008; Ballantyne, 2010). At the upper end of the catchment, Everest and Kubik (2008) report cosmogenic nuclide surface exposure ages from moraines located c. 15 km upstream from the study site, with a mean age of 14.6 ± 0.6 ka. However, Ballantyne (2010) suggests that an earlier deglaciation age of ~ 15 ka for the upper Dee valley may be more likely. Following the LD deglaciation, a period of minor corrie-glaciation occurred in the catchment headwaters during the YD (c. 12.9 − 11.7 ka, Everest and Kubik, 2008; Ballantyne, 2010; Golledge, 2010). The available data suggest that the Linn of Dee was deglaciated sometime between ~15 and 14 ka and was followed by rapid deposition of glacio-fluvial terraces, alluvial fans and alluvial terraces on the valley floor. It is hypothesised that the Type 3 strath terraces at the Linn of Dee were formed as the postglacial river excavated the valley floor sediment cover, exposing a knickpoint in the buried bedrock valley floor which was then incised to form the bedrock gorge. Exposure and abandonment of the Type 3 strath (Figure 5-4 D) occurred due to narrowing of the channel on the transition from alluvial to bedrock substrate.

5.3.1.2   *Little Garve, Blackwater*

The Blackwater is a tributary of the River Conon, which was fully glaciated during the LD glaciation and was drained by a major outlet glacier the fed the Moray Firth ice stream via the Cromarty Firth (e.g., Merritt et al., 1995). The timing of the retreat of the ice is poorly known, but the ice front is likely to have reached the current coastline between 15 and 14 ka (Firth, 1989; Phillips et al., 2008; Ballantyne, 2010). Carbon-14 dates from organic material in a small lake in the catchment headwaters, ~15 km upstream from the study site, indicate that the upper valley was ice free by 14.0 − 12.9 ka (Kirk and Godwin, 1963; Finlayson et al., 2011). Thus, the retreat of the LD glacier across the study site is interpreted to have occurred between 14.5 and 13.5 ka, with glacio-fluvial and/or alluvial sediments deposited on the valley floor during or soon-after ice retreat. During the YD outlet glaciers from the Beinn Dearg ice cap (cf. Figure 2-3) occupied tributary valleys in the upper catchment, with ice margins located ~ 12 km upstream from the strath site (Finlayson et al., 2011). The Type 3 strath terraces at Little Garve (Figure 5-4 C) are hypothesised to have formed due to lateral migration and narrowing of the postglacial channel as the Blackwater excavated the valley-floor sediment and incised the bedrock gorge.

5.3.1.3   Croick Schoolhouse Gorge, River Carron

A detailed overview of the glacial history of this catchment is given in section 2.3.1.1, and is briefly reviewed here. The catchment was glaciated during the LD by a tributary glacier of the Dornoch Firth ice stream. During the latter part of the LD, c. 16 – 14 ka, the ice front retreated up the Dornoch Firth, separating the tributary glaciers as the ice margin reached the modern coastline along the marine inlet of the Kyle of Sutherland (Hansom, 1991). The chronology of retreat of the LD ice front up the Carron valley is poorly known, however Finlayson et al. (2011) report two cosmogenic nuclide surface exposure ages of 12.4 ± 1.2 and 11.6 ± 1.4 ka (calculated using the Lm scaling scheme of Balco et al. (2008)), from a YD moraine approximately 10 km upstream from the strath site. These ages suggest that the site at Croick Schoolhouse was probably deglaciated from under LD ice between 14.5 and 13.5 ka, with ice retreating into the catchment headwaters before the YD re-advance (cf. Finlayson et al., 2011). Alluvial terraces at the study site were probably formed rapidly following LD glacier retreat and were later excavated by the river during excavation of the Type 3 strath surfaces and incision of the bedrock gorge (Figure 5-4 B).

5.3.1.4   Dog Falls, River Affric

The River Affric is a major tributary of the River Glass, in the upper part of the Beauly catchment, which was fully glaciated during the LD glaciation, with the Beauly glacier feeding the Moray Firth ice stream via the inner Beauly Firth. The timing of glacier retreat up the outer Moray Firth and inner Beauly Firth is estimated at 16 – 15 ka (Firth, 1989; Phillips et al., 2008; Ballantyne, 2010). There are no published dates with define the chronology of glacier retreat within the Beauly catchment. However, the position of the YD ice margin in Glen Affric is reasonably well defined from field data and numerical modelling (Bennett and Boulton, 1993; Golledge 2010). This ice margin position is approximately 1 – 2 km upstream from the study site and, assuming an early YD age (c. 12.9 – 12.5 ka) for this maximum ice advance (Golledge, 2010), suggests that deglaciation of the study site occurred sometime between 14 and 13 ka, with ice retreat into the catchment headwaters by the close of the Lateglacial interstadial followed by re-advance of the Affric glacier during the YD. The Type 2 straths at Dog Falls, shown in Figure 5-4 A, are interpreted to have formed during fluvial incision sometime after the LD deglaciation.
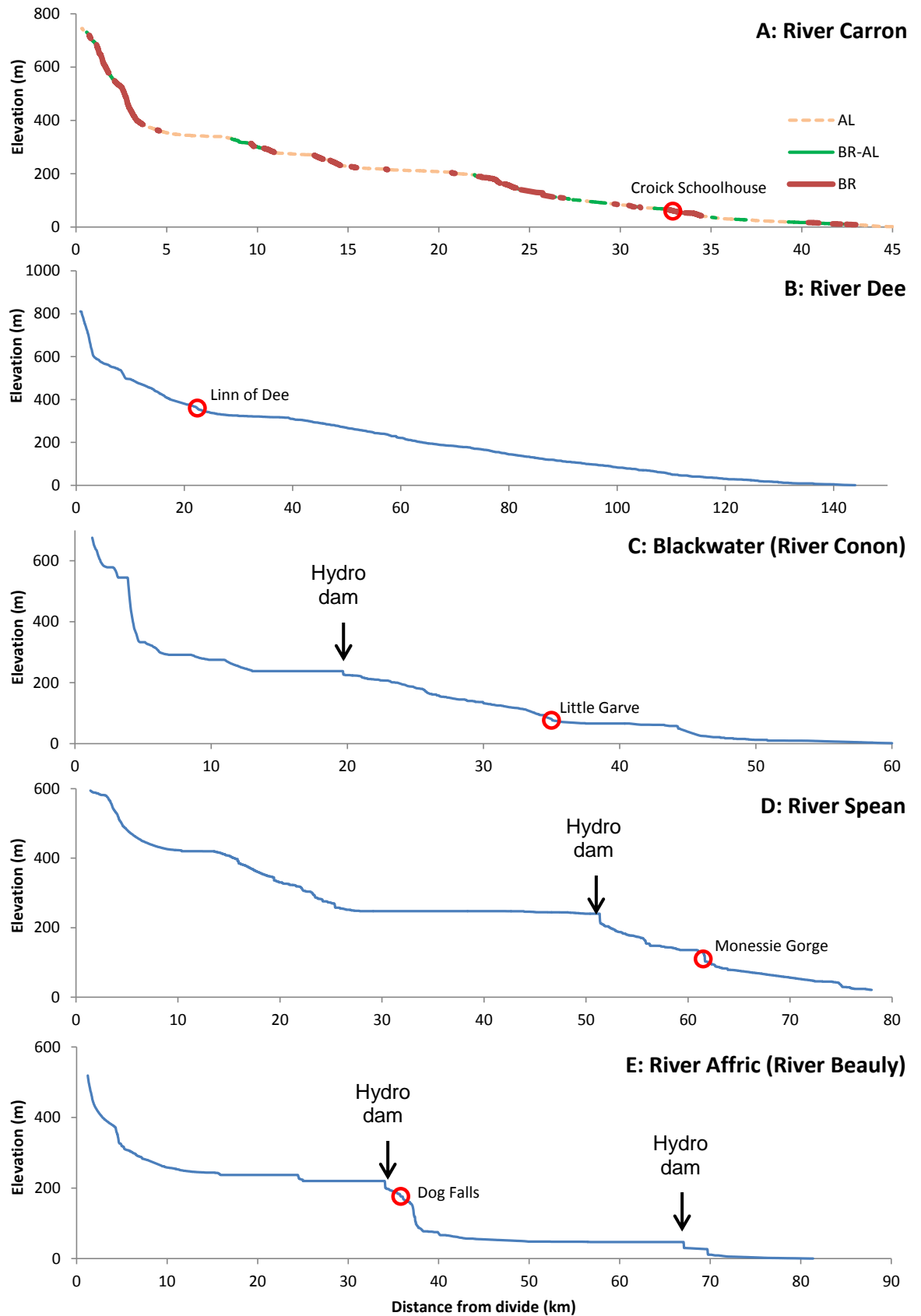
Figure 5-3. Stream long-profiles and locations of strath sites (red open circles). A: Croick Schoolhouse on the River Carron. Distribution of reach types (chapter 3) also shown. B: Linn of Dee, River Dee. C: Little Garve, Blackwater, tributary of the River Conon. D: Monessie gorge on the River Spean. E: Dog Falls on the River Affric, tributary of the River Beauly.
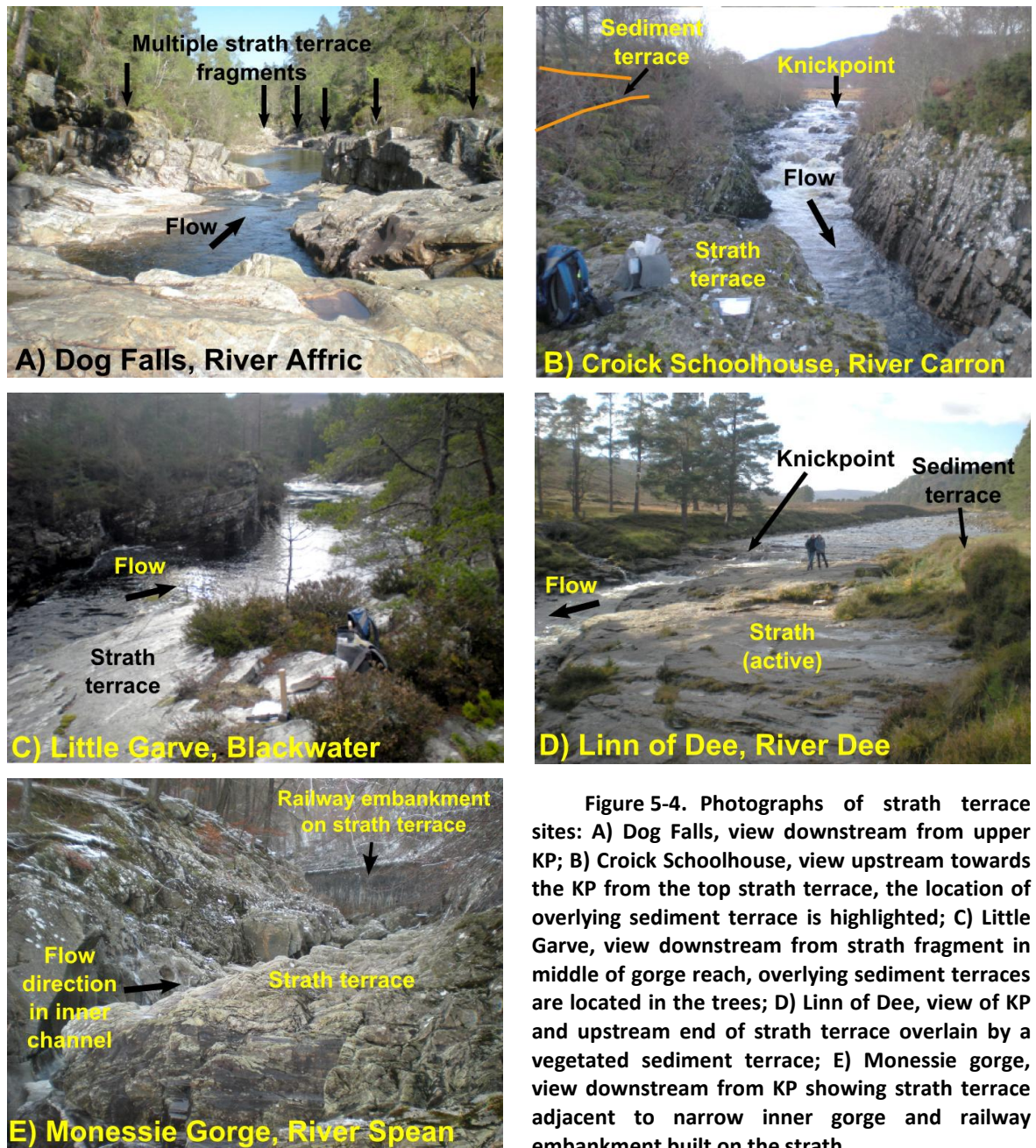
Figure 5-4. Photographs of strath terrace sites: A) Dog Falls, view downstream from upper KP; B) Croick Schoolhouse, view upstream towards the KP from the top strath terrace, the location of overlying sediment terrace is highlighted; C) Little Garve, view downstream from strath fragment in middle of gorge reach, overlying sediment terraces are located in the trees; D) Linn of Dee, view of KP and upstream end of strath terrace overlain by a vegetated sediment terrace; E) Monessie gorge, view downstream from KP showing strath terrace adjacent to narrow inner gorge and railway embankment built on the strath.

5.3.1.5   Monessie Gorge, River Spean

The lower and middle parts of the Spean catchment were glaciated during the YD (Sissons, 1979; Fabel et al., 2010). The YD glacier advanced up-valley from the west forcing the development of a large glacial lake in the upper half of the catchment. At its maximum extent YD ice covered the study site, with the ice margin probably located c. 8 km upstream (Fabel et al., 2010). As the ice margin retreated down-valley during the later YD, the glacial lake expanded, covering the study site until the thinning glacier dam in the lower Spean was breached and the lake drained into the Great Glen (cf. Sissons, 1979a; Fabel et al., 2010). The timing of drainage of the glacial lake at the close of the YD (c. 11.5 ka) is supported by cosmogenic nuclide surface exposure ages from lake shorelines and

varve chronologies in the adjacent valley of Glen Roy (Fabel et al., 2010). This date is hypothesised to be the upper limit for strath surface ages, with Type 2 strath formation likely to have occurred during fluvial erosion in the Holocene.

5.3.2   Cosmogenic nuclide analysis

5.3.2.1   Sampling strategy and procedure

The strath sampling procedure used in this study is based on that of Jansen et al. (2011). The strath terraces at the study sites consist of either a single long, narrow terrace surface adjacent to the entrenched bedrock channel, or a number of smaller strath terrace fragments at similar elevations located at the channel margins. As shown in Figure 5-5, samples were taken at several points along the strath terrace surface, or from several strath fragments, at increasing distances downstream from a knickpoint (KP) at the head of the study reach. Three to five samples were taken at each study site, with horizontal spacing of c. 50 – 200 m. As well as providing a basis for determining the strath age, this sampling strategy allows an assessment of potential differences in surface ages along the strath which may be used to infer the mechanism of fluvial incision (Figure 5-5). Declining strath terrace ages towards the upper KP suggest that the KP is retreating (cf. Jansen et al., 2011). If all samples yield similar ages, then horizontal KP retreat was either too rapid to produce a resolvable difference in surface exposure ages, or incision at the site has been dominated by parallel lowering of the channel bed.
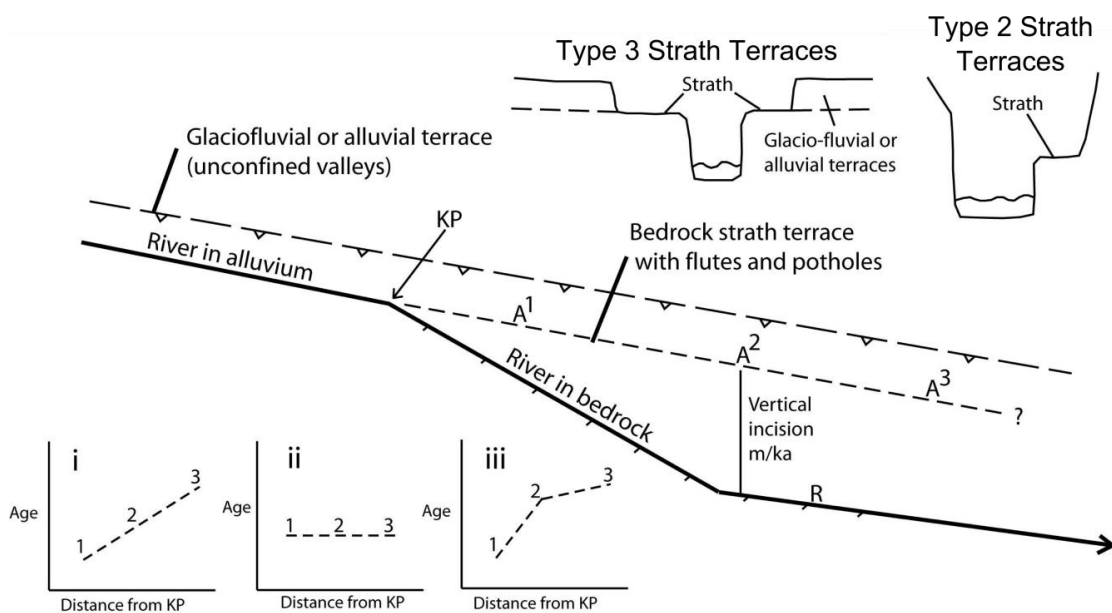
Figure 5-5. Sketch of generalised strath site form in long-profile. Overlying sediment terrace tread, shown by long-dashed line with arrow symbols, is only applicable to Type 3 sites. A[1-3] are locations of strath terrace samples. Sketch cross-sections in upper right depict Type 2 and Type 3 strath terraces. Sketch graphs in bottom left depict possible sample exposure age vs. distance plots for i) constant KP retreat rate, ii) vertical lowering or iii) variable KP retreat rates.

Surface samples 0.5 – 2 cm thick were taken from quartz veins/lenses or from quartz rich psammite or quartzite bedrock using hammer and chisel. Areas affected by plucking and topographic lows associated with flutes and potholes were avoided. Other criteria for sample-point selection were based on the detailed recommendations of Gosse and Phillips (2001). Shielding data, consisting of the azimuth and angle of major breaks-in-slope of the horizon line visible from the sample point, were taken in the field using a compass and clinometer. The dip and orientation of the sample surface were also recorded. These data were used to calculate the shielding factor following the procedure outlined by Dunne et al. (1999). The potential effect of shielding by snow cover is discussed in section 5.4.2.1.

5.3.2.2   <u>Sample processing: Quartz to ^{10}Be concentrations</u>

All rock samples from the strath terraces were processed to extract quartz in the Mineral Separation Laboratory at the University of Glasgow following standard procedures (Kohl and Nishiizumi, 1992). Samples were crushed and sieved to extract the 250 – 500 μm grain-size fraction, then washed to remove organic material and dust. Approximately 100 g of crushed rock was then processed to isolate the quartz during several stages:

1) Samples were leached with HNO_3 and HCl to remove carbonates and metals

2) Flotation was conducted to remove micas and feldspar grains. This procedure exploits a contrast in hydrophyllic versus hydrophobic properties of mineral grains after light leaching in HF.

3) Biotite and other metals were removed by magnetic separation (when necessary)

4) Samples were leached in HF to dissolve the remaining micas and feldspars and etch the surface of the quartz grains. Removing the outer layer of the quartz grains removes any meteoric ^{10}Be from rainwater that may have coated the grains.

5) The purity of the quartz was tested by assaying for aluminium using atomic absorption spectrophotometry. High aluminium suggests the presence of feldspar and/or mica indicating that the sample needs further cleaning.

The second stage of the processing, extracting Be from clean quartz and producing the AMS target (explained below), was carried out in laboratories at the Scottish Universities Environmental Research Centre (SUERC). Seven samples from the River Affric (and one procedural blank), forming a pilot study, were processed to target stage by the author in the Centre for Geosciences - Cosmogenic Nuclide Laboratory (part of the University of Glasgow). The remaining samples from all other sites (fifteen plus two procedural blanks) were processed from quartz to target by the Cosmogenic Isotope Analysis Facility (CIAF),

funded by a CIAF grant award from the Natural Environment Research Council (NERC). Similar procedures for the processing were used for both sets of samples, as detailed by Gosse and Philips (2001):

6) Quartz was weighed, dissolved in HF and spiked with a known concentration of ^{9}Be (the native element) to increase the overall concentration and facilitate measurement.

7) Unwanted elements such as Mg, Ca, Fe and Ti were removed using ion chromatography.

8) Be was precipitated as hydroxide (Be(OH)$_2$) and then fired in a hot oven to produce BeO.

9) BeO was pressed into targets for measurement in the SUERC accelerator mass spectrometer (AMS).

The ratios of ^{10}Be/^{9}Be for all samples were measured on the SUERC AMS (Freeman et al., 2004; Xu et al., 2010). The AMS measurement of pilot study samples from the River Affric were funded by a Scottish Universities AMS Consortium grant. The AMS measurements for the other 15 strath samples were processed as part of the NERC-funded CIAF grant allocation. Sample ^{10}Be/^{9}Be ratios were corrected by subtracting the ^{10}Be/^{9}Be ratio of the procedural blanks (ranging from 3.6 to 5.2 x 10^{-15}). Blank-corrected ^{10}Be/^{9}Be ratios range from 0.3 – 1.7 x 10^{-13}. The primary standard used to determine the ^{10}Be concentration from the ^{10}Be/^{9}Be for samples AFF 07, AFF 08, AFF 10, AFF 13, AFF 14 and AFF 16R from Glen Affric was NIST SRM4325 (^{10}Be/^{9}Be ratio of 3.06 x 10^{-11}). The standard used for all other data was NIST SRM4325 (^{10}Be/^{9}Be ratio of 2.79 x 10^{-11}, Nishiizumi et al., 2007). The resulting concentrations (in at/g) are presented in section 5.4.2 with systematic uncertainties (at 1σ or 2σ as stated).

5.3.2.3   Production rates and surface exposure ages

Surface exposure ages for the samples were calculated from the concentration of ^{10}Be following the procedures of Balco et al. (2008). In principle, surface exposure ages can be calculated from the concentration of ^{10}Be in the samples if the assumptions outlined in section 5.2 are justified and the rate of ^{10}Be production in quartz is known. The rate of ^{10}Be production in quartz in a rock surface depends on the rate of cosmic ray flux to the surface, which is a function of air pressure and the Earth's magnetic field. Thus, the cosmic ray flux depends on latitude and elevation (Lal, 1991; Stone, 2000). Temporal changes in the earth's magnetic field will also have affected the cosmic ray flux, and the Lal/Stone

production rate scaling scheme has been adapted by Balco et al. (2008) to account for these changes (termed 'time-dependant Lal/Stone'). This scaling scheme was used here for consistency with other cosmogenic nuclide studies in Scotland (e.g. Ballantyne, 2010; Jansen et al., 2011). Surface exposure ages calculated from the sample [10]Be concentrations using other available scaling schemes are given in Appendix A5-2.

The production rate at a particular point also depends on the amount of sky the sample is exposed to. Surrounding hills or gorge walls lower the cosmic ray flux to the surface, reducing the long-term production rate. This effect is accounted for through the calculation of a shielding factor for each sample which is, in effect, the ratio of the production rate for a hypothetical unobstructed sample point to that of the actual sample. This was calculated using the horizon data described in section 5.3.2.1 and the topographic shielding calculator of Balco et al. (2008). Production rates, surface exposure ages and associated 'internal' and 'external' uncertainties for the samples were calculated using the CRONUS calculator (Balco et al., 2008) (section 5.4.2). Internal uncertainty is the 1σ uncertainty on the exposure age derived from the measurement uncertainty and does not account for uncertainties associated with the production rate. Internal uncertainties (at 2σ) are <10% of the surface exposure age and are used when comparing sample ages for the same site. The external uncertainty includes uncertainty associated with the scaling of the production rate and is used when comparing surface exposure ages between sites or between different studies. At 1σ, the external uncertainty is generally ~10% of the sample age. The derivation of external uncertainties is described in detail by Balco et al. (2008).

5.3.2.4   Cosmogenic erosion rates

Two of the samples from the Dog Falls site on the River Affric were taken from the active channel bed; one ~ 150 m upstream from the strath site, and one within the site, ~15m downstream from the knickpoint at the head of the study reach. These samples were processed in the same manner as the strath surface samples, but the resultant [10]Be concentrations are interpreted to depend on the rate of active erosion of the channel bed. Erosion rates were calculated using the same standards and scaling schemes as described for surface exposure ages, using the CRONUS calculator (Balco et al., 2008). The term 'modern' is used to denote erosion rates from active channel bed surfaces as compared to long-term (e.g. Holocene) average erosion rates derived from strath surface exposure dating.

5.3.3   Topographic survey

Fluvial vertical incision rates (m/kyr) and erosion fluxes (m^3/m/kyr) were calculated using the cosmogenic exposure age of the strath surface and the site geometry. The site geometry was surveyed using a Leica GPS1200+ differential Global Positioning System (dGPS) with a published accuracy of 10mm horizontal and 20mm vertical (Leica Geosystems, 2008). In confined gorge reaches the actual uncertainty of measurements recorded using the dGPS was found to be greater than the published accuracy for approximately 40% of the readings, with an upper limit of c. 50 mm. This value is used as a conservative estimate of the uncertainty on all survey data. Positions of the sample points, strath terrace surfaces (including outer and inner edges, and centre line), sediment terraces, gorge rim, knickpoint, low and high flow levels and channel bed were surveyed where accessible. At the study sites, some areas of the channel bed were too deep to measure using the 2 m dGPS survey pole. To obtain a channel depth estimate in these areas, a weighted tape was used to gauge the channel depth from a surveyed point at the water line. Three to five weighted tape readings (measured to the nearest 5 cm) were taken at each point and the average taken as the channel depth. This particularly affected channel bed readings in the Monessie gorge and Linn of Dee, where deep inner gorges are formed from amalgamated potholes and direct access to the channel bed was restricted to the upstream and downstream ends of the reach. At these sites, the weighted tape measured to sediment on the bed of the inner gorge, thus underestimating the depth of the actual bedrock bed by an unknown amount. Erosion rates and fluxes estimated for these sites are therefore minima.

A range of channel geometry parameters were quantified through GIS and regression analysis of the dGPS survey data (Table 5-2). The derivation of uncertainty for these parameters varies with the data type: for inner channel and pre-strath widths, derived from averaging $5 - 10$ values per reach, uncertainty at 1σ is equivalent to the standard error of the mean; for channel bed slope, strath surface slope and the average strath height, which were derived from linear regressions, the uncertainty (at 1σ) is the standard error of the regression slope (S_{CB} and S_{ST}) or intercept (H_{ST}); for other data systematic uncertainties were calculated from individual measurement uncertainties (H_P, L_R, X_{IC} and V_{IC}).

Geometry parameter	Term	Units	Description
Sample point height	H_P	m	Height of sample point above the channel bed
Strath terrace height	H_{ST}	m	Average height of the strath terrace above the channel bed; derived from linear regressions of channel bed and strath surface elevations
Reach length	L_R	m	Reach length from KP to downstream end of strath terrace
Inner channel width	w_{IC}	m	Reach-average width of inner channel
Pre-strath channel width	w_{ST}	m	Total width of strath terraces and active channel (reach-average)
Inner channel w/d ratio	$(w/d)_{IC}$	-	Width to depth ratio of the inner channel (reach-average)
Channel bed slope	S_{CB}	m/m	Average slope of channel bed derived from linear regression of surveyed channel bed elevations
Strath surface slope	S_{ST}	m/m	Average slope of the strath terrace surface derived from linear regression of surveyed strath elevations
Inner channel cross section area	X_{IC}	m^2	Inner channel cross-section area; derived from w_{IC} and H_{ST}
Inner channel volume	V_{IC}	m^3	Inner channel volume; derived from w_{IC}, H_{ST} and L_R

Table 5-2.   Strath site geometry parameters: descriptions and terminology.

5.4   Results

In this section the geometry of the strath terraces and associated inner channels are assessed, followed by the the results of the cosmogenic nuclide analysis study.

5.4.1   Strath terrace form and formation

5.4.1.1   Strath terraces and channel geometry

The Type 2 and Type 3 strath terraces assessed in this study are formed due to long-term changes in channel width (Figure 5-6 A, Table 5-3). At the Type 2 strath sites the inner gorge (i.e. modern channel) is approximately half the pre-strath channel width. Both pre-strath channel widths and inner gorge widths at Dog Falls are within the range of reach-averaged bedrock channel widths measured in the three study catchments in the NW Highlands, presented in chapter 4 (Figure 5-6 A, Table 5-3). For the Monessie gorge, the pre-strath channel width is consistent with other bedrock channel widths, but the inner gorge width appears narrower than expected; although at 550 km^2 the drainage area is considerably greater than that of the channel survey data. These findings are consistent with the interpretation that Type 2 straths form by narrowing in an actively incising bedrock channel. The inner gorge widths at the Type 3 sites are also within the range of reach-averaged bedrock channel widths from three study catchments. But the pre-strath channel widths for the Type 3 straths are higher, falling within, or above the range of alluvial channel widths measured in the NW Highlands (Figure 5-6 A). This finding is consistent with the interpretation that these straths formed during a switch from alluvial to

bedrock channels. High pre-strath widths for the Linn of Dee and Little Garve sites may be due to some lateral migration of the channel during excavation of the strath surface.

Inner gorge *w/d* ratios for the study sites are also within the range of other bedrock channels measured during field survey (Figure 5-6 B), with only the Monessie gorge showing a slightly lower ratio than expected. The slopes of the modern channel bed and strath terrace surfaces at each site (Table 5-3) were statistically indistinguishable when tested using ANCOVA (p>0.05). This finding indicates that inner channel incision and strath formation has not been accompanied by a long-term change in channel bed slope. Channel (and strath) slopes at the study sites are at the higher end of the range of bedrock channel slopes for similar drainage areas in the surveyed streams discussed in chapter 3, reflecting their location at riegel and hanging-valley knickpoints (Figure 5-6 C).

Parameter		Site (strath type)				
		Croick (3)	Garve (3)	Dee (3)	Monessie* (2)	Dog Falls^ (2)
Reach length (L_R)	(m)	540	478	168	244	140
Strath terrace height (H_{ST})	(m)	6.2	7.0	14.1	9.6	3.7
$u(H_{ST})$	(m)	1.0	1.3	2.9	0.4	0.3
Channel bed slope (S_{CB})	(m/m)	0.022	0.030	0.068	0.043	0.027
$u(S_{CB})$	(m/m)	0.002	0.003	0.015	0.009	0.005
Strath surface slope (S_{ST})	(m/m)	0.021	0.028	0.052	0.074	0.037
$u(S_{ST})$	(m/m)	0.002	0.002	0.017	0.004	0.003
Inner gorge width (w_{IC})	(m)	23.3	31.9	16.6	9.3	13.4
$u(w_{IC})$	(m)	1.8	2.2	1.3	1.4	1.5
Pre-strath channel width (w_{ST})	(m)	35.1	65"	76.5"	20.2	20.1
$u(w_{ST})$	(m)	1.0	10.0"	10.0"	2.8	1.0
Inner channel shape		R	T	R	R	R
Inner channel width-depth ratio (w/d)$_{IC}$		4.48	5.32	1.50	1.08	3.62
$u(w/d)_{IC}$		0.18	0.20	0.22	0.16	0.14

Table 5-3.   Strath site geometry data derived from analysis of dGPS survey data. Bracketed number refers to the strath 'Type'. Inner channel shape refers to the general shape of the channel cross-section, which is roughly rectangular (R) or triangular (T).

* Channel bed and strath surface elevation versus distance regressions not significant for this site, i.e. the channel bed and strath terraces in the study reach are effectively flat.

^ Only data for lower strath shown (cf. section 5.4.2.1).

" High pre-strath widths for the Linn of Dee and Little Garve (Type 3) may be due to the effects of lateral migration of the channel during exposure and abandonment of the strath. Uncertainty for these sites is estimated to account for this unknown, for all other sites it is the standard error.
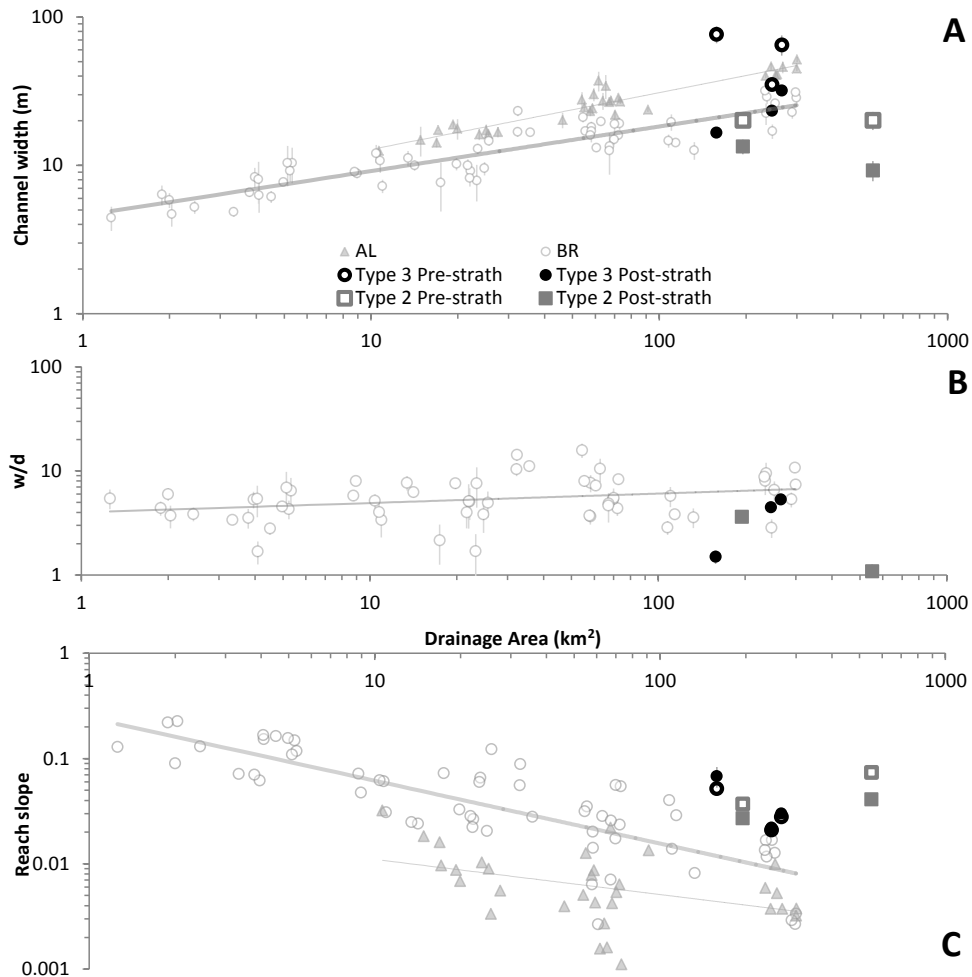
Figure 5-6. Strath site geometry: comparison with data from mapped channels. A) Pre-strath channel width and inner channel width versus drainage area. B) Inner channel w/d ratio versus drainage area. C) Reach-average slopes of strath surface and active channel bed versus drainage area. Key shown in plot A, uncertainties are given in Table 5-3, and are smaller than symbols in plots B and C. AL and BR channel data as presented in chapters 3 (plot C) and 4 (plots A and B).

5.4.1.2   Inner channel form and erosion processes

Two characteristic types of inner channels were seen at the study sites (Figure 5-7). Inner gorges at the Linn of Dee (Type 3) and in the Monessie Gorge (Type 2) have strongly undulating walls and were apparently formed by the coalescence of a series of large potholes which increase in depth and diameter downstream from the knickpoint. At the other three sites, Croick Schoolhouse (Type 3), Little Garve (Type 3) and Dog Falls (Type 2), the form of the inner gorge was more angular with joint and bedding control on the walls and locally on the channel orientation. This suggests differences in the dominant fluvial incision processes at the study sites, with abrasion dominating at the Linn of Dee and Monessie Gorge, and plucking dominating at the other sites. This difference in form and process appears to be related to differences in rock hardness and joint density, with the Linn of Dee and Monessie gorge characterised by lower intact rock strength and lower joint density than seen at the other sites (Table 5-1).
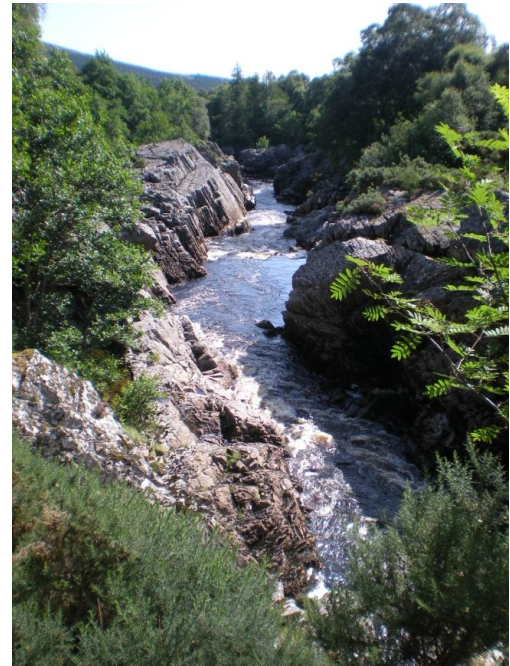
A: Linn of Dee   B: Croick Schoolhouse gorge

Figure 5-7. Field photographs of contrasting inner channel forms. A) Linn of Dee in schist with undulating walled inner gorge (view upstream). B) Croick Schoolhouse Gorge in psammite with irregular, bedding and joint controlled inner gorge wall (view downstream).

5.4.2   Timing of strath formation

5.4.2.1   Surface exposure ages: timing of strath abandonment

[10]Be concentrations and corresponding surface exposure ages for 18 strath terrace samples from the five study sites range from 3.5 ± 0.4 to 13.7 ± 1.0 ka (with internal uncertainty at 2σ) (Table 5-4). The distribution of sample points, and associated ages are shown in the context of site long-profiles in Figure 5-8. Detailed site and calculation data are given in Appendix A5-1 and A5-2 respectively. Strath surface exposure/abandonment ages are discussed for each site below.

All the strath terrace exposure/abandonment ages postdate the expected timing of deglaciation (cf. Table 5-1). The selected strath surfaces are interpreted to have been generally free from post-abandonment sediment cover and to have experienced very limited erosion since their formation. However, localised effects of cover by rock fall debris or block removal from strath surfaces may have lowered the observed surface age in some cases. These effects are discussed in detail for specific sites and samples below.

Site	Sample No.	Sample height (H_P)	u(H_P)	Conc. ^{10}Be^	Uncert.	Sample 'age'*	Internal uncert. (2σ)	External uncert. (2σ)
		(m)	(m)	(at/g)	(at/g)	(ka)	(ka)	(ka)
Garve	*GRV 01*	*7.4*	*0.6*	*17870*	*1130*	*3.5*	*0.4*	*0.7*
	GRV 02	6.4	0.6	56360	2667	11.0	1.0	2.1
	GRV 03	**8.1**	**0.6**	**69460**	**2619**	**13.7**	**1.0**	**2.5**
	GRV 04	4.1	0.2	63510	2304	12.6	0.9	2.3
Croick Schoolhouse	CRK 01	8.0	0.2	49690	3126	9.9	1.2	2.1
	CRK 02	*8.5*	*0.6*	*17700*	*1063*	*3.6*	*0.4*	*0.7*
	CRK 03	10.4	0.6	51960	2105	10.5	0.8	1.9
Linn of Dee	DEE 02	16.0	0.6	80130	3167	12.2	0.9	2.2
	DEE 03	16.6	0.6	74080	2955	11.3	0.9	2.1
	DEE 04	*8.0*	*0.6*	*57410*	*2317*	*8.8*	*0.7*	*1.6*
Monessie Gorge	MON 01	11.0	0.6	41070	1848	7.9	0.7	1.5
	MON 02	8.6	0.6	34070	1590	6.7	0.6	1.3
	MON 03	*8.2*	*0.6*	*19390*	*932*	*3.8*	*0.4*	*0.7*
Dog Falls	AFF 07	3.6	0.2	59527	2397	10.0	0.8	1.8
	AFF 08	*3.3*	*0.2*	*31198*	*1824*	*5.3*	*0.6*	*1.1*
	AFF 10	**5.2**	**0.2**	**75968**	**2859**	**12.6**	**0.9**	**2.3**
	AFF 13	3.4	0.5	52938	2253	9.2	0.7	1.7
	AFF 14	2.3	0.5	59850	2265	10.3	0.7	1.9

Table 5-4. Cosmogenic ^{10}Be results for strath terraces at the five study sites. Italicised data not used to derive average strath age; plain italicised font indicates age under-estimates possibly resulting from post-exposure erosion or cover at the sample point; bold italicised font indicates samples with older ages (discussed in the text). Systematic uncertainties for sample ages include sources of uncertainty in analytical procedures (internal) and production rate uncertainty (external).

^ Based on 2.79E-11 ^{10}Be/^{9}Be for NIST SRM4325 (Nishiizumi et al., 2007)

*Calculated for zero erosion case using the CRONUS calculator with time-dependent Lal (1991)/ Stone (2000) production rate scaling (Balco et al., 2008).

The shielding effects of water and snow have the potential to lower ^{10}Be concentrations in strath surfaces (cf. Reusser et al., 2006). Reusser et al. (2006) used flow modelling to assess the effects of shielding by water on cosmogenic nuclide surface exposure ages from strath terraces in the Holtwood gorge (eastern USA). They showed that for samples taken from higher strath surfaces, which are inundated only during major flood events, the ^{10}Be ages represented > 99% of the total exposure history. This situation is similar to the strath sites assessed in this study, and occasional inundation by water during major floods is not considered to have caused substantial shielding of the samples at any of the study sites over the period of exposure.

The effects of shielding by snow were assessed using a simple numerical simulation which assumes 4 months of cover by snow of density 0.15 g/cm^2 per year (cf. Gosse et al., 1995).

Under these conditions, average snow depths of 2m, considerably higher than is typical for northern Scotland today, would cause only a 3% reduction in the observed exposure age. This value is consistent with the 1 – 4% reduction in production rate predicted for elevations <400 m OD by Schildgen et al. (2005) using a snow accumulation model for the Cairngorm Mountains (where the Linn of Dee is located). Thus shielding by snow cover is not thought to have substantially affected the observed exposure ages. In fact for shielding by snow to account for the observed lag between deglaciation and strath exposure ages (>25% of the observed age, discussed below) snow would have to be double the density, >3 m deep and present for between 8 – 12 months of the year over the whole exposure period. These conditions are extremely unlikely to have persisted during the Holocene in northern Scotland.

Little Garve, Blackwater

Four samples from strath surfaces at Little Garve yielded a range of exposure ages of 3.5 ± 0.4 to 13.7 ± 1.0 ka (internal uncertainties at 2σ). The youngest age comes from the most upstream sample, from a strath surface c. 60m downstream of the knickpoint at the head of the reach (Figure 5-8 A). The surface is lightly vegetated, with smooth and relatively 'clean' bedrock and may still experience some erosion during high flow events. The remaining three ages of 11.0 ± 1.0, 12.6 ± 0.9 and 13.7 ± 1.0 ka come from strath surfaces 175 – 475 m downstream from the knickpoint. The pattern of exposure ages for the site (Figure 5-8 A) suggests that ages may be declining towards the knickpoint, which is consistent with predictions of knickpoint retreat, but the uncertainties for these samples overlap, meaning that they are statistically indistinguishable. The mean age for the strath terrace, calculated from these three samples, is 12.4 ± 1.2 ka.

The location of the 13.7 ka sample, from a bedrock knoll on a broad area of bedrock strath 20 m away from the edge of the active gorge, suggests the possibility that inheritance of [10]Be accumulated during burial under thin sediment cover (<1m) may have contributed to the apparently older exposure age of this sample. This older age is close to the expected deglaciation age for the site (14.5 – 13.5 ka), and may thus be a minimum deglaciation age. The 12.6 and 11.0 ka sample ages are thus probably the most reliable estimates of the true age of excavation and abandonment of the strath surface, suggesting that it was formed between ~12.6 and 11 ka (mean value 11.8 ka).
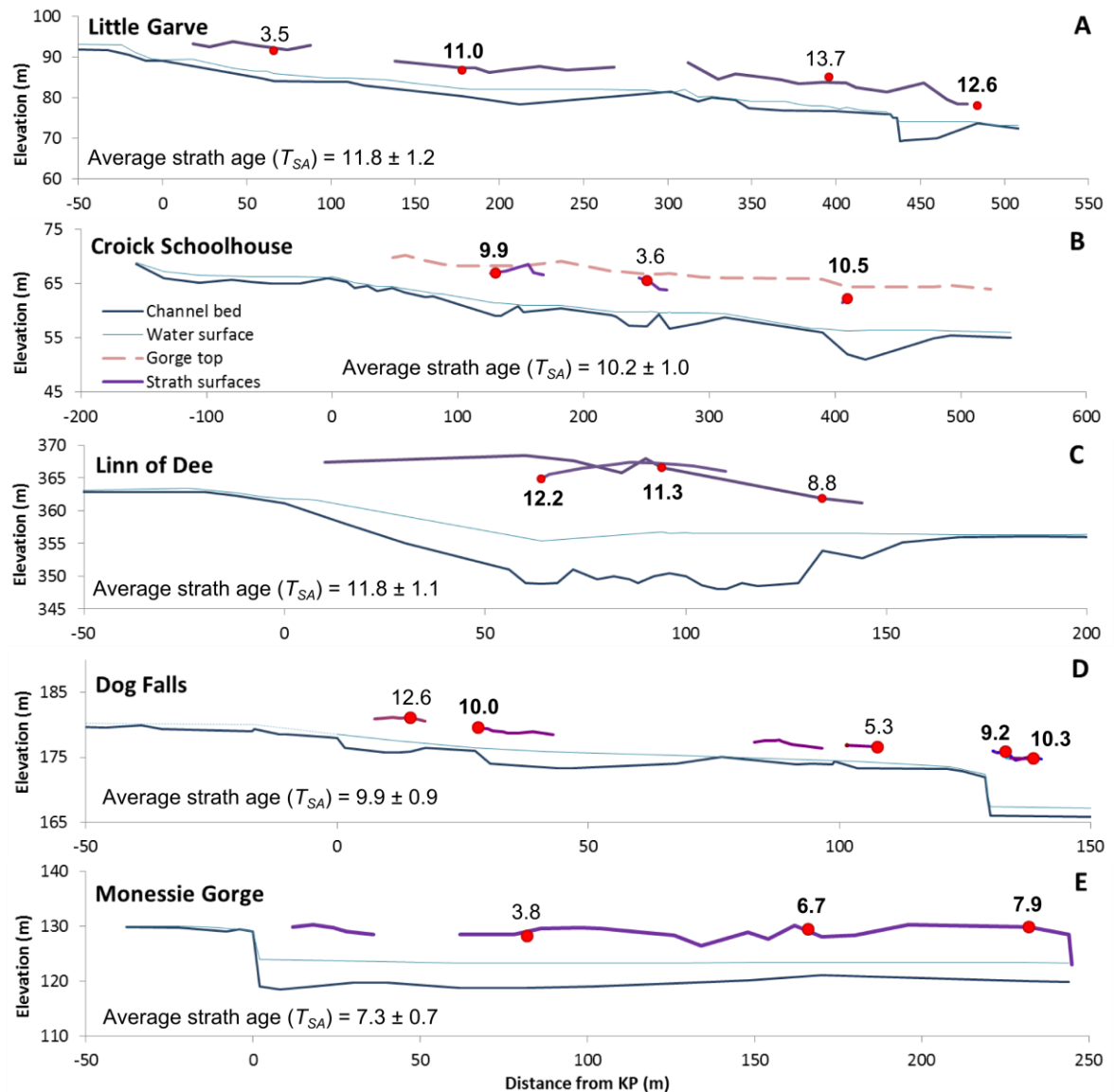
Figure 5-8. Distance versus elevation profiles for the study sites constructed from dGPS survey data (key in plot B) showing locations of sample points (red circles) and associated cosmogenic [10]**Be ages (uncertainty given in Table 5-4). Numbers in bold have been used to derive the average strath age (**T_{SA}**) quoted on the plots (with systematic uncertainty at 1σ). A) Little Garve, Blackwater. B) Croick Schoolhouse, River Carron. C) Linn of Dee, River Dee (note: both right bank and left bank straths shown). D) Dog Falls, River Affric. E) Monessie Gorge, River Spean.**

Croick schoolhouse gorge, River Carron

The three samples from strath terraces at Croick Schoolhouse, yield ages between 3.6 ± 0.4 and 10.5 ± 0.8 ka (Figure 5-8 B). The young age comes from a small strath fragment protruding into the inside of a bend in the middle of the reach. The strath is formed on a shallowly dipping joint surface, and it is possible that recent block plucking during flood-stage flows over this exposed surface, possibly aided by vegetation growth, may be the cause of the young exposure age of this surface. The two other strath samples, from the upper and lower ends of the gorge yield exposure ages of 9.9 ± 1.2 and 10.5 ± 0.8 ka. The ages are within uncertainty and are probably reasonable estimates of the true exposure/abandonment age of the strath surface at this site (mean value 10.2 ± 1.0 ka).

The pattern of strath surface ages is consistent with predictions for 'parallel' lowering of the channel bed, but could equally result from a phase of rapid knickpoint retreat.

Linn of Dee, River Dee

The three samples from strath terraces at the Linn of Dee yield exposure ages ranging from 8.8 ± 0.7 to 12.2 ± 0.9 ka (Figure 5-8 C). The younger age is from a quartz vein at the downstream end of the strath surface. An angular surface to the vein suggests that there may have been some erosion since it was formed and consequently this age is thought not to be representative of the timing of exposure and abandonment of the strath surface. The two other samples from the upper and middle parts of the site yield ages of 12.2 ± 0.9 ka and 11.3 ± 0.9 ka. Again, the uncertainty ranges overlap and these ages are judged to be reasonable estimates of the true exposure/abandonment age of the strath at the site (mean value 11.8 ± 1.1 ka). The ages are consistent with predictions for 'parallel' lowering, or a phase of rapid knickpoint retreat.

Monessie gorge, River Spean

Three strath terrace samples yield exposure ages of 3.8 ± 0.4 to 7.9 ± 0.7 ka for the Monessie Gorge (Figure 5-8 E). The youngest age comes from the most upstream strath which may be actively eroded at high flow (no local vegetation and 'clean' bedrock), or may have been damaged during the construction of a large railway embankment built on the strath surface approximately 2m from the sample point. The decrease in exposure ages towards the knickpoint shown in Figure 5-8 E suggests that strath may have formed during knickpoint retreat. However, the two other ages of 6.7 ± 0.6 and 7.9 ± 0.7 ka have overlapping uncertainty ranges meaning that differences in age cannot be distinguished (mean value 7.3 ± 0.7), precluding a clear interpretation of knickpoint retreat.

Dog Falls, River Affric

Five strath terrace samples from Dog Falls yield exposure ages ranging from 5.3 ± 0.6 to 12.6 ± 0.9 ka (Figure 5-8 D). The youngest age is from a small strath in the middle of the gorge. A landslip scarp on the gorge wall above the upstream end of the strath, and large angular boulders located upstream and in the channel near the strath suggest that the strath terrace may have been partially buried by a landslip deposit following abandonment by the river. Shielding by landslide material may thus be the cause of the apparently young surface age and this value is not thought to be an accurate strath abandonment age. Three of the strath samples yield surface exposure ages of 9.2 ± 0.7, 10.0 ± 0.8 and 10.3 ± 0.7 ka,

which are all within uncertainty and are judged to be reliable estimates of the true strath abandonment age (mean value 9.9 ± 0.9 ka). The final strath sample yields an older age of 12.7 ± 0.9 ka, close to the expected deglaciation age of the site (14 – 13 ka). This sample is from a small strath terrace at a slightly higher elevation (5.2 m above channel bed) than the more extensive lower surface from which the samples with the three 'similar' ages were derived (average ~3 m above channel bed) (Figure 5-9). The difference between the average upper strath elevation (181m>OD) and the projected elevation of the lower strath at the mid-point of the upper strath is 1.1m. Although this elevation difference is small, the upper strath surface lies above the projected 99% confidence interval on the lower surface elevation-distance regression indicating that this is a higher strath level (Figure 5-9).

Numerical simulations were used to assess the potential effect of inheritance in the lower surface due to excavation of only 1.1 m of bedrock from the level of the upper strath. Using the constraints from the site geometry and 12.6 ka exposure age for the upper surface, and assuming the lower strath was cut instantaneously, it was found that the measured exposure ages of 9.2 – 10.3 ka for the lower strath could only be produced if the surface was abandoned between 8.5 and 10 ka. This range is within the range of uncertainty on the measured ages, hence it is probable that inheritance has had a negligible impact on the observed surface exposure age.
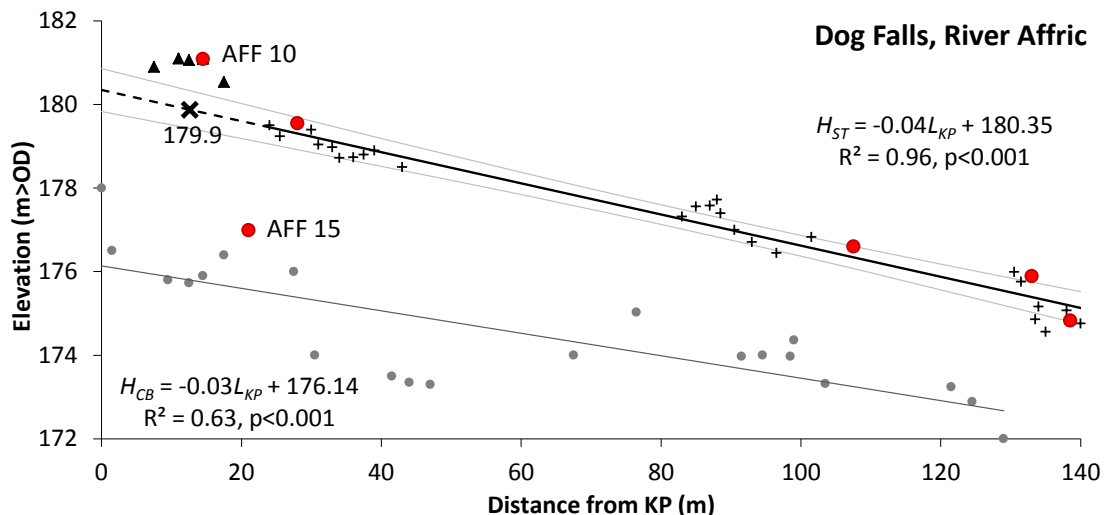
Figure 5-9. Distance from the knickpoint (L_{KP}) versus elevation for dGPS survey points from Dog Falls showing relationship of two strath levels; lower strath terrace (crosses), upper strath terrace (filled triangles) and channel bed grey circles). Regressions for lower strath terrace (black line, H_{ST}) with 99% confidence interval (light grey line) and channel bed (dark grey line, H_{CB}) shown. Locations of sample points marked by red circles. Lower strath elevation projected between 0 and 24 m downstream from KP (dashed black line) with estimated elevation (179.9m) at point level with mid-point of upper strath marked by black diagonal cross. Labelled sample points give sample numbers for upper strath sample (AFF 10) and channel bed sample (AFF 15).

5.4.2.2   Timing of strath abandonment: site comparison

Overlapping uncertainty ranges for all data preclude a detailed comparison of the timing of strath formation between sites (Figure 5-10). However, a pattern in the distribution of average surface exposure ages is inferred by the data (Table 5-5, Figure 5-10). The timing of strath exposure/abandonment at the Linn of Dee and Little Garve sites (11.0 ± 2.1 to 12.6 ± 2.3 ka, 2σ external uncertainty) appears to have been c. 1.5 to 2 kyr earlier than at Croick Schoolhouse and Dog Falls (9.2 ± 1.7 to 10.5 ± 1.9 ka), and ages from the Monessie gorge are younger (6.7 ± 1.3 to 7.9 ± 1.5 ka) (Figure 5-10).

Site	Strath Type	Area	Q	Average strath age (T_{SA})	Uncert.	LD deglaciation	YD glaciation context	Lag time
		(km^2)	(m^3/s)	(ka)	(ka)	(ka)		kyr
Croick Schoolhouse	3	246	121	10.2	1.0	14.5-13.5	Glacier 10km upstream	4.3 – 3.3
Little Garve	3	266	128	11.8	1.2	14.5-13.5	Headwater glaciers	2.7 – 1.7
Linn of Dee	3	158	90	11.8	1.1	15-14	Not glaciated	3.2 – 2.2
Monessie gorge	2	551	228	7.3	0.7	-	11.7 ka glacier retreat and glacial lake drainage	4.2 – 3.2
Dog Falls	2	195	101	9.9	0.9	14-13	Glacier 1km upstream	4.1 – 3.1

Table 5-5.   Average strath ages (T_{SA}) for each site calculated from sample ages shown in Table 5-4 (not italicised values). Drainage area, discharge and deglaciation data discussed in section 5.3.1 and shown here for reference. 'Lag time' is the time between deglaciation and strath abandonment, discussed in the text.

The strath exposure ages from all sites lag the probable deglaciation of the site by ~ 2 – 4 kyr (Table 5-5). The delay in strath exposure/abandonment suggests that strath formation may be related to, but not directly caused by, deglaciation. Both the pattern of surface exposure ages, and the lag time appear to depend on the glacial history of the catchment. Sites in catchments that experienced little glaciation during the YD (Little Garve and the Linn of Dee) have generally older surface exposure ages (11 – 12.6 ka) and slightly shorter lag times between deglaciation and strath formation (~2 – 3 kyr). The other sites, which were glaciated during the YD (Monessie) or were located downstream from large YD valley glaciers (Dog Falls and Croick Schoolhouse) have slightly longer lag times (~ 3 – 4 kyr), and slightly younger surface ages (~9 – 10.5 ka for Dog Falls and Croick, ~7.2 ka for the Monessie gorge). Potential controls on the timing of strath terrace formation are discussed in section 5.5.1.3.

5.4.2.3   Summary of 'age' results

- Strath surface exposure ages all post-date deglaciation.

- Two or more ages from the same strath at each site are within uncertainty of each other suggesting that these ages are good estimates of the timing of strath formation.

- Strath surface exposure ages appear to depend on the extent of YD glaciation of the catchment.
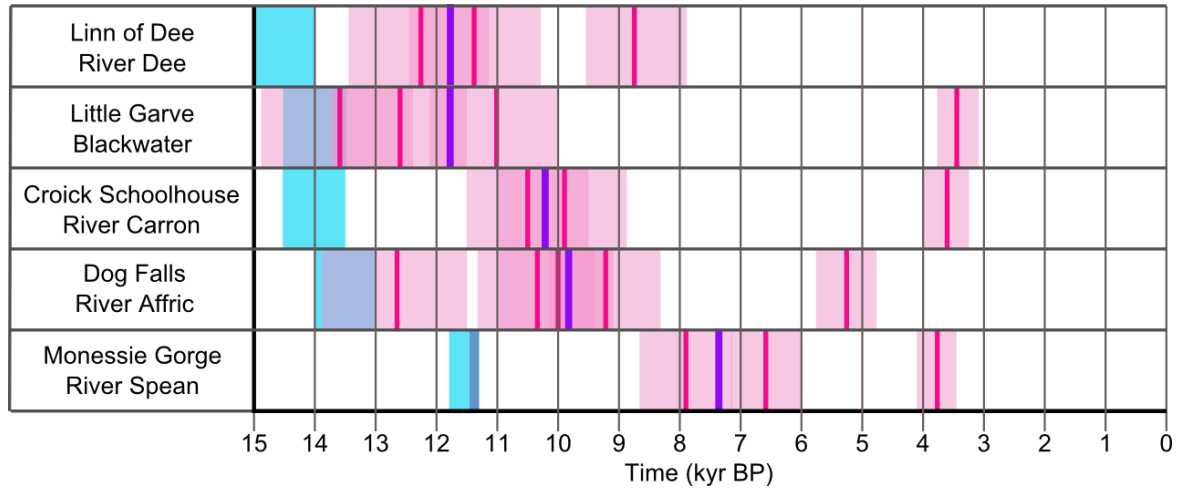
Figure 5-10.   Comparison of sample ages for each site (strong pink lines) with the probable deglaciation age (blue boxes). Average strath terrace age (T_{SA}) shown as dark purple line, ignoring outliers (see Table 5-4 and section 5.4.2.1). Pink boxes represent 2σ internal uncertainty on each exposure age.

5.4.3   Incision rates and erosion fluxes

5.4.3.1   Cosmogenic [10]Be erosion rates

In addition to the strath terrace samples, two samples from the active channel bed were taken at the Dog Falls site. AFF 15R was taken 20 m downstream of the small upper KP at the head of the reach (Figure 5-9). AFF 16R was sited 96 m upstream of the study reach, in an area of bedrock channel flanked by coarse sediment terraces and displaying limited bedrock entrenchment. The concentration of cosmogenic [10]Be in these samples is interpreted to depend on the rate of erosion (Lal, 1991) and the degree of shielding by water (discussed below).

The erosion rate derived for AFF 15R, within the incising bedrock reach downstream from the KP, is slightly higher (0.13 ± 0.02 m/kyr) than that from the channel bed upstream (0.10 ± 0.01 m/kyr) (Table 5-6). Both values are relatively low and are consistent with published [10]Be erosion rates of 0.07 – 0.24 m/kyr from channel bed samples from rivers in the western Highlands (Jansen et al., 2011). However, shielding by water is likely to have influenced the concentration of [10]Be in these samples as they are located within 0.3m of the

base flow level, and the erosion rates in Table 5-6 should be considered as maximum values. A lack of gauging records for the River Affric means that a detailed flood frequency-magnitude model such as that used by Reusser et al. (2006) to assess water shielding in the Holtwood Gorge, is not possible to derive. However, assuming that the average flow depth over the sample sites for the past $1 - 5$ kyr is up to twice the current base-flow depth (up to 0.5m), shielding by water may have resulted in up to a 14% reduction in measured ^{10}Be in the sampled surfaces. This suggests that erosion rates over the past few kyr in the study channels are likely to have been lower than 0.1 m/kyr.

Site, River	Sample	L$_{KP}$	Conc. ^{10}Be	Uncert.	Erosion rate (ε_{CB})	Internal uncert. (2σ)	External uncert. (2σ)
		(m)	(at/g)	(at/g)	(m/kyr)	(m/kyr)	(m/kyr)
Dog Fall, River Affric	AFF 15R	20	38010	2413	0.126	0.016	0.023
	AFF 16R	96 (upstream)	51150	1973	0.103	0.008	0.015

Table 5-6. Cosmogenic ^{10}Be erosion rates for channel bed samples (ε_{CB}) from the River Affric. Calculation data and details of standards used are given in Appendix A5-3. These rates are maximum rates as shielding by water has not been accounted for.

5.4.3.2   Vertical incision rates from strath surface ages

Time-averaged vertical incision rates (m/kyr) were calculated for each sample point from the ^{10}Be age (ka) and height of the strath surface sample above the channel bed (m) (Table 5-7). This mode of calculation assumes that strath surfaces begin to accumulate ^{10}Be as soon as inner channel incision is initiated, an assumption consistent with the relatively low erosion rates expected for Scottish Highland rivers and the interpretation that sediment clearing from the channel margins is an intrinsic part of strath formation (section 5.2.3).

The highest long-term incision rates are from samples at the Linn of Dee and Monessie gorge (1.28 ± 0.3 to 1.47 ± 0.21 m/kyr); the lowest incision rates are, generally, associated with samples from Dog Falls (0.22 ± 0.09 to 0.41 ± 0.09 m/kyr) (Table 5-7). Average incision rates for each site derived from the sample point rates (ε_{PA}) range from 0.33 ± 0.17 m/kyr at Dog Falls to 1.39 ± 0.28 m/kyr at the Linn of Dee.

Sample	Distance from KP	Sample height (H_P)^	$u(H_P)$	Sample age (T_p)	Ext. Uncert	Erosion rate (ε_P)*	$u(\varepsilon_P)$	Average erosion rate (ε_{PA})	$u(\varepsilon_{PA})$
	(m)	(m)	(m)	(ka)	(ka)	(m/kyr)	(m/kyr)	(m/kyr)	(m/kyr)
GRV 01	*66*	*7.4*	*0.6*	*3.5*	*0.4*	*2.13*	*0.44*		
GRV 02	178	6.4	0.6	11.0	1.1	0.58	0.12	0.50	0.17
GRV 03	396	8.1	0.6	13.7	1.3	0.59	0.11		
GRV 04	484	4.1	0.2	12.6	1.2	0.33	0.05		
CRK 01	130	8.0	0.6	9.9	1.0	0.80	0.16		
CRK 02	*250*	*8.5*	*0.6*	*3.6*	*0.4*	*2.37*	*0.46*	0.90	0.23
CRK 03	410	10.4	0.6	10.5	1.0	0.99	0.17		
DEE 02	64	16.0	0.6	12.2	1.1	1.31	0.19		
DEE 03	94	16.6	0.6	11.3	1.1	1.47	0.21	1.39	0.28
DEE 04	*134*	*8.0*	*0.6*	*8.8*	*0.8*	*0.91*	*0.17*		
MON 01	232	11.0	1.0	7.9	0.8	1.39	0.29		
MON 02	166	8.6	1.0	6.7	0.6	1.28	0.30	1.34	0.42
MON 03	*82*	*8.2*	*1.0*	*3.8*	*0.4*	*2.13*	*0.51*		
AFF 07	28	3.6	0.6	10.0	0.9	0.35	0.10		
AFF 08	*108*	*3.5*	*0.2*	*5.3*	*0.5*	*0.66*	*0.12*		
AFF 10	15	5.2	0.6	12.6	1.2	0.41	0.09	0.33	0.17
AFF 13	133	3.2	0.6	9.2	0.9	0.35	0.11		
AFF 14	139	2.2	0.6	10.3	1.0	0.22	0.09		

Table 5-7. **Vertical incision rates calculated for individual sample points (ε_P) and averaged for site (ε_{PA}). Italicised data denotes samples with [10]Be ages that are not judged reasonable estimates of the timing of strath formation/abandonment (section 5.4.2.1).**

^ Note that at channel bed elevation measurements for the Linn of Dee and Monessie gorge are to the surface of sediment fill at the base of the inner gorge. Strath heights and erosion rates for these sites are therefore minimum estimates.

***Strath height/sample exposure age. Uncertainty is derived from the range of maximum and minimum incision rates for the given strath height and exposure age uncertainties.**

5.4.3.3   Reach incision rates and 'erosion fluxes'

Vertical incision rates representative of each site as a whole (ε_R, m/kyr) were derived using the average strath age and strath height (Table 5-5). Volumetric erosion rates per unit length ('erosion fluxes', E_F, m^3/m/kyr) were also calculated for the study channels using the inner channel cross-section area and the reach length. Erosion fluxes are less widely reported in quantitative fluvial studies but they account for channel width and so their use would improve comparisons of erosion rates within and between studies.

Comparison of reach erosion rates (ε_R) with the average rate derived from individual sample points at a site (ε_{PA}) shows a similar general pattern in the data, but there are differences for the individual sites (compare Table 5-7 and Table 5-8). The largest difference between these rates is seen at Croick Schoolhouse (ε_R=0.61 m/kyr, ε_{PA}=0.90

m/kyr). This difference arises due to the distribution of sample points with respect to the undulating form of the channel bed. The sample points at Croick Schoolhouse are located on strath surfaces adjacent to deep pools in the inner gorge (Figure 5-8), meaning that the strath height at these points is higher than the average strath height and thus the calculated erosion rates are greater. The same effect causes lesser differences between ε_R and ε_{PA} at Little Garve and the Linn of Dee. Similar rates found for the Monessie gorge and Dog Falls sites reflect similar H_P and H_{ST} values for these sites. The reach erosion rate (ε_R) is thought to better represent the overall site erosion rate and is used in the remainder of this analysis.

Parameters		Croick	Garve	Dee	Monessie	Dog Falls
Area	(km^2)	246	266	158	551	195
Q	(m^2/s)	121	128	90	228	101
S_{CB}	(m/m)	0.022	0.030	0.068	0.043	0.039
S_{ST}	(m/m)	0.021	0.029	0.052	0.002	0.037
Ω	(W/m)	26065	37807	60062	96332	38458
ω	(W/m/m)	1118	1185	3618	10414	2866
R_h	m	4.04	4.87	5.22	3.12	2.37
X_{IC}	(m^2)	144	112	233	88	49
$u_c(X_{IC})$	(m^2)	26	23	51	14	21
V_{IC}	(m^3)	76279	62867	32774	29433	8054
$u_c(V_{IC})$	(m^3)	9658	7592	4139	5419	1217
T_{SA}	(ka)	10.2	11.8	11.8	7.3	9.9
$u_c(T_{SA})$	(ka)	1.0	1.2	1.1	0.7	0.9
ε_R	(m/kyr)	0.61	0.59	1.19	1.31	0.35
$u_c(\varepsilon_R)$	(m/kyr)	0.11	0.13	0.27	0.14	0.08
E_F	(m^3/m/kyr)	13.8	11.1	16.6	16.5	5.8
$u_c(E_F)$	(m^3/m/kyr)	2.2	1.7	2.6	3.4	1.0

Table 5-8. Holocene-average erosion rates (ε_R) and erosion fluxes (E_F) for the strath sites. Terms defined in Table 5-2.

Spatial variations in incision rate

Controls on the reach erosion rate (ε_R) and erosion flux (E_F) at the study sites were assessed through linear regression with potential control variables. Figure 5-11 indicates that ε_R is positively scaled with total stream power ($p<0.1$, $R^2=0.74$), and both ε_R and E_F are negatively scaled with intact rock strength (i.e. Schmidt hammer 'R' value) ($p<0.05$, $R^2=0.89$ and 0.78). These significant correlations indicate that bedrock incision rates depend strongly on lithological resistance and less strongly on stream power. A best fit equation relating ε_R to total stream power (Ω) and the Schmidt hammer 'R' value was derived from the data:

$$\varepsilon_R = 1.62 + 6 \times 10^{-6}\Omega - 0.0239R \qquad\qquad \text{Eq 5.3} \quad (R^2=0.97, p=0.028)$$

This equation is used in chapter 6 to predict postglacial erosion rates throughout the three NW Highland study streams (rivers Carron, Elchaig and Canaird).

Temporal variations in incision rate

The Holocene-average incision rates derived from the strath exposure ages are all higher than the cosmogenic ^{10}Be erosion rates derived from the active channel bed (c. 0.1 m/kyr). This indicates that modern erosion rates are lower than they have been in the past, and implies that maximum Holocene incision rates may have been considerably higher than the long-term average derived from the strath surface ages. Assuming incision rates at the strath sites have been 0.1 m/kyr for the past 4000 years, average incision rates during the preceding 6 – 10 kyr would have been 0.5 – 2.8 m/kyr.

Findings from the Dog Falls site in Glen Affric also suggest that early Holocene incision rates may have been higher. In section 5.4.2.1 it was noted that there are two strath levels at the Dog Falls site, with the sample from the upper strath (AFF 10) yielding an older exposure age (12.6 ± 0.9 ka) than samples from the lower strath (average 9.9 ± 0.9 ka). Assuming that the 12.6 ka and ~9.9 ka strath ages define a 2.7 ka time period during which the 9.9 ka strath was excavated, the erosion rate calculated during this period is 0.46 ± 0.16 m/kyr (based on an elevation difference of 1.24 ± 0.22 m between AFF 10 and the projected level of the lower strath directly below, Figure 5-9). This YD/early Holocene rate is slightly higher than the reach erosion rate (ε_R) derived from the lower strath (i.e. for the time period ~9.9 ka to present) of 0.35 ± 0.08 m/kyr. However, the overlap in the 2σ uncertainties of the incision rates precludes a firm conclusion from this data.

5.4.3.4   Summary of rate results

- Incision rates derived from the strath terrace ages range from 0.35 to 1.31 m/kyr
- The incision rate depends on lithology and stream power
- Incision rates have declined over the Holocene.
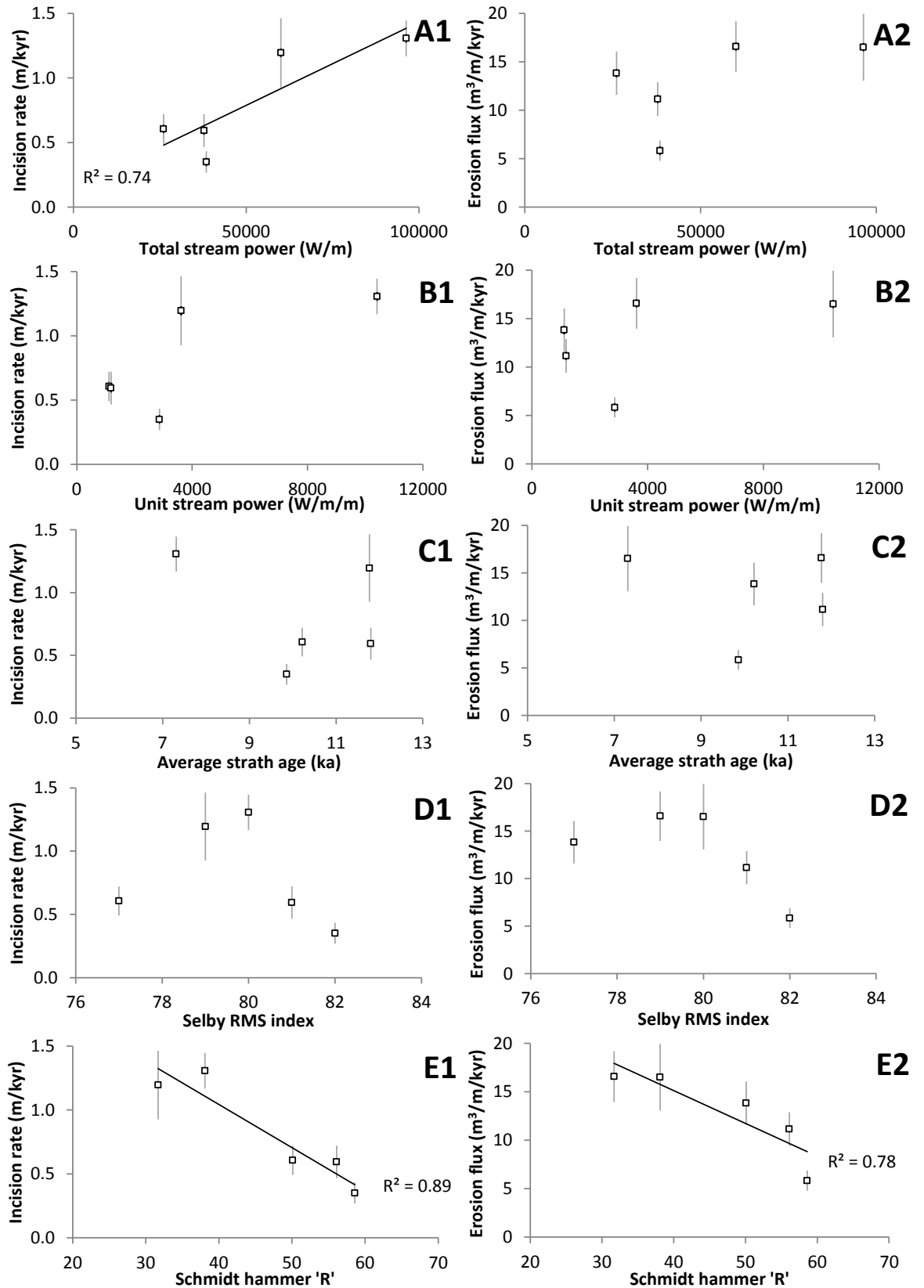
Figure 5-11. Erosion rate (ε_R, m/kyr) and erosion flux (E_F, m³/m/kyr) values for the strath sites, plotted against total stream power (A), unit stream power (B), strath age (C), Selby RMS index (D) and the Schmidt hammer 'R' value (E). Regressions in E1 and E2 are significant at p<0.05, regression in A1 significant at p<0.1, no other regressions are significant at p<0.1.

5.5   Discussion

5.5.1   Mechanisms and timing of strath terrace formation

5.5.1.1   Strath terraces: records of postglacial incision?

Evidence from the study sites supporting the interpretation that the strath terraces and associated inner gorges are postglacial features was outlined in section 5.2.4.1. This interpretation is further supported by the results of the quantitative assessment of the site geometry and cosmogenic nuclide surface exposure ages presented above.

The fact that the inner gorges at all sites have geometries consistent with that expected for hydraulically scaled channels in the NW Highlands is clear evidence that they are adjusted to postglacial discharge conditions. The consistency of the postglacial ^{10}Be exposure ages indicates that these sites are unlikely to be pre-glacial features preserved by sediment cover/fill during glaciation (cf. Montgomery and Korup, 2011). Finally, the measured erosion rates from these sites are within the range of other postglacial fluvial erosion rates quantified in comparable settings in Scotland and Norway (McEwen et al., 2002; Jansen et al., 2011). These findings are strong evidence that the strath terraces and inner gorges at the study sites were not cut by pre-glacial fluvial incision or sub-glacial erosion by meltwater streams, and that the measured erosion rates are thus good estimates of postglacial fluvial incision rates.

Though this finding shows that postglacial rivers *can* and *do* incise into the bedrock valley floor, it does not preclude the possibility that pre- or sub-glacially carved gorges exist elsewhere in the Scottish Highlands. The distribution of postglacial fluvial incision and the extent of inheritance of pre-existing gorges are assessed in the three NW Highland study rivers (Carron, Elchaig and Canaird) in chapter 6.

5.5.1.2   Incision processes and strath formation mechanisms

The channel narrowing resulting in inner gorge formation and the abandonment of straths can occur during KP retreat (Reusser et al., 2006; Jansen et al., 2011) or during 'parallel' lowering of the channel bed (often termed 'diffusive' incision) (e.g. Burbank et al., 1996; Leland et al., 1998; Reusser et al., 2006). The pattern of strath surface ^{10}Be exposure ages can be used to distinguish between these incision mechanisms (Figure 5-5; Reusser et al., 2006; Jansen et al., 2011). Only Little Garve and the Monessie Gorge sites in this study

show possible upstream younging in the ^{10}Be ages towards the KP. However, even at these sites, overlapping uncertainty ranges for two of the strath samples preclude a clear case for KP retreat. If KP retreat was the strath forming mechanism, calculated retreat rates of ~22 – 57 m/kyr would be within the range of rates found by Jansen et al. (2011) for retreating glacio-isostatic knickpoints in western Scotland. The rates of KP retreat for each site also appear to decline over time (e.g. from c. 57 m/kyr at ~7 ka to ~22 m/kyr within the past ~4 ka at the Monessie gorge), a similar pattern to that seen by Jansen et al. (2011). However, the similarities in surface exposure ages at the sites indicate that KP retreat may have been too rapid to be resolved at current levels of analytical precision. Alternatively, incision of the inner gorge at the study sites may have resulted in 'replacement' (*sensu* Gardner, 1983) or decay of the KP during headward retreat.

5.5.1.3   Controls on strath formation in postglacial landscapes

Because both Type 2 and Type 3 strath terraces are formed due to long-term changes in channel width, the timing of formation of strath terraces may be used to identify key factors controlling the channel geometry.

Type 3 strath formation results from channel narrowing due to changes in substrate resistance on transition from alluvial to bedrock channels (chapter 4 and section 5.2.3). The findings that pre-strath channel widths are consistent with alluvial channel widths, and that the inner channel geometry is similar to the geometry of hydraulically-scaled bedrock channels, are consistent with this interpretation. As discussed in chapter 3, declining paraglacial sediment flux is the most likely cause of most alluvial to bedrock channel transitions.

Numerous potential causes of bedrock channel narrowing resulting in Type 2 strath formation have been suggested; including lithological control (Wohl, 2008), climatically driven discharge changes (e.g. Reusser et al., 2006), and declining sediment flux (Finnegan et al., 2007). The possibility that lithological constraints during fluvial incision may result in Type 2 strath formation is important: it may mean that Type 2 strath formation is not indicative of changing external conditions, but is simply a result of factors intrinsic to the incision process. Wohl (2008) noted that strath terraces in crystalline bedrock in streams in Colorado are formed on strong sub-horizontal joint planes, suggesting that strong jointing may constrain bedrock channel geometry, and the distribution of joints may drive temporal variations in channel geometry as incision proceeds. At the two Type 2 strath sites, strong

joint control is only apparent in the strath terraces at Dog Falls, where plucking is the dominant incision mechanism. In the Monessie gorge, where abrasion is the dominant incision mechanism, the long, continuous, strath surface is not formed along a joint plane. The observation that channels at both sites have had a tendency to narrow despite different incision mechanisms, and the fact that the straths at Dog Falls have been preserved over 10 – 12 kyr since their formation, suggest that the channel narrowing, and hence strath formation, at Dog Falls is not simply a function of joint control during incision. It is also clear from the assessment of channel geometry in section 4.3.3 that strong jointing has no significant impact on bedrock channel width. Finally, the consistency of the surface ages from Dog Falls with those of the Type 3 sites, and of the timing of strath formation with respect to deglaciation at all sites, also supports the assertion that the timing of strath abandonment at Dog Falls is related to changing external conditions.

The limited resolution of early Holocene climatic records for the Scottish Highlands, especially for precipitation patterns and sediment flux (section 2.2.3.3), means that it is not possible to link strath ages with climatic variations. However, there appears to be a relation between the timing of strath formation (relative to deglaciation) and the glacial history of the catchment (section 5.4.2.2). This observation, though tentative due to the large uncertainties on both exposure ages and deglaciation times, is consistent with the potential control on strath formation by declining paraglacial sediment flux.

A lag between deglaciation and strath formation would be expected for both Type 3 and Type 2 strath terraces because of the time needed for the pulse of paraglacial sediment to pass through the site prior to strath formation. The subsequent decline in sediment supply may then;

- drive a switch from depositional to erosional fluvial systems that results in excavation of the bedrock valley floor and channel narrowing as rivers incise across the sediment-bedrock boundary (Type 3 straths), or
- drive narrowing in incising bedrock channels due to sediment focusing in topographic lows on the channel bed (Type 2 straths, cf. Finnegan et al., 2007).

Partial glaciation of catchments during the YD may have prolonged the increased sediment pulse following the LD deglaciation, delaying strath formation at sites with substantial YD glaciation of the upper catchment (Dog Falls and Croick Schoolhouse), and causing the slightly longer lag times (3 – 4 kyr) prior to strath formation. By contrast, sites in

catchments which experienced limited YD glaciation of the upper catchment, Little Garve and the Linn of Dee, have shorter lag times of 2 – 3 kyr.

The longer lag time of 3 – 4 kyr for strath formation in the Monessie gorge following the end of the YD glaciation may also be due to specific glacial history of the upper catchment. A relatively large volume of lacustrine sediment is stored in the River Spean catchment, stemming from accumulation in a glacial lake formed during the YD due to a glacier dam in the lower Spean valley (e.g. Sissons, 1979a; Palmer, 2010). Remobilisation of these lacustrine sediments, as well as underlying glacial and glacio-fluvial sediments, following lake drainage at the end of the YD may have elevated sediment flux in the River Spean, possibly causing a higher and longer peak postglacial sediment flux (therefore a longer lag-time) relative to the other catchments.

The general model of declining paraglacial sediment flux also suggests that peak in sediment flux occurs later in downstream areas due to the time needed for the downstream propagation of the sediment 'wave' (Slaymaker, 2009). Hence, it may be expected that strath formation in the lower parts of catchments may occur later than in more upstream areas. This prediction is supported by comparison of strath exposure ages in the Monessie gorge with those for the Spean Gorge, 12 km downstream on the same river, as measured by Jansen et al. (2011). The oldest strath surface exposure age from the Spean Gorge is 4.9 ± 0.3 ka (Jansen et al., 2011), compared with an average strath age of 7.3 ± 0.7 ka from the Monessie gorge in this study. These ages are consistent with a later peak in paraglacial sediment flux through the lower Spean Gorge delaying the onset of strath formation, and suggest that the paraglacial sediment 'wave' may migrate downstream at a rate of ~ 5 m/yr.

Despite the consistency of these observations with those expected for rivers responding to declining paraglacial sediment flux, it must be noted that climate-controlled changes in discharge as well as non-linear responses to channel slope changes during ongoing fluvial adjustment following deglaciation may also drive both Type 2 and Type 3 strath formation (cf. Reusser et al, 2006; Wohl, 2008; chapter 3). It is acknowledged that interpretation of strath surface ages in the early Holocene is largely speculative and more detailed Holocene climatic records and sediment flux estimates for the Scottish Highlands are needed before controls on postglacial strath formation can be properly evaluated.

5.5.2   Incision rates and fluxes

5.5.2.1   <u>Fluvial incision and denudation in Scotland</u>

Holocene vertical incision rates of 0.4 – 2.4 m/kyr and modern erosion rates of 0.07 – 0.24 m/kyr were reported by Jansen et al. (2011) for channels responding to glacio-isostatic uplift in the western Highlands. These are similar to the Holocene incision rates of 0.3 – 1.3 m/kyr and modern rates of ~0.1 m/kyr found in this study over a similar range in drainage areas. The slightly lower maximum erosion rates found in this study may be due to the older strath ages, i.e. the longer period of time-averaging. Incision rates for younger surfaces are commonly greater than those quantified using older surfaces, especially where incision rates are likely to have declined with time (e.g. Hancock and Anderson, 2002).

Long-term denudation rates (10^6 – 10^7 year timescales) for Scotland of 0.02 – 0.03 m/kyr (Persano et al., 2007) are an order of magnitude lower than the Holocene fluvial incision rates quantified in this study. The difference in rate may indicate that landscape instability caused by inheritance of glacially conditioned landscape form and sediment flux is responsible for elevated rates of erosion in rivers, and potentially in the wider landscape following deglaciation (Jansen et al., 2011). However, the disparity may also arise if slow transfer of the fluvial incision signal to surrounding hillslopes limits the rate of erosion over the wider landscape. This is discussed further in chapter 7.

5.5.2.2   <u>Controls on postglacial fluvial incision rates</u>

Postglacial fluvial incision rates were found to be a function of stream power and intact rock strength (as measured by the Schmidt hammer 'R' value). The data from the five study sites were used to derive an empirical incision rate equation that may be used to predict Holocene erosion rates in Scottish Highland rivers from channel slope, drainage area and estimates of rock strength (Schmidt hammer 'R' values) for major lithological units. In chapter 6, this equation is used to model postglacial fluvial incision rates in the three surveyed channels (rivers Carron, Elchaig and Canaird), forming the basis for an assessment of the extent of inheritance of pre-existing gorges and the distribution of postglacial incision at reach to catchment scales.

Stream power control on long-term Holocene vertical incision rates was reported by Jansen et al. (2011) in western Scotland, but modern incision rates were independent of stream power with rates of ~0.1 – 0.2 m/kyr measured at drainage areas ranging from 50 – 200

km^2. The low modern incision rates from Dog Falls (~0.1 m/kyr at 195 km^2) are consistent with those reported by Jansen et al. (2011), and taken with the published data suggests that modern fluvial erosion rates across the whole of the Scottish Highlands are low. Jansen et al. (2011) suggest that declining paraglacial sediment flux is the most reasonable explanation for the differences observed between Holocene and modern incision rates.

The finding of a direct link between rock strength and measured fluvial incision rates is a key result from this study, and was made possible by the analysis of multiple sites. Previously, a direct rock strength control on fluvial incision rates has only been demonstrated in experimental studies designed to quantify rates of abrasion (e.g. Sklar and Dietrich, 2001). The results from this study show that softer schist and pelite rocks erode more rapidly than resistant psammites and quartzites. However, the different rock types also have different styles of inner channel incision, with softer rocks eroded by abrasion-dominated potholing and more resistant rocks eroding by plucking with limited abrasion. Rapid erosion in abrasion-dominated channels may be due to positive feedbacks involved in pothole formation which mean that local incision rates at the base of potholes may be an order of magnitude greater than 'background' abrasion rates (Whipple et al., 2000). This effect, combined with the moderately wide spacing of joints in the plucking-dominated reaches, may explain why rates of abrasion are higher than rates of plucking in the study channels despite contrary observations in other areas (Whipple et al., 2000, Whipple, 2004). The findings suggest that the relationship between lithological resistance, of which intact rock strength is only one component, and incision rates are complex, with rock strength and joint densities controlling both the spatial distribution of the dominant incision processes as well as the overall incision rate. The role of lithology in fluvial incision is analysed further in sections 6.4.2 and 7.2.2.

5.6   Conclusions

The data presented in this chapter show that the formation of strath terraces in postglacial rivers lags deglaciation, suggesting that declining paraglacial sediment flux influences channel geometry through a direct control on bedrock channel width (Type 2 straths) and by driving long term changes in channel type (Type 3 straths). The formation of Type 3 straths occurs because the 'stable' width of bedrock channels in the Scottish Highlands is narrower than that for alluvial channels (see chapter 4). In landscapes with weaker bedrock, undergoing similar channel type transitions, Type 3 straths may not be expected

to form as stable channel geometries for both alluvial and bedrock channel types are not sufficiently different (cf. section 4.4.1).

The quantification of Holocene incision rates at multiple sites highlights the importance of stream power and lithological resistance in controlling fluvial incision, but sediment flux is also a fundamental control on incision rates; under sediment-starved conditions incision rates are low regardless of stream power. The results define an empirical equation for Holocene-average incision rates which is used in the following chapter to assess the distribution of entrenchment in the three NW Highland study channels.

All strath terraces examined here were formed at glacially inherited knickpoints (reigels or hanging valleys), suggesting that these steep reaches act as foci for postglacial bedrock incision. The presence of Type 2 strath terraces near the base of bedrock gorges suggests that postglacial incision may add to pre-existing gorges. Where Type 3 straths are formed, postglacial rivers have cut new inner gorges in the floors of glacial troughs.

Chapter 6

Postglacial fluvial incision

6.1   Introduction

6.1.1   Context

The distribution and magnitude of fluvial incision within catchments are major controls on the overall landscape response to climatic change or base-level fall. In postglacial landscapes, glacially-conditioned valley-floor slopes and sediment flux control the distribution of bedrock channels (chapter 3) and the timing and rate of fluvial incision (chapter 5). Postglacial fluvial incision leads to bedrock channel entrenchment, forming inner gorges inset into the floor of glaciated valleys, with the degree of entrenchment reflecting the duration and rate of fluvial incision. However, some inner gorges may be inherited from periods of pre-glacial fluvial incision or erosion by sub-glacial meltwater streams (Holtedahl, 1967; Tricart, 1970; McEwen et al., 2002; Montgomery and Korup, 2011). In order to assess the distribution and magnitude of fluvial incision in postglacial settings, the history of these inner gorges must be unravelled.

The distribution and magnitude of channel entrenchment were mapped at reach scales during the field survey of the rivers Carron, Elchaig and Canaird. Comparison of observed entrenchment with predicted entrenchment depths, derived using an empirical incision rate equation (section 5.4.3), forms the basis for assessment of the distribution and magnitude of postglacial incision in the NW Scottish Highlands. The degree of inheritance of pre-

existing gorges is estimated and the results form the basis for further assessment of potential controls on the timing and rate of postglacial fluvial incision.

6.1.2   Research questions and approach

The analysis presented in this chapter aims to answer two main research questions:

1. How much of the observed entrenchment of bedrock channels is due to postglacial incision?
2. What is the distribution of postglacial incision within catchments?
   a. What are the main mechanisms of fluvial incision?
   b. How do the main controls on fluvial incision influence the distribution and magnitude of erosion in postglacial streams?

A variety of methods have been used to assess the origin of inner gorges in postglacial settings; field-based approaches utilise the geomorphic context of the gorge and associated landforms to interpret its origin (Holtdahl, 1967; McEwen et al, 2002), surface exposure dating has been used to quantify the timing of gorge excavation (Valla et al., 2010a), and digital topographic data have been used to make quantitative comparisons between different scenarios for gorge excavation (Montgomery and Korup, 2011).

The jointed rocks of the NW Highlands study area mean that gorge walls are relatively unstable and are therefore not suitable for surface exposure dating. The following analysis is thus based upon data and observations from field survey and digital topographic analysis. The derivation of an empirical fluvial erosion rate equation from independently measured incision rates in section 5.4.3 provided a new method for assessing the origin of inner gorges in the NW Highlands. The empirical erosion rate function (Eq 5.3) was used to derive predicted postglacial entrenchment depths for each bedrock reach and the degree of inheritance of pre-existing gorges was estimated by comparing observed entrenchment depths with predicted postglacial entrenchment. Classification of channels according to their observed depth of entrenchment relative to the predicted depth also forms the basis for further assessment of the mechanisms and controls on postglacial fluvial incision.

6.2   Data and methods

The techniques used to measure entrenchment in alluvial and bedrock channels during the field survey are outlined in section 6.2.1. The method used to calculate predicted

postglacial incision rates and entrenchment depths for the bedrock reaches is presented in section 6.2.2.

6.2.1   Measuring reach-scale channel entrenchment

Entrenchment of channels into bedrock, alluvial or glacio-fluvial terraces was assessed at reach scales by measuring the depth of bedrock gorges (H_G in Figure 4-1) and height of sediment terraces (H_T in Figure 4-1) using the vertical distance and vertical height functions on the Impulse 200R Laser Range finder. Where terrace heights or entrenched bedrock gorge depths are less than 1.9 m, the measurement was made using a measuring pole (to the nearest 5 cm). Gorge depth and sediment terrace heights were measured to the low flow water surface, and were taken at multiple points along each entrenched reach. The values for each reach were then averaged to give a mean entrenchment depth or terrace height for each entrenched reach. Finally, the reach-averaged low flow channel depth (section 4.2.1) was added to the mean entrenchment depth of the bedrock reaches to give a reach-averaged total entrenchment depth (H_{GT}). Where channels were entrenched into valley-fill, including glacial till, talus and raised marine sediment, the depth of entrenchment was estimated from the height of the steep scarp at the toe of the sediment deposit.

Gorge volumes were calculated as the volume of a rectangular prism of the reach length, the reach-averaged high flow width (w_r – see section 4.2.1) and the reach-averaged total entrenchment depth (H_{GT}). The high flow width, rather than the gorge width (Figure 4-1) was used because the gorge width is affected by rockfall and landslip from the unstable gorge walls.

Uncertainty for the reach-average entrenchment depth and reach-averaged low flow depth were calculated as the standard error of the mean (1σ) of the sample populations. The combined standard uncertainty (at 1σ) for the total entrenchment depth ($u(H_{GT})$), was derived from these standard errors using summation in quadrature (e.g. Bell, 1999):

$$u(H_{GT}) = \sqrt{u(reach\ average\ entrenchment\ depth)^2 + u(low\ flow\ channel\ depth)^2} \qquad \text{Eq 6.1}$$

Uncertainty values for terrace heights and valley scarp heights above the channel were not derived as these values are used for reference only.

Detailed sub-reach scale mapping of channels was beyond the scope of this study and the limited resolution of channel slope data means that the form of entrenched reaches at sub-

reach scales has not been quantitatively assessed (cf. section 2.3.3.2). The implications of the results for the mechanism of entrenchment at reach to catchment scales, e.g. knickpoint retreat or parallel lowering of the channel bed, is discussed using findings from the strath sites (chapter 5) and observations from the surveyed streams in section 6.4.2.3.

6.2.2   Identifying postglacial inner gorges

6.2.2.1   Modelling fluvial erosion rates at reach scales

Postglacial fluvial erosion rates for each bedrock reach in the mapped catchments were estimated from the empirical erosion rate equation derived in chapter 5,

$$\varepsilon = 1.62 - 0.0239R + 6 \times 10^{-6}\Omega \qquad\qquad\qquad \text{Eq 5.3}$$

where R is the corrected Schmidt hammer 'R' value and Ω is the total stream power (ΥQS). Values of R in the study streams range from 40 – 53 (Table 2-5) and Ω varies from 430– 24800 W m^{-1}. These ranges are different to the ranges of R and Ω for the strath sites (31 – 59 and 26000 – 96300 W m^{-1} respectively), hence it is assumed that the linear relationship may be extrapolated to lower and higher values of Ω and R. Spatial variations in sediment flux and the density of jointing may also influence fluvial incision rates. These factors are not accounted for in the calculation of estimated postglacial fluvial incision rates for the study streams but their role is explored in the analysis in the following sections.

6.2.2.2   Classification of channels by entrenchment

The predicted postglacial erosion rates were used in conjunction with an estimated deglaciation time to calculate a predicted postglacial entrenchment depth (h_{pg}) for the bedrock reaches. The deglaciation time for each reach was estimated on the basis of the deglaciation histories for the catchments (section 2.3.1.1). Bedrock reaches were ascribed to one of three classes: i) 'postglacial-entrenched' where predicted postglacial entrenchment depths are equivalent to the observed entrenchment; ii) 'over-entrenched' where the predicted postglacial entrenchment is less than the observed entrenchment and; iii) 'under-entrenched' where the predicted entrenchment is greater than the observed entrenchment.

The range of potential errors associated with the prediction of postglacial incision rates by this method means that a relatively high level of uncertainty is assumed for the predicted entrenchment depth. Observed entrenchment values within ±25% of predicted are deemed

to be consistent with postglacial entrenchment. This means that under-entrenched reaches have observed entrenchment depths <75% of the predicted postglacial entrenchment and over-entrenched reaches have observed entrenchment depths >125% of predicted values.

This classification of bedrock channels forms the basis for assessment of the main controls on the entrenchment of postglacial channels. In particular, the level of inheritance of pre- or sub-glacially cut inner gorges, and the implications for controls on the timing and rate of fluvial incision are addressed in the following analysis.

6.3   Results

The results of the assessment of bedrock channel entrenchment are presented in two sections. In section 6.3.1 the overall distribution and magnitude of channel entrenchment in the study rivers are assessed. In section 6.3.2 the distributions of postglacial-entrenched, under-entrenched and over-entrenched channels are analysed in the context of potential controls on postglacial channel entrenchment.

6.3.1   Distribution and magnitude of entrenchment

The distribution and magnitude of channel entrenchment into bedrock are shown for the study rivers in Figure 6-1, Figure 6-2 andFigure 6-3. There is a general correlation between the location of entrenched bedrock reaches and peaks in total stream power for the River Carron, but the magnitude of peaks does not appear to correlate well with the depth of entrenchment (Figure 6-1). For the rivers Elchaig and Canaird, many deeply entrenched channels are associated with small peaks in stream power, and some larger stream power peaks correspond to only small amounts of entrenchment (Figure 6-2 and Figure 6-3).

If the entrenchment of bedrock channels is due to ongoing postglacial incision, the depth of entrenchment would be expected to depend on the erosion rate and the time since deglaciation. The erosion rates derived from strath terraces in chapter 5 are correlated with stream power and lithological resistance, so if the entrenchment in the surveyed channels began soon after deglaciation, the observed entrenchment depth may be positively correlated with stream power and negatively correlated with rock resistance. If channels have inherited pre-existing gorges, however, or if the timing of the onset of incision is spatially variable, then the degree of entrenchment may not be related directly to the erosion rate.
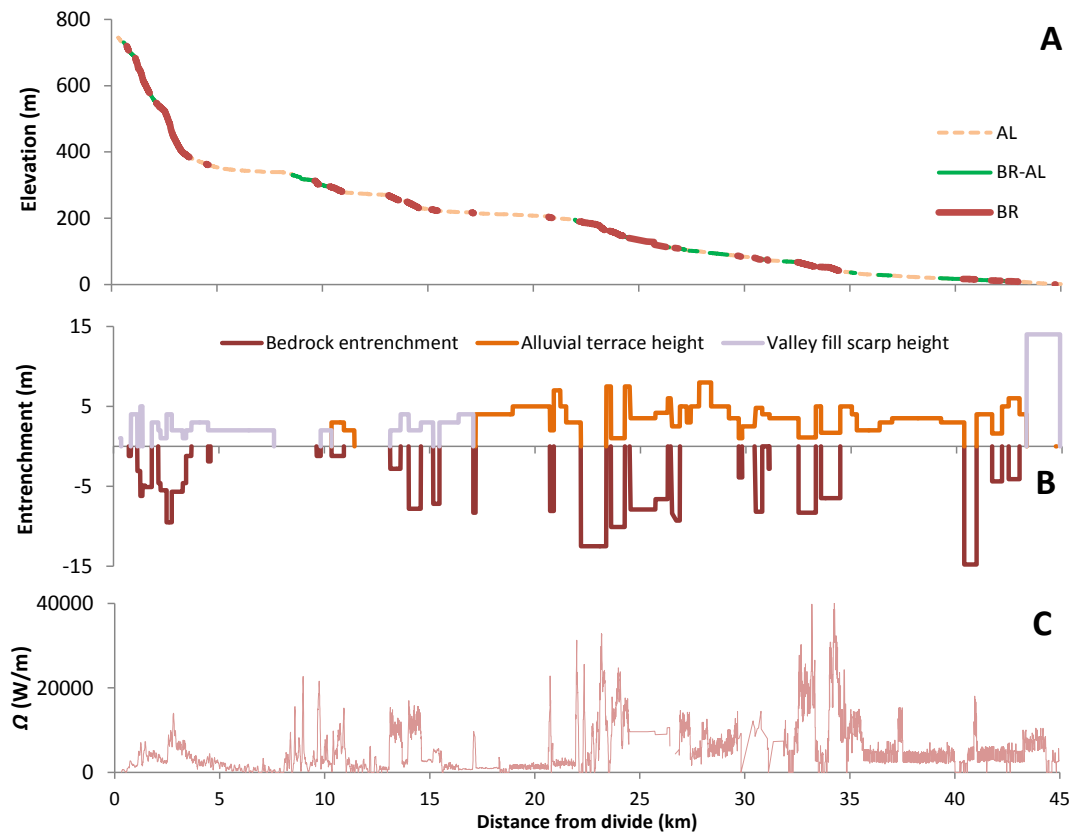
Figure 6-1. **River Carron – Distribution of bedrock channel entrenchment. Depth of bedrock channel entrenchment shown in plot B (negative values), with height of alluvial terraces and valley fill scarp height above channel (positive values). Key on plot B. Note that valley fill consists of glacial till, talus and debris fan deposits. The channel long-profile and distribution of channel types (A) and the total stream power (Ω) (C) are shown for reference.**
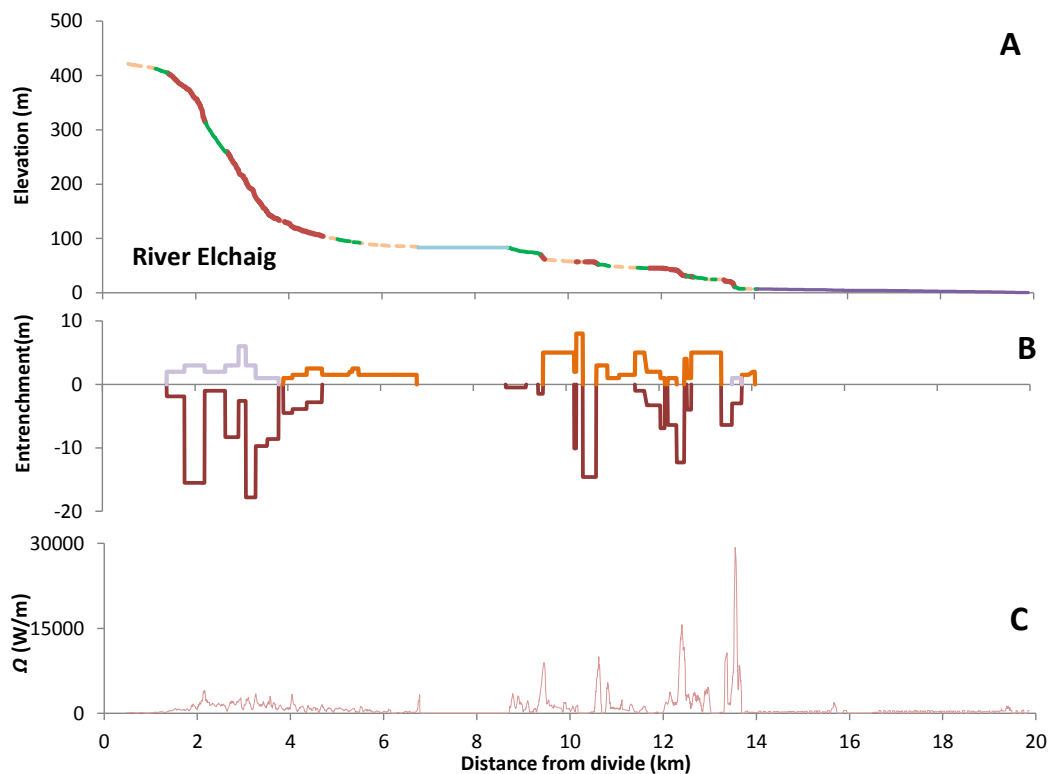
Figure 6-2. **River Elchaig – Channel entrenchment, data as for Figure 6-1.**
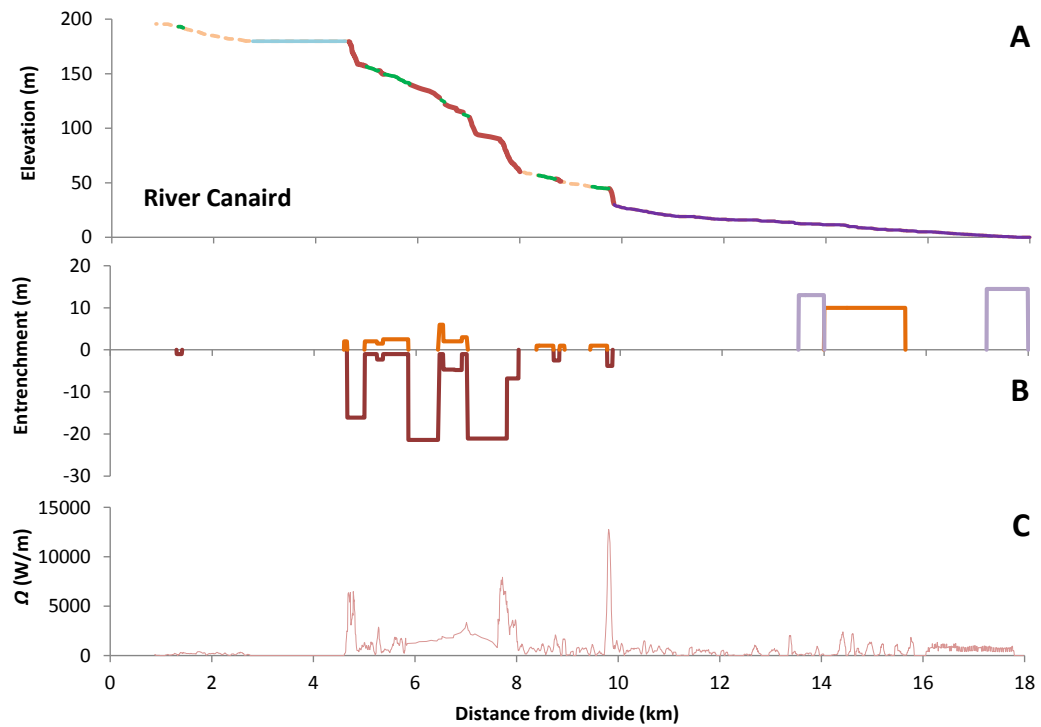
Figure 6-3.   **River Canaird – Channel entrenchment, data as for Figure 6-1.**

The scatter plots in Figure 6-4 A, B and C indicate that the observed entrenchment is not correlated with total stream power (Ω) or unit stream power (ω). Classifying the data according to lithology (Figure 6-4 B) suggests that reaches in pelite have generally low entrenchment whilst reaches in flaggy psammites are generally more deeply entrenched. Reaches in pelite are the only lithological group to show a significant correlation between observed entrenchment and total stream power ($p<0.1$, Figure 6-4). Overall, the observed bedrock channel entrenchment is not dependent on the time since deglaciation (Figure 6-4 D), or rock hardness (R) (Figure 6-4 E) and there is a large range in entrenchment for all values of the Selby rock mass strength (RMS) index. However, the maximum entrenchment depth does appear to be inversely related to the Selby RMS index (Figure 6-4 F), suggesting that there may be a lithological control on entrenchment, but that other factors may limit the depth of incision even in weaker lithologies. Assessment of gorge volume versus Ω, ω, R, the Selby RMS index, and time since deglaciation show results similar to those for the entrenchment depth (Appendix 6). These results indicate that inheritance of pre-existing gorges and/or delays in the onset of incision are likely to have influenced entrenchment in the study channels.
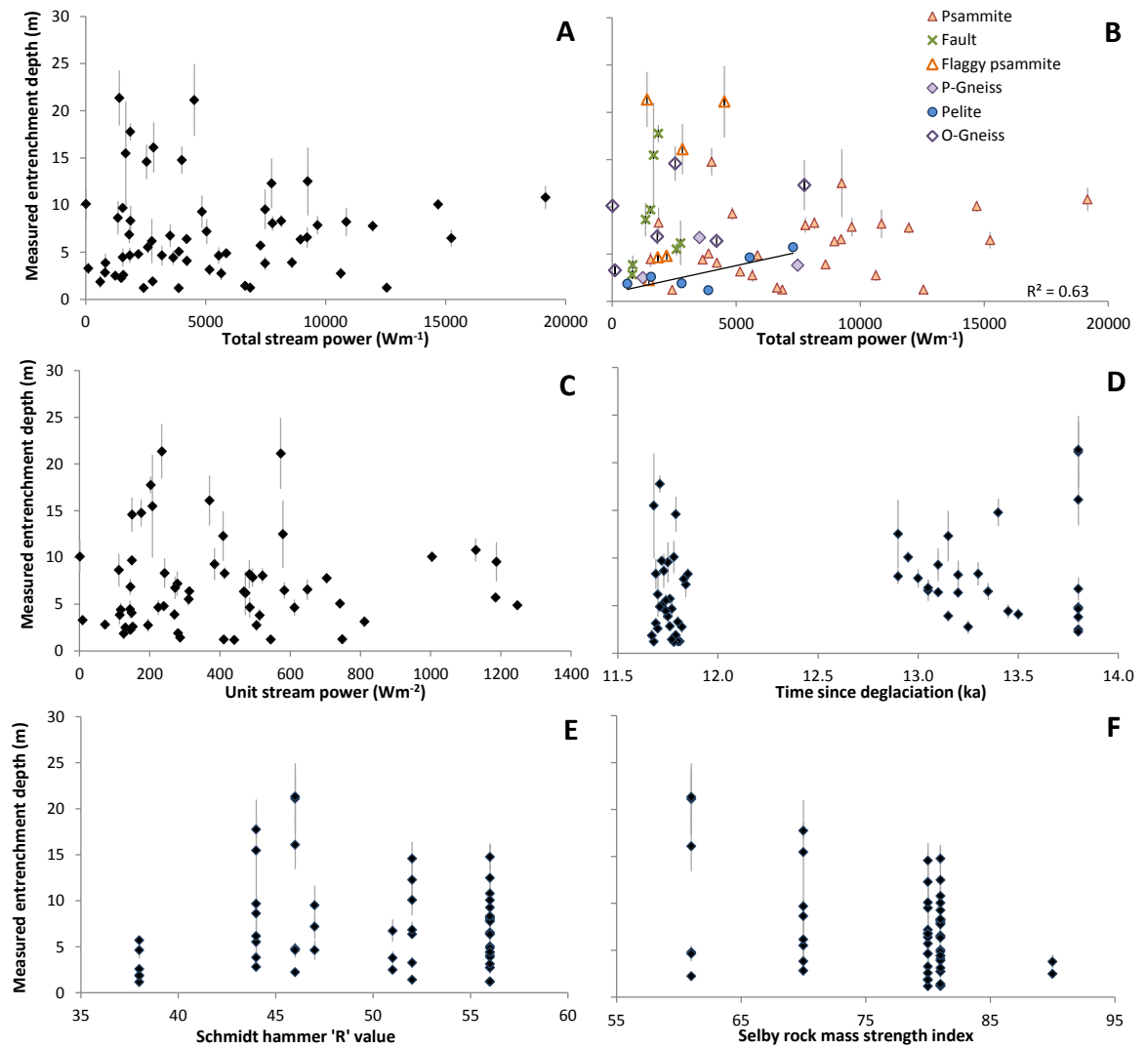
Figure 6-4.   Scatter plots of entrenchment depth (H_{GT}) versus total stream power (Ω) for all data (A) and classified according to lithology (B). Key to lithological symbols shown in plot B, linear regression for pelite is significant at p<0.1. H_{GT} for all data versus unit stream power (ω) (C), time since deglaciation (T_{DG}, D), Schmidt hammer R value (E) and the Selby RMS index for the dominant rock type in the reach (F). Error bars show combined standard uncertainty at 1σ.

6.3.2   Postglacial bedrock channel entrenchment

Comparison of observed versus predicted entrenchment depth is used in the following analysis to identify channels that have been incised by postglacial rivers (cf. section 6.2.2). Where observed entrenchment and predicted entrenchment depths are similar, it is concluded that the channel has been incised by postglacial fluvial incision initiated soon after deglaciation ("postglacial-entrenched"). Under-entrenchment of channels may be due to a delay in the onset of fluvial incision following deglaciation. Over-entrenchment of channels is expected for reaches that have inherited pre-existing inner gorges.
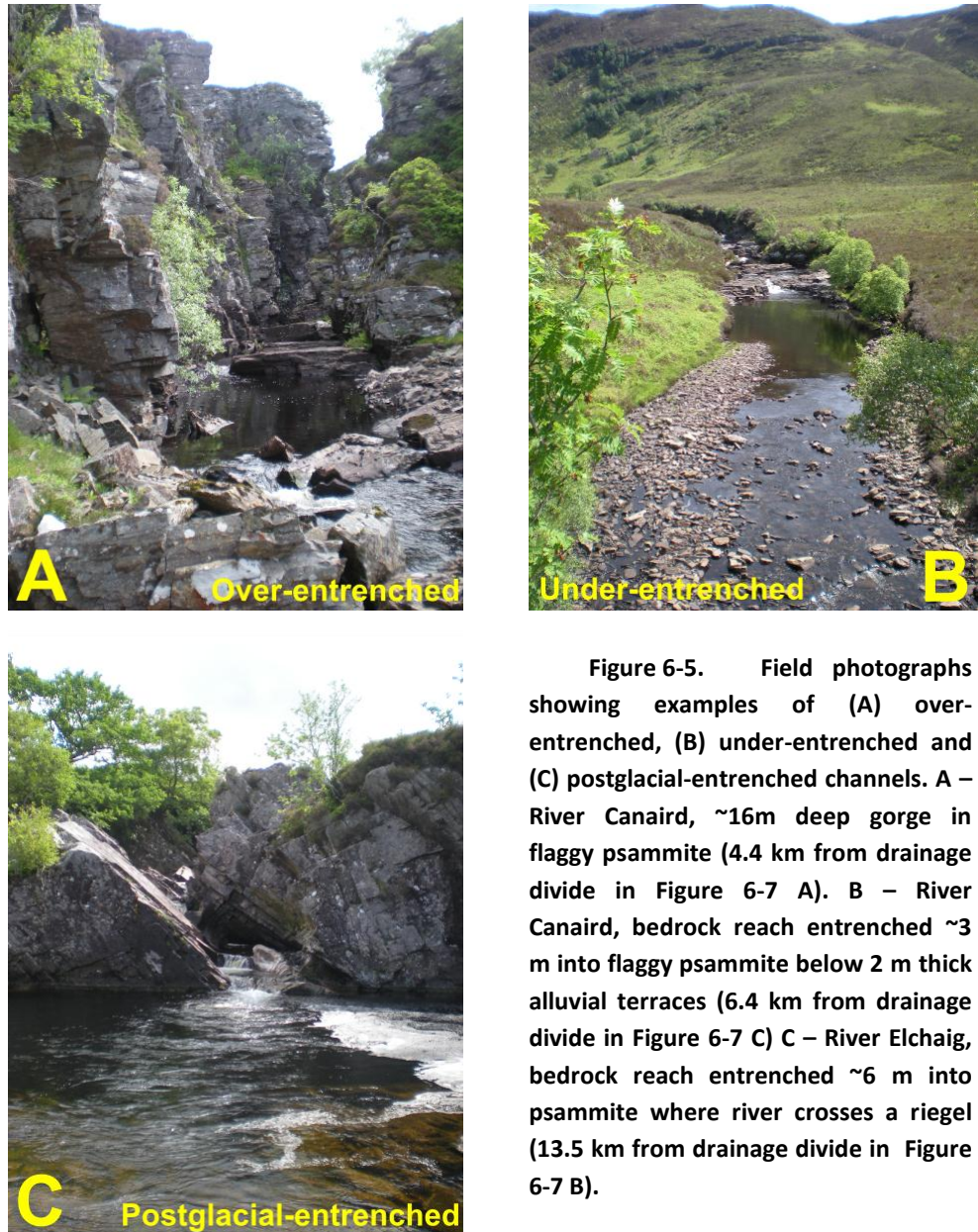
Figure 6-5. Field photographs showing examples of (A) over-entrenched, (B) under-entrenched and (C) postglacial-entrenched channels. A – River Canaird, ~16m deep gorge in flaggy psammite (4.4 km from drainage divide in Figure 6-7 A). B – River Canaird, bedrock reach entrenched ~3 m into flaggy psammite below 2 m thick alluvial terraces (6.4 km from drainage divide in Figure 6-7 C) C – River Elchaig, bedrock reach entrenched ~6 m into psammite where river crosses a riegel (13.5 km from drainage divide in Figure 6-7 B).

The observed entrenchment and the predicted depth of postglacial entrenchment are compared for each bedrock reach in Figure 6-6, with downstream patterns shown in Figure 6-7. Of the 59 bedrock reaches in the study streams, 24% were found to have observed entrenchment depths similar to those predicted using equation 5.3, 39% were found to be 'under-entrenched' (i.e. have entrenchment depths less than <75% of predicted), and 37% are 'over-entrenched' (i.e. with observed entrenchment depths >125% of predicted) (Figure 6-6). As both postglacial-entrenched and under-entrenched reaches have been incised since deglaciation, the results indicate that 63% of the bedrock reaches have been entrenched into the valley floor by postglacial fluvial incision (see plots A2, B2 and C2 in Figure 6-7).

Postglacial-entrenched channels are found at riegels and in some steep channels in the headwall of the upper Carron (Figure 6-5 C and Figure 6-7 A2). Over-entrenched channels

are distributed throughout catchments, but are extensive in steep channels downstream of major profile convexities, particularly in the upper River Elchaig and middle sections of the rivers Carron and Canaird (Figure 6-5 A and Figure 6-7). Under-entrenched channels are generally found at smaller riegels and in lower parts of the headwall sections of the Elchaig and Carron. The larger knickpoints in the lower Canaird are also under-entrenched (Figure 6-7 C2).
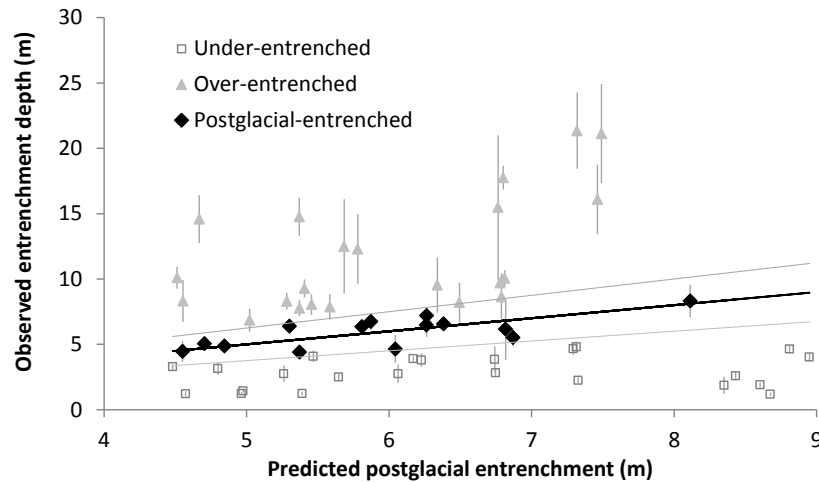
Figure 6-6. **Predicted entrenchment versus observed entrenchment for the different classes of entrenched channel. Systematic uncertainty at 1σ. Black line marks point where observed entrenchment equals predicted entrenchment, with ±25% limits shown by grey lines.**

Comparison of the degree of postglacial entrenchment between the study catchments was made by calculating the total volume of 'missing rock'; effectively the sum of all the inner gorge volumes for each river. Gorge volumes were calculated from the average entrenchment depth, reach length and the high-flow channel width. The total volume of postglacially entrenched gorges was also derived for each stream from the sum of the volumes of all postglacial-entrenched and under-entrenched reaches (Table 6-1).

The ratio of the postglacial gorge volume to the total gorge volume for the three study channels indicates that in the River Carron, 77% of the observed entrenchment is postglacial, compared to 66% for the River Elchaig and 47% for the River Canaird. This result suggests that over half of the observed entrenchment in the River Canaird and two thirds of that in the River Elchaig may be due to inheritance of pre-existing inner gorges. The ratio appears to be inversely related to the reference channel steepness (S_r) and positively related to the breach depth ratio (Table 6-1) suggesting a possible link between inheritance of pre-existing gorges and the degree of breaching of drainage divides (Table 6-1). This is discussed further in section 6.4.1.
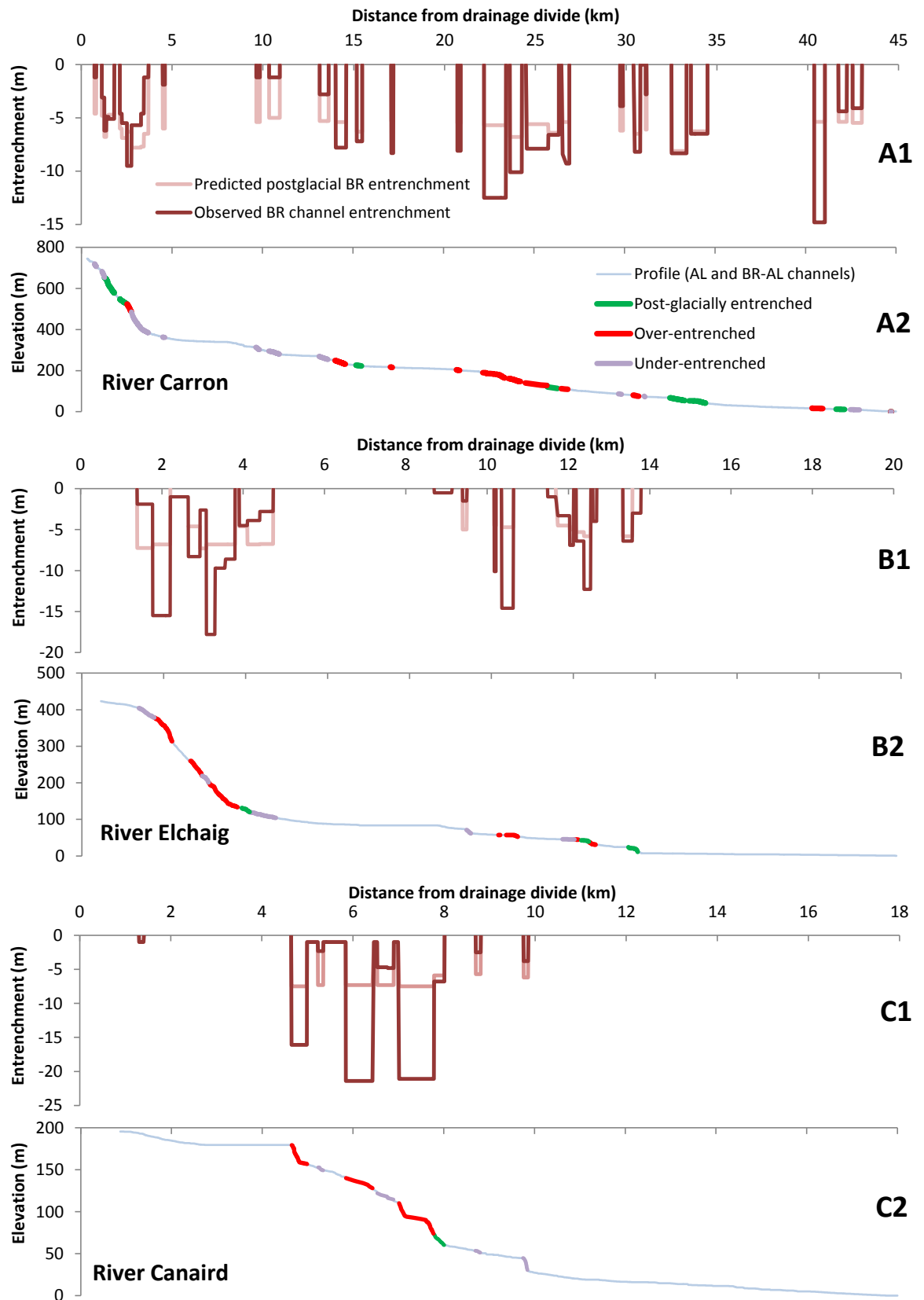
Figure 6-7. Comparison of the distribution of observed bedrock channel entrenchment (H_{GT}) with predicted postglacial entrenchment (h_{pg}) for the River Carron (A1), Elchaig (B1) and Canaird (C1). Long-profiles of the study streams showing distribution of postglacial-entrenched, under-entrenched and over-entrenched bedrock channels (A2, B2 and C2). Key in plots A1 and A2.

Parameter		River		
		Carron	Elchaig	Canaird
Proportion of BR channel	%	28.8	23.7	16.1
Total stream length	km	44.7	19.5	17.1
Reference channel steepness (S_r)		0.035	0.023	0.010
Concavity index (θ)		0.682	0.959	0.289
Breach depth ratio		0.09	0.33	0.36
Total gorge volume	m^3	1264524	308367	284824
Postglacial gorge volume	m^3	970368	202262	132427
Ratio of postglacial gorge volume to total gorge volume		0.77	0.66	0.47

Table 6-1.   Catchment scale entrenchment parameters. The derivation of the reference channel steepness, the concavity index and the breach depth ratio are described in section 3.3.1.1.

6.3.2.1   Postglacial-entrenched channels: fluvial incision rates

Postglacial-entrenched bedrock channels are located throughout the study catchments, in a range of rock types, including psammite, orthogneiss and fault-affected reaches. Vertical incision rates were calculated for the postglacial-entrenched reaches by dividing the observed entrenchment depth by the time since deglaciation (ε_{PG} in m/kyr). Volumetric erosion fluxes per unit channel length were also calculated for these reaches from the gorge volume (E_f^{PG} in m^3/m/kyr). Postglacial fluvial incision rates range between 0.33 and 0.63 ± 0.15 m/kyr and erosion fluxes range between 2 and 13 ± 3 m^3/m/kyr. As may be expected from the method of selecting the postglacial-entrenched reaches (cf. section 6.2.2), these rates are similar to those quantified using cosmogenic nuclide analysis of strath terrace surfaces in chapter 5 (ε_R =0.35 – 1.31 m/ka and E_f =5.8 – 16.6 m^3/m/kyr). The postglacial incision rates and erosion fluxes are also positively correlated with total stream power ($p<0.05$; Figure 6-8, Table 6-2), which reflects positive relationship between erosion rate and Ω in equation 5.3. Predicted erosion rates for the study channels were also based on rock strength (R) but the vertical incision rates and erosion fluxes derived from postglacial-entrenched channels are not correlated with this parameter (Table 6-2). The lack of correlation may be due to the narrow range of R values for postglacial-entrenched channels (40 – 53), with scaling obscured by variability in the data. However, the density of jointing is also expected to influence fluvial incision rates and variations in joint spacing in the study streams may be responsible for the lack of scaling with R. This latter point is explored in more detail in the following analysis and discussion.
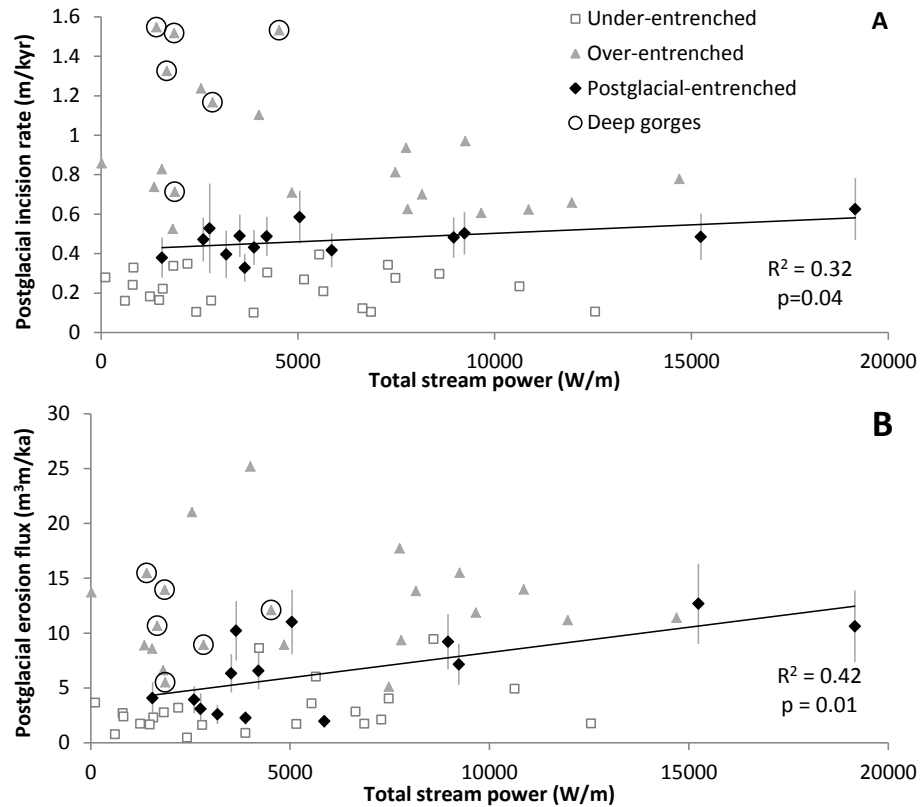
Figure 6-8. Postglacial vertical incision rates (A, ε_{PG}) and erosion fluxes (B, E_f^{PG}) derived from postglacial-entrenched channels (blue diamonds) versus stream power. Equivalent erosion rate estimates from under- and over-entrenched channels shown for reference only as these channels may be affected by delayed incision or inheritance respectively (key in plot A). Deep gorges in the upper River Elchaig and middle River Canaird, discussed in the text, are highlighted. Error bars are systematic uncertainties at 1σ and are shown only for postglacial-entrenched channel data.

| Parameter | Postglacial-entrenched channels | | | |
| | ε_{PG} (m/ka) | | E_f^{pg} (m^3/m/ka) | |
	R^2	p	R^2	p
Ω	0.32	*0.047*	0.42	*0.012*
R	0.05	0.460	0.10	0.279
Selby index	<0.01	0.744	0.08	0.336

Table 6-2. Regression statistics for postglacial-erosion rate (ε_{PG}) and erosion flux per unit channel length per kyr (E_f^{pg}) calculated for postglacial-entrenched channels. Linear regressions calculated for potential controlling variables in Minitab. Shading and italics indicates significant correlations where $p<0.05$. All correlations are positive.

6.3.2.2   Under-entrenched channels: controls on the timing and rate of postglacial fluvial incision

Under-entrenchment of channels with respect to predicted postglacial entrenchment may arise where incision has been delayed by a preceding period of excavation into sediments. In support of this proposition, ~50% of the under-entrenched channels are reaches that

have undergone a switch from alluvial to bedrock channel types over the Holocene
(chapter 3).

Assuming that postglacial fluvial erosion in these under-entrenched 'switch' reaches
occurred at the modelled erosion rate (calculated from Eq 5.3), the duration of incision
required to produce the observed entrenchment ranges from 1.6 to 10.1 kyr. If this erosion
occurred in a continuous period ending at the present, the duration of the lag between
deglaciation and the onset of bedrock incision ranges between 3 and 10 kyr (mean value of
6.7 ± 0.5 kyr (standard error at 1σ)). The mean potential lag time of 6.7 kyr is greater than
the duration of the lag between deglaciation and the excavation of the Type 3 strath terrace
surfaces quantified using cosmogenic nuclide analysis in chapter 5 (2 − 4.5 kyr). The
longer lag time in the surveyed channels may be due to lower stream power (smaller
drainage areas), hence lower rates of excavation of the overlying sediment. However, no
correlation between the lag time and total stream power (calculated using the modern
channel slope) is seen (Figure 6-9 B). The potential lag time is not scaled with the time
since deglaciation (Figure 6-9 A), catchment area or the distance from the drainage divide
(expressed as a fraction of the total stream length).
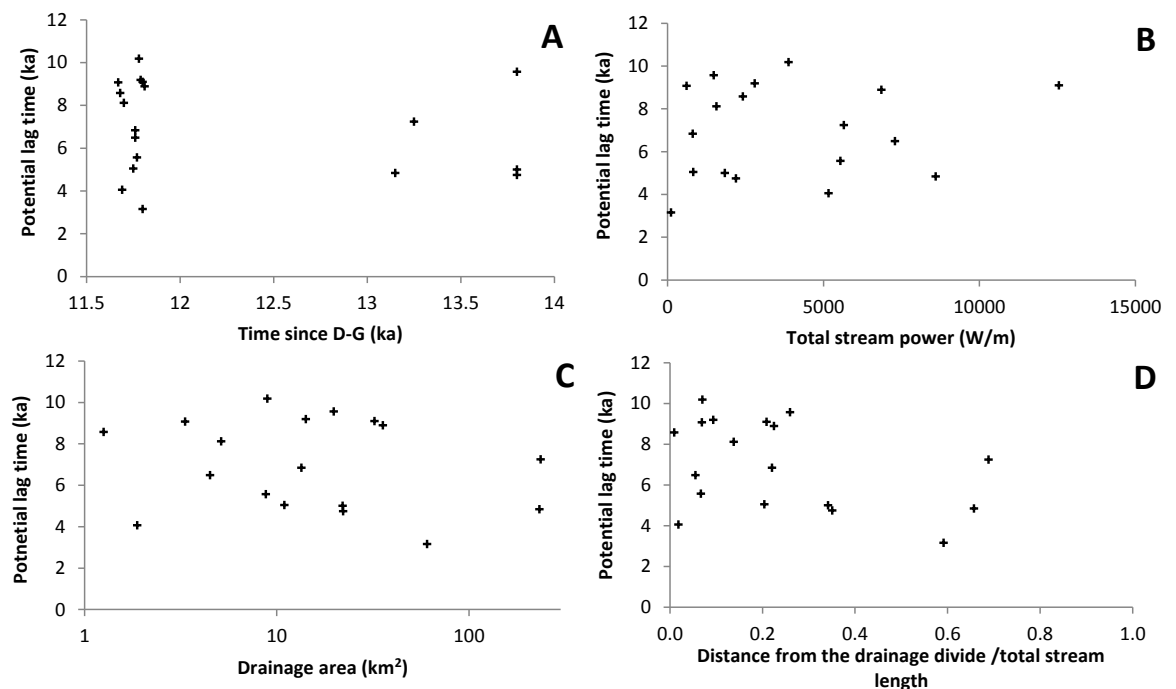
Figure 6-9.   **Potential lag between deglaciation and the onset of fluvial incision in under-
entrenched reaches associated with alluvial to bedrock channel transitions, plotted against A) time since
deglaciation, B) total stream power, C) drainage area (log axis) and D) the distance from the drainage
divide as a fraction of the total stream length.**

The remaining 50% of under-entrenched reaches are not 'switch' channels, and were interpreted in chapter 3 as having been bedrock since deglaciation. The apparent under-entrenchment of these reaches is probably due to overestimation of the postglacial erosion rate by equation 5.3, which does not account for slow erosion in hard, poorly jointed bedrock or spatial variations in sediment flux caused by lakes (see section 6.4.2).

6.3.2.3   Over-entrenched channels: gorge inheritance and controls on postglacial fluvial incision

Over-entrenchment of channels with respect to predicted postglacial erosion is expected where channels inherit pre-existing gorges after deglaciation. Over-entrenched reaches are found throughout the study catchments, but are concentrated in the upper Elchaig and the middle reaches of the rivers Canaird and Carron (Figure 6-7). In these reaches, the predicted postglacial fluvial erosion accounts for only 34 – 79% of the total gorge depth.

The most deeply entrenched bedrock channels are in the middle Canaird and upper Elchaig (15 – 21 m), accounting for 27% of all over-entrenched reaches. This deep entrenchment occurs despite low stream power and causes the observed entrenchment depth of over-entrenched reaches to be, counter-intuitively, inversely correlated with total stream power (Figure 6-10 C). The deeply entrenched reaches of the middle Canaird and upper Elchaig are in strongly jointed flaggy psammites and fault-affected rocks, resulting in a strong negative correlation with lithological resistance, especially with the Selby RMS index (Figure 6-10 A and B). This suggests that the deep entrenchment of these reaches may be due, at least in part, to rapid incision by plucking. If postglacial incision alone was responsible for the entrenchment of the deep gorges in the middle Canaird and upper Elchaig, average vertical incision rates of up to 1.5 m/kyr would have been required during the Holocene (Figure 6-8). This value is higher than the erosion rates quantified for the strath sites in chapter 5 despite stream power values that are an order of magnitude lower ($1.4 – 4.5 \times 10^3$ Wm^{-1} compared to $2.6 – 9.6 \times 10^4$ W m^{-1} for the strath sites). It is likely that inheritance of pre-existing gorges has also contributed to the deep entrenchment seen in the bedrock channels of the middle Canaird and upper Elchaig. This is discussed further in section 6.4.1.
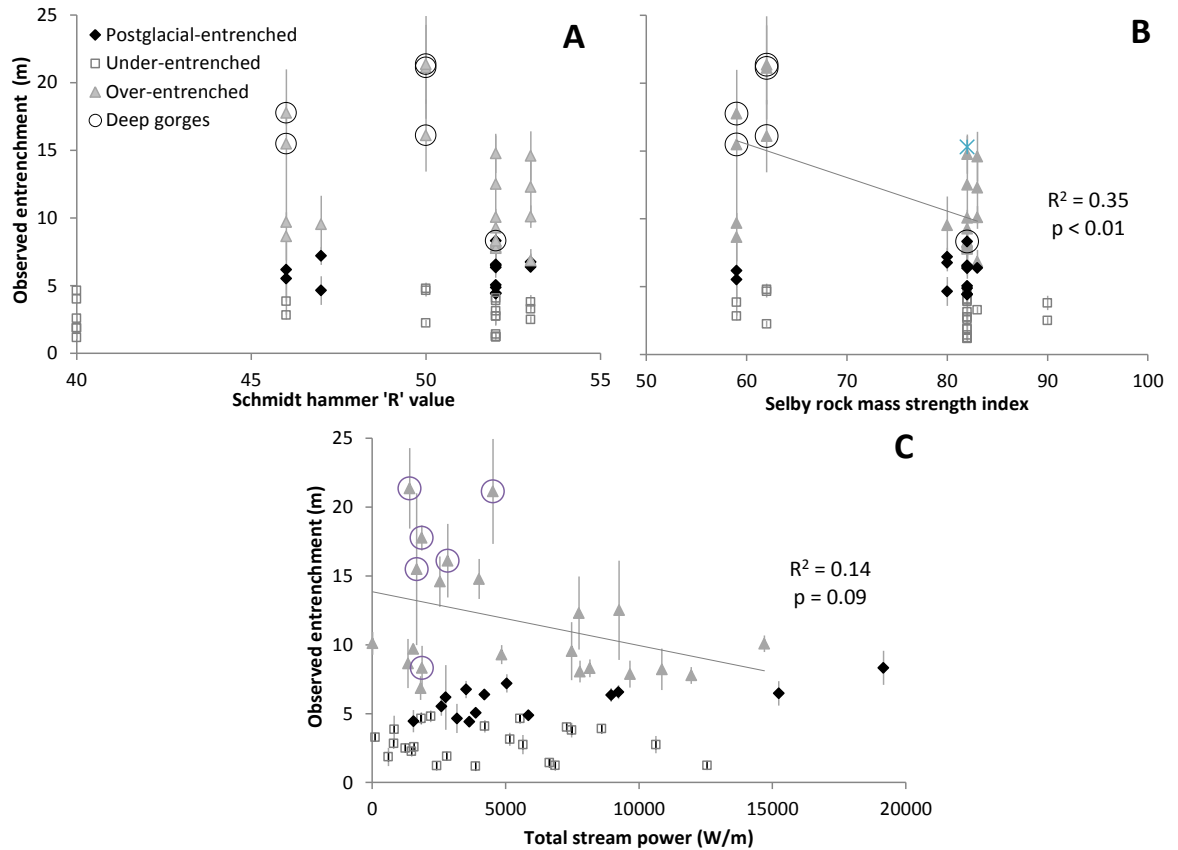
Figure 6-10. Scatter plots of over-entrenched reach depths (observed) versus A) the Schmidt hammer 'R' value and B) the Selby rock mass strength index and C) total stream power (Ω). Postglacial and under-entrenched channel data shown for reference, key in plot C. Linear regressions only shown for over-entrenched channel data (grey lines).

The over-entrenched bedrock reaches located in the middle section of the River Carron are cut in resistant psammite rocks that are not strongly jointed (Figure 6-7 A2). These reaches are located just a few kilometres downstream of the maximum position of Younger Dryas (YD) ice front (Figure 6-11). In this area, the valley floor is mantled by thick, very coarse-grained, glacio-fluvial deposits that are almost certainly proglacial in origin (Finlayson et al., 2011) (Figure 6-11). Incision into the glacio-fluvial sediment and underlying bedrock is likely to have occurred under proglacial conditions during the YD, either during floods triggered by sub-glacial lake drainage (from Glen Alladale, cf. Finlayson and Bradwell, 2007) or due to temporal variations in sediment flux and discharge during the YD glaciation and deglaciation. Thus rapid erosion by proglacial streams, characterised by high discharges and sediment flux (e.g. Gurnell, 2000), is probably responsible for the over-entrenchment of the bedrock reaches in middle Carron. Assuming that Holocene erosion occurred at the predicted postglacial erosion rate, average rates of incision during the YD of 1.9 – 5.7 m/kyr would be needed to produce the observed entrenchment depths. These values are consistent with measured rates of erosion of resistant substrates in

proglacial streams in the European Alps (1 – 20 m/kyr: Vivian, 1970; de Graaff, 1996). Over-entrenched bedrock channels are also located in the middle of the River Elchaig (Figure 6-7 B), just downstream from the position of the YD ice margin as suggested by Bennett and Boulton (1993). However, the debate over the extent of YD ice in this catchment (section 2.3.1.1) means that the interpretation of this gorge as a proglacial feature is tentative.

The deeply entrenched reaches of the middle Canaird and upper Elchaig, and the proglacially incised reaches of the middle Carron account for 50% of the over-entrenched reaches in the study streams. The remaining over-entrenched reaches are located at riegels throughout the rivers Carron and Elchaig (Figure 6-7) and are entrenched into relatively resistant psammite and orthogneiss. The reasons for over-entrenchment of these reaches are discussed further in section 6.4.1.
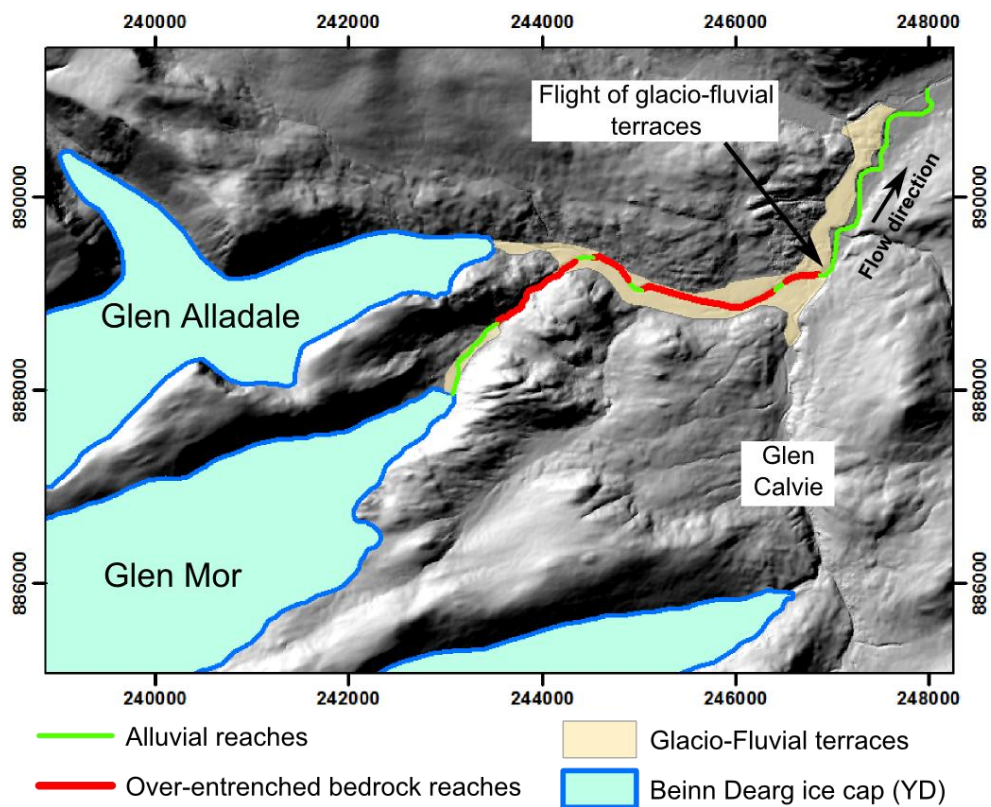
Figure 6-11.   **Map showing location of over-entrenched reaches with respect to the maximum extent of the Younger Dryas glaciers in the middle section of the River Carron (c. 20 – 25 km from the drainage divide). YD outlet glaciers from the Beinn Dearg ice cap after Finlayson et al. (2011). Topography indicated by hillshade derivation of the 5m horizontal resolution NextMap dtm (InterMap, processed using ARC GIS). Grid scale is British National Grid in metres.**

6.3.2.4   Summary of entrenchment results

- Reach-averaged entrenchment depths for bedrock channels range between 1.5 and 21m.
- Postglacial fluvial incision can be responsible for the observed channel entrenchment in 63% of bedrock reaches.
- Postglacial vertical incision rates range from 0.33 to 0.63 m/ka.
- Inheritance of pre-existing inner gorges, or gorges cut by proglacial meltwater streams affects 37% of bedrock reaches.
- There is an apparent lithological control on the dominant erosion process (i.e. plucking versus abrasion).

6.4   Discussion

6.4.1   Origin and significance of pre-existing inner gorges

In previous studies of postglacial settings, inner gorges cut into the floors of glaciated troughs have been interpreted as pre-existing features cut during periods of pre-glacial fluvial erosion (e.g. Montgomery and Korup, 2011), or by sub-glacial meltwater streams (e.g. Holtedahl, 1967; McEwen et al., 2002). Substantial inheritance of pre-existing gorges by postglacial streams would be a strong control on channel morphology and therefore postglacial fluvial erosion processes. It would also imply that postglacial fluvial incision has, at best, a minimal impact on deglaciated landscapes (e.g. Montgomery and Korup, 2011), rather than having a key role in readjusting landscape form after deglaciation (e.g. Tomkin, 2009).

6.4.1.1   The origin of pre-existing gorges in the NW Highlands

Over-entrenched reaches in the NW Highland study streams are located in steep headwall areas of the middle Canaird and upper Elchaig, downstream of major convex breaks in the valley floor below breached drainage divides (Figure 6-7 B and C). Shorter over-entrenched sections are also found at smaller riegels throughout the rivers Elchaig and Carron (Figure 6-7). The distribution of these channels suggests that the over-entrenched inner gorges may have been formed by erosion by sub-glacial meltwater streams. Large convexities in the valley floor cause crevassing in glaciers which transfers supra- and en-glacial meltwater to the glacier bed (Hooke, 1991). It is thought that the resultant high sub-glacial meltwater discharge combined with relatively narrow valley floors channelizes the

meltwater, driving incision into the bedrock valley floor (Holtedahl, 1967; Benn and Evans, 1998).

Deep sub-glacial gorges are seen in comparable locations in other Scottish catchments (Werrity and McEwen, 1997; Benn and Evans, 1998) and in Norway (Holtedahl, 1967), and have also been found beneath active glaciers (Tricart, 1970). This mechanism for the formation of these gorges is consistent with the location of over-entrenched reaches at and below large valley-floor convexities, and the apparent relationship between the degree of over-entrenchment at catchment scales and the extent of divide breaching (section 6.3.2). A sub-glacial meltwater origin for these gorges also explains the presence of a small, dry, incised slot-gorge approximately 20 m long and up to 5 m deep that is a 'tributary' of the lower gorge on the River Canaird. This dry slot has no upstream catchment and has remnants of large potholes in the gorge walls. Similar features were described for sub-glacial gorges in Norway by Holtdahl (1967) and were also found associated with another sub-glacial gorge in the NW Highlands, the Corrieshalloch gorge near Loch Broom (McEwen, 1997), during reconnaissance work for this study. Sub-glacial erosion during the last glaciation is thus the most likely origin for the over-entrenchment of bedrock channels in the steep headwall zones of the upper Elchaig and middle Canaird and at riegels throughout the Carron and lower Elchaig catchments. Yet, some entrenchment of these reaches during preceding glacial and interglacial phases of sub-glacial and fluvial erosion cannot be ruled out.

6.4.1.2   Inheritance and postglacial channel entrenchment

It was shown in chapter 4 that bedrock channel widths are strongly scaled with discharge and that postglacial-entrenched and over-entrenched channels have similar cross-sectional geometries. These findings indicate that postglacial fluvial incision has 'remodelled' the inherited gorges since deglaciation. If postglacial incision occurred at the predicted postglacial incision rate, 32 – 79% of the depth of the over-entrenched gorges will have been added by fluvial incision since deglaciation. This amount of postglacial excavation is similar to that seen by McEwen et al. (2002) in four gorges cut in metamorphic bedrock on the Storutla River in Norway. They found that postglacial fluvial incision accounts for 24 to 97% of the total gorge depth using a volumetric assessment of gorge-fan pairs, with the remaining entrenchment attributed to sub-glacial erosion by meltwater streams.

Channels with no inherited entrenchment account for 63% of the bedrock reaches in the study catchments. In these reaches, postglacial fluvial incision has resulted in $2 - 8$ m of entrenchment. Assuming that similar amounts of postglacial fluvial erosion occurred during the last interglacial, glacial erosion during the Late Devensian and Younger Dryas glaciations must have been sufficient to 'reset' the valley floor topography in many areas of the catchments. The cosmogenic nuclide surface exposure ages from the Type 3 strath terraces sampled in this study (chapter 5) suggest that this may be the case. The Type 3 straths are sections of the bedrock valley floor that have been cleared of sediment cover by rivers. Postglacial ages for all samples indicate that >3m of surface lowering occurred along the valley axis to reset the bedrock surface ^{10}Be concentration during the last glaciation. Fabel et al. (2004) quantified a similar degree of glacial erosion in metasedimentary rocks in the Sierra Nevada (USA), finding that Late Devensian glaciers eroded $2 - 10$ m of bedrock near the valley axis. Furthermore, Dühnforth et al. (2010) noted that cosmogenic nuclide concentrations from a glacial trough floor at Yosemite indicate that over 3 m of glacial erosion has occurred in flatter areas of the trough floors, whereas in granitic rocks associated with riegels, glacial erosion during the last glaciation was less than 3 m in depth. The findings of these studies suggest that $2 - 8$ m of glacial erosion in the axes of glacial troughs in the NW Highlands during the last glaciation is probable, with the preservation of sub-glacial gorges in headwalls and at some riegels likely due to spatial variations in glacial erosion rates.

The finding that most channel entrenchment in post-orogenic landscapes, such as the Scottish Highlands and Norway, is due to postglacial fluvial incision contrasts with recent findings from the actively orogenic region of the Swiss Alps (Montgomery and Korup, 2011). There, large inner gorges are preferentially formed in weak sedimentary rocks and have been interpreted to be pre-glacial features preserved during glaciation, most probably due to 'sealing' of the gorge with sediment fill as glaciers advance (Montgomery and Korup, 2011). That postglacial fluvial incision should be a more significant feature of the landscape response to deglaciation in postglacial terrains characterised by resistant bedrock and low rates of tectonic uplift seems counter-intuitive. A likely reason for this contrast in geomorphic response is a difference in the rate of sediment production during glaciations. Hallet et al., (1996) found that in post-orogenic terrains, with resistant bedrock and relatively low topographic relief, glaciers produce relatively small amounts of sediment and most erosion occurs beneath larger, bedrock-floored valley glaciers. By comparison, in the softer rocks and steeper terrain of the Swiss Alps, glaciers produce more sediment, with more sourced from erosion in cirque glaciers in the upper catchment. This abundant

sediment in Alpine catchments forms thick valley fills in glacial troughs which, according to Montgomery and Korup (2011), 'seal' the pre-glacial bedrock gorges and protect the valley floor from glacial erosion. The abundance of sediment in the major valleys of the Swiss Alps means that postglacial rivers re-excavate the pre-existing gorges, with little bedrock erosion. However, in the NW Highlands postglacial bedrock rivers form at, or soon after, deglaciation leading to longer periods of postglacial bedrock incision.

6.4.2   Controls on postglacial fluvial incision

Predicted postglacial erosion rates, calculated using the empirical function (Eq 5.3) derived from the erosion rates quantified from strath terraces, range from 0.3 to 0.75 m/kyr. These incision rates equate to predicted entrenchment of 2 – 8 m in bedrock channels since deglaciation. Channels with limited entrenchment due to delayed onset of postglacial incision, and those with deep entrenchment arising from inheritance of pre-existing gorges were successfully discriminated by comparison of predicted entrenchment with observed entrenchment in the study channels. This finding suggests that equation 5.3, from which postglacial erosion rates are estimated as a linear function of stream power and rock hardness (Schmidt hammer 'R' value), provides a reasonable approximation of postglacial incision rates in the study streams. The advantage of using this function to predict erosion rates is that it can be applied easily throughout the study catchments using topographic data and a simple geological assessment. However, other factors may influence fluvial incision rates in the study streams, including the density of jointing and sediment flux. Assessment of channels classified as over- and under-entrenched provides further insights into the control of these factors on fluvial incision processes in the NW Highlands.

6.4.2.1   Lithological control of fluvial incision rates

The distribution of over-entrenched reaches highlights that deeply entrenched channels in the middle Canaird and upper Elchaig are cut in strongly jointed flaggy psammites and fault-affected rocks. Although erosion by sub-glacial meltwater streams is the main cause of the deep entrenchment of these channels (discussed above), it is possible that some of the 'over-entrenchment' may be due to an underestimation of the postglacial erosion rate in the strongly jointed rocks where plucking is the dominant incision mechanism (section 6.3.2.3). If dense joints generally increase incision rates in the study streams, then an absence of joints, especially in resistant rocks, would be expected to result in postglacial erosion rates that are substantially lower than predicted. Observations from a detailed assessment of under-entrenched reaches suggest that this may be the case.

Two under-entrenched bedrock reaches in the resistant protomylonitic gneiss in the lower River Canaird, located where the stream crosses valley-spanning reigels (c. 8.5 and 9.7 km from the drainage divide in Figure 6-7 B), are not flanked by alluvial or valley-floor sediment deposits. They are thus not thought to have experienced a delay in the onset of incision. The protomylonitic gneiss has a rock-strength (R value) similar to psammite, but has a broadly isotropic structure with very few continuous joints (and thus a Selby RMS index of 90, the highest value in the study streams) (Figure 2-4; Table 2-5). A slow rate of fluvial incision in this resistant rock explains the apparent under-entrenchment of these channels with respect to the predicted postglacial entrenchment. Assuming incision started soon after deglaciation, the entrenchment of these reaches in protomylonitic gneiss equates to postglacial incision rates of 0.18 and 0.28 ± 0.07 m/kyr (Figure 6-12 A).

Angular bedforms indicate that plucking is the dominant incision mechanism in reaches in faulted rocks, flaggy psammite and psammite. Plucking also appears to be dominant in protomylomitic gneiss but some potholes and flutes indicate that abrasion is also occurring (cf. Figure 7-5). Average postglacial incision rates calculated from all plucking-dominated reaches interpreted to have been entrenched by postglacial fluvial incision show that the rate of incision for the different rock types increases with stream power at similar rates, but suggest that the intercept may be sensitive to the joint spacing (Figure 6-12 A). This finding is consistent with the results of previous research (Whipple et al., 2000), and highlights that equation 5.3 is successful at predicting postglacial incision rates in moderately jointed psammites but poorly predicts incision rates in more and less jointed rocks.

Bedrock incision into pelite occurs largely by abrasion, most probably from bedload sediment impacts, as indicated by smoothed and fluted bedforms in the study rivers and at the strath sites (Figure 5-6). Three of the under-entrenched reaches that have not undergone alluvial to bedrock transitions are in pelite bedrock. The pelite has a low 'R' value (~40) and consequently incision rates predicted by equation 5.3 are relatively high and appear to overestimate the real incision rate. Postglacial incision rates calculated from the entrenchment of these pelite reaches are 0.16 – 0.49 m/kyr compared to the predicted rates of ~0.7 m/kyr. The postglacial incision rates from the pelite reaches increase more rapidly with stream power than plucking-dominated psammites, with lower incision rates than psammite reaches at low stream powers, but similar rates at moderate stream power values (Figure 6-12 B).
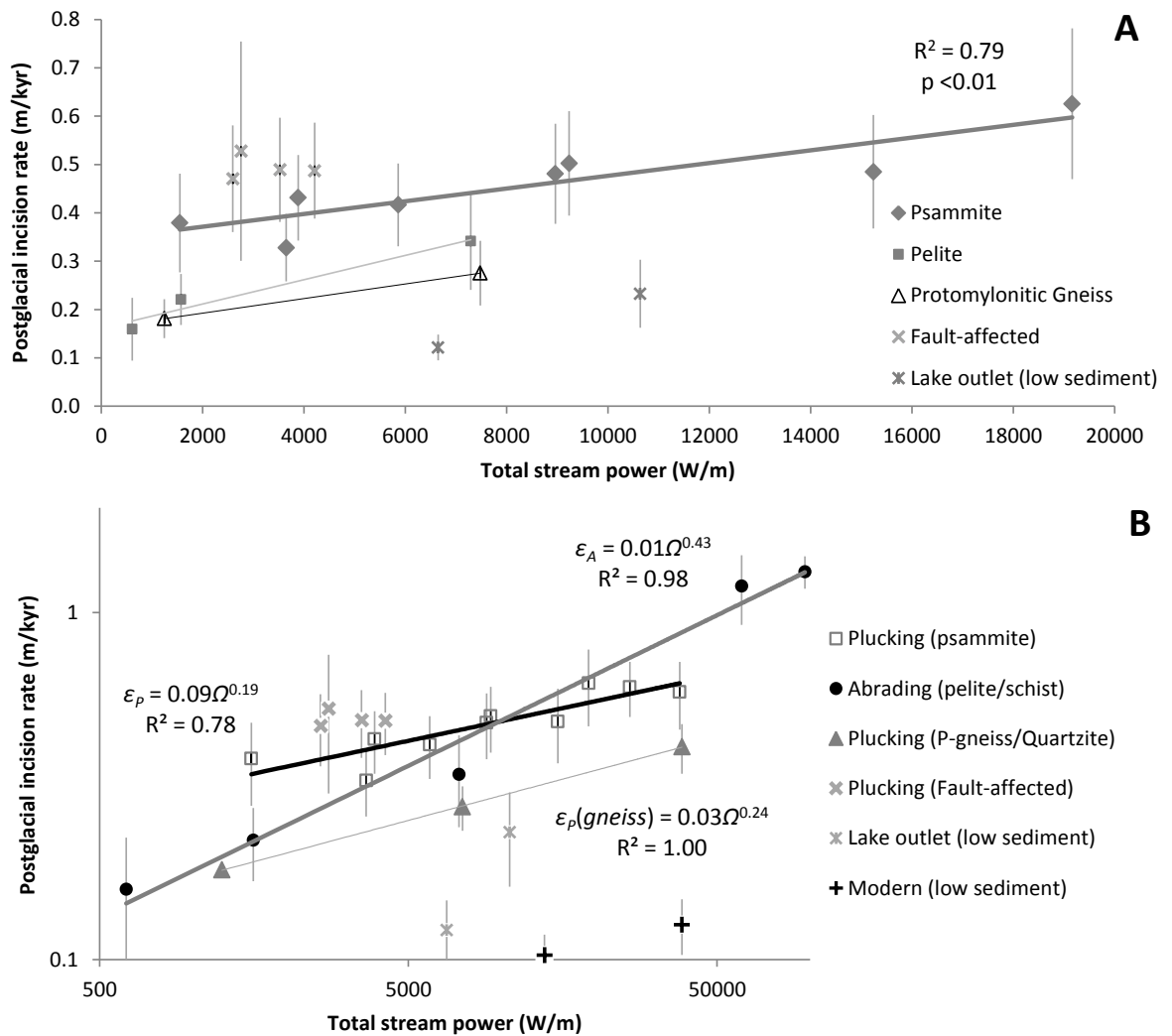
Figure 6-12. **A) Scatter plot of postglacial incision rates versus total stream power. Postglacial incision rates calculated from the observed entrenchment depths for postglacial-entrenched reaches and under-entrenched reaches in protomylonitic gneiss, pelite and downstream from lake outlets (psammite). Linear regressions for psammite (thick grey line) and pelite (thin grey line) are significant at p<0.05. Thin black line shows approximate relationship for protomylonitic gneiss. B) Log-log plot of postglacial incision rate versus total stream power for data from entrenched channels and strath terrace cosmogenic nuclide analysis (chapter 5) grouped according to the main incision mechanism. Power law regressions for plucking-dominated (psammite) reaches (thick black line) and abrasion-dominated reaches (thick grey line) are significant at p≤0.001 and are discussed in the text, power law regression for plucking dominated reaches in more resistant quartzite and protomylonitic gneiss (thin line) is significant at p<0.1. Error bars show uncertainty at 1σ**

Combination of the erosion rates derived from all postglacially entrenched channels and those derived from the strath terrace sites (chapter 5) reinforces the different relationships between erosion rate and stream power for abrasion and plucking (Figure 6-12 B). Power law regression of abrasion rates (ε_A) with total stream power yields:

$$\varepsilon_A = 0.01\Omega^{0.43} \qquad\qquad (R^2=0.98, p<0.001) \quad \text{Eq. 6.2}$$

Whereas rates of plucking (ε_B) in moderately jointed psammites (joint spacing of ~0.2 – 0.5m) scale as:

$$\varepsilon_B = 0.09\Omega^{0.19} \qquad\qquad\qquad (R^2=0.78, \text{p}=0.001) \quad \text{Eq. 6.3}$$

The exponents of these scaling relationships are significantly different (ANCOVA p<0.001). The higher scaling exponent and stronger correlation for abrasion indicates that abrasion rates are more strongly dependent on stream power than plucking rates. For the latter, joint spacing appears to be a stronger control on the incision rate; the scaling relationship for plucking in sparsely jointed protomylonitic gneiss and quartzite (0.6 – 0.9 m) has a similar exponent (0.24) but a lower coefficient of 0.03 compared to the moderately jointed psammites. The narrow spread of data for more densely jointed fault-affected rocks (~0.02 – 0.2 m) means that correlations between the erosion rate and stream power are not significant (p>0.1), but the data are consistent with an exponent of ~0.19 and a higher coefficient of ~0.1 (Figure 6-12 B).

Formulated in terms of drainage area (A) and slope (S) (Eq 1.3), the relationship between stream power and the abrasion rate becomes:

$$\varepsilon_A = 1.43A^{0.55}S^{1.13} \qquad\qquad\qquad (R^2=0.97, \text{p}=0.03) \quad \text{Eq 6.4}$$

And the plucking rate:

$$\varepsilon_B = 0.53A^{0.18}S^{0.24} \qquad\qquad\qquad (R^2=0.78, \text{p}=0.004) \quad \text{Eq 6.5}$$

These values of the slope and area exponents (*n* and *m* respectively in Eq 1.3) follow a similar pattern to the numerical predictions of Whipple et al. (2000) of a slope exponent (*n*) for plucking of ~2/3 and for abrasion (by suspended load) of ~5/3. However, abrasion in the study channels is more likely to result from bedload sediment impacts (Sklar and Dietrich, 1998; Whipple et al., 2000). Process-specific models for bedload abrasion represent erosion rates as a function of shear stress, sediment flux, and the inverse of the rock tensile strength (Sklar and Dietrich, 1998, 2004). The relative roles of sediment, rock strength and shear stress/stream power in controlling both abrasion and plucking in the study rivers are explored further in section 7.2.

Although lithology is clearly a strong control on incision, the Schmidt hammer R value, and the Selby RMS index are relatively poor predictors of both the erosion process and the incision rate in the study channels (Figure 6-13). Low R values result in a dominance of abrasion in pelite reaches, a finding similar to that from the strath sites, but the abrasion rates are relatively low (Figure 6-12 A) and there is no overall scaling between R and the erosion rate (compare Figure 6-13 A with Figure 5-10 E1). The Selby RMS index is a poor

predictor of the erosion process, with both abrasion-dominated pelites and plucking-dominated psammites falling in the centre of the range (Figure 6-12 B). However, erosion rates for plucking-dominated reaches do appear to be negatively correlated with the Selby RMS index, in contrast to the finding from the strath sites where the erosion rates were not correlated with the Selby RMS index. These findings indicate that these two lithological parameters do not adequately account for substrate control on erosion in the study streams. In section 7.2.2 a new lithological index, applicable to fluvial systems, is derived on the basis of the results from this study.
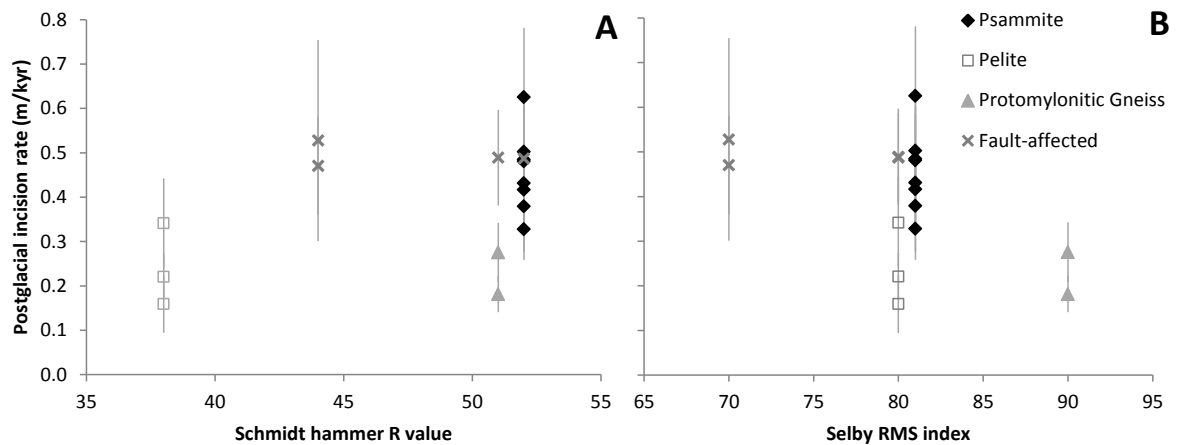
Figure 6-13. **Postglacial erosion rates derived from postglacially entrenched channels, grouped according to lithology and plotted against A) the Schmidt hammer R value and B) the Selby rock mass strength index. Key on plot B.**

6.4.2.2   Sediment flux control on fluvial incision rates

An absence of sediment is known to limit the rates of fluvial incision because sediment impacts on the channel bed drive abrasion and contribute to the loosening and detachment of joint-bound blocks during plucking (Whipple et al., 2000; Sklar and Dietrich, 2001). Thus low sediment flux downstream of lakes in the study channels may be expected to result in slow rates of postglacial fluvial incision and limited entrenchment of bedrock channels close the lake outlets.

This prediction is supported by observations from the River Elchaig where a bedrock reach (E27), formed at a riegel downstream of the outlet of Loch na Leitreach, has very limited entrenchment despite a relatively high stream power. There are no alluvial terraces flanking the bedrock channel and no substantial sediment sources between the lake outlet and E27. The reach has a notable lack of the well-rounded coarse-grained bedload sediment that is commonly found in pockets in hollows or as inner-channel and pool fills

in other bedrock reaches (Figure 6-14). The limited incision of E27 is contrasted with an incised tributary stream (the Allt a Ghlomach), which joins the main stream at the base of E27 (Figure 6-14). These channels have the same bedrock lithology and the Allt a Ghlomach has a slightly smaller upstream drainage area. But the incised tributary stream, with no upstream sediment trap, has abundant bedload sediment in the channel thalweg and a large bar of well-rounded cobble- to boulder-grade sediment deposited at the confluence, implying a relatively high sediment flux. The marked contrast in the degrees of entrenchment of the River Elchaig and Allt a' Ghlomach near their confluence strongly suggests that low sediment flux downstream from the outlet of Loch na Leitreach has restricted long-term fluvial incision rates (Figure 6-14). A similar situation, with under-entrenched channels located downstream of the outlet of an in-filled glacial lake, is seen in the River Carron (~10 km from the drainage divide, Figure 6-7).

Postglacial erosion rates for the two under-entrenched bedrock reaches (in psammite) at lake, or former lake, outlets are 0.12 and 0.23 ± 0.07 m/kyr, compared to predicted rates of 0.42 and 0.45 calculated from the stream power and lithology (Figure 6-12 A). These results indicate that low sediment flux causes a break-down in the psammite erosion rate scaling with stream power, implying therefore that sediment flux is a first order control on the rate of plucking, and most probably also abrasion, in the study streams.

The effect of lakes on erosion rates is spatially restricted to reaches within 1 km of the lake outlet. Erosion rates appear to be 'reset' with the first substantial sediment input to the stream below the lake. The erosion rate scaling relationships with stream power for the different lithologies (Figure 6-12 A) are consistent despite potential local variations in sediment flux associated with 'point' sources such as tributary inputs. These observations suggest that there may be a non-linear, or threshold relationship between sediment flux and incision. Below the threshold, incision is restricted due to a lack of 'tools' for erosive work (Sklar and Dietrich, 2001), and above the threshold incision proceeds at a rate dictated largely by stream power and lithological resistance, with spatial variations in sediment flux causing relatively minor variations in erosion rates.
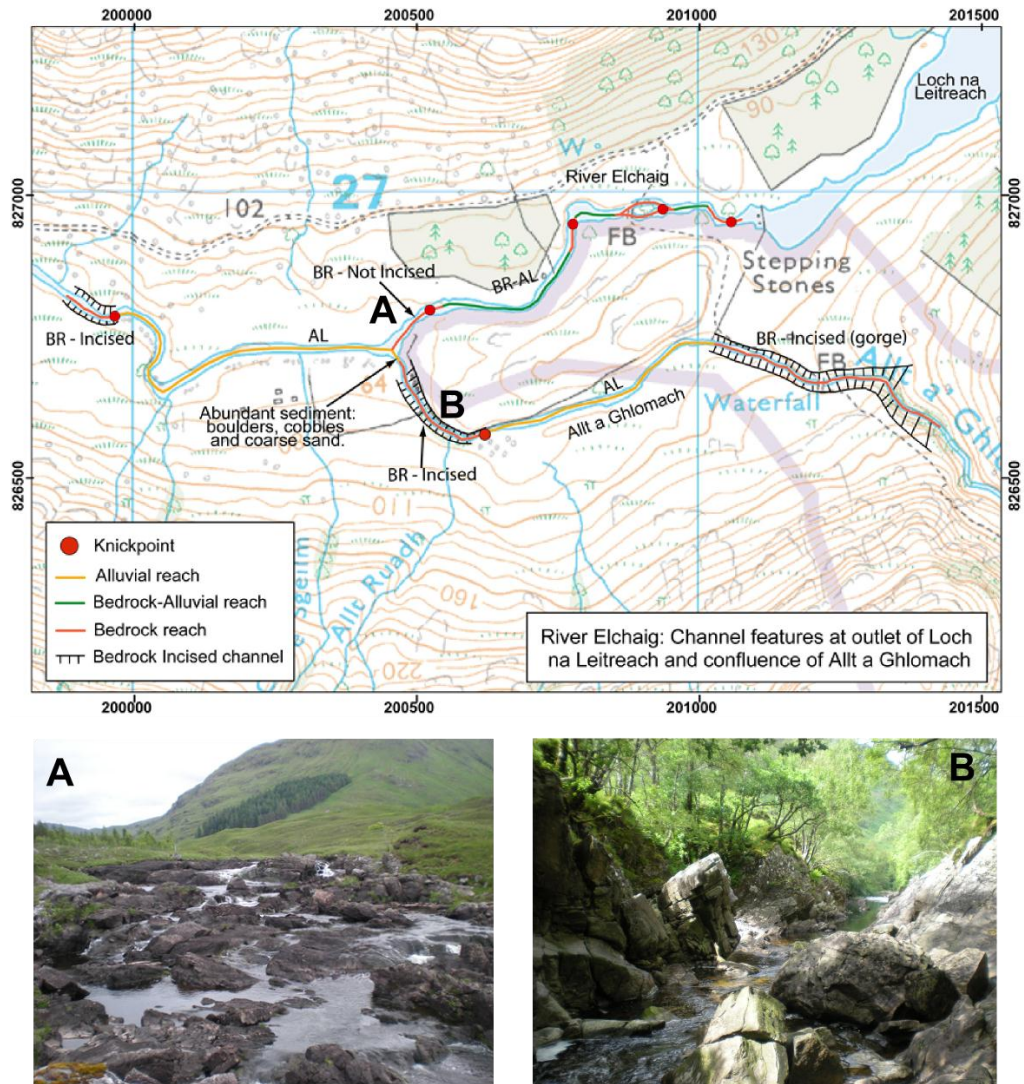
Figure 6-14.   **Map of section of River Elchaig below outlet of Loch na Leitreach (between ~8-10 km from the divide). (Base map is digital Ordnance Survey 1:25,000 scale topographic map). Under-entrenched bedrock reach on trunk stream below lake (marked A), with photograph. Note lack of sediment in thalweg. Contrast with entrenched bedrock reach in tributary stream the Allt a Ghlomach just upstream from the confluence (marked B) – with representative photograph. Note coarse gravel to boulder-grade sediment in thalweg as well as blocks from the gorge walls.**

6.4.2.3   Stream power and the distribution of fluvial incision

Postglacial fluvial incision is occurring at multiple points along the channel profile, with the distribution controlled by the spatial variations in stream power associated with knickpoints at inherited riegels and steep reaches in the headwalls of upland troughs. Over the Holocene this incision has resulted in $2 - 8$ m of channel bed lowering, but this depth of entrenchment is low relative to the relief on major knickpoints, and the channel profiles remain strongly influenced by the inherited, glacially-conditioned landscape form.

Although the mechanisms of incision at sub-reach scales were not assessed in this study (see section 6.2.1), the distribution of postglacial fluvial entrenchment is not consistent

with substantial horizontal retreat of knickpoints. Rather, it suggests that progressive lowering or 'replacement' (Gardner, 1983) may be occurring, similar to the patterns of incision seen at the strath sites in chapter 5. By contrast, knickpoints initiated by glacio-isostatic uplift of rivers in eastern and western Scotland show horizontal retreat (0.5-20 km) that scales with catchment area (Bishop et al., 2005; Jansen et al., 2011). The lack of observable lateral 'migration' of incision signals in the study catchments implies that the location of riegels acts as a long-term control on the distribution of postglacial fluvial incision.

Spatio-temporal changes in the distribution of incision do occur in the study rivers, as the result of alluvial to bedrock channel transitions driven by declining paraglacial sediment flux. The long term decline in sediment flux increases the proportion of the channel system in which the transport capacity exceeds the sediment supply and progressively smaller knickpoints form erosional 'response points' within the catchments.

6.5   Conclusions and implications

An empirical erosion rate function was used to predict postglacial entrenchment in bedrock channels, providing a yardstick against which to assess the observed channel entrenchment. This approach was successful in discriminating inherited sub-glacial gorges, and channels in which postglacial incision has been delayed by excavation of sediment cover. Because of the sensitivity of this method, the results shed new light on the complex dynamics of fluvial incision in a postglacial landscape. The results also highlight the importance of lithological resistance and sediment flux in controlling fluvial incision, providing a basis for further development of empirical erosion rate models for different erosion processes. The finding that postglacial fluvial incision is the main cause of channel entrenchment the NW Highlands contrasts with the results of recent work in other postglacial settings, suggesting that the complex interplay between glacial and fluvial erosion may be conditioned by the wider geological, climatic and tectonic contexts.

Chapter 7

Fluvial incision and postglacial landscape evolution: Further analysis and discussion

7.1   Introduction

The results of this study show that fluvial incision is an important component of the river response to deglaciation in post-orogenic terrains, and is thus likely to be a key agent of postglacial landscape evolution. Fluvial incision in the NW Scottish Highlands has driven entrenchment of streams into the valley floor and the adjustment of channel cross-sections over timescales of ~10 kyr. As in non-glaciated areas, the rate of fluvial incision is controlled by stream power and sediment flux, but in postglacial terrains these factors are strongly influenced by glacially-conditioning. Inherited glacial valley floor slopes determine the distribution and magnitude of incision within catchments and declining paraglacial sediment supply drives spatial and temporal variations in incision rates. This inheritance results in a pulse of rapid fluvial incision following deglaciation, but over longer timescales low sediment flux and feedbacks arising from changes in channel geometry appear to inhibit incision. The findings of this study thus shed light on the complex controls on fluvial incision in detachment-limited channels and are discussed further in section 7.2.

Postglacial channel adjustment has fundamental implications for the wider landscape response to deglaciation. In the NW Highlands, bedrock channel entrenchment alters the form of adjacent hillslopes, and thus is likely to influence channel-hillslope coupling and rates of sediment supply to the channel network. Coupling between channels and hillslopes is required if fluvial incision is to drive long-term postglacial landscape adjustment. This coupling is influenced by the form of hillslopes and nature of sediment deposits, thus the sensitivity of hillslopes to postglacial fluvial adjustment may also depend on glacial inheritance. The influence of bedrock channel evolution on channel-hillslope coupling and the implications for the wider landscape response to deglaciation in post-orogenic terrains are discussed in section 7.3.

7.2   Postglacial fluvial incision: processes and controls

In recent years, our understanding of the controls on fluvial incision has advanced in tandem with the development of numerical frameworks describing erosion. General stream power models for fluvial incision, in which erosion rates are a function of channel slope and discharge, have been successful in predicting erosion rates and describing channel profile morphologies in numerous settings (e.g. Whipple, 2004). However, lithology and sediment flux are also recognised as key controls and it is becoming clear that the different erosion processes of plucking and abrasion have fundamentally different relationships with stream power and sediment flux (Whipple et al., 2000). The recognition that sediment flux is a first-order, and non-linear, control on fluvial incision has been a key step forward (Sklar and Dietrich, 1998, 2001, 2004), but its inclusion into numerical frameworks is currently restricted to abrasion-specific process models; the role that sediment flux plays in plucking remains poorly understood (Whipple et al., 2000). Intact rock strength has also been recognised as a fundamental control on abrasion rates (Sklar and Dietrich, 2001) but despite wide acceptance that joint spacing and rock strength together determine the dominant erosion process (Whipple et al, 2000), consideration of lithological control on fluvial incision process and rate remains rudimentary.

Fluvial erosion rates quantified in this study show that total stream power is the dominant control on fluvial incision rates over Holocene timescales, regardless of incision process. However, the data indicate that the scaling relationships between stream power and incision rate break down where (or when) sediment flux is extremely limited (Figure 7-1). Lithology is also a major control on erosion process and rate in the study rivers and rates of

abrasion and plucking scale differently with stream power. These results are consistent with the findings and predictions of previous research, and the erosion rate data from this study provide the opportunity to test numerical frameworks and develop our understanding of the sediment and lithological controls on incision in detachment-limited channels. The erosion rate data and key variables for each of the datasets are summarised in Table 7-1.
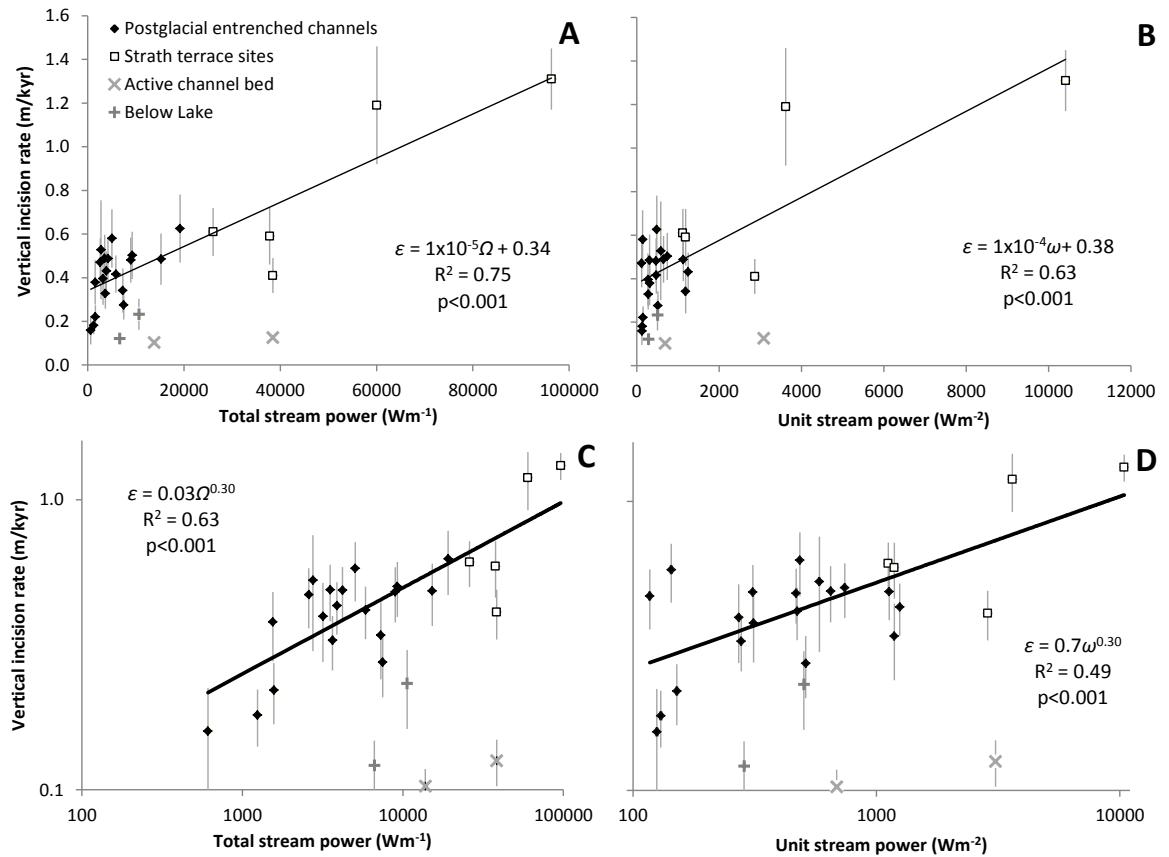
Figure 7-1. Fluvial incision rate versus total stream power (A and C) and unit stream power (B and D), on linear (A and B) and log-log (C and D) axes. All average Holocene incision rates from strath terrace sites (chapter 5) and postglacially entrenched channels (chapter 6) shown. Holocene average incision rates from sites below lakes, and modern erosion rates from [10]Be concentrations in channel bed samples at Dog Falls also shown. Key on plot A. Linear (thin lines) and power law (thick lines) regressions for all Holocene data except 'Below Lake' rates are significant at p<0.001.

Several studies have highlighted the importance of seasonal freezing and the effects of ground ice on erosion processes in 'cold landscape' rivers; for example, crack propagation due to expansion of water on freezing was noted by McEwen and Matthews (1998) and McEwen et al. (2002) to be the main 'block loosening' mechanism in bedrock channels in Norway. Seasonal freezing still occurs in the NW Highlands and is likely to have occurred throughout the Holocene, with relatively intense periods during short-lived cold climate oscillations such as the 8.2 ka event and the Little Ice Age (c.f. Sissons, 1979b; Brooks and Birks, 2000; Ballantyne, 2008). Seasonal freezing and ground ice may have influenced

fluvial erosion in NW Scotland but there is no apparent morphological evidence to confirm this. Furthermore, little is known about the mechanisms by which ice-driven crack propagation contributes to erosion of the channel boundary and there is a need for further research in this area.

Parameter	Strath terrace derived erosion rates (ch 5)	Postglacially entrenched channel erosion rates (ch 6)
Postglacial vertical incision rate (m/kyr) (ε_R and ε_{PG})	0.35 – 1.31	0.10 – 0.63
Postglacial erosion flux (m^3/m/kyr) (E_F and E_F^{PG})	5.8 – 16.6	2.0 – 12.7
Total stream power (Wm^{-1})	2.6 – 9.6 x 10^4	0.15 – 1.9 x 10^4
Drainage area (km^2)	150 – 550	2 – 300
Slope (m/m)	0.022 – 0.068	0.002 – 0.13
Schmidt hammer 'R' value	31 – 56	38 – 52
Selby rock mass strength index	77 – 82	61 – 90

Table 7-1. **Comparison of erosion rates derived from strath terrace sites (ε_R and E_F; chapter 5) and from postglacially entrenched channels in the three surveyed streams (ε_{PG} and E_F^{PG}; chapter 6). Note that the strath terrace derived erosion rates were used to classify postglacial-entrenched channels but ε_{PG} is otherwise independent of ε_R.**

7.2.1   *Sediment flux and postglacial fluvial incision*

In the NW Highlands, the finding that modern incision rates (~0.1 m/kyr) and average Holocene incision rates in reaches downstream from lake outlets (0.1 – 0.2 m/kyr) are substantially lower than average Holocene incision rates (0.4 – 1.3 m/kyr) indicates a strong sediment flux control on fluvial incision (section 5.4.3; section 6.4.2). Jansen et al. (2011) found that modern incision rates and knickpoint (KP) retreat rates in western Scotland are not scaled with discharge or stream power, whereas average Holocene incision rates increase with stream power, and KP retreat rates scale with catchment area (a surrogate for discharge) (cf. also Bishop et al., 2005). The 'Below lake' and 'Modern' incision rates from this study together with the results of Jansen et al. (2011) indicate that a lack of sediment flux causes a breakdown in the scaling of erosion rate with stream power (Figure 7-1).

The low 'Modern' and 'Below lake' incision rates are from reaches in psammite and quartzite where plucking is the main incision process, implying that sediment has a strong control on the rate of plucking. Whipple et al. (2000) suggested that a direct relationship between plucking and sediment flux may only be expected in resistant rocks where crack propagation due to the impact of saltating grains or 'hydraulic-wedging' of sediment into

cracks are main mechanisms of block loosening. The finding that rates of plucking are extremely low in reaches with restricted sediment flux suggest that sediment is required for block loosening in the study channels and where/when sediment is limited, crack propagation is probably restricted by low rates of weathering in the resistant metamorphic rocks. With sediment available to loosen blocks, the rate of plucking depends mainly on stream power and the spacing of joints (Figure 6-12). This finding implies that sediment effectively acts as a 'switch' that turns plucking 'on' or 'off'. Furthermore, once turned 'on', spatial and temporal variations in sediment flux have a limited effect on the rate of plucking. Thus there appears to be a threshold sediment flux below which the rate of erosion is limited by the rate of block loosening, but above which the rate of erosion is limited by capacity of the flow to remove and transport the blocks (Figure 7-2).
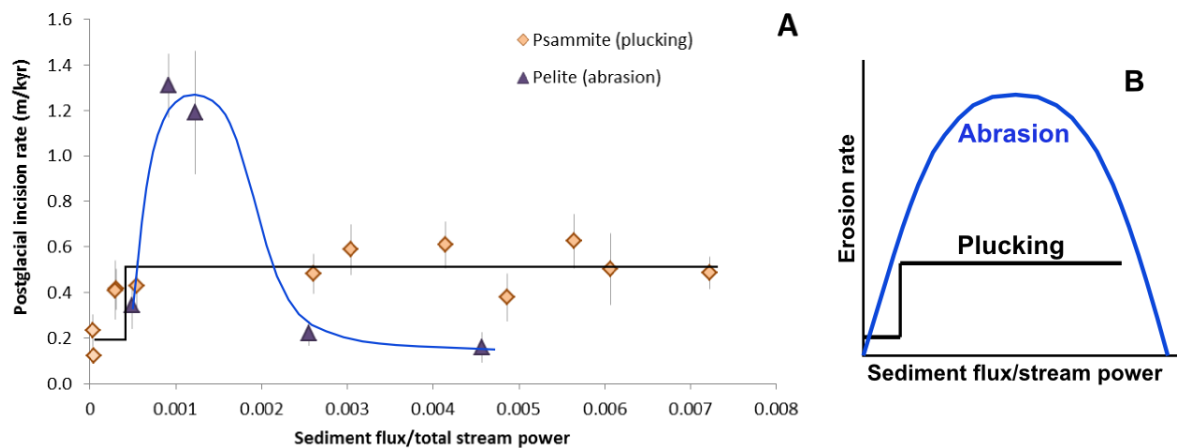
Figure 7-2.   A) Postglacial incision rates for plucking-dominated psammite, abrasion dominated-pelite and lake outlet (low sediment) reaches versus the ratio of a sediment flux index (~q_s) to total stream power (i.e. q_c). The derivation of the sediment flux index is discussed in the text and is not empirically calibrated hence the q_s/q_c values highlight relative differences between reaches but are not otherwise meaningful. B) Sketch graph of saltation-abrasion model of Sklar and Dietrich (blue line) compared with the relationship for plucking dominated reaches suggested by these data.

Channels where abrasion is the dominant erosion mechanism may be expected to show more variation in incision rate with sediment flux. The saltation-abrasion model of Sklar and Dietrich (1998, 2004) predicts that low sediment flux restricts fluvial incision rates due to a lack of 'tools' for erosive work, and high sediment flux also limits fluvial incision due to the 'cover' effect of sediment deposited on the channel bed. Sklar and Dietrich (2001) show that abrasion rates are greatest at intermediate values of the ratio between sediment supply and transport capacity (q_s/q_c) (Figure 7-2 B).

A sediment flux 'index' for each study reach was derived by assuming a power law scaling relationship between sediment flux and drainage area where q_s~$A^{0.85}$, with q_s reset to zero

at lake outlets to account for the effect of sediment trapping. This relation was employed on the assumption that sediment flux increases with discharge but there will be some storage of sediment in floodplains (Leopold and Maddock, 1953; Massong and Montgomery, 2000). Although only five of the study reaches are dominated by abrasion, abrasion rates do appear to reach a maximum at intermediate values of the q_s/q_c ratio (Figure 7-2 A). This finding suggests that although NW Highland channels are interpreted as being generally detachment-limited, incision in abrading reaches may be inhibited by increased bed cover at higher q_s/q_c ratios.

7.2.2   Lithological control of fluvial incision

Both the dominant erosion process and the incision rate in the study channels are strongly controlled by lithological resistance. At the strath terrace sites intact rock strength is a major control on the incision rate and determines the main incision process, with abrasion dominating in rocks with Schmidt hammer 'R' values <40. The same control by intact rock strength on erosion process is seen in bedrock channels in the three study rivers but the average Holocene incision rates in these channels are not directly dependent on intact rock strength (section 6.4.2.1). The Selby rock mass strength (RMS) index, which includes both intact rock strength and joint spacing (section 2.3.2.3), does not discriminate between the dominant erosion processes or relate to incision rates in either dataset. These results are highlighted for all the data in Figure 7-3 A1 and B1.

In order to explore the role of lithological resistance in controlling erosion, vertical incision rates derived from the strath sites (ε_R) and the postglacially entrenched reaches (ε_{PG}) in the three study channels were scaled with total stream power (Ω):

$$\varepsilon_n = \frac{\varepsilon_R \ or \ \varepsilon_{PG}}{1 \times 10^{-5} \Omega + 0.341}$$ Eq 7.1

where the denominator is the relationship of the erosion rate with total stream power derived by linear regression of all erosion rate data (Table 7-1). The linear regression of total stream power was used as this has the strongest correlation with the incision rates (Figure 7-1). The effects of normalisation can be seen by comparing plots A1 and B1 with A2 and B2 in Figure 7-3. For plucking-dominated reaches, normalised erosion rates show no relation with the Schmidt hammer 'R' value but do show a significant negative correlation with the Selby RMS index (p<0.01, Figure 7-3 B2). High Selby RMS values denote rocks with both high intact rock strength and sparse joints, thus the decrease in the rate of plucking with increasing Selby RMS values is probably due to the influence of

increasing joint spacing (cf. section 6.4.2.1). But, as noted for the non-normalised data, the Selby RMS does not account for differences in erosion process and is not correlated with abrasion rates.
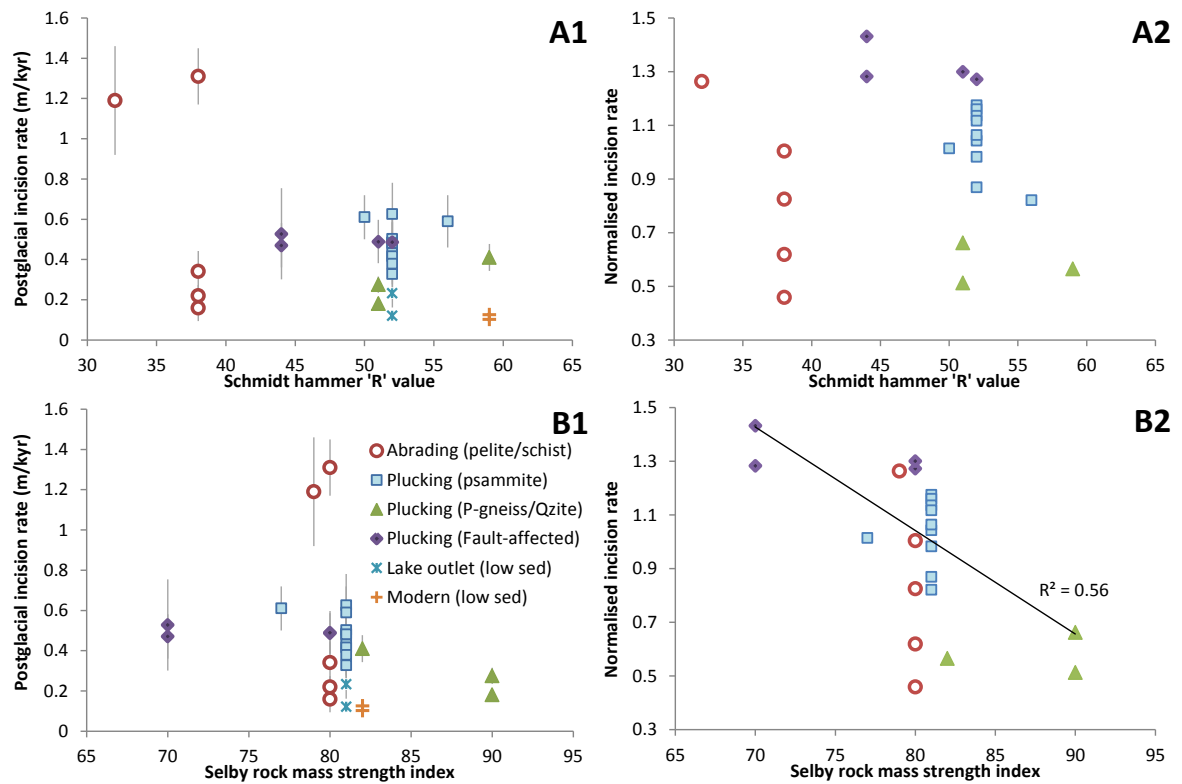
Figure 7-3. **Erosion rates, grouped according to lithology versus A) the Schmidt hammer 'R' value and B) the Selby RMS index. Key in plot B1. A1 and B1 show actual erosion rate data from the strath sites and postglacially entrenched bedrock reaches in the study channels. A2 and B2 show erosion rates normalised for stream power (ε_n) calculated using equation 7.1. Linear regression for all data from plucking-dominated reaches, shown in B2, is significant at p<0.01.**

As discussed in section 2.3.2.3, the Selby RMS index is measure of rock strength developed to assess hillslope stability. It has been used in field studies of fluvial systems because there is currently no other method of deriving a single 'lithological resistance' metric that incorporates both intact rock strength and joint density (Whittaker et al., 2008; Wohl and David, 2008). The Selby RMS is calculated as the sum of semi-quantitative sub-indices accounting for joint density, continuity, orientation, and width as well as the Schmidt hammer 'R' value and the degree of weathering. Importantly, high joint densities result in low values of the joint spacing sub-index (I_j), whilst the intact rock strength sub-index (I_s) increases with Schmidt hammer 'R' values (cf. Table 2-5). In effect this means that these factors cancel out: soft rocks with sparse joints (low I_s, high I_j) and hard rocks with dense joints (high I_s, low I_j) yield similar Selby RMS values. This is significant because these combinations of rock characteristics represent end-member criteria for the

two main incision processes and mean that the Selby RMS index is inherently unable to distinguish lithological differences that lead to abrasion-dominated and plucking-dominated conditions (Figure 7-3 B1 and B2).

Another potential problem of the use of Selby RMS index in studies of fluvial incision is the fact that, collectively, the 'joint indices' make up 70% of the total Selby RMS index, with the intact rock strength accounting for 20% and the degree of weathering 10% (Selby, 1993). This ratio means that lithologies with large variations in rock strength but similar joint densities, such as those at the strath sites in this study, have similar values of the Selby RMS index. By contrast, lithologies in the surveyed channels have limited variation in intact rock strength but a greater variation in the joint index, and therefore a large range of the Selby RMS index (Table 7-1).

7.2.2.1   New lithological resistance index for assessing lithological control on fluvial erosion

Data from this study have been used to derive a revised lithological classification system for fluvial studies. The two key components are the joint index (I_j) and the intact rock strength (I_s). As for the Selby scheme, I_s is quantified on the basis of the Schmidt hammer 'R' value, but I_j is simplified to include only the joint spacing (quantitative) and the joint continuity (qualitative). The sum of these two parameters is the 'resistance index' (I_R), and both I_s and I_j are equally weighted with respect to I_R, reflecting the potential importance of rock hardness in both plucking and abrasion. The most important component of this new classification is the 'resistance ratio' (I_j/I_S), which represents the balance between the intact rock strength and the joint density. Values of the resistance ratio $\ll 1$ indicate soft rocks with sparse joints, where abrasion is expected to dominate; values $\gg 1$ indicate hard rocks with dense joints, where plucking is expected to dominate. Further details of the new lithological resistance index are given in Appendix 7.

Figure 7-4 A shows that the resistance ratio (I_j/I_s) successfully discriminates between abrasion-dominated and plucking-dominated channels. It also highlights contrasting trends in erosion rates with variations in the ratio for abrasion and plucking. All plucking-dominated channels have resistance ratio values <1 and their associated erosion rates decrease as I_j/I_s approaches 1, i.e. as the joint density decreases relative to the intact rock strength. By contrast, channels dominated by abrasion have I_j/I_s values >1 and erosion rates increase as I_j/I_s increases, i.e. as the rock strength decreases relative to the joint density.

Erosion rates reach a minimum at the intersection of these trends, at I_j/I_s values around 1, indicating that rocks with moderate joint density and intermediate values of the intact rock strength have the lowest erosion rates (~50% of average rates) because rates of both plucking and abrasion are relatively low. Field observations are consistent with this finding, and confirm that both abrasion and plucking occur in reaches with resistance ratios close to one (Figure 7-5). At high and low values of the resistance ratio, rates of abrasion and plucking are similar for a given stream power and approximately 25% higher than average incision rates (Figure 7-4 A). The success of the 'resistance ratio' in defining the lithological control on both erosion processes and rates is a key contribution of this research, with the potential for wide application in field and numerical studies of fluvial incision (section 8.1.2).
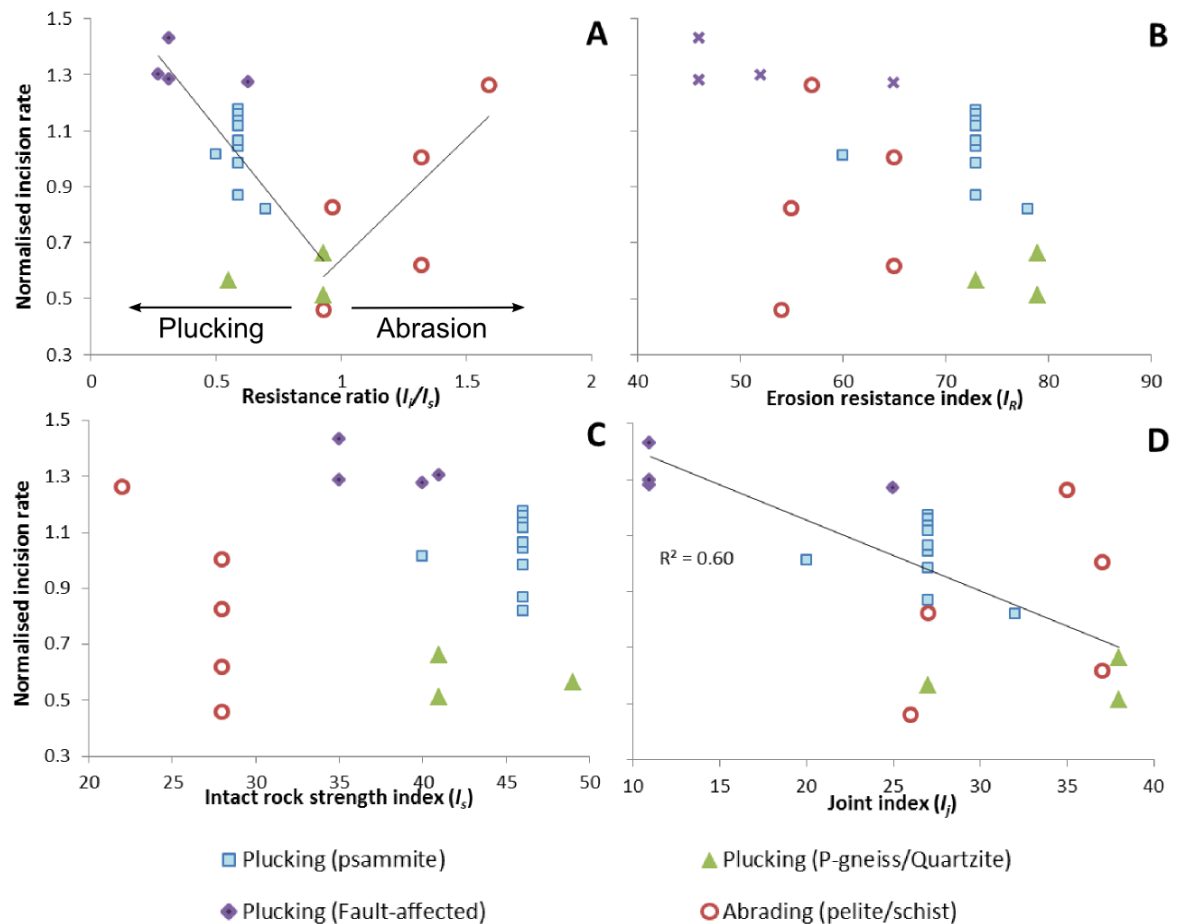
Figure 7-4. Normalised erosion rates (ε_n; Eq 7.1) versus A) the resistance ratio (I_j/I_s), B) the erosion resistance index (I_R) C) the rock strength index (I_s), D) the joint index (I_j). Data grouped according to erosion process and lithology. Linear regressions in plot A highlight contrasting trends in plucking-dominated and abrasion-dominated channels discussed in the text.
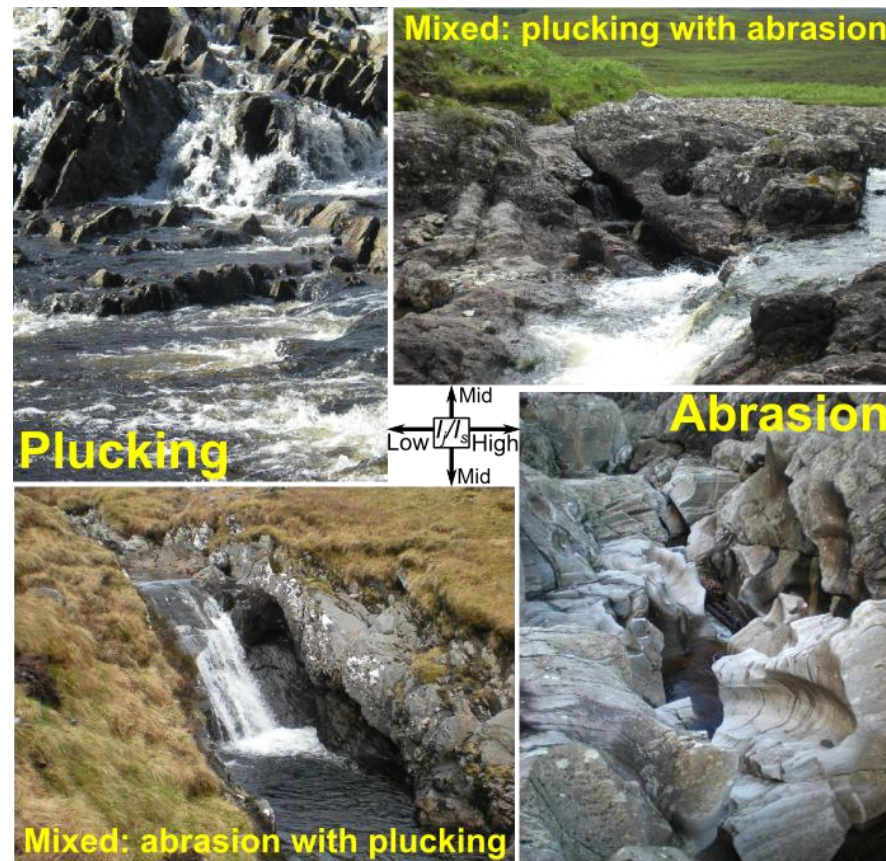
Figure 7-5.   Field photographs showing bedforms associated with the major incision processes and their relation to the resistance ratio (I_i/I_s). 'Abrasion' image: inner gorge in pelite in the Monessie gorge, River Spean. 'Plucking' image: psammite in the River Carron. 'Mixed: plucking with abrasion' image: protomylonitic gneiss in the River Elchaig. 'Mixed: abrasion with plucking' image: pelite in the River Carron.

7.2.3   *Stream power, thresholds and internal feedbacks*

Where sediment is present, erosion rates in the study channels increase with total stream power (Ω) and different scaling relationships exist for abrasion and plucking (Figure 6-12). Abrasion rates scale as $\sim\Omega^{0.43}$ or $\sim A^{0.55}S^{1.13}$, whereas plucking rate scales as $\sim\Omega^{0.19}$ or $\sim A^{0.18}S^{0.24}$. These empirical values are consistent with theoretical predictions (section 6.4.2.1, Whipple et al., 2000).

Elevated stream power arising from high discharges in proglacial areas during the Younger Dryas (YD) is the most likely cause of deep entrenchment of bedrock channels in the middle River Carron (section 6.3.2.3). On the basis of estimated YD incision rates of up to $\sim$5.7 m/kyr in these reaches, total stream power (estimated using the equation $\varepsilon = 1 \times 10^{-5} + 0.34$, Figure 7-1 A) may have been $\sim$36 times greater than average Holocene values (5.4×10^5 compared to $\sim1.5\times10^4$ Wm^{-1}). Precipitation-driven fluctuations in discharge during the Holocene were probably small in comparison to the difference

between proglacial and postglacial discharges (Maizels and Aitkin, 1991) and the effects of short term climate variations cannot be addressed using the average Holocene rates derived in this study. Moreover, modern erosion rates are lower than the Holocene average despite an increase in flood frequency since ~4 ka (cf. Jansen et al., 2011), suggesting that during the later Holocene the lack of sediment flux means that discharge variations have not had a substantial impact on fluvial incision rates.

7.2.3.1   Channel morphology and internal feedbacks

Feedbacks between channel geometry, stream power and fluvial incision rates are likely to have resulted in long-term changes in erosion rates during the postglacial evolution of the study channels (section 1.3.3.2). Fluvial incision has driven the narrowing and deepening of bedrock channels, with adjusted, hydraulically-scaled cross-section geometries established within 8 – 17 kyr of deglaciation. But channel slopes require longer timescales to adjust and the long profiles of NW Highland channels remain strongly glacially-conditioned.

The tendency for channels to narrow and deepen during the early stage of postglacial incision will increase (unit) stream power, whereas the lowering of channel slopes will tend to reduce stream power. Hypothetically, the rate of lowering of channel slopes slows when the stream power required for sediment transport balances the rate of sediment supply and sediment cover forms in the channel, limiting the rate of fluvial incision. This negative feedback leads to the development of 'stable' channel geometries, adjusted to the prevailing climate and tectonic conditions. Thus, in channels undergoing transient responses to changing conditions, a natural 'pulse' of incision is expected as channels adjust (e.g. Schumm et al., 1984).

In section 4.3.5.2, channels with limited entrenchment (i.e. 'under-entrenched' channels) were shown to be wider than channels in which entrenchment is more advanced (i.e. 'postglacial-entrenched channels', cf. section 6.2.2.2). Channel widths at a reference drainage area of 50 km^2, calculated from the width–area scaling relationships for under-entrenched and postglacial-entrenched channels, are 16.4 m and 14.7 m respectively. On the basis of these channel widths, unit stream power in an 'adjusted' postglacial bedrock channel is ~12% higher than in partially adjusted channels, and 62% higher than an alluvial channel at the same drainage area. This increase in unit stream power corresponds to slight increase in fluvial incision rates from ~0.40 m/kyr to 0.43 m/kyr in the 'reference'

reach (based on scaling relationship in figure 7-1 B) implying that channel narrowing during incision in the study rivers may have caused an increase in the erosion rate of ~8%. This value is within the range of uncertainty of the measured erosion rates.

Vertical lowering of the channel bed in the study streams has been limited, and the geometry of entrenched channels, including those at the strath sites, show that there has been no significant change in reach-scale channel slope over the Holocene. This finding indicates that the paraglacial decline in sediment flux, and the consequent reduction in erosion rate, has checked the channel response before slope can be adjusted. Thus, in the study channels, narrowing has effectively driven a long term increase in unit stream power over the Holocene, but the effects of this increase on incision rates have been restricted by declining sediment flux.

7.3   Paraglacial bedrock rivers

Bedrock channels form a substantial component of the river systems of the NW Highlands. Long-term changes in bedrock exposure, geometry, and erosion processes and rates indicate that bedrock channels undergo a 'paraglacial' response to deglaciation, adjusting their initial glacially-conditioned form with respect to postglacial climatic conditions and regional uplift rates. The pattern and rate of changes in postglacial bedrock channels are reviewed below.

Bedrock channels form the lower boundary of adjacent hillslopes, thus changes in channel elevation and geometry may affect hillslope processes throughout catchments and influence the production and routing of sediment through the landscape. Thus, the rate at which the surrounding hillslopes respond to postglacial bedrock channel entrenchment is a fundamental constraint on the wider landscape response to deglaciation. The coupling of bedrock channels and hillslopes, and the downstream routing of sediment through the channel system are discussed in section 7.3.2.

7.3.1   Review of postglacial bedrock channel change

At deglaciation, the distribution of bedrock and alluvial channels in the NW Highlands was determined by the glacial valley-floor slopes and sediment supplied from the reworking of glacial sediment deposits and mass wasting from unstable hillslopes. The high sediment supply resulted in a relatively high critical slope for the bedrock-alluvial channel transition

(where $q_s=q_c$), and even channels with moderate slopes were alluvial at this stage. Bedrock channels in early postglacial times were confined to knickpoints associated with riegels, steep valley headwalls and narrow, pre-existing gorges. Due to the prevalence of resistant, jointed rocks, incision was mainly by plucking, with the incision rate largely controlled by stream power and the spacing of joints. With relatively abundant sediment available to drive incision, vertical incision rates may have been up to ~2 m/kyr for the first few thousand years after deglaciation. Entrenchment of bedrock channels of 2 – 8 m over the Holocene has resulted in the adjustment of the cross-section geometry to the postglacial discharge regime.

Although the postglacial sediment flux regime is poorly constrained, the timing of Type 3 strath formation suggests that a substantial decline in sediment flux from initial levels had occurred within 2 – 4 kyr of deglaciation. The decline in sediment flux drove a shift in q_s/q_c throughout the channel system and the entrenchment of alluvial channels with moderate slopes. This entrenchment led to an increase in the proportion of bedrock exposure from 15% to 25% of the total stream length, and a 'second wave' of bedrock channel incision in the 'new' bedrock reaches. Progressive entrenchment of these channels, accompanied by channel narrowing, has led to the formation of Type 3 strath terraces. But the delay in the onset of incision means that the cross-sectional geometry of many of these channels is not yet fully adjusted to the postglacial discharge and many of the 'switch' channels are slightly wider than expected for a given drainage area. The decline in sediment flux has also driven channel narrowing in some of the 'original' bedrock channels, resulting in the formation of Type 2 strath terraces.

Continuation of the decline in paraglacial sediment flux has resulted in extremely low rates of fluvial incision during the latter parts of the Holocene. The slowing of incision irrespective of stream power suggests a virtual 'cessation' of erosion in bedrock channels. Thus, sediment-starved conditions in post-orogenic, postglacial terrains, such as the NW Highlands, may considerably prolong the timescale of channel adjustment following deglaciation.

The Holocene base level fall resulting from glacio-isostatic uplift of the land surface has been largely accommodated by incision and re-grading of sediment deposits in the lower reaches of the study channels. In channels with bedrock at the outlet, such as those studied by Bishop et al. (2005) and Jansen et al. (2011) in eastern and western Scotland, knickpoints (KPs) initiated during base level fall retreated upstream and downstream of the

KP the channel has re-graded to the new base level. However, the retreat of KPs is locally retarded by resistant bedrock outcrops (Jansen et al., 2010) and, like the incision upstream, has been slowed by the depletion of paraglacial sediment (Jansen et al., 2011).

7.3.2   *Bedrock channels and the postglacial landscape*

The fluvial incision rates quantified in this study are considerably higher than Cenozoic denudation rates for the Scottish Highlands (0.02 – 0.03 m/kyr; Persano et al., 2007). Superficially, this finding suggests a rapid period of postglacial landscape adjustment. However, if the transfer of this incision signal to the wider landscape is slow, overall postglacial denudation rates may be consistent with the Cenozoic average (section 5.5.2.1) (e.g. Reinhardt et al., 2007).

Although not assessed specifically in this study, the coupling of bedrock channels and hillslopes in the NW Highland study streams is here reviewed on the basis of field observations. In particular, the influence of glacial inheritance on the connectivity of the river – hillslope systems and the extent to which fluvial incision *drives* the paraglacial response of hillslopes to deglaciation are considered.

7.3.2.1   <u>Local scale channel-hillslope and reach-reach coupling</u>

In postglacial settings, the coupling between channels and hillslopes is strongly influenced by the inheritance of glacial valleys (cf. Ballantyne, 2002a; Brardinoni and Hassan, 2006). Where rivers inherit wide valley floors, direct coupling between channels and hillslopes is limited, but in the narrower, confined reaches found in steep valley headwalls and at major hanging valleys, channels are strongly coupled to hillslopes (Brardinoni and Hassan, 2006). Glacial control on spatial variations in channel-hillslope coupling is evident in the NW Highland study catchments (Figure 7-6); channels in inherited gorges receive sediment directly from the gorge walls through rockfalls and landslips (Figure 7-6 B), whereas in wider troughs, sediment from hillslopes is deposited at the foot of the valley wall as talus, debris fans and debris cones. Where the glacial troughs are relatively narrow these 'foot-slope' deposits are being partially reworked by the rivers (Figure 7-6 A) but in wider troughs the rivers are effectively decoupled from adjacent hillslopes. The impact of fluvial incision on adjacent hillslopes will thus depend on the form of the valley floor and the extent of entrenchment of the bedrock channel.

Figure 7-6. Field photographs showing relationship between channel and hillslopes. A) View of the River Carron in Glean Beag facing downstream. The alluvial channel meandering in the trough floor is locally reworking debris fans at apex of meanders but overall the channel is poorly coupled to hillslopes. B) River Canaird in an 18m deep inherited inner gorge, blocks in the foreground are part of a small landslip, highlighting strong connection between the channel and the gorge walls.

In confined inner gorges, bedrock channels are directly coupled to the gorge walls but are currently disconnected from the valley walls above the gorge (c.f. Korup and Schlunegger, 2007; Norton et al., 2008). Channel bed lowering and changes in channel width are likely to increase the instability of gorge walls, leading to higher rates of sediment supply to the channel through rock falls and landslips. However, in the resistant rocks of the study area, the steep gorge walls appear to be meta-stable and bedrock incision has resulted in little widening of the inner gorges (Figure 7-6 B; cf. Augustinus, 1995; Korup and Schlunegger, 2007). Therefore no overall increase has occurred in the proportion of the valley side that is directly connected to the channel. Stabilised, inactive gully systems on hillslopes above the inner gorges in the upper Elchaig and Carron (section 3.4.3; Figure 7-7) suggest that channels and the upper valley-wall were formerly connected, and debris fans and gullies supplied sediment directly to the channel. It is possible that deepening of the inner gorge may have encouraged gullying in upper Carron and upper Elchaig, but, over the Holocene, stabilisation of the hillslopes through exhaustion of sediment and vegetation growth has led to decoupling of the upper valley-wall and the inner gorge.

The transmission of sediment between steep, coupled gorge reaches and uncoupled reaches in flatter valley floors may be limited by the grain size of sediment supplied and by the abrupt changes in channel slope. In the gorge reaches, extremely coarse sediment is supplied to the channel through rockfalls and landslips (cf. Figure 7-6 B). As some of the

material is too large to be moved by the flow, boulders are deposited in the gorge and break-down in situ (e.g. Figure 6-14 B). Boulder and cobble grade sediment that *is* mobilised in the gorge is generally deposited just beyond the gorge outlet where the channel widens and slope decreases abruptly (section 3.3.2.1). These observations suggest that only a fraction of the sediment sourced in gorges is actually transported downstream. Thus, despite being coupled with hillslopes, gorges may not contribute much sediment to the downstream channel system (cf. Hooke, 2003). The deposition of coarse sediment in the gorges reduces the rate of fluvial incision, potentially driving a negative feedback that results in stabilisation of the gorge morphology (c.f. Schlunegger, 2002; Hooke, 2003; Korup and Montgomery, 2008).

In wider glacial troughs, alluvial channels rework floodplain sediments and constitute sediment storage and transport 'zones' with the fluvial system (Figure 7-7). Where fluvial incision results in the conversion of alluvial channels to bedrock and entrenchment of an inner gorge cut into the valley floor, channels become disconnected from both valley-walls and the floodplain (cf. Schumm, 1984; Fryirs et al., 2007). This incision-driven decoupling of channels contributes to the paraglacial decline in sediment flux and suggests that a negative feedback with sediment supply may make fluvial incision a self-limiting process in post-orogenic, postglacial terrains.

7.3.2.2   Sub-catchment scale coupling

Large-scale spatial variations in channel-hillslope and reach-reach scaling in the study channels are related to the overall form of the channel profiles, and can be summarised in the context of the glacio-morphological domains identified in section 3.3.1.2 (Figure 7-7).

Glacial breaching of divides (Domain I) has a major impact on the nature of postglacial channel coupling in the catchment headwaters (e.g. Harvey, 2007). Low channel slopes and relatively wide valleys lead to uncoupled segments in upper reaches with limited sediment input from hillslopes. The downstream transfer of sediment in Domain I channels is restricted by low stream power (low discharge and channel slope) and by headwater lakes where drainage divides are overdeepened, as in the rivers Canaird and Elchaig. By contrast, channels with steep coupled headwaters, such as those studied by Brardinoni and Hassan (2006) in British Columbia (i.e. channels that lack Domain I), have greater rates of sediment supply from the headwaters. These differences have major implications for the sensitivity of catchments to climatic change, and the 'recovery' time of the channel system

following flood events. Harvey (2007) showed that channels with headwaters in a glacially breached divide were stabilised more rapidly following a major flood than channels with steep, coupled headwater channels. As the extent of breaching of drainage divides depends on the nature of glacial erosion and is regionally variable (section 2.2.2), corresponding regional variations in the sensitivity of postglacial rivers to climatic change may be expected. Areas affected by areal-scouring beneath ice sheets, with widespread breaching of drainage divides, may be less sensitive to postglacial environmental change than landscapes of Alpine-type glaciation where breaching is less extensive.

Where drainage divides are partially breached or un-breached, the upper part of the catchment is dominated by the 'hyper-concave' upper valley of Domain II (Figure 7-7). The steep headwall is effectively a source area, with the flat valley-floor, or overdeepened lake basin in the lower half of the domain, acting as a long-term sediment sink. The overdeepening of the valley profile in Domain II with respect to a typical fluvial profile dampens both the upstream and downstream coupling of the channel system. The flat or overdeepened valley floor restricts the throughput of sediment, especially in valleys with lakes. Incision of the riegel at the lake outlet is required to 'rejuvenate' the system but this may be inhibited by the lack of sediment below the lake (e.g. River Elchaig, section 6.4.2.2). Where lakes are completely filled with sediment following deglaciation, the lower part of Domain II changes from a sediment sink to a 'transport' zone, reconnecting the upper and lower halves of the catchment. This process has probably occurred at Deanich on the River Carron (Figure 7-7, location in Figure 2-5) and may have resulted in some incision in bedrock reaches downstream; the average Holocene incision rate at the bedrock reach on the riegel below Deanich is ~0.23 ± 0.07 m/kyr, which is significantly faster than the 0.12 ± 0.03 m/kyr incision rate measured at the outlet of Loch na Leitreach on the River Elchaig.

The variable channel slopes in the lower parts of the catchments (Domain III) produce a stepped sequence of floodplains deposited on 'flats' in the trough floor (transport zones) separated by knickpoints (KPs) and/or bedrock gorges forming steep 'steps' (source zones) (Figure 7-7). Entrenchment of alluvium down to bedrock in many of the 'flats' has disconnected many of the former alluvial reaches from the floodplain. As discussed in section 3.4 and section 6.3, the incision into sediments and bedrock in the 'flats' is largely due to the paraglacial decline in sediment supplied from upstream, and lowering of the local base level through incision at the KPs has had limited effect. This result indicates that rates of upstream migration of base level adjustment are substantially slower than rates of

downstream change in sediment supply. Effectively, the upstream-coupling is slower to respond than the downstream-coupling; hillslopes are not rejuvenated and sediment-starved conditions prevail.
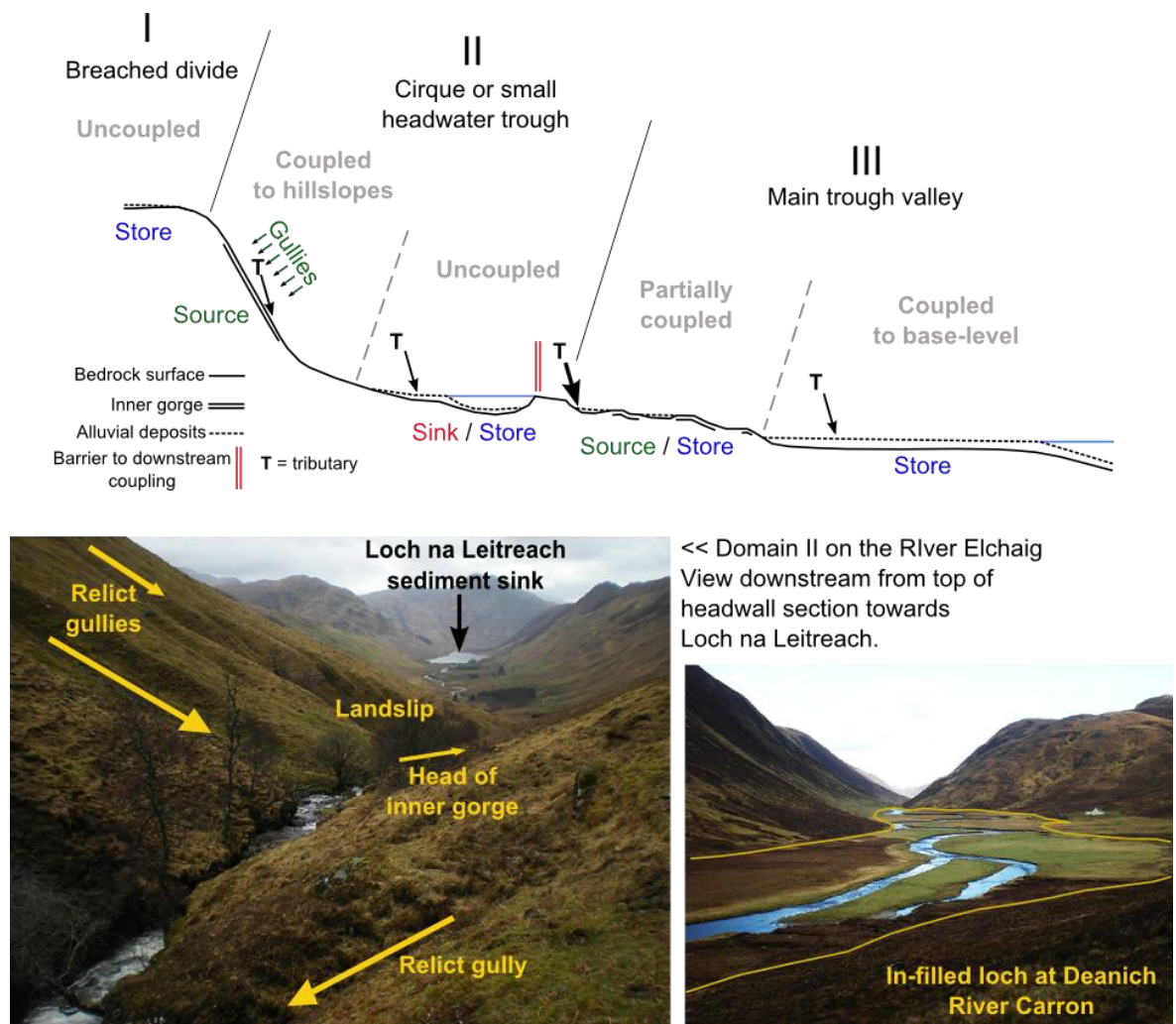
Figure 7-7. **Glacio-morphological domains, channel coupling and locations of main sediment sources and sinks in the River Elchaig (cf. Figure 3-4). Field photographs of Domain II in the upper Elchaig (bottom left) and in-filled lake near Deanich lodge on the River Carron are discussed in the text (location shown in figure 2-5).**

7.3.2.3   Catchment to regional scale landscape adjustment

The discussion above highlights that resistant bedrock, and the wide and overdeepened valleys produced by glacial erosion, combine to limit postglacial fluvial incision and restrict the rate at which the wider landscape responds to channel entrenchment. Despite a pulse of relatively rapid postglacial fluvial erosion, overall denudation rates following deglaciation are likely to have been extremely low, reflecting the declining and subsequently very low rates of sediment supply and the poor coupling between entrenched

channels and valley-walls. In fact, it is conceivable that postglacial denudation rates may be even lower than the Cenozoic average noted at the start of this section.

In their discussion of landscape sensitivity to environmental change, Brunsden and Thornes (1979) note that "if a 'harsh' environment precedes a more gentle one then it is likely that some [landscape] forms will be produced which are morphologically 'too flat' to be altered in the new system. As far as the new state is concerned they are 'over-adjusted' and therefore remain unchanged for very long periods" (p. 478). In the post-orogenic, postglacial landscape of the NW Scottish Highlands, glacial erosion has effectively overdeepened and 'beheaded' the long profiles of postglacial streams and produced resistant rock barriers. The overdeepening of the long profile, lowering of channel relief and widening of valleys through glacial erosion have reduced the sensitivity of the landscape to postglacial climatic and base level change. Without substantial tectonic uplift to steepen the topography the landscape response to deglaciation is restricted by sediment availability (a supply-limited system). Even with more sediment available to sustain erosion, channel incision may only continue until the transport capacity of a particular reach balances the sediment supply (a transport-limited system), and the channel profile may remain largely glacially conditioned indefinitely.

In postglacial terrains with higher rates of tectonic uplift glacial valley profiles are locally overdeepened, but have greater relief than those in low uplift zones (Brocklehurst and Whipple, 2007; figure 3-4 D). Inheritance of irregular glacial valley floor profiles and ongoing tectonic uplift after glaciation may combine to drive fluvial incision that results in a substantial 'reconfiguring' of the landscape (Braun et al., 1999; Tomkin, 2009). But, even in tectonically active areas postglacial fluvial incision may be limited by the presence of thick glacial sediment (Korup and Montgomery, 2008; Montgomery and Korup, 2011), or by the deposition of landslide debris on the valley floor (Schlunegger, 2002; Korup, 2005; Hewitt, 2006).

Chapter 8

Conclusions

8.1   Study objectives, scope and methods

The overall research objective was to *assess the erosional fluvial response to inheritance of a landscape conditioned by glacial erosion*, with the aim of testing hypotheses concerning the role of fluvial incision in postglacial landscape evolution. This objective has been addressed through analysis of the distribution, geometry and entrenchment of bedrock channels in the NW Scottish Highlands together with the quantification of postglacial fluvial incision rates.

The scope of the study is broad and the holistic approach was facilitated by the integration of field and digital topographic data with cosmogenic nuclide surface exposure dating. The large dataset, particularly for the channel distribution and geometry, and the use of novel combinations of data analysis techniques, has made it possible to identify key controls on channel form and incision process in addition to quantifying the nature, extent and rate of postglacial channel change.

8.1.1   Summary of key contributions

The key contributions of this study are:
- An overview of postglacial bedrock channel evolution in a post-orogenic terrain, including quantification of the timescale of channel cross-section adjustment.

- Quantification of Holocene-averaged fluvial incision rates for the NW Scottish Highlands and the derivation of empirical erosion rate equations.

- A re-evaluation of strath terrace forms and formation models, providing a new classification system and assessment of the implications for cosmogenic nuclide analysis.

- Insights into the impact of declining (paraglacial) sediment flux on the channel system and rate of fluvial incision.

- Quantitative assessment of the nature of lithological control on fluvial incision and substrate control on channel geometry.

8.1.2   Advances in methods

8.1.2.1   Strath terrace interpretation and dating procedures

A core component of this research is the measurement of fluvial incision rates using cosmogenic nuclide surface exposure dating of strath terraces (chapter 5). The application of this technique in a post-orogenic terrain, characterised by relatively low fluvial incision rates, prompted a reassessment of the geomorphic considerations that underpin the procedure. The result of this reassessment is a new process-form classification of strath terrace types (section 5.2.3). This classification resolves previous conflicts over the interpretation of strath terrace ages by clarifying three different mechanisms of strath formation. The geomorphic formation models associated with the classification were used in conjunction with numerical simulations to assess quantitatively the 'geomorphic pre-requisites' required for reliable determination of fluvial incision rates, namely: i) no inheritance of cosmogenic nuclides; ii) rapid strath abandonment; and iii) no post-abandonment burial or erosion. There is potential for these simulations to be combined with two and three-dimensional channel geometry models to improve site and sample selection in future studies.

8.1.2.2   Timing of gorge formation

The postglacial incision rates quantified from strath terrace surface exposure ages were used to derive an empirical equation relating incision rates to stream power and intact rock strength. This result enabled postglacial erosion rates to be predicted throughout catchments and provided a basis for the assessment of the extent of inheritance of pre-existing gorges and the identification of channels in which fluvial incision has been delayed by sediment cover. The success of this method in the NW Highlands suggests that similar approaches using empirical, or empirically-calibrated, stream power based erosion

rate equations may be tested in other postglacial settings. In the Scottish Highlands, more incision rate data from other catchments, and/or the use of the process-specific models derived here, may be used in future to widen the assessment of postglacial fluvial incision and to help to develop regional empirical erosion rate models.

8.1.2.3   Lithological resistance metrics for fluvial incision

The findings of this study highlight the control of lithology on incision process and rate. Revision of lithological resistance metrics for fluvial incision has highlighted that a simple 'resistance ratio', effectively the density of joints divided by the rock strength, may be used to predict the dominant incision process in a particular reach. This finding potentially also paves the way for inclusion of process-specific erosion rate equations into two and three dimensional landscape evolution models on the basis of the distribution of geological units and faults. The ratio also highlights a non-linear, process-dependent relationship between the resistance ratio and the rate of fluvial incision. With further development, this ratio has the potential for wide application in fluvial studies.

8.1.2.4   Topographic data requirements

The use of digital topographic data to derive channel elevation, stream length, slope and drainage area at reach-to-catchment scales for channels also assessed in the field meant that the full length of main-stem channel in three catchments (total of 71 km) could be surveyed, forming the core of the large dataset in this study. Potential limitations to the use of DTM-derived data have been discussed (chapters 2 and 3), and improvements in DTM resolution and GIS processing methods will enhance the accuracy of future work.

8.2   Paraglacial bedrock rivers

The findings from this study confirm that bedrock channel erosion is a major part of landscape response to deglaciation, and suggest that these processes should be considered as a central element of paraglacial systems. Importantly, inclusion of bedrock channels and fluvial incision processes provides conceptual and numerical frameworks for assessing the trajectory and rate of landscape change in paraglacial systems (Slaymaker, 2009).

8.2.1   Declining sediment flux and channel evolution

A range of observations highlights the fundamental influence of declining paraglacial sediment flux on the channel system. Although changes in sediment flux rates through the

Holocene have not been directly measured, an increase in the distribution of bedrock channels, local channel narrowing, the formation of Type 3 strath terraces, and a slowing of incision rates over time all tally with predicted effects of a decline in sediment flux (cf. section 1.3.2.2). In the post-orogenic NW Highlands, paraglacial sediment flux appears to drive a pulse of incision for several thousand years after deglaciation but subsequently, fluvial erosion is retarded by an absence of erosive 'tools'. In fact, the pulse of incision appears to contribute to the decline in sediment flux by 'disconnecting' channels from flood plains and other valley-floor sediment sources.

8.2.2   Post-orogenic, paraglacial terrains

The finding that erosion is largely focused at knickpoints inherited from glacial riegels accords with the results of small-scale, quantitative studies in other postglacial terrains (both orogenic and post-orogenic) (McEwen et al., 2002; Valla et al., 2010a, 2010b). Furthermore, the observation that, at catchment scales, fluvial incision has yet to drive substantial readjustment of channel long-profiles or surrounding hillslopes also supports the findings of larger-scale studies where long-term glacial inheritance has been observed (Brardinoni and Hassan, 2006). The strong hydraulic scaling of bedrock channel widths highlights the different timescales of channel response to deglaciation for different aspects of the channel system.

The wide, overdeepened glacial valleys of the NW Highlands mean that channel-hillsope and reach-reach coupling in postglacial streams is poor. When combined with resistant metamorphic bedrock, this inheritance results in generally low sediment availability and, despite an initial pulse of relatively rapid fluvial incision, limits the capacity of the system to respond to changing base level and prolongs the adjustment of glacially eroded valley walls. This is, in effect, a paraglacial 'tools-effect', and 're-fluvialisation' of post-orogenic postglacial landscapes in the absence of further glaciations is likely to require renewed tectonic uplift over 'geological' timescales ($>10^5$ years).

8.2.3   Implications for orogenic postglacial terrains?

The regional tectonic regime may constrain the trajectory of paraglacial landscape change due to the nature of glacial inheritance. High rates of tectonic uplift are associated with steeper glacial valley long profiles, greater hillslope relief (Brocklehurst and Whipple, 2007) and greater volumes of glacial sediment (Hallet et al., 1996). In New Zealand postglacial river incision drives landsliding on valley walls (Hovius et al., 1997),

suggesting that postglacial fluvial incision in orogenic terrains may increase coupling between hillslopes and channels. A greater capacity for fluvial erosion and strong channel-hillslope coupling would eventually lead to 're-fluvialisation' of postglacial orogenic landscapes. The modelling of Tomkin (2009) suggests that such re-fluvialisation may occur over timescales of 10^4-10^5 years without significant change to tectonic uplift rates. However, landscape readjustment in orogenic settings may be prolonged by abundant glacial and paraglacial sediment which protects valley floors from rejuvenation by fluvial incision (Hewitt, 1998; Korup, 2005; Montgomery and Korup, 2011). In orogenic terrains, glacial and paraglacial sediment supply to valley floors may thus result in a paraglacial 'cover effect'.

8.3   Further research opportunities

A detailed assessment of channel-hillslope coupling in the study catchments, possibly through a sediment budget approach, is needed to build on the analysis of bedrock channel evolution presented in this study. Combined with dating of 'relict' sediment deposits and alluvial terraces, catchment sediment budgets may also provide constraints on the paraglacial sediment flux regime. In this regard, a pilot study aimed at establishing the timing of alluvial terrace deposition with respect to strath formation and the onset of bedrock incision at one of the Type 3 strath sites from this study is underway. Samples for optically stimulated luminescence dating have been taken from alluvial terrace sections overlying the bedrock strath terraces at Croick Schoolhouse on the River Carron. It is hypothesised that the alluvial terraces will have postglacial ages, with deposition prior to strath exposure (i.e. ages between ~14 and 10 ka).

The findings from this research have implications for the development and testing of combined glacial-fluvial landscape evolution models (e.g. Braun et al., 1999; Tomkin, 2009). Such models have been applied to the tectonically-active terrain of the Southern Alps in New Zealand, but widening their application to the post-orogenic terrain of the Scottish Highlands would develop our understanding of landscape evolution in this region. This approach may also enable us to test whether geological control of glacial inheritance ultimately constrains the 'trajectory' of postglacial landscape change. Data from this study may serve to test and/or calibrate numerical landscape evolution models. The results of numerical modelling may provide an interesting contribution to the debate surrounding the role of Quaternary denudation in the uplift of North Atlantic passive margins (cf. Nielsen et al., 2002, 2009).

Combinations of field observations and developments in numerical modelling may also be used to predict postglacial landscape evolution in currently glaciated areas that may be deglaciated through contemporary climate change. Constraints on the nature and timescales of different aspects of the landscape response to deglaciation may be constructive for long-term mitigation plans and forward modelling of climate change.

List of References

Addy, S., 2010. Hierarchical controls on channel morphology in montane catchments in the Cairngorms, north-east Scotland, University of Aberdeen, Unpublished PhD Thesis.

Addy, S., Soulsby, C., Hartley, A.J. and Tetzlaff, D., 2011. Characterisation of channel reach morphology and associated controls in deglaciated montane catchments in the Cairngorms, Scotland. Geomorphology, 132(3-4): 176-186.

Ahnert, F., 1994. Equilibrium, scale and inheritance in geomorphology. Geomorphology, 11(2): 125-140.

Anderson, D.E., 1998. A reconstruction of Holocene climatic changes from peat bogs in north-west Scotland. Boreas, 27(3): 208-224.

Anderson, R.S., Molnar, P. and Kessler, M.A., 2006. Features of glacial valley profiles simply explained. J. Geophys. Res., 111(F1): F01004.

Attal, M., Cowie, P.A., Whittaker, A.C., Hobley, D., Tucker, G.E. and Roberts, G.P., 2011. Testing fluvial erosion models using the transient response of bedrock rivers to tectonic forcing in the Apennines, Italy. J. Geophys. Res., 116(F2): F02005.

Attal, M., Tucker, G.E., Whittaker, A.C., Cowie, P.A. and Roberts, G.P., 2008. Modeling fluvial incision and transient landscape evolution: Influence of dynamic channel adjustment. J. Geophys. Res., 113(F3): F03013.

Augustinus, P.C., 1995. Glacial valley cross-profile development: the influence of in situ rock stress and rock mass strength, with examples from the Southern Alps, New Zealand. Geomorphology, 14(2): 87-97.

Bagnold, R.A., 1966. An approach to the sediment transport problem from general physics.

Balco, G., Stone, J.O., Lifton, N.A. and Dunai, T.J., 2008. A complete and easily accessible means of calculating surface exposure ages or erosion rates from 10Be and 26Al measurements. Quaternary Geochronology, 3(3): 174-195.

Ballantyne, C.K., 1986. Landslides and slope failures in Scotland: A review. Scottish Geographical Magazine, 102(3): 134-150.

Ballantyne, C.K., 2002a. A general model of paraglacial landscape response. The Holocene, 12(3): 371-376.

Ballantyne, C.K., 2002b. Paraglacial geomorphology. Quaternary Science Reviews, 21(18-19): 1935-2017.

Ballantyne, C.K., 2008. After the Ice: Holocene Geomorphic Activity in the Scottish Highlands. Scottish Geographical Journal, 124(1): 8-52.

Ballantyne, C.K., 2010. Extent and deglacial chronology of the last British–Irish Ice Sheet: implications of exposure dating using cosmogenic isotopes. Journal of Quaternary Science, 25(4): 515-534.

Barker, D.M., Lawler, D.M., Knight, D.W., Morris, D.G., Davies, H.N. and Stewart, E.J., 2009. Longitudinal distributions of river flood power: the combined automated flood, elevation and stream power (CAFES) methodology. Earth Surface Processes and Landforms, 34(2): 280-290.

Barnes, H.L., 1956. Cavitation as a geological agent. American Journal of Science, 254(8): 493-505.

Basu, A. and Aydin, A., 2004. A method for normalization of Schmidt hammer rebound values. International Journal of Rock Mechanics and Mining Sciences, 41(7): 1211-1214.

Bell, S., 1999. A Beginners Guide to Uncertainty of Measurement. National Physical Laboratory, HMSO.

Benda, L. and Dunne, T., 1997. Stochastic forcing of sediment routing and storage in channel networks. Water Resour. Res., 33(12): 2865-2880.

Benn, D.I. and Evans, D.J.A., 1998. Glaciers and Glaciation. Arnold, London.

Bennett, M.R. and Boulton, G.S., 1993. Deglaciation of the younger dryas or Loch Lomond Stadial ice-field in the northern Highlands, Scotland. Journal of Quaternary Science, 8(2): 133-145.

Bishop, P., Hoey, T.B., Jansen, J.D. and Artza, I.L., 2005. Knickpoint recession rate and catchment area: the case of uplifted rivers in Eastern Scotland. Earth Surface Processes and Landforms, 30(6): 767-778.

Bradwell, T., Fabel, D., Stoker, M., Mathers, H., McHargue, L. and Howe, J., 2008a. Ice caps existed throughout the Lateglacial Interstadial in northern Scotland. Journal of Quaternary Science, 23(5): 401-407.

Bradwell, T., Stoker, M. and Krabbendam, M., 2008b. Megagrooves and streamlined bedrock in NW Scotland: The role of ice streams in landscape evolution. Geomorphology, 97(1–2): 135-156.

Bradwell, T., Stoker, M.S., Golledge, N.R., Wilson, C.K., Merritt, J.W., Long, D., Everest, J.D., Hestvik, O.B., Stevenson, A.G., Hubbard, A.L., Finlayson, A.G. and Mathers, H.E., 2008c. The northern sector of the last British Ice Sheet: Maximum extent and demise. Earth-Science Reviews, 88(3–4): 207-226.

Brardinoni, F. and Hassan, M.A., 2006. Glacial erosion, evolution of river long profiles, and the organization of process domains in mountain drainage basins of coastal British Columbia. J. Geophys. Res., 111(F1): F01013.

Brardinoni, F. and Hassan, M.A., 2007. Glacially induced organization of channel-reach morphology in mountain streams. J. Geophys. Res., 112(F3): F03013.

Braun, J., Zwartz, D. and Tomkin, J.H., 1999. A new surface-processes model combining glacial and fluvial erosion. Annals of Glaciology, 28(1): 282-290.

Bray, D., 1982. Regime equations for gravel-bed rivers. In: R.D. Hey, J.C. Bathurst and C.R. Thorne (Editors), Gravel-Bed Rivers. John Wiley and Sons, Chichester, England, pp. 517-552.

Brazier, V., Whittington, G. and Ballantyne, C.K., 1988. Holocene debris cone evolution in Glen Etive, Western Grampian Highlands, Scotland. Earth Surface Processes and Landforms, 13(6): 525-531.

Brocard, G.Y. and van der Beek, P.A., 2006. Influence of incision rate, rock strength, and bedload supply on bedrock river gradients and valley-flat widths: Field-based evidence and calibrations from western Alpine rivers (southeast France). Geological Society of America Special Papers, 398: 101-126.

Brocard, G.Y., van der Beek, P.A., Bourlès, D.L., Siame, L.L. and Mugnier, J.L., 2003. Long-term fluvial incision rates and postglacial river relaxation time in the French Western Alps from 10Be dating of alluvial terraces with assessment of inheritance, soil development and wind ablation effects. Earth and Planetary Science Letters, 209(1–2): 197-214.

Brocklehurst, S.H. and Whipple, K.X., 2002. Glacial erosion and relief production in the Eastern Sierra Nevada, California. Geomorphology, 42(1–2): 1-24.

Brocklehurst, S.H. and Whipple, K.X., 2004. Hypsometry of Glaciated Landscapes. Earth Surface Processes and Landforms, 29(7): 907-926.

Brocklehurst, S.H. and Whipple, K.X., 2007. Response of glacial landscapes to spatial variations in rock uplift rate. J. Geophys. Res., 112(F2): F02035.

Brooks, S.J. and Birks, H.J.B., 2000. Chironomid-inferred Late-glacial air temperatures at Whitrig Bog, Southeast Scotland. Journal of Quaternary Science, 15(8): 759-764.

Brown, I.M., 1993. Pattern of deglaciation of the last (Late Devensian) Scottish ice sheet: Evidence from ice-marginal deposits in the Dee valley, Northeast Scotland. Journal of Quaternary Science, 8(3): 235-250.

Brunsden, D. and Thornes, J.B., 1979. Landscape Sensitivity and Change. Transactions of the Institute of British Geographers, 4(4): 463-484.

Büdel, J., 1982. Climatic Geomorphology. Princeton University Press, Princeton, N.J., 443 pp.

Bull, W.B., 1979. Threshold of critical power in streams. Geological Society of America Bulletin, 90(5): 453-464.

Burbank, D.W., Leland, J., Fielding, E., Anderson, R.S., Brozovic, N., Reid, M.R. and Duncan, C., 1996. Bedrock incision, rock uplift and threshold hillslopes in the northwestern Himalayas. Nature, 379(6565): 505-510.

Castillo-Rodriguez, M.E., 2011. Base-level fall, knickpoint retreat and transient channel morphology: The case of small bedrock rivers on resistant quartzite (Isle of Jura, western Scotland), Unversity of Glasgow, Unpublished PhD Thesis.

Chatanantavet, P., Lajeunesse, E., Parker, G., Malverti, L. and Meunier, P., 2010. Physically based model of downstream fining in bedrock streams with lateral input. Water Resour. Res., 46(2): W02518.

Church, M. and Ryder, J.M., 1972. Paraglacial Sedimentation: A Consideration of Fluvial Processes Conditioned by Glaciation. Geological Society of America Bulletin, 83(10): 3059-3072.

Clayton, K., 1996. Quantification of the impact of glacial erosion on the British Isles. Transactions of the Institute of British Geographers, 21(1): 124-140.

Collins, B.D. and Dunne, T., 1989. Gravel transport, gravel harvesting, and channel-bed degradation in rivers draining the southern olympic mountains, Washington, U.S.A. Environmental Geology, 13(3): 213-224.

Cotton, C.A., 1941. The Longitudinal Profiles of Glaciated Valleys. The Journal of Geology, 49(2): 113-128.

Crosby, B.T. and Whipple, K.X., 2006. Knickpoint initiation and distribution within fluvial networks: 236 waterfalls in the Waipaoa River, North Island, New Zealand. Geomorphology, 82(1-2): 16-38.

Curry, A.M., 2000. Holocene reworking of drift-mantled hillslopes in the Scottish Highlands. Journal of Quaternary Science, 15(5): 529-541.

Curry, A.M., 1999. Paraglacial modification of slope form. Earth Surface Processes and Landforms, 24(13): 1213-1228.

Dadson, S.J. and Church, M., 2005. Postglacial topographic evolution of glaciated valleys: a stochastic landscape evolution model. Earth Surface Processes and Landforms, 30(11): 1387-1403.

Day, M.J., 1980. Rock Hardness: Field Assessment and Geomorphic Importance. The Professional Geographer, 32(1): 72-81.

de Graaff, L.W.S., 1996. The fluvial factor in the evolution of alpine valleys and of ice marginal topography in Vorarlberg (W-Austria) during the upper Pleistocene and Holocene. Zeitschrift fur Geomorphologie, 104: 129-159.

Dühnforth, M., Anderson, R.S., Ward, D. and Stock, G.M., 2010. Bedrock fracture control of glacial erosion processes and rates. Geology, 38(5): 423-426.

Dunne, J., Elmore, D. and Muzikar, P., 1999. Scaling factors for the rates of production of cosmogenic nuclides for geometric shielding and attenuation at depth on sloped surfaces. Geomorphology, 27(1–2): 3-11.

Edwards, K.J. and Whittington, G., 2001. Lake sediments, erosion and landscape change during the Holocene in Britain and Ireland. CATENA, 42(2–4): 143-173.

Ehlers, J. and Gibbard, P.L., 2007. The extent and chronology of Cenozoic Global Glaciation. Quaternary International, 164–165(0): 6-20.

Evans, I.S., 1997. Process and form in the erosion of glaciated mountains. In: D.R. Stoddart (Editor), Process and form in geomorphology. Routledge, London, pp. 145-174.

Everest, J. and Kubik, P., 2006. The deglaciation of eastern Scotland: cosmogenic 10Be evidence for a Lateglacial stillstand. Journal of Quaternary Science, 21(1): 95-104.

Fabel, D., Harbor, J., Dahms, D., James, A., Elmore, D., Horn, L., Daley, K. and Steele, C., 2004. Spatial Patterns of Glacial Erosion at a Valley Scale Derived From Terrestrial Cosmogenic 10Be and 26Al Concentrations in Rock. Annals of the Association of American Geographers, 94(2): 241-255.

Fabel, D., Small, D., Miguens-Rodriguez, M. and Freeman, S.P.H.T., 2010. Cosmogenic nuclide exposure ages from the 'Parallel Roads' of Glen Roy, Scotland. Journal of Quaternary Science, 25(4): 597-603.

Finlayson, A. and Bradwell, T., 2007. Evidence for Loch Lomond Stadial ice cap glaciation of the Beinn Dearg massif, northern Scotland. Quaternary Newsletter, 113: 10-17.

Finlayson, A., Golledge, N., Bradwell, T.O.M. and Fabel, D., 2011. Evolution of a Lateglacial mountain icecap in northern Scotland. Boreas, 40(3): 536-554.

Finnegan, N.J., Roe, G., Montgomery, D.R. and Hallet, B., 2005. Controls on the channel width of rivers: Implications for modeling fluvial incision of bedrock. Geology, 33(3): 229-232.

Finnegan, N.J., Sklar, L.S. and Fuller, T.K., 2007. Interplay of sediment supply, river incision, and channel morphology revealed by the transient evolution of an experimental bedrock channel. J. Geophys. Res., 112(F3): F03S11.

Firth, C.R., 1989. Late Devensian raised shorelines and ice limits in the inner Moray Firth area, northern Scotland. Boreas, 18(1): 5-21.

Firth, C.R. and Stewart, I.S., 2000. Postglacial tectonics of the Scottish glacio-isostatic uplift centre. Quaternary Science Reviews, 19(14–15): 1469-1493.

Flint, J.J., 1974. Stream gradient as a function of order, magnitude, and discharge. Water Resour. Res., 10(5): 969-973.

Freeman, S., Bishop, P., Bryant, C., Cook, G., Fallick, A., Harkness, D., Metcalfe, S., Scott, M., Scott, R. and Summerfield, M., 2004. A new environmental sciences AMS laboratory in Scotland. Nuclear Instruments and Methods in Physics Research Section B: Beam Interactions with Materials and Atoms, 223-224(0): 31-34.

Fryirs, K.A., Brierley, G.J., Preston, N.J. and Kasai, M., 2007. Buffers, barriers and blankets: The (dis)connectivity of catchment-scale sediment cascades. CATENA, 70(1): 49-67.

Fuller, T.K., Perg, L.A., Willenbring, J.K. and Lepper, K., 2009. Field evidence for climate-driven changes in sediment supply leading to strath terrace formation. Geology, 37(5): 467-470.

Galster, J.C., 2009. Testing the linear relationship between peak annual river discharge and drainage area using long-term USGS river gauging records. Geological Society of America Special Papers, 451: 159-171.

Gardner, T.W., 1983. Experimental study of knickpoint and longitudinal profile evolution in cohesive, homogeneous material. Geological Society of America Bulletin, 94(5): 664-672.

Gibbard, P.L. and Lewin, J., 2009. River incision and terrace formation in the Late Cenozoic of Europe. Tectonophysics, 474(1–2): 41-55.

Gilbert, G.K., 1877. Geology of the Henry Mountains. Government Printing Office, Washington, D.C.

Gilvear, D.J., Heal, K.V. and Stephen, A., 2002. Hydrology and the ecological quality of Scottish river ecosystems. Science of The Total Environment, 294(1–3): 131-159.

Golledge, N.R., 2010. Glaciation of Scotland during the Younger Dryas stadial: a review. Journal of Quaternary Science, 25(4): 550-566.

Golledge, N.R., Hubbard, A. and Sugden, D.E., 2008. High-resolution numerical simulation of Younger Dryas glaciation in Scotland. Quaternary Science Reviews, 27(9–10): 888-904.

Gordon, J.E., 1981. Ice-Scoured Topography and Its Relationships to Bedrock Structure and Ice Movement in Parts of Northern Scotland and West Greenland. Geografiska Annaler. Series A, Physical Geography, 63(1/2): 55-65.

Gosse, J.C., Klein, J., Lawn, B., Middleton, R. and Evenson, E.B., 1995. Beryllium-10 Dating of the Duration and Retreat of the Last Pinedale Glacial Sequence. Science, 268(5215): 1329-1333.

Gosse, J.C. and Phillips, F.M., 2001. Terrestrial in situ cosmogenic nuclides: theory and application. Quaternary Science Reviews, 20(14): 1475-1560.

Gurnell, A.M., Edwards, P.J., Petts, G.E. and Ward, J.V., 2000. A conceptual model for alpine proglacial river channel evolution under changing climatic conditions. CATENA, 38(3): 223-242.

Haggart, B.A., 1986. Relative sea-level change in the Beauly Firth, Scotland. Boreas, 15(2): 191-207.

Hall, A., 1991. Pre-Quaternary landscape evolution in the Scottish Highlands. Transactions of the Royal Society of Edinburgh, 82: 1-26.

Hall, A. and Bishop, P., 2002. Scotland's denudational history: an integrated view of erosion and sedimentation at an uplifted passive margin. Geological Society, London, Special Publications, 196(1): 271-290.

Hallet, B., Hunter, L. and Bogen, J., 1996. Rates of erosion and sediment evacuation by glaciers: A review of field data and their implications. Global and Planetary Change, 12(1–4): 213-235.

Hancock, G.R., Anderson, R.S. and Whipple, K.X., 1998. Beyond Power: Bedrock River Incision Process and Form. In: K. Tinkler and E. Wohl (Editors), Rivers over Rock: Fluvial processes in bedrock channels. American Geophysical Union, Washington DC, pp. 35-60.

Hancock, G.S. and Anderson, R.S., 2002. Numerical modeling of fluvial strath-terrace formation in response to oscillating climate. Geological Society of America Bulletin, 114(9): 1131-1142.

Hansom, J.D., 1991. Holocene coastal development in the Dornoch Firth. In: C.R. Firth and B.A. Haggart (Editors), LAte Quaternary coastal evolution in the Inner Moray Firth: Field Guide West. London Inst., London, pp. 45-54.

Harbor, J. and Warburton, J., 1993. Relative rates of glacial and nonglacial erosion in alpine environments. Arctic and Alpine Research, 25(1): 1-7.

Harbor, J.M., Hallet, B. and Raymond, C.F., 1988. A numerical model of landform development by glacial erosion. Nature, 333(6171): 347-349.

Hartshorn, K., Hovius, N., Dade, W.B. and Slingerland, R.L., 2002. Climate-Driven Bedrock Incision in an Active Mountain Belt. Science, 297(5589): 2036-2038.

Harvey, A.M., 2007. Differential recovery from the effects of a 100-year storm: Significance of long-term hillslope–channel coupling; Howgill Fells, northwest England. Geomorphology, 84(3–4): 192-208.

Haynes, V.M., 1977. The Modification of Valley Patterns by Ice-Sheet Activity. Geografiska Annaler. Series A, Physical Geography, 59(3/4): 195-207.

Hewitt, K., 1998. Catastrophic landslides and their effects on the Upper Indus streams, Karakoram Himalaya, northern Pakistan. Geomorphology, 26(1): 47-80.

Hewitt, K., 2006. Disturbance regime landscapes: mountain drainage systems interrupted by large rockslides. Progress in Physical Geography, 30(3): 365-393.

Hewitt, K., Clague, J.J. and Orwin, J.F., 2008. Legacies of catastrophic rock slope failures in mountain landscapes. Earth-Science Reviews, 87(1–2): 1-38.

Hey, R.D. and Thorne, C.R., 1986. Stable Channels with Mobile Gravel Beds. Journal of Hydraulic Engineering, 112(8): 671-689.

Hirano, M. and Aniya, M., 1988. A rational explanation of cross-profile morphology for glacial valleys and of glacial valley development. Earth Surface Processes and Landforms, 13(8): 707-716.

Hobley, D.E.J., Sinclair, H.D. and Cowie, P.A., 2010. Processes, rates, and time scales of fluvial response in an ancient postglacial landscape of the northwest Indian Himalaya. Geological Society of America Bulletin, 122(9-10): 1569-1584.

Hoey, T.B. and Bluck, B.J., 1999. Identifying the controls over downstream fining of river gravels. Journal of Sedimentary Research, 69(1): 40-50.

Holtedahl, H., 1967. Notes on the Formation of Fjords and Fjord-Valleys. Geografiska Annaler. Series A, Physical Geography, 49(2/4): 188-203.

Hooke, J., 2003. Coarse sediment connectivity in river channel systems: a conceptual framework and methodology. Geomorphology, 56(1–2): 79-94.

Hooke, R., 1991. Positive feedbacks associated with erosion of glacial cirques and overdeepenings. Geological Society of America Bulletin, 103(8): 1104-1108.

Hovius, N., Stark, C.P. and Allen, P.A., 1997. Sediment flux from a mountain belt derived by landslide mapping. Geology, 25(3): 231-234.

Howard, A.D., Dietrich, W.E. and Seidl, M.A., 1994. Modeling fluvial erosion on regional to continental scales. J. Geophys. Res., 99(B7): 13971-13986.

Howard, A.D. and Kerby, G., 1983. Channel changes in badlands. Geological Society of America Bulletin, 94(6): 739-752.

IntermapTechnologies, 2004. Intermap Product Handbook and Quick Start Guide version 3.3. In: I.T. Inc. (Editor). Intermap Technologies Inc.

IntermapTechnologies, 2007. NEXTMap Britain: Digital terrain mapping of the UK, NERC Earth Observation Data Centre.

Jain, V., Preston, N., Fryirs, K. and Brierley, G., 2006. Comparative assessment of three approaches for deriving stream power plots along long profiles in the upper Hunter River catchment, New South Wales, Australia. Geomorphology, 74(1–4): 297-317.

Jansen, J.D., 2006. Flood magnitude–frequency and lithologic control on bedrock river incision in post-orogenic terrain. Geomorphology, 82(1-2): 39-57.

Jansen, John D., Codilean, Alexandru T., Bishop, P. and Hoey, Trevor B., 2010. Scale Dependence of Lithological Control on Topography: Bedrock Channel Geometry and Catchment Morphometry in Western Scotland. The Journal of Geology, 118(3): 223-246.

Jansen, J.D., Fabel, D., Bishop, P., Xu, S., Schnabel, C. and Codilean, A.T., 2011. Does decreasing paraglacial sediment supply slow knickpoint retreat? Geology, 39(6): 543-546.

Johnson, J.P. and Whipple, K.X., 2007. Feedbacks between erosion and sediment transport in experimental bedrock channels. Earth Surface Processes and Landforms, 32(7): 1048-1062.

Johnson, J.P.L. and Whipple, K.X., 2010. Evaluating the controls of shear stress, sediment supply, alluvial cover, and channel morphology on experimental bedrock incision rate. J. Geophys. Res., 115(F2): F02018.

Johnstone, G.S., 1989. The Northern Highlands of Scotland. British Regional Geology. H.M.S.O., London.

Kirk, W. and Godwin, H., 1963. A late-glacial site at Loch Droma, Ross and Cromarty. Transactions of the Royal Society of Edinburgh, 65: 225-249.

Kirkbride, M. and Matthews, D., 1997. The role of fluvial and Glacial erosion in landscape evolution: The Ben Ohau Range, New Zealand. Earth Surface Processes and Landforms, 22(3): 317-327.

Klecka, W.R., 1980. Discriminant Analysis. Sage University Paper series on Quantitative Applications in the Social Sciences. Sage, Beverly Hills, CA.

Klitgaard-Kristensen, D., Sejrup, H.P., Haflidason, H., Johnsen, S. and Spurk, M., 1998. A regional 8200 cal. yr BP cooling event in northwest Europe, induced by final stages of the Laurentide ice-sheet deglaciation? Journal of Quaternary Science, 13(2): 165-169.

Knighton, D., 1998. Fluvial forms and processes: a new perspective. Arnold, London.

Kohl, C.P. and Nishiizumi, K., 1992. Chemical isolation of quartz for measurement of in-situ - produced cosmogenic nuclides. Geochimica et Cosmochimica Acta, 56(9): 3583-3587.

Korup, O., 2005. Geomorphic imprint of landslides on alpine river systems, southwest New Zealand. Earth Surface Processes and Landforms, 30(7): 783-800.

Korup, O., 2006. Rock-slope failure and the river long profile. Geology, 34(1): 45-48.

Korup, O. and Montgomery, D.R., 2008. Tibetan plateau river incision inhibited by glacial stabilization of the Tsangpo gorge. Nature, 455(7214): 786-789.

Korup, O. and Schlunegger, F., 2007. Bedrock landsliding, river incision, and transience of geomorphic hillslope-channel coupling: Evidence from inner gorges in the Swiss Alps. J. Geophys. Res., 112(F3): F03027.

Korup, O., Strom, A.L. and Weidinger, J.T., 2006. Fluvial response to large rock-slope failures: Examples from the Himalayas, the Tien Shan, and the Southern Alps in New Zealand. Geomorphology, 78(1–2): 3-21.

Lague, D., 2010. Reduction of long-term bedrock incision efficiency by short-term alluvial cover intermittency. J. Geophys. Res., 115: F02011.

Lal, D., 1988. In Situ-Produced Cosmogenic Isotopes in Terrestrial Rocks. Annual Review of Earth and Planetary Sciences, 16(1): 355-388.

Lal, D., 1991. Cosmic ray labeling of erosion surfaces: in situ nuclide production rates and erosion models. Earth and Planetary Science Letters, 104(2–4): 424-439.

Lambeck, K., 1993. Glacial rebound of the British Isles. Preliminary model results. Geophyscial Journal International, 115(3): 941-959.

Lee, J.R., Rose, J., Hamblin, R.J.O., Moorlock, B.S.P., Riding, J.B., Phillips, E., Barendregt, R.W. and Candy, I., 2011. Chapter 6 - The Glacial History of the British Isles during the Early and Middle Pleistocene: Implications for the long-term development of the British Ice Sheet. In: Gibbard, P.L., Ehlers, J. and Hughes, D. (Editors), Developments in Quaternary Sciences. Elsevier, pp. 59-74.

Leica Geosystems, 2008. Leica GPS1200+ Series. Leica Geosystems (Editor), Switzerland.

Leland, J., Reid, M.R., Burbank, D.W., Finkel, R. and Caffee, M., 1998. Incision and differential bedrock uplift along the Indus River near Nanga Parbat, Pakistan Himalaya, from [10]Be and [26]Al exposure age dating of bedrock straths. Earth and Planetary Science Letters, 154(1-4): 93-107.

Leopold, L.B. and Maddock, T., 1953. The hydraulic geometry of stream channels and some physiographic implications. U.S. Geol. Surv. Prof. Pap., 252: p. 56.

Lewin, J. and Macklin, M.G., 2003. Preservation potential for Late Quaternary river alluvium. Journal of Quaternary Science, 18(2): 107-120.

Lewin, J., Macklin, M.G. and Johnstone, E., 2005. Interpreting alluvial archives: sedimentological factors in the British Holocene fluvial record. Quaternary Science Reviews, 24(16-17): 1873-1889.

Linton, D.L., 1949. Watershed breaching by ice in Scotland. Transactions of the Institute of British Geographers, 15: 1-16.

Linton, D.L., 1963. The Forms of Glacial Erosion. Transactions and Papers (Institute of British Geographers)(33): 1-28.

Litchfield, N. and Berryman, K., 2006. Relations between postglacial fluvial incision rates and uplift rates in the North Island, New Zealand. J. Geophys. Res., 111(F2): F02007.

Lowe, J.J., Rasmussen, S.O., Björck, S., Hoek, W.Z., Steffensen, J.P., Walker, M.J.C. and Yu, Z.C., 2008. Synchronisation of palaeoenvironmental events in the North Atlantic region during the Last Termination: a revised protocol recommended by the INTIMATE group. Quaternary Science Reviews, 27(1–2): 6-17.

MacGregor, K.R., Anderson, R.S., Anderson, S.P. and Waddington, E.D., 2000. Numerical simulations of glacial-valley longitudinal profile evolution. Geology, 28(11): 1031-1034.

Macklin, M.G., Johnstone, E. and Lewin, J., 2005. Pervasive and long-term forcing of Holocene river instability and flooding in Great Britain by centennial-scale climate change. The Holocene, 15(7): 937-943.

Maizels, J. and Aitken, J., 1991. Palaeohydrological Change During Deglaciation in Upland Britain: A Case Study from Northeast Scotland. In: L. Starkel, K.J. Gregory and J.B. Thornes (Editors), Temperate Palaeohydrology: Fluvial processes in the Temperate zone during the last 15000 years. John Wiley and Sons Ltd, Chichester.

Marsh, T.J. and Hannaford, J., 2008. UK Hydrometric Register. Hydrological data UK series. Centre for Ecology & Hydrology, 210 pp.

Massong, T.M. and Montgomery, D.R., 2000. Influence of sediment supply, lithology, and wood debris on the distribution of bedrock and alluvial channels. Geological Society of America Bulletin, 112(4): 591-599.

May, F., Peacock, J.D. and Smith, D.I., 1993. Geology of the Kintail district: Memoir for 1:50 000 geological sheet 72W and part of 71E (Scotland). HMSO, London.

McEwen, L., 1997. Corrieshalloch Gorge. In: K.J. Gregory (Editor), Fluvial Geomorphology of Great Britain. Geological Conservation Review Series. Chapman & Hall, London, pp. 32.

McEwen, L.J. and Matthews, J.A., 1998. Channel Form, Bed Material and Sediment Sources of the Sprongdøla, Southern Norway: Evidence for a Distinct Periglacio-Fluvial System. Geografiska Annaler: Series A, Physical Geography, 80(1): 17-36.

McEwen, L.J., Matthews, J.A., Shakesby, R.A. and Berrisford, M.S., 2002. Holocene Gorge Excavation Linked to Boulder Fan Formation and Frost Weathering in a Norwegian Alpine Periglaciofluvial System. Arctic, Antarctic, and Alpine Research, 34(3): 345-357.

Meigs, A., Krugh, W.C., Davis, K. and Bank, G., 2006. Ultra-rapid landscape response and sediment yield following glacier retreat, Icy Bay, southern Alaska. Geomorphology, 78(3–4): 207-221.

Merritt, J.W., Auton, C.A. and Firth, C.R., 1995. Ice-proximal glaciomarine sedimentation and sea-level change in the inverness area, Scotland: A review of the deglaciation of a major ice stream of the British Late Devensian ice sheet. Quaternary Science Reviews, 14(3): 289-329.

Merritts, D.J., Vincent, K.R. and Wohl, E.E., 1994. Long river profiles, tectonism, and eustasy: A guide to interpreting fluvial terraces. J. Geophys. Res., 99(B7): 14031-14050.

Millar, R.G., 2005. Theoretical regime equations for mobile gravel-bed rivers with stable banks. Geomorphology, 64(3-4): 207-220.

Miller, J.R., 1991. The Influence of Bedrock Geology on Knickpoint Development and Channel-Bed Degradation along Downcutting Streams in South-Central Indiana. The Journal of Geology, 99(4): 591-605.

Montgomery, D.R., 2004. Observations on the role of lithology in strath terrace formation and bedrock channel width. American Journal of Science, 304(5): 454-476.

Montgomery, D.R., Abbe, T.B., Buffington, J.M., Peterson, N.P., Schmidt, K.M. and Stock, J.D., 1996. Distribution of bedrock and alluvial channels in forested mountain drainage basins. Nature, 381(6583): 587-589.

Montgomery, D.R. and Buffington, J.M., 1997. Channel-reach morphology in mountain drainage basins. Geological Society of America Bulletin, 109(5): 596-611.

Montgomery, D.R. and Foufoula-Georgiou, E., 1993. Channel network source representation using digital elevation models. Water Resour. Res., 29(12): 3925-3934.

Montgomery, D.R. and Gran, K.B., 2001. Downstream variations in the width of bedrock channels. Water Resour. Res., 37(6): 1841-1846.

Montgomery, D.R. and Korup, O., 2011. Preservation of inner gorges through repeated Alpine glaciations. Nature Geosci, 4(1): 62-67.

Murton, J.B. and Belshaw, R.K., 2011. A conceptual model of valley incision, planation and terrace formation during cold and arid permafrost conditions of Pleistocene southern England. Quaternary Research, 75(2): 385-394.

Nielsen, S.B., Gallagher, K., Leighton, C., Balling, N., Svenningsen, L., Jacobsen, B.H., Thomsen, E., Nielsen, O.B., Heilmann-Clausen, C., Egholm, D.L., Summerfield, M.A., Clausen, O.R., Piotrowski, J.A., Thorsen, M.R., Huuse, M., Abrahamsen, N., King, C. and Lykke-Andersen, H., 2009. The evolution of western Scandinavian topography: A review of Neogene uplift versus the ICE (isostasy–climate–erosion) hypothesis. Journal of Geodynamics, 47(2–3): 72-95.

Nielsen, S.B., Paulsen, G.E., Hansen, D.L., Gemmer, L., Clausen, O.R., Jacobsen, B.H., Balling, N., Huuse, M. and Gallagher, K., 2002. Paleocene initiation of Cenozoic uplift in Norway. Geological Society, London, Special Publications, 196(1): 45-65.

Nishiizumi, K., Imamura, M., Caffee, M.W., Southon, J.R., Finkel, R.C. and McAninch, J., 2007. Absolute calibration of 10Be AMS standards. Nuclear Instruments and Methods in Physics Research Section B: Beam Interactions with Materials and Atoms, 258(2): 403-413.

Norton, K.P., von Blanckenburg, F. and Kubik, P.W., 2010. Cosmogenic nuclide-derived rates of diffusive and episodic erosion in the glacially sculpted upper Rhone Valley, Swiss Alps. Earth Surface Processes and Landforms, 35(6): 651-662.

Norton, K.P., von Blanckenburg, F., Schlunegger, F., Schwab, M. and Kubik, P.W., 2008. Cosmogenic nuclide-based investigation of spatial erosion and hillslope channel coupling in the transient foreland of the Swiss Alps. Geomorphology, 95(3–4): 474-486.

Oerlemans, J., 1984. Numerical experiments on large-scale glacial erosion. Zeitschrift Fur Gletscherkunde und Glazialgeologie, 20: 107-126.

Ouimet, W.B., Whipple, K.X., Crosby, B.T., Johnson, J.P. and Schildgen, T.F., 2008. Epigenetic gorges in fluvial landscapes. Earth Surface Processes and Landforms, 33(13): 1993-2009.

Palmer, A.P., Rose, J., Lowe, J.J. and MacLeod, A., 2010. Annually resolved events of Younger Dryas glaciation in Lochaber (Glen Roy and Glen Spean), western Scottish Highlands. Journal of Quaternary Science, 25(4): 581-596.

Parker, G., Toro-Escobar, C.M., Ramey, M. and Beck, S., 2003. Effect of Floodwater Extraction on Mountain Stream Morphology. Journal of Hydraulic Engineering, 129(11): 885-895.

Parker, G., Wilcock, P.R., Paola, C., Dietrich, W.E. and Pitlick, J., 2007. Physical basis for quasi-universal relations describing bankfull hydraulic geometry of single-thread gravel bed rivers. J. Geophys. Res., 112(F4): F04005.

Persano, C., Barfod, D.N., Stuart, F.M. and Bishop, P., 2007. Constraints on early Cenozoic underplating-driven uplift and denudation of western Scotland from low temperature thermochronometry. Earth and Planetary Science Letters, 263(3–4): 404-419.

Phillips, W.M., Hall, A.M., Ballantyne, C.K., Binnie, S., Kubik, P.W. and Freeman, S., 2008. Extent of the last ice sheet in northern Scotland tested with cosmogenic 10Be exposure ages. Journal of Quaternary Science, 23(2): 101-107.

Pickup, G., 1976. Adjustment of stream-channel shape to hydrologic regime. Journal of Hydrology, 30(4): 365-373.

Pickup, G. and Rieger, W.A., 1979. A conceptual model of the relationship between channel characteristics and discharge. Earth Surface Processes, 4(1): 37-42.

Pizzuto, J.E., 1992. The morphology of graded gravel rivers: a network perspective. Geomorphology, 5(3-5): 457-474.

Rea, B.R. and Evans, D.J.A., 1996. Landscapes of areal scouring in N.W. Scotland. Scottish Geographical Magazine, 112(1): 47-50.

Reinfelds, I., Cohen, T., Batten, P. and Brierley, G., 2004. Assessment of downstream trends in channel gradient, total and specific stream power: a GIS approach. Geomorphology, 60(3–4): 403-416.

Reinhardt, L.J., Bishop, P., Hoey, T.B., Dempster, T.J. and Sanderson, D.C.W., 2007. Quantification of the transient response to base-level fall in a small mountain catchment: Sierra Nevada, southern Spain. J. Geophys. Res., 112(F3): F03S05.

Reusser, L., Bierman, P., Pavich, M., Larsen, J. and Finkel, R., 2006. An Episode of Rapid Bedrock Channel Incision During the Last Glacial Cycle, Measured with 10Be. American Journal of Science, 306(2): 69-102.

Roberts, M.C. and Rood, K.M., 1984. The role of ice contributing area in the morphology of transverse fjords, British Columbia. Geografiska Annaler. Series A, Physical Geography, 66(4): 381-393.

Schildgen, T.F., Phillips, W.M. and Purves, R.S., 2005. Simulation of snow shielding corrections for cosmogenic nuclide surface exposure studies. Geomorphology, 64(1–2): 67-85.

Schlunegger, F., 2002. Impact of hillslope-derived sediment supply on drainage basin development in small watersheds at the northern border of the central Alps of Switzerland. Geomorphology, 46(3–4): 285-305.

Schumm, S.A., 1993. River Response to Baselevel Change: Implications for Sequence Stratigraphy. The Journal of Geology, 101(2): 279-294.

Schumm, S.A., Harvey, M.D. and Watson, C.C., 1984. Incised channels morphology, dynamics and control. Water Resources Publications, Michigan.

Schumm, S.A. and Rea, D.K., 1995. Sediment yield from disturbed earth systems. Geology, 23(5): 391-394.

Sejrup, H.P., Hjelstuen, B.O., Torbjørn Dahlgren, K.I., Haflidason, H., Kuijpers, A., Nygård, A., Praeg, D., Stoker, M.S. and Vorren, T.O., 2005. Pleistocene glacial history of the NW European continental margin. Marine and Petroleum Geology, 22(9–10): 1111-1129.

Selby, M.J., 1982. Rock mass strength and the form of some inselbergs in the central namib desert. Earth Surface Processes and Landforms, 7(5): 489-497.

Selby, M.J., 1993. Hillslope materials and processes. Oxford University Press, Oxford.

Shennan, I., Hamilton, S., Hillier, C. and Woodroffe, S., 2005. A 16,000-year record of near-field relative sea-level changes, northwest Scotland, United Kingdom. Quaternary International, 133–134(0): 95-106.

Shennan, I., Lambeck, K., Horton, B., Innes, J., Lloyd, J., McArthur, J., Purcell, T. and Rutherford, M., 2000. Late Devensian and Holocene records of relative sea-level changes in northwest Scotland and their implications for glacio-hydro-isostatic modelling. Quaternary Science Reviews, 19(11): 1103-1135.

Sissons, J.B., 1967. The evolution of Scotland's scenery. Oliver & Boyd, Edinburgh.

Sissons, J.B., 1979a. Catastrophic lake drainage in Glen Spean and the Great Glen, Scotland. Journal of the Geological Society, 136(2): 215-224.

Sissons, J.B., 1979b. Palaeoclimatic inferences from former glaciers in Scotland and the Lake District. Nature, 278(5704): 518-521.

Sissons, J.B., 1983. Shorelines and isostasy in Scotland. In: D.E. Smith and A.G. Dawson (Editors), Shorelines and Isostasy. Academic Press, London, pp. 209-205.

Sklar, L.S. and Dietrich, W.E., 1998. River Longitudinal Profiles and Bedrock Incision Models: Stream Power and the Influence of Sediment Supply. In: K. Tinkler and E. Wohl (Editors), Rivers over Rock: Fluvial Processes in Bedrock Channels. American Geophysical Union, USA, pp. 237-260.

Sklar, L.S. and Dietrich, W.E., 2001. Sediment and rock strength controls on river incision into bedrock. Geology, 29(12): 1087-1090.

Sklar, L.S. and Dietrich, W.E., 2004. A mechanistic model for river incision into bedrock by saltating bed load. Water Resour. Res., 40(6): W06301.

Slaymaker, O., 2009. Proglacial, periglacial or paraglacial? Geological Society, London, Special Publications, 320(1): 71-84.

Smith, D.E., Firth, C.R., Turbayne, S.C. and Brooks, C.L., 1992. Holocene relative sea-level changes and shoreline displacement in the Dornoch Firth area, Scotland. Proceedings of the Geologists' Association, 103, Part 3(0): 237-257.

Snyder, N.P., Whipple, K.X., Tucker, G.E. and Merritts, D.J., 2000. Landscape response to tectonic forcing: Digital elevation model analysis of stream profiles in the Mendocino triple junction region, northern California. Geological Society of America Bulletin, 112(8): 1250-1263.

Snyder, N.P., Whipple, K.X., Tucker, G.E. and Merritts, D.J., 2002. Interactions between onshore bedrock-channel incision and nearshore wave-base erosion forced by eustasy and tectonics. Basin Research, 14(2): 105-127.

Snyder, N.P., Whipple, K.X., Tucker, G.E. and Merritts, D.J., 2003. Channel response to tectonic forcing: field analysis of stream morphology and hydrology in the Mendocino triple junction region, northern California. Geomorphology, 53(1-2): 97-127.

Sternberg, H., 1875. Unterschungen über längen- und querprofil geschiebeführender Flüss. Z. Bauwesen, 25: 483-506.

Stone, J.O., 2000. Air pressure and cosmogenic isotope production. J. Geophys. Res., 105(B10): 23753-23759.

Strachan, R.A., Smith, M., Harris, A.L. and Fettes, D.J., 2002. The northern Higland and Grampian terranes. In: N.H. Trewin (Editor), The Geology of Scotland. The Geological Society, Bath, pp. 81-148.

Sugden, D.E. and John, B.S., 1976. Glaciers and landscape: a geomorphological approach. Edward Arnold, London.

Tinkler, K. and Wohl, E., 1998. Field studies of bedrock channels. In: K. Tinkler and E. Wohl (Editors), Rivers over rock: Fluvial processes in bedrock channels. American Geophysical Union, Washington, pp. 269-278.

Tomkin, J.H., 2009. Numerically simulating alpine landscapes: The geomorphologic consequences of incorporating glacial erosion in surface process models. Geomorphology, 103(2): 180-188.

Tomkin, J.H. and Braun, J., 2002. The influence of alpine glaciation on the relief of tectonically active mountain belts. American Journal of Science, 302(3): 169-190.

Trewin, N.H. and Thirlwall, M.F., 2002. Old Red Sandstone. In: N.H. Trewin (Editor), The Geology of Scotland. The Geological Society, Bath.

Tricart, J., 1970. Geomorphology of Cold Environments. Macmillan, London.

Tucker, G.E. and Hancock, G.R., 2010. Modelling landscape evolution. Earth Surface Processes and Landforms, 35(1): 28-50.

Turowski, J.M., Lague, D., Crave, A. and Hovius, N., 2006. Experimental channel response to tectonic uplift. J. Geophys. Res., 111(F3): F03008.

Turowski, J.M., Lague, D. and Hovius, N., 2007. Cover effect in bedrock abrasion: A new derivation and its implications for the modeling of bedrock channel morphology. J. Geophys. Res., 112(F4): F04006.

Valla, P.G., Van Der Beek, P.A. and Carcaillet, J., 2010a. Dating bedrock gorge incision in the French Western Alps (Ecrins-Pelvoux massif) using cosmogenic 10Be. Terra Nova, 22(1): 18-25.

Valla, P.G., van der Beek, P.A. and Lague, D., 2010b. Fluvial incision into bedrock: Insights from morphometric analysis and numerical modeling of gorges incising glacial hanging valleys (Western Alps, France). J. Geophys. Res., 115(F2): F02010.

Vivian, R., 1970. Hydrologie et érosion sous-glaciaires. PERSEE.

Wang, Y., Mercer, B., Vincent, T.C., Sharma, J. and Crawford, S., 2001. Automatic generation of bald earth digital elevation models from digital surface models created using airborne IfSAR, Intermap Technologies Corporation, Canada.

Werritty, A. and McEwen, L., 1997. The fluvial geomorphology of Scotland. In: K. Gregory (Editor), The fluvial geomorphology of Great Britain. Chapman and Hall, London.

Wharton, G., 1995. The channel-geometry method: Guidelines and applications. Earth Surface Processes and Landforms, 20(7): 649-660.

Whipple, K.X., 2001. Fluvial Landscape Response Time: How Plausible Is Steady-State Denudation? American Journal of Science, 301(4-5): 313-325.

Whipple, K.X., 2004. Bedrock rivers and the geomorphology of active orogens. Annual Review of Earth and Planetary Sciences, 32(1): 151-185.

Whipple, K.X., Hancock, G.S. and Anderson, R.S., 2000. River incision into bedrock: Mechanics and relative efficacy of plucking, abrasion, and cavitation. Geological Society of America Bulletin, 112(3): 490-503.

Whipple, K.X., Kirby, E. and Brocklehurst, S.H., 1999. Geomorphic limits to climate-induced increases in topographic relief. Nature, 401(6748): 39-43.

Whipple, K.X. and Tucker, G.E., 1999. Dynamics of the stream-power river incision model: Implications for height limits of mountain ranges, landscape response timescales, and research needs. J. Geophys. Res., 104(B8): 17661-17674.

Whipple, K.X. and Tucker, G.E., 2002. Implications of sediment-flux-dependent river incision models for landscape evolution. Journal of Geophysical Research, 107(B2).

Whittaker, A.C., Attal, M., Cowie, P.A., Tucker, G.E. and Roberts, G., 2008. Decoding temporal and spatial patterns of fault uplift using transient river long profiles. Geomorphology, 100(3–4): 506-526.

Whittaker, A.C., Cowie, P.A., Attal, M., Tucker, G.E. and Roberts, G.P., 2007. Bedrock channel adjustment to tectonic forcing: Implications for predicting river incision rates. Geology, 35(2): 103-106.

Whittington, G., 1985. The little ice age and Scotland's weather. Scottish Geographical Magazine, 101(3): 174-178.

Wobus, C.W., Kean, J.W., Tucker, G.E. and Anderson, R.S., 2008. Modeling the evolution of channel shape: Balancing computational efficiency with hydraulic fidelity. J. Geophys. Res., 113(F2): F02004.

Wobus, C.W., Tucker, G.E. and Anderson, R.S., 2006. Self-formed bedrock channels. Geophys. Res. Lett., 33(18): L18408.

Wohl, E., 2008. The effect of bedrock jointing on the formation of straths in the Cache la Poudre River drainage, Colorado Front Range. J. Geophys. Res., 113(F1): F01007.

Wohl, E., 2004. Limits of downstream hydraulic geometry. Geology, 32(10): 897-900.

Wohl, E., 1998. Berock channel morphology in relation to erosional process. In: K. Tinkler and E. Wohl (Editors), Rivers over Rock: Fluvial processes in bedrock channels. American Geomphysical Union, Washington, pp. 133-152.

Wohl, E.E., 1992. Bedrock benches and boulder bars: Floods in the Burdekin Gorge of Australia. Geological Society of America Bulletin, 104(6): 770-778.

Wohl, E. and David, G.C.L., 2008. Consistency of scaling relations among bedrock and alluvial channels. J. Geophys. Res., 113(F4): F04013.

Wohl, E. and Merritt, D.M., 2008. Reach-scale channel geometry of mountain streams. Geomorphology, 93(3-4): 168-185.

Wohl, E.E. and Merritt, D.M., 2001. Bedrock channel morphology. Geological Society of America Bulletin, 113(9): 1205-1212.

Wolman, M.G. and Miller, J.P., 1960. Magnitude and Frequency of Forces in Geomorphic Processes. The Journal of Geology, 68(1): 54-74.

Xu, S., Dougans, A.B., Freeman, S.P.H.T., Schnabel, C. and Wilcken, K.M., 2010. Improved 10Be and 26Al-AMS with a 5MV spectrometer. Nuclear Instruments and Methods in Physics Research Section B: Beam Interactions with Materials and Atoms, 268(7-8): 736-738.

Yanites, B.J. and Tucker, G.E., 2010. Controls and limits on bedrock channel geometry. J. Geophys. Res., 115(F4): F04019.

Appendix 1 - Details of analytical procedures

A 1.1 *Longitudinal profile derivation using ArcGIS Hydrology tools*

Stream lines, elevation profiles, stream length and drainage area were calculated from the 5 m resolution NEXTMap dtm using ArcGIS Hydrology processing tools following this procedure:

1. Mosaic separate dtm tiles for the catchment area

Using Hydrology tools:

2. Fill holes in the dtm
3. Calculate flow direction raster
4. Calculate flow accumulation raster (number of contributing cells)
5. Derive basin area raster and convert to shapefile
6. Calculate flow length raster

Using raster calculator and other raster processing tools:

7. Calculate contributing area (m^2) from flow accumulation raster using cell size (5x5m)
8. Extract stream lines from flow accumulation raster using an accumulation area filter set at 0.5-1km^2
9. Convert stream line raster to point and line shapefiles: The point shapefiles represent the channel line with points spaced every 5-7.5m along the channel line (depending on whether they are horizontally or diagonally spaced)

Using the stream shapefiles:

10. Isolate main channel and tributaries
11. Extract elevation, stream length and drainage area for each point in the stream line.
12. Plot longitudinal profiles (in Excel)
13. Check stream lines and longitudinal profiles against digital Ordnance Survey 1:10,000 and 1:25,000 scale topographic maps and correct major errors.

A 1.2 *Canonical discriminant analysis: R code*

R code used to derive critical slope function for the alluvial to bedrock channel transition through canonical discriminant analysis of reach slope and drainage area (Naylor, M., pers comm).

```
data=read.table("FILE NAME.csv", header=T, sep=",")

library(MASS)

cata=data[,2]
symb=c()
symb[ which(cata =="AL") ] = 1
symb[ which(cata =="BR") ] = 2

Length = log10(data[,3])
Slope = log10(data[,4])
Area = log10(data[,5])

### Slope vs Area
```

```
model<-help(cata~Slope+Area)
pAL=model[[1]][1] ; pBR=model[[1]][2]
yMeanAL <- model[[3]][1] ; yMeanBR <- model[[3]][2]
xMeanAL <- model[[3]][3] ; xMeanBR <- model[[3]][4]
xMid=pBR*xMeanAL+ pAL*xMeanBR ; yMid=pBR*yMeanAL+ pAL*yMeanBR
xL = c(0.5-xMid,4-xMid) ; yL= -xL*model[[4]][2]/model[[4]][1]

plot(Area, Slope, pch=symb, col=symb)
points(xMid,yMid, col=3)
points(xL+xMid,yL+yMid,type="l", col=2)
```

Appendix 2 - Chapter 3 additional results
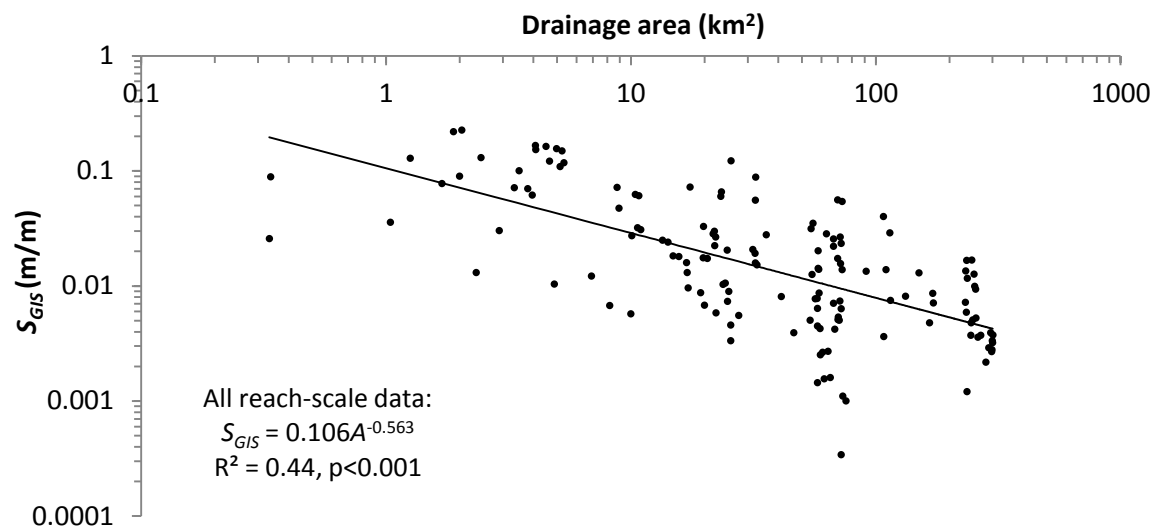
Figure A2-1 Log-log plot of channel slope versus drainage area for all reach-scale channel data showing power law regression (black line). Standard errors for the coefficient and exponent are 0.010 and 0.053 respectively. The regression equation is used in section 3.3.1.2 to normalise channel slope for drainage area.

River	Drainage area (km²)	Profile data Max E (m)	Profile data Length (m)	Morphometric indices S_r	Morphometric indices θ	Lithology indices Quartzite fraction	Lithology indices Fault fraction	Glacial divide breaching Breach relief ratio	Glacial divide breaching Breach cross-section area (m²)
Northwest Highlands									
Carron	300.8	723.5	44934.1	0.035	0.682	*0.00*	0.070	0.095	38700
Elchaig	97.0	423.1	20480.0	0.023	0.959	0.01	0.450	0.333	141991
Canaird	96.7	195.7	17113.0	0.010	0.289	0.09	0.194	0.365	265478
Oykel-Cassley	653.4	483.2	50409.1	0.016	0.334	*0.00*	0.001	0.473	776296
Oykel	653.4	458.5	51520.6	0.026	0.844	0.01	0.001	*0.000*	0
Oykel-Einig	653.4	442.5	45960.3	0.022	0.780	*0.00*	0.127	*0.000*	0
Conon-Blackwater	1169.0	263.7	48581.5	0.012	0.416	*0.00*	0.180	0.450	338337
Conon-Bran	1169.0	228.3	66357.8	0.010	0.290	*0.00*	0.060	0.573	528907
Conon-Meig	1169.0	316.6	57710.5	0.012	0.450	*0.00*	0.119	0.384	312969
Beauly-Farrer	996.0	345.2	75064.8	0.018	0.532	*0.00*	*0.000*	0.406	301582
Beauly-Cannich	996.0	284.3	75708.7	0.023	0.647	0.01	0.213	0.387	257655
Beauly-Affric	996.0	326.2	82113.7	0.011	0.463	0.02	0.248	0.442	472538
Broom-Droma	146.9	276.7	18639.2	0.004	-0.516	*0.00*	*0.000*	0.573	528907
Broom-Cuileig	146.9	317.7	21956.2	0.022	0.315	*0.00*	0.221	0.381	380495
Carron (W)	139.3	176.6	26619.0	0.012	0.266	0.10	0.511	0.514	604494
Ling-Blackwater	133.7	439.2	23500.9	0.023	0.431	*0.00*	0.152	0.235	91000
Ling	133.7	398.3	25840.8	0.011	0.125	*0.00*	0.146	0.360	217296
Elchaig-Ghlomach	97.0	387.9	20046.2	0.013	0.655	*0.00*	0.273	0.350	305693
Western Highlands									
Spean	821.0	1044	63.484	0.019	0.398	0.050	0.766	0.393	569680
Leven	192.0	659	26.731	0.009	0.444	0.059	*0.000*	0.321	500172
Etive	158.0	437	21.184	0.015	0.177	0.036	0.367	0.375	307544
Nevis	77.0	986	22.866	0.029	0.461	0.214	0.041	0.337	369578
Kinglass	74.2	724	18.133	0.028	0.516	0.005	0.024	*0.000*	0
Coe	55.0	345	12.272	0.023	-0.054	0.074	0.370	0.375	307544
Kiachnish	48.3	867	14.321	0.023	0.176	0.063	0.056	0.388	274059
Creran	29.1	739	9.245	0.038	0.351	0.083	0.168	0.205	116974
Salachan	21.9	604	7.310	0.044	0.357	0.242	*0.000*	*0.000*	0
Duror	21.7	749	8.788	0.028	-0.177	0.215	0.105	0.394	305320
Righ	19.9	554	8.713	0.005	0.636	0.391	*0.000*	0.504	324967
Ure	18.7	685	7.410	0.052	0.110	0.036	*0.000*	0.156	57176
Easragan	14.9	499	7.022	0.100	-0.135	0.241	0.342	0.208	45932
Laroch	12.8	579	5.988	0.042	0.251	0.305	0.743	0.394	305320

Table A2 Catchment scale metrics for channels in the NW Highlands, including the three surveyed streams and 15 other trunk stream and major tributary channels. Data for western Highland rivers taken from Jansen et al., (2010), with addition of divide breaching data. Derivation of metrics described in section 3.3.1.

Appendix 3 - Hydraulic geometry regression and analysis of covariance (ANCOVA) results

	Data	Coefficient	St error	Exponent	St error	R^2	p
All data	All data	-1.049 (0.089)	0.088	-0.528	0.053	0.40	<0.001
	AL	-1.705 (0.020)	0.124	-0.299	0.072	0.26	<0.001
	BR	-0.614 (0.243)	0.087	-0.598	0.056	0.66	<0.001
	BR-AL	-1.26 (0.055)	0.149	-0.477	0.086	0.44	<0.001
Carron	All data	-1.064 (0.086)	0.098	-0.498	0.053	0.52	<0.001
	AL	-1.700 (0.020)	0.146	-0.283	0.077	0.33	0.001
	BR	-0.647 (0.225)	0.091	-0.575	0.054	0.79	<0.001
	BR-AL	-1.25 (0.056)	0.155	-0.447	0.078	0.65	<0.001
Elchaig	All data	-0.608 (0.247)	0.221	-0.862	0.149	0.43	<0.001
	AL	-1.264 (0.055)	0.383	-0.610	0.245	0.32	0.027
	BR	-0.498 (0.318)	0.228	-0.708	0.166	0.52	0.001
	BR-AL	-0.677 (0.210)	0.492	-0.901	0.315	0.43	0.015
Canaird	All data	-2.603 (0.003)	0.540	+0.655	0.424	0.10	0.137
	AL	-2.193 (0.006)	0.464	+0.053	0.410	0.00	0.904
	BR	-1.759 (0.017)	2.706	+0.284	2.011	0.00	0.892
	BR-AL	-1.84 (0.015)	0.599	-0.096	0.464	0.01	0.843

Table A3-1 Regression statistics for linear regressions of log S and log A from the surveyed rivers in the NW Highlands calculated using Minitab. Values in brackets are powerlaw coefficients calculated from the intercept of the log S-log A relationship.

Data groups	Regression test	Exponent p value	Coefficient p value
All data – river	Carron vs. Elchaig	0.012	-
All data – channel type	AL vs. BR	0.001	-
	AL vs. BR-AL	0.112	0.040
	BR vs. BR-AL	0.218	<0.001
River – channel type	Carron BR vs. Elchaig BR	0.370	0.751
	Carron AL vs. Elchaig AL	0.147	0.528
Carron – channel type	AL vs. BR	0.002	-
	AL vs. BR-AL	0.137	0.076
	BR vs. BR-AL	0.165	<0.001
Elchaig – channel type	AL vs. BR	0.739	<0.001
	AL vs. BR-AL	0.470	0.388
	BR vs. BR-AL	0.561	0.008

Table A3-2 Results of ANCOVA on S-A regressions for the reach data from the surveyed rivers. Note that the lack of significant S-A correlation for the River Canaird precludes comparison with data from the other rivers, however, as it falls within a similar range to the rivers Elchaig and Carron it is included in the 'All data' regressions.

DRAINAGE AREA		Width-area				Depth-area			
		Intercept	Exponent	R²	p	Intercept	Exponent	R²	p
All data	Individual data	0.593 (3.917)	0.389	0.747	<0.001	-0.066 (0.859)	0.218	0.381	<0.001
	Reach-average	0.594 (3.926)	0.391	0.818	<0.001	-0.057 (0.877)	0.218	0.446	<0.001
River	Carron	0.642 (4.385)	0.368	0.872	<0.001	-0.027 (0.940)	0.212	0.624	<0.001
	Elchaig	0.566 (3.681)	0.435	0.696	<0.001	0.090 (1.230)	0.113	0.123	**0.018**
	Canaird	0.053 (1.130)	0.744	0.650	<0.001	-0.745 (0.180)	0.693	0.317	0.005
Substrate	Alluvial	0.732 (5.395)	0.379	0.891	<0.001	-0.121 (0.757)	0.216	0.336	<0.001
	Bedrock	0.662 (4.591)	0.300	0.814	<0.001	0.061 (1.151)	0.209	0.494	<0.001
	Bedrock - Alluvial	0.657 (4.539)	0.366	0.849	<0.001	-0.299 (0.502)	0.326	0.671	<0.001
River and substrate	Carron AL	0.692 (4.920)	0.397	0.801	<0.001	-0.031 (0.931)	0.186	0.281	0.011
	Elchaig AL	0.609 (4.064)	0.484	0.668	0.004	0.252 (1.787)	-0.082	0.093	0.391
	Canaird AL	-	-	-	-	-	-	-	-
	Carron BR	0.652 (4.488)	0.309	0.899	<0.001	0.035 (1.084)	0.215	0.595	<0.001
	Elchaig BR	0.734 (5.420)	0.267	0.651	<0.001	0.079 (1.200)	0.209	0.457	0.002
	Canaird BR	-0.582 (0.262)	1.152	0.244	0.176	0.116 (1.306)	0.187	0.003	0.891

Table A3-3 Regression data for reach average channel width and depth with drainage area for all data and data groups defined by river and substrate calculated as log-linear relationships in Minitab. Bracketed values for intercepts are converted to power-law coefficients, slope values from the log linear relationship are equivalent to the power-law exponents. Scaling relationships for alluvial channels on the River Canaird were not calculated due too little data.

DRAINAGE AREA	Test	Width p values		Depth p values	
		Exponent	Intercept	Exponent	Intercept
Data type	Individual data vs Reach-average	0.918	0.754	0.994	0.591
River	Carron vs Elchaig	0.115	0.387	0.036	-
	Carron vs Canaird	0.002	-	<0.001	-
	Elchaig vs Canaird	0.038	-	0.003	-
Substrate	AL vs BR	0.038	-	0.832	<0.001
	AL vs BR-Al	0.663	<0.001	0.060	0.435
	BR vs BR-AL	0.080	<0.001	0.035	-
River and Substrate	Carron AL vs Elchaig AL	0.414	0.161	0.042	-
	Carron BR vs Elchaig BR	0.389	0.297	0.667	0.384
	Carron AL vs Carron BR	0.085	<0.001	0.722	0.003
	Elchaig AL vs Elchaig BR	0.084	<0.001	0.026	-

Table A3-4 ANCOVA p values for comparisons of *w-A* and *d-A* regression relationships for subsets of the data grouped according to river and substrate (test). Where exponents are significantly different, it is not possible to compare intercepts.

DISCHARGE		Width-discharge				Depth-discharge			
		Intercept	Exponent	R^2	p	Intercept	Exponent	R^2	p
All data	**Individual data**	0.729 (5.358)	0.373	0.691	<0.001	0.008 (1.019)	0.211	0.358	<0.001
	Reach-average	0.742 (5.521)	0.380	0.751	<0.001	0.018 (1.042)	0.219	0.436	<0.001
River	**Carron**	0.552 (3.565)	0.466	0.872	<0.001	-0.079 (0.834)	0.269	0.624	<0.001
	Elchaig	0.814 (6.516)	0.435	0.696	<0.001	0.155 (1.429)	0.113	0.123	**0.018**
	Canaird	0.490 (3.090)	0.724	0.615	<0.001	0.346 (2.218)	0.685	0.310	0.006
Substrate	**Alluvial**	0.964 (9.205)	0.306	0.810	<0.001	-0.467 (0.341)	0.212	0.456	<0.001
	Bedrock	0.775 (5.957)	0.287	0.695	<0.001	0.152 (1.419)	0.189	0.375	<0.001
	Bedrock-Alluvial	0.923 (8.375)	0.288	0.790	<0.001	-0.077 (0.838)	0.268	0.679	<0.001
River and substrate	**Carron AL**	0.596 (3.945)	0.502	0.801	<0.001	-0.076 (0.840)	0.235	0.281	0.011
	Elchaig AL	0.884 (7.656)	0.484	0.668	0.004	0.205 (1.603)	-0.082	0.093	0.391
	Canaird AL	-	-	-	-	-	-	-	-
	Carron BR	0.576 (3.767)	0.391	0.899	<0.001	-0.018 (0.959)	0.273	0.595	<0.001
	Elchaig BR	0.886 (7.691)	0.267	0.651	<0.001	0.198 (1.578)	0.209	0.457	0.002
	Canaird BR	0.073 (1.183)	1.152	0.244	0.176	0.222 (1.667)	0.187	0.003	0.891

Table A3-5 Regression data for reach average channel width and depth with discharge for all data and data groups defined by river and substrate calculated as log-linear relationships in Minitab. Bracketed values for intercepts are converted to power-law coefficients, slope values from the log linear relationship are equivalent to the power-law exponents. Scaling relationships for alluvial channels on the River Canaird were not calculated due too little data.

DISCHARGE	Test	Width p values		Depth p values	
		Exponent	Intercept	Exponent	Intercept
Data type	Individual data vs Reach-average	0.751	0.161	0.763	0.276
River	Carron vs Elchaig	0.477	<0.001	0.002	-
	Carron vs Canaird	0.034	-	0.011	-
	Elchaig vs Canaird	0.054	0.001	0.004	-
Substrate	Alluvial vs Bedrock	0.660	<0.001	0.693	<0.001
	Alluvial vs BR-Al	0.635	0.002	0.296	0.088
	Bedrock vs BR-AL	0.971	<0.001	0.126	<0.001
River and Substrate	Carron AL vs Elchaig AL	0.878	<0.001	0.026	-
	Carron BR vs Elchaig BR	0.018	-	0.404	0.001
	Carron AL vs Carron BR	0.085	<0.001	0.722	0.003
	Elchaig AL vs Elchaig BR	0.084	<0.001	0.026	-

Table A3-6 Ancova p values for comparisons of *w-Q* and *d-Q* regression relationships for subsets of the data grouped according to river and substrate (test). Where exponents are significantly different, it is not possible to compare intercepts.

Appendix 4 - Chapter 4 additional results

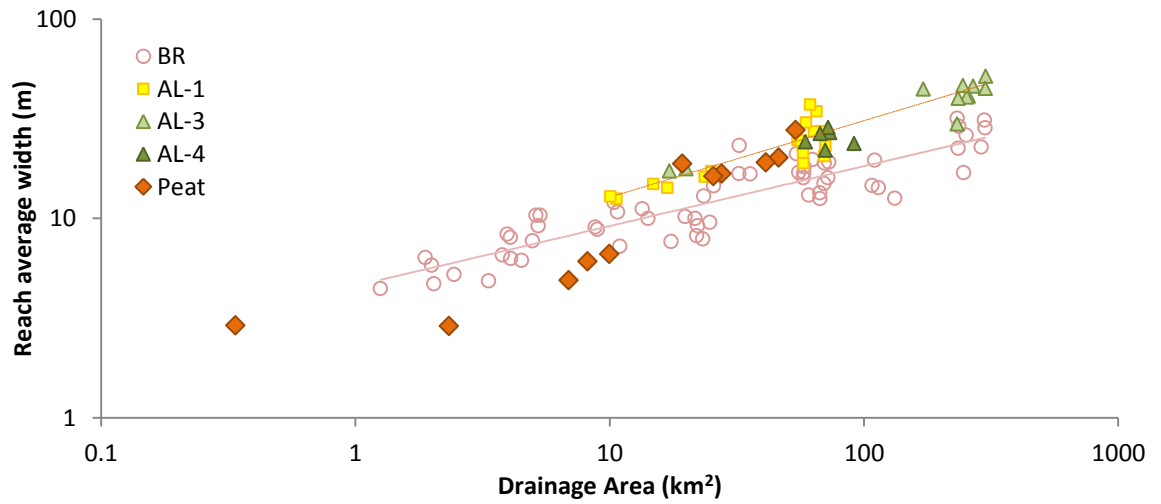**Figure A4-1 Log-log *w-A* plot for alluvial channels grouped according to bank vegetation type after Hay and Thorne (1986). AL-1 = grass or grass and light heather, AL-3=grass and heather with few trees, AL-4 = abundant trees. Power law regression for all alluvial channels, not including peat (dashed orange line). Bedrock channel data and power law regression (light pink, solid line) shown for reference.**

Appendix 5 - Chapter 5 additional data

Site, River	Sample No.	Lat. (°N)	Long. (°E)	Elevation (m > OD)	Strath height (m)	Sample thickness (cm)	Lithology	Shielding	Surface slope	Shielding factor	Rate or Age
Garve, Blackwater	GRV 01	57.83	-4.97	91.5	7.4	1	Qz vein	070 8, 108 9, 190 3, 200 6, 242 4, 288 4, 326 9, 020 3, 050 5	4 135	0.999	A
	GRV 02	57.83	-4.97	86.7	6.4	0.75	Psammite	037 6, 082 12, 122 11, 174 3, 204 5, 250 4, 318 9, 010 8	20 136	0.993	A
	GRV 03	57.83	-4.97	84.9	8.1	0.75	Qz vein	148 1, 172 1, 207 7, 268 5, 318 8, 355 5, 013 9, 032 4, 074 6, 116 13	10 220	0.999	A
	GRV 04	57.83	-4.97	77.9	4.1	1.5	Psammite	165 2, 200 8, 283 6, 304 4, 328 8, 352 4, 031 8, 059 11, 124 11, 160 4	8 228	0.998	A
Croick Schoolhouse, River Carron	CRK 01	57.86	-4.95	59.0	8.0	0.75	Qz vein	243 4, 261 6, 286 4, 331 14, 348 9, 010 11, 082 4, 156 6, 207 6, 233 5	8 080	0.999	A
	CRK 02	57.86	-4.95	57.1	8.5	1	Psammite	240 3, 262 6, 284 5, 322 14, 345 9, 010 12, 075 7, 088 2, 138 9, 150 6, 228 7	5 028	0.998	A
	CRK 03	57.86	-4.95	51.9	10.4	1.25	Qz vein + psammite	088 2, 170 7, 241 4, 293 9, 324 12, 338 10, 001 11, 074 6	14 249	0.997	A
Linn of Dee, River Dee	DEE 02	56.99	-3.55	364.8	16.0	1.25	Qz lens	083 1, 110 2, 141 13, 178 12, 228 8, 262 3, 282 3, 311 11, 334 7	14 168	0.997	A
	DEE 03	56.99	-3.55	366.6	16.6	1.5	Qz lens	254 4, 270 3, 282 8, 300 8, 083 5, 106 1, 149 14, 212 13	08 080	0.998	A
	DEE 04	56.99	-3.54	361.9	8.0	1.25	Qz lens	104 01, 122 04, 154 14, 176 14, 250 08, 275 06, 303 10, 040 09, 085 01	flat	0.997	A
Monessie Gorge, River Spean	MON 01	56.89	-4.80	118.8	11.0	1.25	Qz lens	084 7, 107 15, 176 23, 222 6, 237 5, 275 20, 046 12, 060 10	10 131	0.986	A
	MON 02	56.89	-4.80	120.8	8.6	1	Qz lens	092 7, 119 20, 190 26, 227 11, 236 6, 265 11, 299 32, 063 14	flat	0.965	A
	MON 03	56.89	-4.79	120.0	8.2	1.5	Qz lens	106 9, 126 04, 140 16, 194 34, 234 24, 253 6, 286 14, 332 32*, 080 16*	flat	0.962	A
Dog Fall, River Affric	AFF 07	57.31	-4.85	179.6	3.6	1.75	Quartzitic psammite	094 1, 115 11, 188 18, 243 4, 261 5, 281 12, 310 18, 060 24	flat	0.984	A
	AFF 08	57.31	-4.84	176.6	3.3	1.75	Quartzitic psammite	102 8, 121 16, 153 21, 236 16, 264 6, 271 9, 278 7, 300 15, 309 30, 004 48	flat	0.976	A
	AFF 10	57.31	-4.85	181.1	5.2	0.75	Quartzite	083 6, 140 8, 191 21, 199 24, 222 20, 248 5, 270 7, 288 10, 011 24	6 026	0.986	A
	AFF 13	57.31	-4.84	175.9	3.4	1.25	Quartzite	080 4, 090 2, 106 19, 140 33, 151 32, 187 34, 222 32, 275 13, 271 06	flat	0.948	A
	AFF 14	57.31	-4.84	174.8	2.3	0.75	Quartzitic psammite	098 8, 142 30, 150 33, 165 31, 179 31, 262 7, 268 8, 280 9, 296 13, 332 25, 011 31, 088 19	15 238	0.950	A
Dog Fall, River Affric	AFF 16R	57.31	-4.85	180.6	-	0.75	Quartzite	081 3, 157 21, 165 24, 204 16, 248 3, 265 5, 291 15, 328 22, 009 24	4 108	0.983	R
	AFF 15R	57.31	-4.85	177.0	-	1.25	Pegmatite	100 6, 114 12, 143 16, 167 21, 186 23, 251 5, 261 5, 287 16, 332 32, 013 35, 071 13, 089 7	16 182	0.959	R

Table A5-1 Sample data used in cosmogenic nuclide analysis. Shielding factor calcualted using CRONUS topographic shileding calcualator (Balco et al., 2008).

Sample code	Thickness factor	Shielding factor	¹⁰Be conc.	Measurement uncert. 1σ	Internal uncert. 1σ	Muon prod.	Time indep Lal/Stone			Desilets et al. (2003, 2006)		Dunai (2001)		Lifton et al. (2005)		Time dep Lal/Stone	
							Spallation prod.	Exposure Age	External uncert. 1σ	Exposure Age	External uncert. 1σ	Exposure Age	External uncert. 1σ	Exposure Age	External uncert. 1σ	Exposure Age	External uncert. 1σ
			at/g	at/g	ka	at/g/yr	at/g/yr	ka	ka	ka	ka	ka	ka	ka	ka	ka	ka
GRV 01	0.992	0.999	17870	1130	0.2	0.188	5.08	3.4	0.4	3.6	0.5	3.6	0.5	3.4	0.4	3.5	0.4
GRV 02	0.994	0.993	56360	2667	0.5	0.188	5.06	10.8	1.1	11.3	1.4	11.3	1.4	10.9	1.2	11.0	1.1
GRV 03	0.994	0.999	69460	2619	0.5	0.188	5.02	13.4	1.3	14.0	1.7	14.0	1.7	13.5	1.4	13.7	1.3
GRV 04	0.987	0.998	63510	2304	0.5	0.187	4.97	12.4	1.2	12.9	1.6	12.9	1.6	12.5	1.3	12.6	1.2
CRK 01	0.994	0.999	49690	3126	0.6	0.187	4.94	9.7	1.0	10.1	1.4	10.1	1.4	9.8	1.2	9.9	1.1
CRK 02	0.992	0.998	17700	1063	0.2	0.186	4.86	3.5	0.4	3.7	0.5	3.7	0.5	3.5	0.4	3.6	0.4
CRK 03	0.990	0.997	51960	2105	0.4	0.185	4.81	10.4	1.0	10.8	1.4	10.8	1.4	10.5	1.1	10.7	1.0
DEE 02	0.990	0.997	80130	3167	0.5	0.206	6.51	12.0	1.2	12.7	1.6	12.7	1.6	12.3	1.3	12.2	1.1
DEE 03	0.987	0.998	74080	2955	0.4	0.206	6.56	11.0	1.1	11.7	1.5	11.7	1.5	11.3	1.2	11.2	1.1
DEE 04	0.990	0.997	57410	2317	0.4	0.206	6.5	8.6	0.8	9.1	1.1	9.1	1.1	8.8	0.9	8.8	0.8
MON 01	0.990	0.986	41070	1848	0.4	0.190	5.12	7.8	0.8	8.1	1.0	8.2	1.0	7.8	0.9	7.9	0.8
MON 02	0.992	0.965	34070	1590	0.3	0.190	5.03	6.5	0.7	6.9	0.9	6.9	0.9	6.6	0.7	6.7	0.7
MON 03	0.987	0.962	19390	932	0.2	0.189	4.95	3.8	0.4	4.0	0.5	4.0	0.5	3.8	0.4	3.9	0.4
AFF 07	0.985	0.984	59527	2397	0.4	0.194	5.39	9.8	0.9	10.3	1.3	10.3	1.3	9.9	1.1	10.0	0.9
AFF 08	0.985	0.976	31198	1824	0.3	0.193	5.33	5.2	0.5	5.5	0.7	5.5	0.7	5.2	0.6	5.3	0.5
AFF 10	0.994	0.986	75968	2859	0.5	0.194	5.45	12.3	1.2	13.0	1.6	13.0	1.6	12.5	1.3	12.6	1.2
AFF 13	0.990	0.948	52938	2253	0.4	0.193	5.19	9.0	0.9	9.5	1.2	9.5	1.2	9.1	1.0	9.2	0.9
AFF 14	0.994	0.950	59850	2265	0.4	0.193	5.22	10.1	1.0	10.7	1.3	10.7	1.3	10.3	1.1	10.3	1.0
AFF 16R	*0.994*	*0.983*	*51150*	*1973*	*0.4*	*0.194*	*5.44*	*8.3*	*0.8*	*8.8*	*1.1*	*8.8*	*1.1*	*8.4*	*0.9*	*8.5*	*0.8*
AFF 15R	*0.990*	*0.959*	*38010*	*2413*	*0.4*	*0.194*	*5.26*	*7.0*	*0.8*	*7.4*	*1.0*	*7.4*	*1.0*	*7.1*	*0.8*	*7.1*	*0.8*

Table A5-2 Exposure age calcualtion data from CRONUS (cf. Balco et al., 2008). Ages calcualted for zero erosion case. Italicised data is for channel bed samples, i.e. from eroding surfaces.

Sample	Thickness factor	Shielding factor	10Be conc.	Measurement uncert. 1σ	Muon prod.	Internal uncert. 1σ	Time indep Lal/Stone			Desilets et al. (2003, 2006)		Dunai (2001)		Lifton et al. (2005)		Time dep Lal/Stone	
							Spallation prod.	Erosion rate	External uncert. 1σ	Erosion rate	External uncert. 1σ	Erosion rate	External uncert. 1σ	Erosion rate	External uncert. 1σ	Erosion rate	External uncert. 1σ
			at/g	at/g	at/g/yr	m/Myr	at/g/yr	m/Myr	m/Myr	m/Myr	m/Myr	m/Myr	m/Myr	m/Myr	m/Myr	m/Myr	m/Myr
AFF 16R	0.9937	0.983	51150	1973	0.194	3.78	5.47	105.6	7.9	101.9	9.2	101.7	9.16	104.6	8.4	104	7.6
AFF 15R	0.9895	0.959	38010	2413	0.193	8.27	5.32	127.8	11.5	123.5	12.7	123.2	12.7	126.8	12	125.9	11.2

Table A5-3 Erosion rate calculation data from CRONUS for channel bed samples only (Balco et al., 2008). Rates calculated by assuming infinite age.
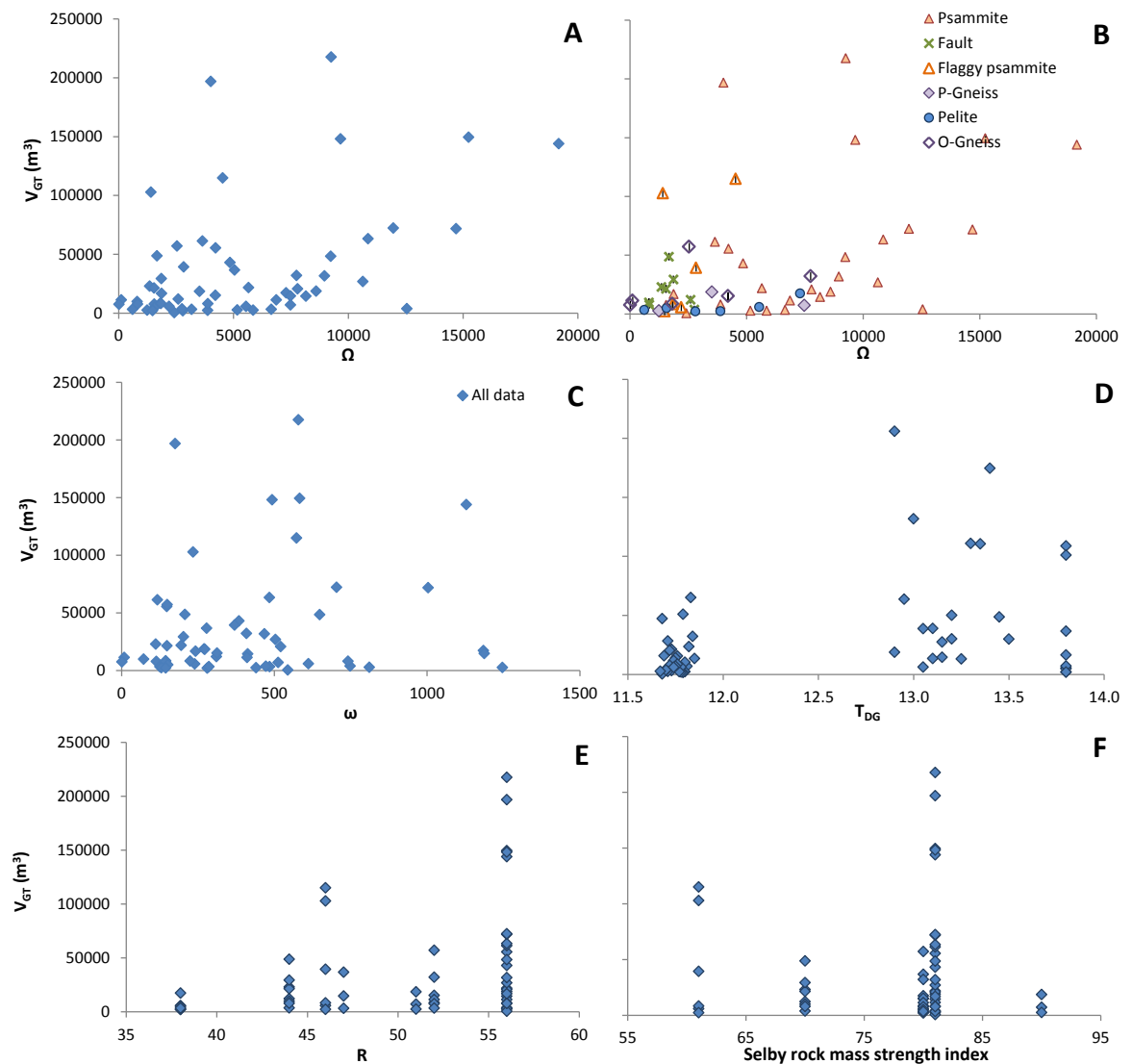
Appendix 6 - Chapter 6 additional results

Figure A6-1 Scatter plots of gorge volume (V$_{GT}$) for all bedrock reaches versus A) total stream power (Ω), B) total stream power, but catagorised for different lithologies, key in plot, C) unit stream power (ω), D) time since deglaication (T$_{DG}$), E) the Schmidt hammer R value and F) the Selby rock mass strength index.

Appendix 7 - Details of new lithological resistance index

The new lithological resistance index discussed in section 7.2.2 is based on a simplified version of the Selby rock mass strength index (see scoring scheme in table 2-5; Selby, 1982). The new scheme contains just two components, a rock strength index and a joint index accounting for the joint spacing and continuity (Tables A7-1 and A7-2). The weathering component of the original Selby index was removed as the rate of fluvial incision outpaces weathering rates in most settings hence rivers are predominantly eroding unweathered rock in the channel bed. Groundwater is not thought to be a significant factor

in fluvial erosion of silicate rocks (but may be important in carbonate rocks). The joint scaling scheme was also simplified by the removal of the joint width and orientation components. As joints may progressively expand through weathering, hydraulic wedging and vegetation growth when exposed at the surface, joint widths measured from surface observations are likely to be function of time rather than a property of the 'intact' rock. Joint orientation may be an important control on the rate of plucking, but complexities arising from the conjugation of joint sets (commonly sub-orthogonal planes) and relative orientations of bedding and jointing mean that further work is needed to assess the importance of different three-dimensional discontinuity patterns in constraining fluvial incision processes and rates.

I_s	Schmidt hammer 'R'			60		50		40		30	
	Score		50		40		30		20		
I_j	Joint spacing (m)		2		1		0.5		0.005		
	Score		40		30		20		10		
	Joint continuity	None		Few		Some		Many			
	Score	10		7		5		3			

Table A7-1 Scoring scheme for rock strength index (I_s) and joint index (I_j) components of the new lithological resistance index

	Schmidt hammer 'R' value	Average joint spacing	Joint continuity	Selby RMS index	I_s	I_j	I_L	I_j/I_s
Protomylonitic gneiss	51	0.7	None	90	41	38	79	0.93
Orthogneiss	50	0.25	Few	83	40	25	65	0.63
Flaggy Psammite	47	0.03	Many	61	37	11	48	0.30
Psammite	56	0.5	Few	83	46	27	73	0.59
Pelite	38	1.0	Few	82	28	37	65	1.32
Schist	32	0.9	Few	79	22	35	57	1.59
Quartzite	59	0.5	Some	82	49	37	65	0.49

Table A7-2 New lithological index metrics for the main lithologies in the NW Highlands study area